An anatomically based mathematical model of the human lungs, applied to gas mixing and water vapour and heat transport

by Merryn Howatson Tawhai

Supervised by Professor Peter Hunter
and Dr. Andrew Pullan

A thesis submitted in partial fulfilment of the requirements for the
degree of Doctor of Philosophy at the University of Auckland

Department of Engineering Science
School of Engineering
The University of Auckland
New Zealand
February 2001

Abstract

This thesis has focused on developing an anatomically-based model of the human lungs, initially to be used for modelling transport problems.

An algorithm is presented for generating three-dimensional conducting airway models into anatomically-based host volumes. The algorithm uses a bifurcating distributive method to generate a three-dimensional tree that fills an anatomically based pleural cavity. Branching, length, and diameter ratios from the generated model are consistent with experimental results, and the mean branch angles are consistent with a theoretical 'ideal' angle. The proportion and number of branches in each of the five model lobes are similar to those from the literature.

A lumped parameter model for respiratory airway gas mixing is developed, based on results from gas mixing in a multi-branching model. Development of a computationally small respiratory airway model for coupling to the asymmetric conducting airway model is necessary to ensure that solution of transport equations in the coupled model are feasible. The lumped parameter model is calibrated using gas mixing results from an anatomically-based multi-branching respiratory airway model, over a wide range of simulation conditions and model sizes. The lumped parameter model is in the form of regression equations that are used to predict transitional bronchiole concentrations throughout expiration, based on inspiratory parameters that are particular to each coupled lumped parameter model.

The lumped parameter respiratory airway model is coupled with the asymmetric conducting airway model to simulate gas mixing in the entire lung system. Results from full lung gas mixing show the importance of respiratory airway asymmetry and incomplete mixing, conducting airway asymmetry, blood gas exchange, and airway mechanics, on generation of a sloping alveolar plateau in phase III of the washout

curve. Respiratory airway asymmetry and incomplete mixing is shown to have the greatest contribution to S_n (the slope of the alveolar plateau normalised by the mean expired gas concentration) in the first breaths of multiple washin tests. Conducting airway asymmetry is shown to increase S_n in a manner consistent with the literature, even when flow is distributed uniformly throughout the model. Blood gas exchange moderates the S_n curve such that the plot of S_n against breath number approaches a plateau after approximately 18 breaths. Airway mechanics are represented in this study by idealised pleural pressure gradients. The pleural pressure gradients are shown to have a complex effect on S_n. This study highlights the import contribution made by each of these factors to generation of S_n over multiple breaths.

A model of water and heat exchange in the asymmetric conducting airway model is developed for investigating penetration of the airways by unconditioned gas, and for investigating airway drying. The water and heat transfer model incorporates radial layers of airway surface liquid, sub-mucosa/tissue, and a surrounding capillary bed. Additional layers can be included in the model to simulate an endotracheal tube and associated condensation. Unlike other models in the literature, the respiratory transfer model presented in this study uses power law curves to describe the velocity, temperature, and concentration across an airway. The model therefore solves coupled transport and transfer equations both axially and radially. The transfer of water vapour or heat is governed by the concentration and temperature gradients at the interface between the surface liquid and the air in the lumen: empirically derived transfer coefficients are not used to predict heat and mass transfer in this model.

Comparison of results from the water and heat transfer model with experimental results shows that the model presented in this study produces airway temperatures close to experimental measurements for ventilation up to $60 \ \mathrm{L \cdot min^{-1}}$ with an inspired temperature of $30.3°C$. For combined higher ventilation rates and lower temperatures the model does not sustain sufficient wall cooling during inspiration. The model simulates temperatures down an endotracheal tube that are close in value to experimental temperatures. Airway drying in the model is shown to be dependent on the rate of replenishment of the airway surface liquid by the surrounding tissue.

Acknowledgements

I have had a large number of friends, family, and colleagues who have supported and encouraged me over the past few years.

The most significant influence on my research has come from Professor Peter Hunter. Peter has been an inspiration to work with - not only because of his outstanding abilities and passion for his work, but also because of his caring, understanding, and genuine concern for the well-being of his students. Thankyou Peter for believing in my ability to complete this project.

I have been fortunate to have been part of a very supportive research group, with students and staff members who have always been willing to answer questions and help me where possible. In particular, Drs Andrew Pullan and Poul Neilsen have always made themselves available to provide me with carefully considered advice. I have valued their input into this project. I would like to thank all of the members of the Bioengineering Research Group - past and present - for their friendship and support, particularly Carey Stevens, Chris Bradley, Karl Tomlinson, and Shane Blackett.

This research was initiated at the suggestion of Dr Edward Harris. He has been a wonderful source of information on lung structure and function (and amusing anecdotes). Thankyou Dr Harris for the enthusiasm and energy you have put into this research.

The first stage of this research was supported by a Graduate Research in Industry Fellowship, in conjunction with Fisher & Paykel Healthcare. I would like to thank the GRIF scheme and Fisher & Paykel Healthcare for the opportunity to undertake this research.

I must thank my family for many years of encouragement and support. My parents always seemed to take it for granted that I could acheive anything I set my mind to.

Their unquestioning faith in me allowed me to come a long way before I began to question myself.

Finally, I have been fortunate to have been backed by an extremely loving, dependable, patient, and understanding husband. He has been my emotional and financial crutch throughout this whole process, ensuring that my life has balance and stability. Thankyou Jamie (and Aimee and Grace) for loving me.

Contents

List of figures

List of Tables

Glossary of Terms

α Parameter describing the shape of the velocity profile for water and heat transfer simulation

ACA   Asymmetric conducting airway (model)

ACA-perfect (model)   ACA model coupled with a LPA model in which gas mixing was assumed to be complete by the end of inspiration

Acinus (acini)   A respiratory unit comprising all airspaces distal to and including a single transitional bronchiole

Alveolar sac   An airspace with alveoli as its only outlets

Alveolus (alveoli)   Half-spherical outpouching, site of gas exchange with blood

AME   Alveolar mixing efficiency

Anatomical dead-space   Volume of gas present in the conducting airways at the end of inspiration that therefore cannot take part in gas exchange

β Parameter describing the shape of the temperature profile for water and heat transfer simulation

Carina   Division of the trachea into left and right major bronchi

CDI   Convection-dependent inhomogeneity, determined by lung mechanics

delta   Difference in Horsfield order of two daughter branches

ΔS_n Difference between the S_n curve values for SF_6 and He

Δy Tissue layer depth in the water and heat transfer model

DCDI   Diffusion- and convection-dependent inhomogeneity, inhomogeneous gas distribution due to interaction of convection and diffusion in an asymmetric lung structure

FD   Flow divider, the value used to divide the Reynolds number, for calculation of parabolic profile parameters

FRC   Functional residual capacity, volume remaining in lungs after a relaxed tidal exhalation

γ Parameter describing the shape of the water vapour concentration profile for water and heat transfer simulation

HBW   Haefeli-Bleuer and Weibel (1988) anatomical data

IC   Inspiratory capacity, volume that can be inhaled from FRC

LLL   Left lower lobe

LPA   Lumped parameter acinar (model), lumped parameter model of a single acinus using a regression equation to predict expiratory parameters

LPA-ACA (model)   Combined LPA and ACA models

LPA-SCA (model)   Combined LPA and SCA models

LUL   Left upper lobe

MBA   Multi-branching acinar (model), asymmetric finite element model of a single acinus

MBA-SCA (model)   Combined MBA and SCA models

MBME   Multiple breath alveolar mixing efficiency

MBW   Multiple breath washin (washout), multiple SBW performed sequentially

MRI   Magnetic resonance imaging

N_w Number of branches in order w

Pe   Peclet number

Phase I   First portion of a SBW curve, representing unmixed inspired gas

Phase II   S-shaped decrease in a SBW curve concentration from inspiratory value

Phase III   Third portion of a SBW curve, where concentrations approach a plateau

QSI   Quasi-stationary interface, interface between unmixed inspired gas and mixed residual and inspired gas

R_b Branching ratio, slope of the plot of log(number of branches) against branch order

R_d Diameter ratio, slope of the plot of log(mean branch diameter) against branch order

Re   Reynolds number

RH   Relative humidity, usually as a percentage (of the maximum possible water content at a given temperature)

R_l Length ratio, slope of the plot of log(mean branch length) against branch order

RLL   Right lower lobe

RML   Right middle lobe

RUL   Right upper lobe

RV   Residual volume, smallest volume of air that the lungs can contain after a

	maximal forced expiration
SCA	Symmetric conducting airway (model), symmetric finite element model of the conducting airways
S_{acin}	Contribution of the respiratory airways to ventilation inhomogeneity
S_{cond}	Contribution of the conducting airways to ventilation inhomogeneity
SBW	Single breath washin (washout), inhalation of a single breath of marker gas at a known concentration, followed by exhalation while recording expired concentrations and volumes
S_n	The slope of the alveolar plateau in Phase III of a SBW curve, normalised by the mean expired concentration of subject gas
TLC	Total lung capacity, largest volume of air that the lungs can contain after a maximal inspiration
T_{lumen}	Temperature in the centre of the airway
T_{mai}	Temperature at the interface between air and airway surface liquid
Transitional (terminal) bronchiole	Most distal conducting airway. Has both a conductive and a respiratory portion.
$\dot{V}$	Ventilation rate, in $L \cdot min^{-1}$
VC	Vital capacity, largest volume that can be inspired or expired
$V_D F$	Fowler's dead-space, estimate of the anatomical dead-space
$V_D V$	Ventilatory dead-space, estimate of the conducting airway volume plus the volume of gas that reaches the respiratory airways but does not take part in mixing
VM	Visual man, sections through a frozen cadaver
V_T	Tidal volume, amount of gas inspired or expired in a breath

Chapter 1

Introduction

The human lungs and upper airway perform a number of important functions: as well as transporting oxygen and carbon dioxide between the environment and the alveolar gas exchange surfaces, they also filter inspired air to remove pathogens and particles of dust, they heat and humidify inspired air to optimal conditions for proper lung function, and they are a site of defence.

Efficient transport of gas between the mouth and alveolar surfaces is achieved by a hierarchical branching structure: the large conducting airways repeatedly divide into two daughter branches with (generally) smaller cross-section and length than their parent branch, such that the summed cross-sectional area with distance from the mouth quickly increases. Because the area through which the inspired gas passes increases with each branch division, its forward rate of movement is slowed until, near the respiratory region, gas transport is predominantly by molecular diffusion. The branching lung structure enables efficient transport of gas to a very large alveolar surface, but the small size of the peripheral airways make it impossible with current technology to take measurements of gas concentration or temperature in the small conducting airways and the respiratory region without disturbing the normal function of the airways. For this reason mathematical models of the lung have proven useful to assist with explaining lung function where it is not possible to gather experimental data.

Historically, mathematical models of the lungs have been developed to provide

information that is not obtainable experimentally, and to assist with interpreting experimental observations. The idealised geometries adopted for these models, and their simplifying assumptions that were necessary at the time of their development to make them computationally feasible, means that they are not capable of reliably simulating experimental data.

Although the lungs are an asymmetric structure with thousands of branches, their geometry has usually been modelled as symmetric. However, simulations of gas mixing and water and heat transfer in these symmetric models have not produced results that compare closely with experimental results. A closer fit to experimental gas mixing results has been attempted by including respiratory airway asymmetry (Paiva & Engel 1984), generation of gas from the blood (Scherer, Neufeld, Baumgardner & Neufeld 1996), and distributed pressure-volume curves (Cruz 1991, Cruz, Jeng, Han, Wu & Flores 1997). These assumptions have each been shown to improve the numerical results, but have not been sufficient to produce results that match the experimental data of Crawford, Makowska, Kelly & Engel (1986). The effect of conducting airway asymmetry on gas mixing has largely been ignored.

Results from Cruz (1991) and Cruz et al. (1997) indicate that pulmonary mechanics have a significant effect on gas mixing. It is therefore sensible to assume that a more realistic description of mechanics than the compartmentalised pressure-volume curves employed by Cruz (1991) and Cruz et al. (1997) would produce a more realistic gas mixing model. For a lung model to incorporate a thorough description of pulmonary mechanics, it will require coupling of the mechanical deformation of the parenchyma to the airflow in the asymmetric branching conducting airway system: a symmetric airway model is not adequate in this case.

Artificially ventilated patients are generally intubated with an endotracheal tube. This tube bypasses the nose and mouth, to deliver air directly into the trachea. The nose and mouth usually condition inspired air to be close to body temperature and to be saturated with water vapour. When this area is bypassed by an endotracheal tube, cold and dry gas must be conditioned by the conducting airways before it reaches the respiratory region. This is accomplished by evaporation of water from the surface liquid that lines normal airways. This surface liquid bathes small hair-like structures (cilia) that line the airway walls. The function of the cilia is to sweep mucus on the

surface of the lining liquid towards the mouth. Their performance is sensitive to the depth of the surface liquid: when the liquid depth is too low, the cilia cannot complete their 'back-sweep' without contacting the mucus on the surface of the lining liquid, and the mucus is hence swept forwards and backwards without any net movement; when the surface liquid depth is too deep the cilia cannot make contact with the mucus and therefore no movement occurs. The optimal function of the cilia is also impaired by contact with air that is cooler than body temperature. Impaired muco-ciliary transport leads to airway blockage, and increased infection. It is therefore vital that air supplied to an artificially ventilated patient is pre-conditioned by an external device to adequate conditions of heat and water content.

There is currently debate in the literature as to the 'correct' level of pre-conditioning that is necessary to prevent airway damage. Some groups advocate conditioning inspired air to body conditions ($37°C$ and saturation) while others recommend lower temperatures and absolute humidities. Fisher & Paykel Healthcare are a New Zealand company who specialise in the manufacture of active respiratory humidifiers. They require a model for simulating respiratory heat and water exchange, so that they can investigate the effect of different ventilation and conditioning strategies on the airway surface liquid.

Previous interest in modelling water and heat transfer in the lungs has arisen largely due to its possible connection with exercise-induced asthma. Although a number of pulmonary water vapour and heat transfer models have been developed, these models have all used symmetric airway geometry, and have usually relied on experimentally-derived heat and mass transfer coefficients to describe the radial movement of water vapour and heat from the airway wall into the lumenal gas. When unconditioned air does not penetrate far beyond the carina, then a symmetric model is preferable to one with a large degree of asymmetry: the symmetric model is computationally less expensive and will produce the same results as the asymmetric model. However, as the unconditioned air moves more distally into the lung, the symmetric model becomes less appropriate. The common reasons for artificial ventilation (damage to the wall structure, muscle weakness, abnormal airway resistance or compliance) mean that the lung may experience more uneven ventilation than under normal conditions. The altered pulmonary mechanics and

hence distribution of flow makes an asymmetric conducting airway model necessary.

Because the airways are susceptible to damage, measurements of airway temperature have usually been gathered under relatively mild experimental conditions. Subjects have inspired very cold dry gas through the mouth at varying rates of ventilation, with the temperatures measured at a range of distances down the airway tree (McFadden, Denison, Waller, Assoufi, Peacock & Sopwith 1982, McFadden, Pichurko, Bowman, Ingenito, Burns, Dowling & Solway 1985). Because the gas has passed through the mouth, the gas entering the trachea is already considerably heated and humidified. Further experiments have been performed where gas colder than body temperature has been introduced through an endotracheal tube (Ryan, Rankin & Williams 2000). This second set of experiments used temperatures closer to body temperature because introducing very cold dry gas directly into the trachea may cause damage to the airway walls or stimulate bronchoconstriction similar to that seen in exercise-induced asthma. Experimental data for model comparison is therefore limited, but the experiments have all demonstrated that unconditioned air can penetrate deep into the lung, and that it causes significant cooling of the airway walls via evaporation and its associated latent heat. These studies show that the airway walls rewarm slowly, facilitating recovery of heat and water vapour from the expired air.

In this thesis development of an algorithm for generation of asymmetric conducting airway models into a three-dimensional description of a pleural cavity is presented. The generated model can be used as a computational mesh for solution of transport problems. In Chapter 2, the conducting airway model is compared extensively with available experimental data, and its close match to these data indicates that the model can be considered representative of a human lung.

The asymmetric conducting airway model is coupled with a lumped parameter respiratory airway model (calibrated using results from a multi-branching acinar model with blood-gas evolution), and is then used to simulate gas mixing in Chapter 4. The influence of conducting airway asymmetry on gas mixing is investigated, and shown to be significant. An idealised pleural pressure gradient is applied, and shown to have a significant effect on the model's gas mixing. This confirms the results of Cruz (1991) and Cruz et al. (1997), and highlights the importance of developing an accurate

description of pulmonary mechanics.

The transfer coefficient approach used in most respiratory water and heat transfer models is only valid over a limited range of inspiratory conditions, and is not applicable when an endotracheal tube is positioned in the trachea. In Chapter 5, the approach used by Saidel, Kruse & Primiano (1983) is extended to include power law descriptions of velocity, temperature and water vapour concentration that vary axially and with Reynolds number. Heat and water vapour transfer equations are solved in a multi-layered model: cylindrical airways with a lumen, airway surface liquid, tissue, and surrounding capillary bed. An endotracheal tube can also be present, with a layer of condensate under appropriate conditions. Solutions of the transport equations in a symmetric and asymmetric model are compared.

The algorithms for conducting and respiratory airway model generation, and the numerical methods for solving the transport equations, were incorporated into the computational back-end of CMISS (Continuum Mechanics, Image analysis, Signal processing, and System identification). CMISS is a mathematical modelling environment that has been developed in the Department of Engineering Science at the University of Auckland, for application of finite element, boundary element, and collocation techniques to bioengineering problems. More information can be found at http://www.esc.auckland.ac.nz/Groups/Bioengineering/CMISS. CMISS command files used to generate the models in this thesis and to solve the transport equations are included in Appendix B.

The animations on the enclosed disk were made by exporting numerical results from the model to the graphical front end of CMISS.

Chapter 2

Modelling the conducting airways

2.1 Introduction

Historically, computational models of the conducting airways have been highly idealised to model various phenomena with constraints on computational power and storage. Symmetric (Weibel 1963) and regular asymmetric (Horsfield, Dart, Olsen, Filley & Cumming 1971) models have been used widely for various lung model simulations, and they have proved useful under certain conditions (see Section 3.2.5 and Section 5.2.6). However, these simplified models have not been able to reliably reproduce experimental results for gas transport. A realistic asymmetric conducting airway model is essential for increasing the accuracy of lung transport models. An asymmetric model will also be essential for coupling airway gas flow to parenchymal mechanics.

Conductive ventilation inhomogeneity arises from the non-uniform distribution of flow, largely because of the pleural pressure gradient that is induced by gravity. Flow through the airways is driven by the difference in pressure between the mouth and alveolar surfaces, and is moderated by the resistance and compliance of the individual airways. Flow through the airways may also be distributed non-uniformly because of the non-uniform deformations of the thoracic cavity that drive ventilation. Solution of equations that describe the mechanical deformation of the lungs under different boundary pleural pressures, and the resulting pressure-driven flows in the airways,

requires a conducting airway model that closely represents characteristics of the real lung.

The number of conducting airways in the human lungs is determined entirely before birth, by division and growth into a constrained space. The asymmetric cavity in which the lungs are space-filling determines that the conducting airways are asymmetric in both branching pattern and dimensions. This asymmetry is present from birth, and persists as the dimensions of the airways change with age.

The asymmetry of the human lungs is not as great as that of other mammals (Scadding & Cumming 1981*a*), but it is significant enough to affect ventilation inhomogeneity and therefore incomplete gas mixing (see Section 3.2.5), particle deposition (Taulbee & Yu 1975, Taulbee, Yu & Heyder 1978, Darquenne & Paiva 1994, Darquenne & Paiva 1996, Darquenne, Paiva, West & Prisk 1997), and water and heat transfer under extreme conditions (see Chapter 5).

The variation in branching pattern between individual lungs is conceivably very large. However, morphometric studies suggest that human lungs share certain structural properties, such as similar branching, length, and diameter ratios, and similar relationships between daughter and parent branch dimensions. For a conducting airway model to be representative of the real human lungs, it must also display the structural properties of the real lung.

This chapter describes the development of an algorithm for generating a three-dimensional conducting airway model - to be used as a computational mesh - using a bifurcating distributive method (Wang, Bassingthwaighte & Weissman 1992). The algorithm generates a conducting airway model into a volume mesh that describes the pleural cavity.

The structure and dimensions of the resulting conducting airway model are compared in Section 2.4 with values from morphometric studies. Branching, length, and diameter ratios, branch numbers, mean lengths, mean diameters, and mean branching angles are all compared with published data. The statistics from the model are found to be close enough to the morphometric data to be able to regard the model as representative of the conducting airways of a human lung.

2.2 Background

2.2.1 Classifying branches in tree-like systems

Like many other biological systems, the lungs have a tree-like structure where the trachea is the 'stem' and the bronchi, bronchioles, ducts and sacs branch out from the trachea in a manner similar to branches arising from the trunk of a tree.

A 'parent' branch gives rise to 'daughter' branches. If the parent divides in two, this is a bifurcation (or, dichotomy); division into three daughter branches is a trifurcation.

A symmetric tree contains airway paths from the stem branch to the peripheral branches that are all identical. That is, a single airway path is representative of all airway paths in the tree. In contrast, asymmetric trees contain non-identical airway paths, either in terms of their dimensions or because of varying numbers of component branches in the airway paths that comprise the tree.

There are several methods for describing the position of a branch in a tree-like system. The most commonly used methods are: Weibel generations (Weibel 1963), Strahler ordering (Strahler 1950), and Horsfield ordering (Horsfield & Cumming 1968).

2.2.1.1 Weibel generations

Weibel generations describe the position of a branch in relation to the stem branch. The numbering begins at the stem branch and continues towards the peripheral branches. The stem branch has the lowest generation number, and each subsequent branch division produces daughter branches that are one generation higher than the parent branch. When Weibel generations are applied to asymmetric trees, terminal branches are classified in a range of generations. Weibel generations may therefore group together branches that are unlike in terms of their dimension or structure.

2.2.1.2 Methods of ordering

2.2.1.2.1 Strahler ordering

Strahler ordering was originally developed for use on river systems. This method begins at the terminal branches, which are assigned the lowest order (usually 1). Strahler ordering has two stages: stage 1 classifies a parent branch as one order higher

than two daughter branches of the same order, or as the same order as the highest ordered daughter branch; stage 2 replaces parent and daughter branches of the same order with a single branch of that order.

2.2.1.2.2   Horsfield ordering

Horsfield & Cumming (1968) developed an ordering system based on Strahler ordering that was more appropriate for a lung tree. Horsfield ordering assigns the lowest order (usually 1) to the terminal branches, and parent branches are one order higher than the daughter branch of highest order. Horsfield ordering produces more branches and orders than Strahler ordering for asymmetrical trees. The number of orders in a Horsfield ordered tree is the same as the number of Weibel generations.

Both Strahler and Horsfield ordering are better at grouping functionally similar branches together in asymmetrical trees than Weibel generations. Orders are useful when describing, classifying, or comparing branching systems within and between species whereas generations are useful for locating a branch in relation to the stem branch. The three classification methods are demonstrated in Figure 2.1. The top branch in the classified tree is generation 1, Strahler order 3, and Horsfield order 5.

(a) Weibel generations   (b) Strahler ordering   (c) Horsfield ordering
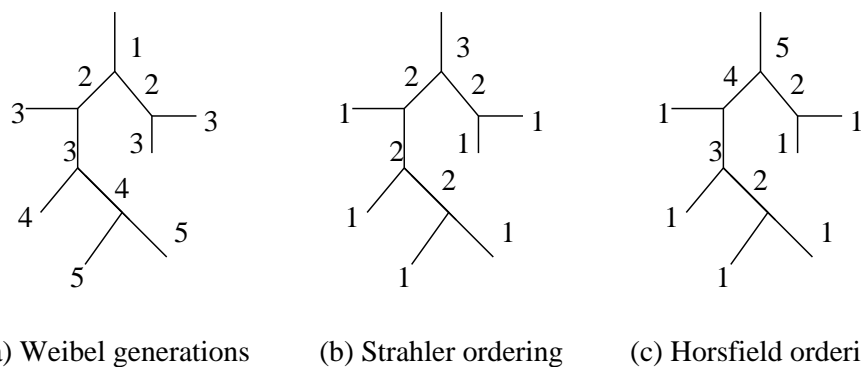
Figure 2.1: *Trees classified using (a) Weibel generations, (b) Strahler ordering, and (c) Horsfield ordering. The stem branch is generation 1, Strahler order 3, and Horsfield order 5.*

To describe and define the asymmetry at a bifurcation, Horsfield et al. (1971) developed the concept of delta, the difference in Horsfield order of two daughter branches that arise from the same parent branch. A tree with delta=0 is symmetric;

delta=1 describes a tree with regular asymmetry of one order difference between daughters; higher delta values describe more asymmetrical trees. For example, in Figure 2.1(c) the order 5 branch (uppermost in the tree) has a delta value of 2, the order 3 branch has a delta value of 1, and the order 2 branches have delta values of 0.

2.2.2 Human lung and conducting airway structure

2.2.2.1 The lungs

The human lungs are housed inside the thoracic cavity. The lungs fill most of the thoracic cavity except for the space occupied by the heart and major blood vessels. The normal live adult human lung weighs about 1000g and consists of about 50% blood and 50% tissue by weight. About 10% of the total lung volume is composed of conducting airways and some connective tissue. The remaining 90% is the respiratory region.

The human lungs have a right and left lung which are housed in two separate pleural cavities and are separated by the heart. The apex of the lungs has a tapering conical shape, and extends into the root of the neck. The broad base of the lungs rest upon the surface of the diaphragm, which separates the lungs from the liver, stomach, and spleen. The right lung is usually larger and heavier than the left lung due to the heart inclining towards the left side of the body. The right lung is also usually shorter than the left lung by about 2 cm, because the diaphragm is higher on the right side to accommodate the liver. The two lungs and typical five lobes are illustrated in Figure 2.2.
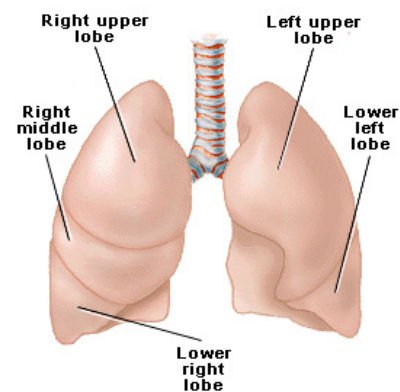
Figure 2.2: *Lung surface anatomy. Image courtesy of gsm.com (http://www.gsm.com) (c)1993-2000 Gold Standard Multimedia Inc. and its licensors.*

The two lungs are divided into distinct, separable lobes: the left lung is typically divided into an upper and a lower lobe by the oblique fissure; the right lung is typically divided into an upper, a middle and a lower lobe by the oblique and horizontal fissures. The lobes are bounded by the visceral pleura whereas the parietal pleura lines the interior surface of the chest wall, diaphragm,

and mediastinum. Therefore the lung and chest wall are separated by a narrow pleural space, which contains a small amount of serosal fluid. The fluid in the pleural space enables the lungs to slide within the chest cavity with minimal energy loss, and maximises the transmission of the forces of breathing from the chest wall to the lungs.

2.2.2.2 The pulmonary airways

The human respiratory tract consists of the nasal cavity, mouth, and larynx (the upper airways), the trachea and bronchi (the central airways), and the bronchioles, ducts, sacs and alveoli distal to the bronchi. The central and lower airways can be visualised as a complex branching 'tree' of bronchi, bronchioles and alveolar ducts. The hierarchy of airways is shown in Figure 2.3. In this figure the trachea is numbered as generation 0, and the subsequent generations are those from Weibel (1963).

The airways fall into two major categories: respiratory and conducting airways. The function of the conducting airways is to transport gas between the mouth and the respiratory airways. They do not take part in oxygen-carbon dioxide (O_2-CO_2) gas exchange, although they are capable of exchanging soluble gases with the bronchial circulation (Tsu, Babb, Ralph & Hlastala 1988). The respiratory airways are the most distal from the trachea, and are the site of all O_2-CO_2 exchange (see Section 3.2.1).
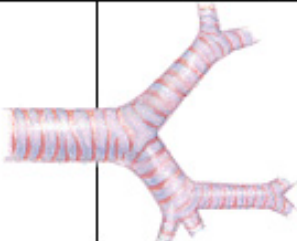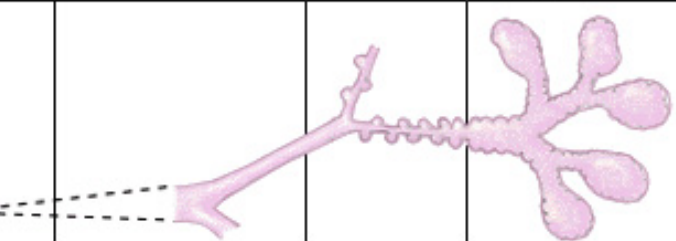
Conducting Airways			Gas Exchange Airway		
Cartilagenous		Membranous	Terminal Respiratory Unit		
Trachea	Bronchi	Bronchioles	R.Bronchioles	A. Ducts	A. Sacs
No alveoli			Alveoli		
Generation 0	1 2 ——→ 10	11-13 ——→ 16	17-19	20 22 23 24	
Bronchial Circulation			Pulmonary Circulation		
Air volume − − − 150 ml			1500 ml	3000 ml	
Smooth muscle					

Figure 2.3: *Hierarchy of airways in a human lung. The terminal respiratory unit (a pulmonary acinus) shows the respiratory (R) bronchioles, alveolar (A) ducts, and alveolar sacs. Image courtesy of gsm.com (http://www.gsm.com) (c)1993-2000 Gold Standard Multimedia Inc. and its licensors.*

2.2.2.3 The conducting airways

The conducting airway tree (beyond the upper airways) begins with the trachea, which divides into left and right principal bronchi that distribute inspired gas to the left and right lungs, respectively. Each principal bronchus divides into secondary bronchi, which in turn divide into tertiary bronchi. The division of branches continues down to the airway endings. The function of the conducting airways is to transport gas between the mouth and the respiratory airways. The most distal conducting airways are the transitional bronchioles (Haefeli-Bleuer & Weibel 1988) which define the boundary between the conducting and respiratory regions in the lung.

The cellular structure of the trachea and bronchi is shown in Figure 2.4. This figure also shows the underlying structure of the tracheal and bronchial walls. The innermost layer of cells lining the trachea and bronchi is composed mostly of ciliated pseudo-stratified columnar epithelial cells. Interspersed amongst the ciliated cells are mucus-secreting Goblet cells. A distinctive feature of the trachea and bronchi is the presence of sub-mucosal gland cells deep within the mucosa. The sub-mucosal gland cells are connected to the lumenal surface by ducts. They are capable of secreting large volumes of liquid and mucus. The sub-mucosal gland cells decrease in abundance and size distally and are not present in the bronchioles.
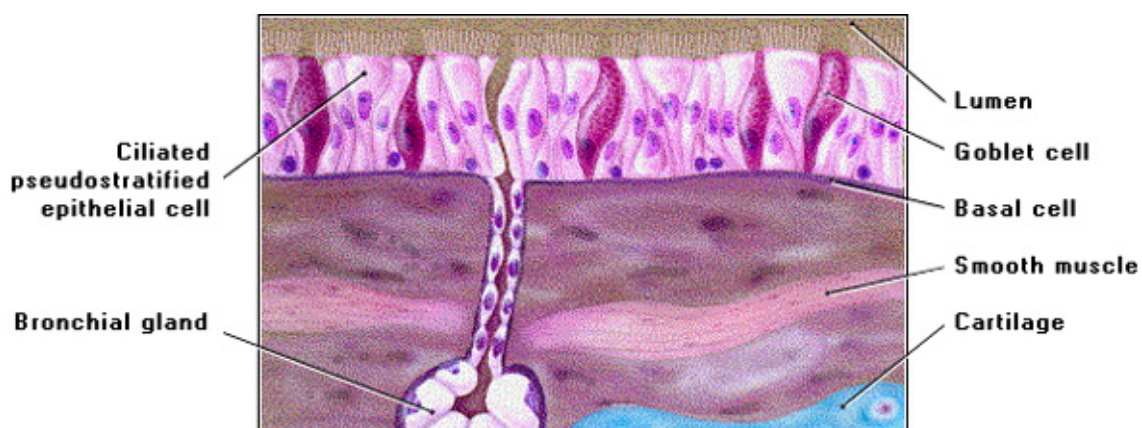
Figure 2.4: *Radial structure of the tracheal and bronchial walls. Image courtesy of gsm.com (http://www.gsm.com) (c)1993-2000 Gold Standard Multimedia Inc. and its licensors.*

The summed cross-sectional area of the airway system is smallest and therefore the flow velocities greatest in the trachea and central airways. In general, tracheal dimensions can be predicted from body size, with a linear relationship between the logarithms of tracheal dimension and body mass (Parent 1992). The ratio of tracheal length to diameter is relatively constant among species, approximating 1:8.

The main structural support for the trachea is provided by 19 to 20 incomplete cartilaginous rings and plates connected by a fibrous layer which is encircled by smooth muscle. The blood supply to the conducting airways is from the bronchial circulation.

The bronchioles make up about 25% of the volume of the conducting airways. They do not have the fibrocartilaginous support of the trachea and bronchi, but are instead embedded in the connective tissue framework of the lungs. This means that they are passively dilated and narrowed during breathing. The bronchioles are surrounded by a circular layer of smooth muscle. The bronchioles, like the bronchi, receive their blood supply from the bronchial circulation.

The bronchioles are lined with ciliated cells, but have fewer Goblet cells and no sub-mucosal gland cells. The Goblet cells tend to disappear distally and are replaced by secretory Clara cells. A circular layer of smooth muscle surrounds the bronchioles. Figure 2.5 illustrates the cell types that line the bronchiolar walls, and also shows the underlying connective tissue and smooth muscle.
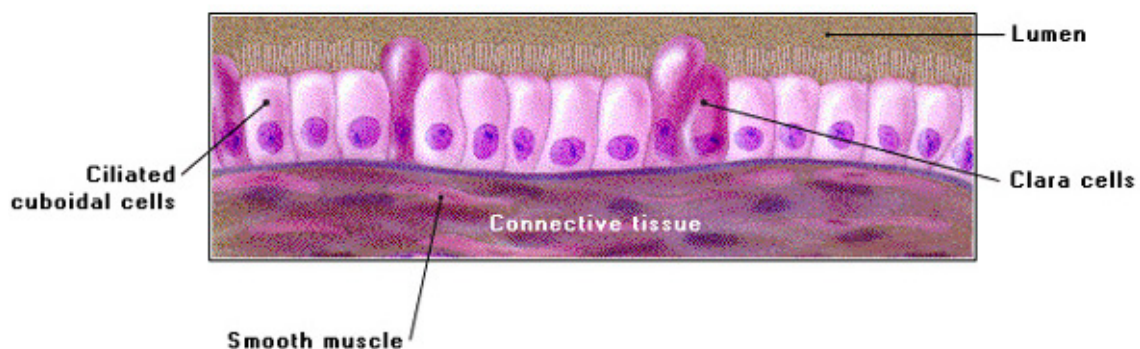
Figure 2.5: *Radial structure of the walls in the bronchioles. Image courtesy of gsm.com (http://www.gsm.com) (c)1993-2000 Gold Standard Multimedia Inc. and its licensors.*

2.2.2.4 Asymmetry in the conducting airways

The conducting airways are generally considered to be a bifurcating system: each parent branch gives rise to two daughter branches which are usually asymmetrical with respect to branch dimension and volume of lung supplied by each daughter branch. The degree of asymmetry in the conducting airways appears to differ among species, and to a lesser extent among lobes in individuals and among airways at different levels in the same lobe.

The human lung is more symmetrical than other species, but asymmetry of branching varies with the level within the lung. In general, the branching of the central airways is markedly asymmetric. Horsfield & Cumming (1968) proposed that branching in the human lung is asymmetric through most of the intra-lobar airways with a delta value of 3 (see Section 2.2.3), but becomes nearly symmetric in the last two orders before the terminal bronchiole. They found that the shortest paths to the transitional bronchioles have about 9 generations, and the longest about 27.

When the logarithm of the number of branches in a conducting airway order is plotted against order, an approximately linear plot is obtained. The slope of this plot is the branching ratio, R_b. Calculation of R_b is demonstrated in Figure 2.6. R_b is the factor by which the number of branches increases with decreasing order down the tree. Because of their slightly different asymmetries, different lobes in the lungs characteristically have different values of R_b. R_b can be calculated using either Horsfield or Strahler ordering.
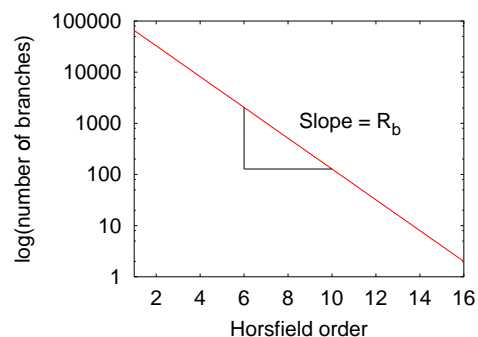
Figure 2.6: *A plot of log(number of branches) against Horsfield order, demonstrating calculation of R_b.*

Values for the diameter ratio (R_d) and length ratio (R_l) can be calculated in a similar manner by plotting the logarithms of mean branch diameter and length, respectively, against order and calculating the slopes.

All of the conducting airways are present before birth, so R_b has also been determined at this stage. The airways grow in both length and diameter for some

years after birth while subjected to air flowing through them, therefore the R_l and R_d are determined later than the R_b.

2.2.2.5   Development of the lung *in utero*

During the fourth week of human fetal development, the first stages of lung morphogenesis occur with the trachea becoming separated from the esophagus, and growth of lateral lung buds. The lung buds branch, which at this early stage involves both the epithelial tube comprising the bud, and the splanchnopleural wrapping enclosing the bud. This first branching produces two branches on the left side and three branches on the right side, resulting in an arrangement that will eventually form the typical five lobes of the human lung. Dichotomous branching of the epithelial tube within the mesenchymal bed of the splanchnopleura then continues repeatedly. The branching process results in a space-filling organ.

The epithelial tubes grow by proliferation of epithelial cells, especially at the 'bronchial buds' (at the ends of the tubes), where the epithelial tube is slightly widened. Division into two branches occurs at the epithelial bud due to interaction between the epithelial cells and the mesenchyme (Hutchins, Haupt & Moore 1981).

The mesenchyme eventually develops into a complex supporting structure for the lung and its components. The airways that will develop into bronchi become enwrapped by a dense sheath of mesenchyme. Smooth muscle fibres, strong connective tissue fibre sheaths, and cartilage develop from the mesenchyme, thus forming the bronchial wall. The arteries and veins also become enwrapped with condensed mesenchyme which forms smooth muscle fibres in varying amounts. The remaining loose mesenchyme forms sheaths that enwrap and separate the airway units that result from branching. These sheaths are all connected directly or indirectly to the splanchnopleura and thus form a complex system of connective tissue which transmits forces from the pleura into the depths of the lung (Weibel 1984).

By 17 weeks the fetal lungs have reached the 'pseudoglandular' stage when the airways have a narrow lumen lined by a thick columnar epithelium. Following this stage, the branches undergo a sequence of histological changes that gradually transform the lung into a gas exchanger.

By about 25 weeks the conducting airways have developed the ability to secrete

mucus and to transport mucus outward by the action of beating cilia. Between the 18th and 20th week, the terminal airways begin to widen and the lung reaches its 'canalicular' stage. The epithelial cells now begin to differentiate into two types: the first type is the thin squamous cell and the second type is the cuboidal secretory cell which is capable of synthesising phospholipids. The phospholipids are needed at birth to reduce surface tension as the air-spaces fill with air (Weibel 1984). At the end of this development the air-spaces have reached the 'saccular' stage.

The fetal lung remains at the saccular stage until birth, when it will be mature enough to act as a gas exchanger. In the months following birth, the lungs undergo structural changes to considerably enlarge the gas exchange surface and to thin the air-blood barrier. This results in an alveolar lung.

2.2.3 Anatomical studies of the conducting airways

There have been numerous studies published on different features of conducting airway morphometry. The studies published by Weibel (1963), Horsfield & Cumming (1968), and Raabe, Yeh, Schum & Phalen (1976) were detailed, and in a form that is easily utilised for development of, and comparison with, models. Most mathematical models of the human lung utilise one of these studies to some degree.

The most influential of these studies was published by Weibel (1963). Weibel (1963) measured dimensions of the major conducting airway branches from a plastic cast of a pair of human lungs. Measurements of branch length and diameter were performed on all branches down to Weibel generation 4, then were less complete down to generation 10 where only 10% of the branches were measured. Difficulty in measuring the small bronchioles was overcome by assuming regular dichotomy and hence predicting the missing measurements. Weibel (1963) approximated 16 generations from the trachea to the estimated 65,536 terminal bronchioles, and a mean branch length to diameter ratio of 3.25.

Horsfield & Cumming (1968) performed detailed measurements on a resin cast of the human lungs. 8,298 branches were measured, from the trachea down to airways 0.7 mm in diameter (defined as the 'lobular branches'). These data were complete down to airways of 2.2 mm diameter, and 90% complete at the lobular branches. The

lobular branches were assumed to be two or three generations proximal to the terminal bronchioles. Therefore, the Horsfield data was incomplete for the last few orders of the conducting airway tree. However, measurements of individual 'lobules' confirmed that branching in the terminal region was nearly symmetrical.

Horsfield & Cumming (1968) measured an average of 14.6 generations from the trachea to the lobular branches, with the shortest path reaching a terminal bronchiole after 8 branchings, and the longest after 25. The distribution of path lengths from the carina (the point where the trachea divides into left and right main bronchi) down to the lobular branches ranged from 7.5 to 21.5 cm. Horsfield & Cumming (1968) estimated there to be 27,992 terminal bronchioles in the lungs .

Raabe et al. (1976) made silicone rubber casts of two human lungs. They made measurements of diameter, length, branching angle, and the angle the branch made with the direction of gravity. For one of the casts, measurements were complete down to branches of 3 mm diameter. The other cast was measured down to a range of diameters, but for three of its lobes these data were 10% complete at the terminal bronchioles.

The length to diameter ratio of approximately 3:1 found by Weibel (1963) was observed by Raabe et al. (1976) for segments with diameters in the range of about 1-2 mm; outside of this range the values were lower. Analysis of this study by Phalen, Yeh, Schum & Raabe (1978) found that the minor daughter branches formed an angle with their parent branch of between 30° and 65°, with the angle of the corresponding major branch about 20° smaller. Phalen et al. (1978) also confirmed the finding of Weibel (1963) that the average ratio of smaller to larger diameters ranged between 0.5 to 1.0, with an average of 0.86 (±0.01), whereas the ratio of lengths averaged 0.62 (±0.2).

Figure 2.7 shows a detailed cast of the human airways, with the pulmonary arteries and veins also cast in the left lung. The white branches are the airways, the pulmonary arteries are coloured red, and the pulmonary veins are coloured blue.
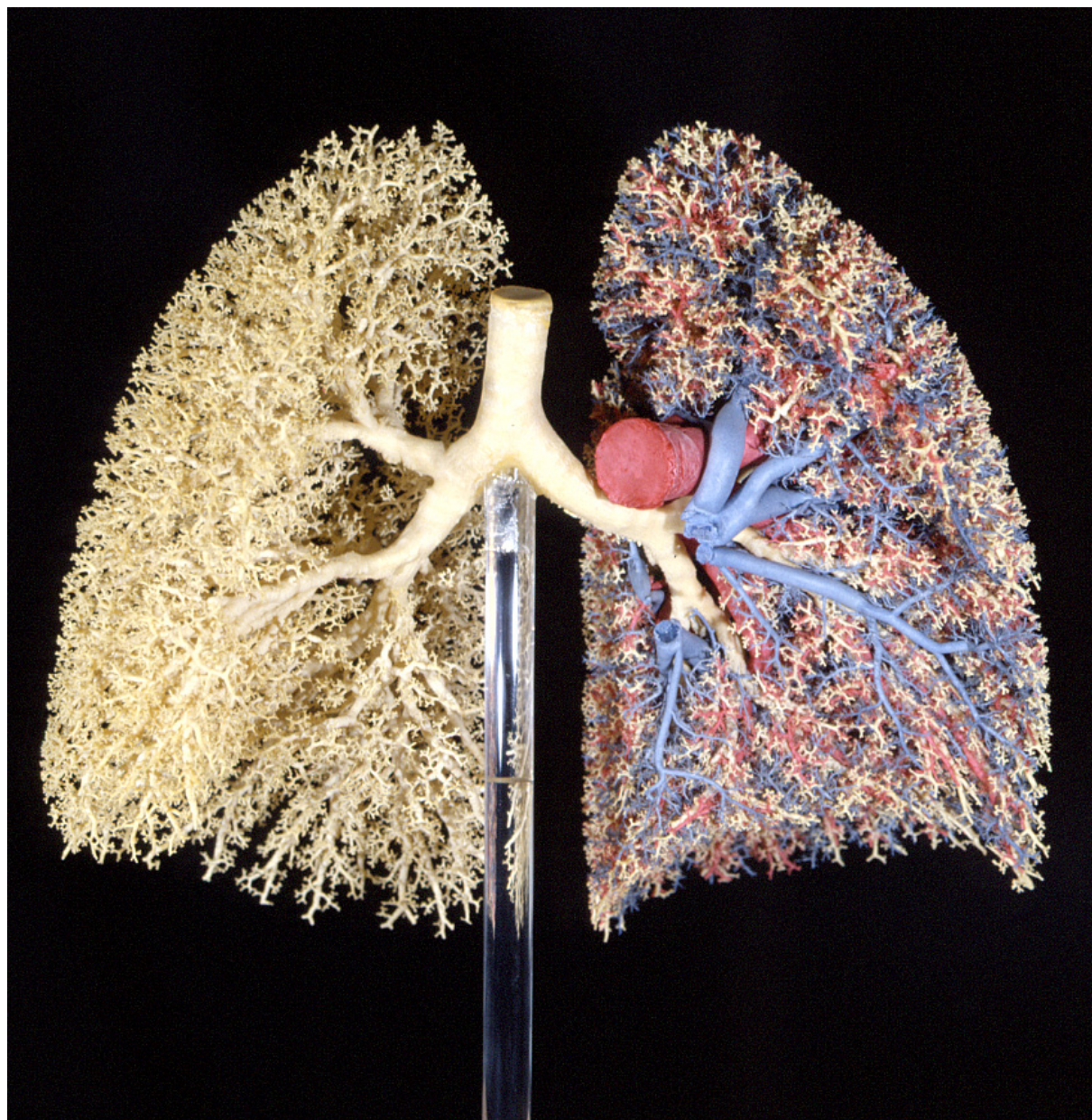
Figure 2.7: *Detailed cast of the human airways (left lung on right, right lung on left). In the left lung the arteries are coloured red, the veins are blue, and the airways are white. Image courtesy of E. Weibel.*

2.2.4   Past conducting airway models and algorithms

The conducting airways in the human lungs are a complex asymmetric branching structure. However, most computational models of the conducting airways have used highly idealised models of airway anatomy to ensure that the amount of computation required to solve the governing equations is relatively small. In this section two simplified topological airway models are first reviewed, followed by a description of three algorithms for generating spatially distributed airway models.

2.2.4.1   Weibel's symmetric model A

The most commonly utilised conducting airway model has been Weibel's symmetric model A, based on the morphometric study of Weibel (1963) (see Section 2.2.3). The symmetric model has been used to investigate gas mixing (La Force & Lewis 1970, Cumming, Horsfield & Preston 1971, Scherer, Shendalman & Green 1972, Paiva 1972, Baker, Ultman & Rhoades 1974, Engel, Paiva, Siegler & Fukuchi 1979), particle deposition (Taulbee & Yu 1975), and water and heat transfer (Hanna & Scherer 1986*c*, Hanna & Scherer 1986*b*, Ingenito, Solway, McFadden, Pichurko, Cravalho & Drazen 1986, Tsu et al. 1988, Daviskas, Gonda & Anderson 1990, Bui, Dabdub & George 1998). The symmetric model has proved popular due to its ease of use: because every pathway from the trachea to the terminal bronchioles is identical, the governing equations need only be solved down one pathway. Although Weibel's symmetric model is computationally cheap, it obviously cannot be used to investigate the effect of anatomical asymmetry on transport problems. Asymmetry of the lung structure becomes important when different regions of the lungs have different mechanical properties, or experience different pressures during breathing. The importance of branching asymmetry for accurately simulating gas mixing has also been recognised (Verbanck & Paiva 1990, Verbanck, Schuermans, van Muylem, Melot, Noppen, Vincken & Paiva 1998).

2.2.4.2   Horsfield's Delta model

Horsfield et al. (1971) derived an asymmetric conducting airway model based on the measurements of Horsfield & Cumming (1968) (see Section 2.2.3). The asymmetric

model was based on the concept of regular asymmetry at different levels in the airway tree. A tree with regular asymmetry has a constant value of delta, the difference in order between daughter branches. Branching ratios can be calculated for these regularly asymmetric trees. Comparison of the branching ratios with those from morphometric studies suggested that branching at different levels in the lungs could be represented by regular asymmetric trees with different values of delta. In the delta model, each daughter pair has a difference in order of 3, corresponding to a branching ratio of 1.38 which is assumed to be valid down to branches of 0.7 mm diameter (Horsfield & Cumming 1968). That is, if the terminal bronchiole is order 1, then the formula $N_w = N_{w-1} + N_{w-4}$ is valid down to Horsfield order 4, where N is the number of branches of order w. Branching is defined to be more symmetric in the lower ordered branches of the delta model. The delta model can be used to describe the numbers of branches in each order, and their connectivity.

Gillis & Lutchen (1999) have used the delta model to predict flow distributions among acini during bronchoconstriction. Although the model has proved useful for this type of study, it does not incorporate spatial positions for the branches, and therefore is not directly useful for investigating gravity- or structure-dependent effects.

2.2.4.3 Spatial method 1: area-splitting method

Nelson & Manchester (1988) described an algorithm to generate a bifurcating tree into a bounded plane. The algorithm can be summarised as:

1. From the end of an initial branch segment, the available space is divided into N subareas;

2. an angle is determined for a line from the end of the initial segment that divides each subarea in half;

3. the branch segment length is set to one-half the distance from the end of the initial branch to the nearest branch or boundary at that angle.

The algorithm relies on area splitting to determine the direction of generated branches. To extend this algorithm to three dimensions would require large numbers of volume splits, and thus incur high computational cost.

(a)   (b)   (c)
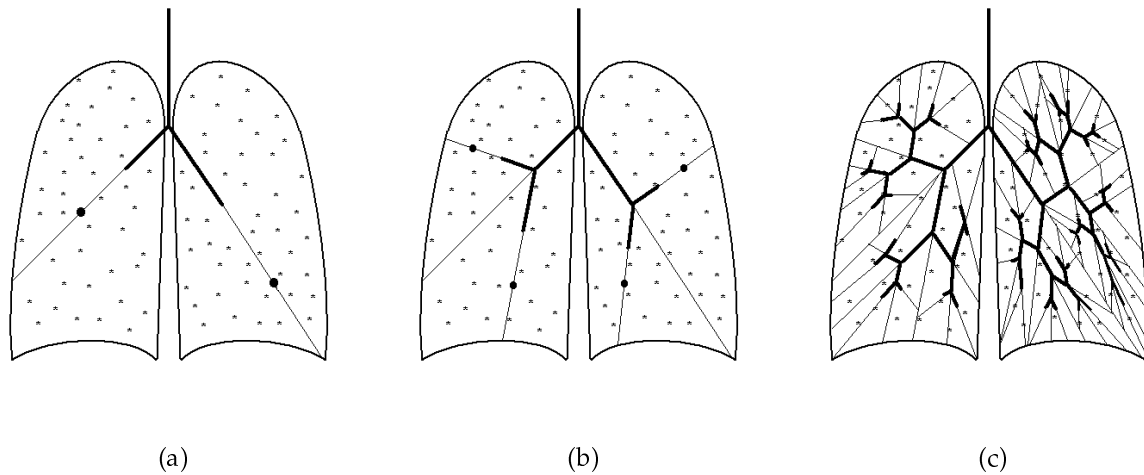
Figure 2.8: *Generation of a two-dimensional tree using the bifurcating-distributive method. (a) Calculation of the centre of mass of the random points; (b) Division of random points, and generation of a new branch; (c) Branching continues until each set contains only one point*

2.2.4.4   Spatial method 2: bifurcating-distributive method

Wang et al. (1992) devised a bifurcating-distributive method, based on the work of Nelson & Manchester (1988), to grow a lung-like tree in two dimensions in response to host geometry. Wang et al. (1992) used division of sets of random points instead of area splitting to provide a more efficient algorithm for tree generation. The first step in the distributive method is to calculate a large collection of random points on a plane, then the following algorithm is used to generate a bifurcating system from these points:

1. The centre of mass of the points is calculated (see Figure 2.8(a));

2. An imaginary dividing line is drawn from a given starting point through the centre of mass to the boundary. A branch is generated from the starting point, lying on the dividing line, and extending a defined fractional distance towards the centre of mass (see Figure 2.8(b));

3. The dividing line is used to define two new subcollections of random points;

4. The end of the generated branch is used as the start point for branching into the subsets of points (see Figure 2.8(c));

5. Branching ends when a subcollection of points contains only one point.

2.2.4.5 Spatial method 3: model based on a relationship between diameter and flow

The deterministic algorithm proposed by Kitaoka & Suki (1997) and used by Kitaoka, Takaki & Suki (1999) to generate a three-dimensional conducting airway model is based on a power law relationship between airway diameter and flow. Although a relationship between diameter and flow exists in the mature lung, the entire conducting airway tree develops in the fetal lung independently of air flow, followed by post-natal changes in branch length and diameter at different rates (Horsfield, Gordon, Kemp & Phillips 1987). Therefore, the diameter-flow relationship would not be suitable for investigating the underlying mechanisms of conducting airway development.

The Kitaoka et al. (1999) algorithm generates a lung-like tree into an idealised pleural cavity by using a diameter-flow relationship to constrain model branch diameter, angle, and length. The approximate number of terminal branches is specified by setting a flow limit. That is, flow decreases with each branch division down to the flow limit, at which point the branch is declared to be terminal. Branches are produced into 'branching planes', where the branching plane of the daughter branches is generally constrained to be perpendicular to the branching plane of the parent branch. Branches that project outside of the host boundary are either forced back inside the host, or are terminal branches.

Fundamental assumptions used in this model were that the terminal units to be supplied with flow (the acini) were close to uniform size and uniformly distributed, and that they each received nearly identical flow. However, the terminal branches in the *in vivo* lung are not distributed uniformly, and flow distribution is known to be non-homogeneous (Anthonisen, Robertson & Roos 1970, Milic-Emili, Henderson, Dolovich, Trop & Kaneko 1966). These assumptions may therefore limit this model's suitability for investigating airway and heterogeneous parenchymal interactions.

The diameter-flow algorithm was based on a set of rules designed to constrain the branching model development, plus a set of supplementary rules to alter the branching when it was deemed necessary. The supplementary rules were essential to ensure that, for example, the shape of a region supplied by a branch did not become long and flat.

The following algorithm summarises the diameter-flow method:

1. Two daughter branches arise from a single parent branch and are constrained to lie in a branching plane at 90° to the parent branching plane.

2. The region supplied by a parent branch is divided into two daughter regions by a 'space-dividing plane' which is perpendicular to the branching plane (a supplementary rule alters the space-dividing plane if the resulting daughter branches have an angle of greater than 10° between them).

3. The ratio of smallest daughter region to parent region is calculated, and the flow-dividing ratio is set equal to this.

4. The diameter-flow relationship is used to calculate the diameters and branching angles of the two daughter branches. A supplementary rule alters the branching angle when it is greater than 90°.

5. The length of each branch is assigned a value three times the diameter.

6. Branching stops when the flow rate becomes less than a specified threshold or the branch extends beyond its own region.

Branching angles, length-to-diameter ratio, and rotation angle of each branching plane down to the segmental branches were assigned in advance. The 'best' tree was determined based on: 1) minimising the number of branches that terminated by extending beyond their own region; 2) ensuring a nearly uniform distribution of acini; 3) minimising the coefficient of variation of acinar volumes; 3) comparison of generated dead-space volume; and, 4) minimising energy loss per terminal branch.

The approximate number of terminal branches in the model was set by defining the flow threshold below which branching would stop. Extension beyond a branches' region arose when a branch ended outside of the host volume, or outside of the subregion into which the branch was generated.

The volume into which the model was generated was a set of initial conditions mimicking the shape of the lung. As more detailed host geometries were used, the number of branches terminating because they extended beyond their own region

increased. This was assumed to be because of the algorithm's inability to cope with the concave surfaces of the real lung.

The model presented by Kitaoka et al. (1999) as satisfying their optimality criteria had a mean and standard deviation for the terminal branch generation number of 17.6 ±3.4 with a minimum value of 8 and a maximum value of 32. The mean was higher and the range wider for the model than was reported by Horsfield et al. (1971). The average terminal bronchiole diameter was smaller than reported in the literature. These results were assumed to be because of higher asymmetry in the model. Although not reported, it can therefore be assumed that the branching ratio from this model would have been higher than published values. Generating more symmetric models using the diameter-flow algorithm resulted in an increased number of branches terminating because they extended beyond their own region.

The diameter-flow relationship relies on an exponent, n. The value of n depends on whether the flow is turbulent or laminar, but Kitaoka et al. (1999) used a single value of n for '...simplicity of the algorithm'. The results showed that the generated model was very sensitive to the value of n chosen. The algorithm was also very sensitive to the rotation angle.

In summary, the diameter-flow method has proven capable of generating a branching structure that is visually similar to the real lungs. However, the resulting model is more asymmetric than the real lungs, and suffers from a lack of robustness when the confining geometry is made more realistic or an attempt is made to make the model more symmetric. Not enough information was provided with the model to support the author's claim that it compared well with morphometric data.

2.2.4.6 Summary

The lungs are a space-filling structure: the conducting airways bifurcate repeatedly to supply around 30,000 respiratory units (Haefeli-Bleuer & Weibel 1988) distributed within two irregularly shaped lung cavities. An algorithm to generate a conducting airway model should therefore consider the supply of respiratory units as well as physical constraints on branch dimensions and orientation.

The area-splitting, bifurcating-distributive, and diameter-flow algorithms all generate branching structures into constraining boundaries, but the diameter-flow

algorithm is the only method to produce a tree in three-dimensional space. However, the diameter-flow algorithm produces a markedly more asymmetric tree than the real human lungs, and is not capable of producing a more realistic tree without incurring large errors.

A new algorithm is required that can generate a conducting airway tree into any given pleural cavity, such that the resulting tree has structural properties very close to those of the real lungs.

2.3   Developing a conducting airway model

2.3.1   Three-dimensional bifurcating-distributive method

The three-dimensional conducting airway model developed in this thesis was based on the two-dimensional bifurcation algorithm described by Wang et al. (1992). The algorithm of Wang et al. (1992) was chosen because it was relatively simple, and it was computationally cheaper to implement in three dimensions than a volume-splitting algorithm. The generated model presented in this section extends from the trachea to the terminal conducting airways, which are the transitional bronchioles as defined by Haefeli-Bleuer & Weibel (1988). The model was generated into an anatomically based finite element mesh of a pleural cavity.

2.3.2   The host mesh

A host volume was defined into which the branching model was generated. The lung surface used for the host volume in this study was originally a surface mesh derived from Magnetic Resonance Imaging (MRI) data (Bradley, Pullan & Hunter 1997). The original surface mesh is shown in Figure 2.9 placed inside a torso, and surrounding the heart. The heart and torso models illustrated in Figure 2.9 have been developed by the University of Auckland Bioengineering Research Group (more information is available at http://www.esc.auckland.ac.nz/Groups/Bioengineering). The surface mesh from Bradley et al. (1997) described only the surface of the lungs, as more detailed information was not visible on the MRI slices.
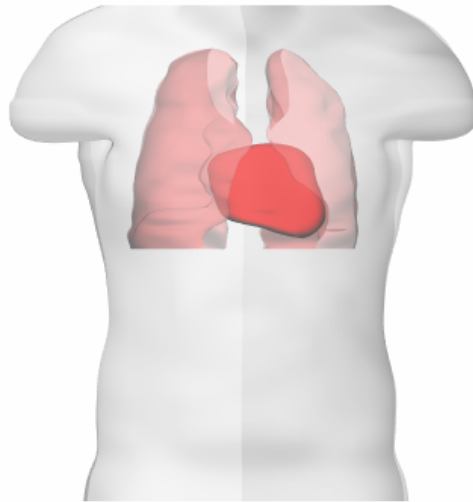
Figure 2.9: *The MRI-derived surface lung mesh in relation to the torso and heart models from the University of Auckland.*

The MRI-derived surface mesh was used as the description of the host boundary because it was sourced from a live subject. This meant that the subject lungs were not distorted by muscle relaxation that occurs after death, as would have been the case if post mortem lung data had been used to describe the pleural surface.

The horizontal and oblique fissures were determined by examination of slices through a torso from the Visual Man project (National Library of Medicine 1996). These torso slices are 1 mm sections through a frozen cadaver, on which the lung fissures are identifiable.

The horizontal and oblique fissures were tracked through the VM (Visual Man) lung, and their positions transferred to the surface lung mesh. Because the VM data are from a lung which has been compressed by the relaxation of surrounding muscles post mortem, the length of the VM lungs (from apex to base) was shorter than for the MRI lung (live subject). The positions of the horizontal and oblique fissures were therefore scaled from the VM lung to their new positions on the surface mesh.

For each MRI lung layer, the corresponding vertical coordinates in the VM lung were calculated, assuming a linear transformation from the compressed VM lung to

the expanded MRI lung. The VM lung layer at the corresponding scaled vertical coordinate was inspected to locate the horizontal and oblique fissures. When a fissure was located, the coordinates of the intersection between the fissure and pleural surface were recorded. A point on the fissure, central to the lung, was also recorded. The VM fissure coordinates were matched to the closest nodes on a refined MRI surface mesh.

To enable a close match between the VM coordinates and the surface mesh nodes, the MRI mesh was refined once running circumferentially around the lung, and twice vertically. This level of refinement enabled the mesh to be fit to the transformed VM data with 1 to 5 mm accuracy.

A line was drawn between the matched boundary nodes to define the fissure at each level. There was uncertainty in the internal position of the fissure, given that the VM lung is compressed. There is also variation in the exact shape of the lobes between human subjects. Therefore, the internal coordinates were not used to define the fissure, but were just used to check that the line joining the boundary nodes was not widely different to the internal coordinates.

Once all of the layers in the refined surface mesh had been matched with VM fissure coordinates, a new set of central nodes were created along the centre of each layer, at the midpoint between nodes on opposite sides of the layer. New nodes were also created at intersections between the fissure lines and lines connecting the midpoints and boundary points. The nodes lying on the fissure lines were then duplicated, such that two nodes with identical coordinates were positioned at each node point along the fissure.

Adjoining layers were pieced together to form a volume mesh. At the fissure face, the duplicate nodes were used such that adjoining lobes contained different nodes with identical coordinates. Each lobe in the volume mesh was therefore described using an independent set of nodes.

Cubic Hermite basis functions were used in the mathematical description of the surfaces, enabling a good description of the curved surfaces with a relatively small number of elements (Bradley et al. 1997).

The host space for the conducting airway mesh generation is in the form of five subspaces - one for each typical human lobe. The volume and number of elements for each host lobe is listed in Table 2.1.

Lobe	# elements	volume (ml)	% host	% Horsfield
RUL	131	702.11	23.14	21
RML	58	314.03	10.35	9
RLL	104	682.35	22.49	25
LUL	182	705.87	23.26	20
LLL	121	629.81	20.76	25
Total	596	3034.17	100	100

Table 2.1: *Numbers of elements, volumes, and % volumes for the host lobe meshes (at FRC) compared with % volumes from Horsfield & Cumming (1968). RUL refers to the Right Upper Lobe, RML to the Right Middle Lobe, RLL to the Right Lower Lobe, LUL to the Left Upper Lobe, and LLL to the Left Lower Lobe.*

The central airways (from the trachea to the lobar bronchi) were based mainly upon the study of Horsfield & Cumming (1968), but have been adjusted to fit the MRI data and model from Bradley et al. (1997). The end of each lobar bronchus provided a starting point for model generation into each corresponding lobe. Table 2.2 lists the lengths and diameters for each of the central airway branches.

Figure 2.10(a) shows the host mesh surfaces and central airways used for model generation viewed from the front; Figure 2.10(b) shows them viewed from the back. The central airways and the host element boundaries are illustrated in Figure 2.11.

Branch	Length (mm)	Diameter (mm)
trachea	100.0	16.0
right main bronchus	22.0	11.1
RUL bronchus	15.6	7.3
right lower bronchus	26.0	8.9
RML bronchus	16.3	5.2
RLL bronchus	26.1	6.4
left main bronchus	50.0	12.0
LUL bronchus	18.2	7.5
LLL bronchus	16.1	8.0

Table 2.2: *Length and diameter of central airway branches used for conducting airway mesh generation. Dimensions are based upon measurements by Horsfield & Cumming (1968), and adjusted to fit the data and model from Bradley et al. (1997).*
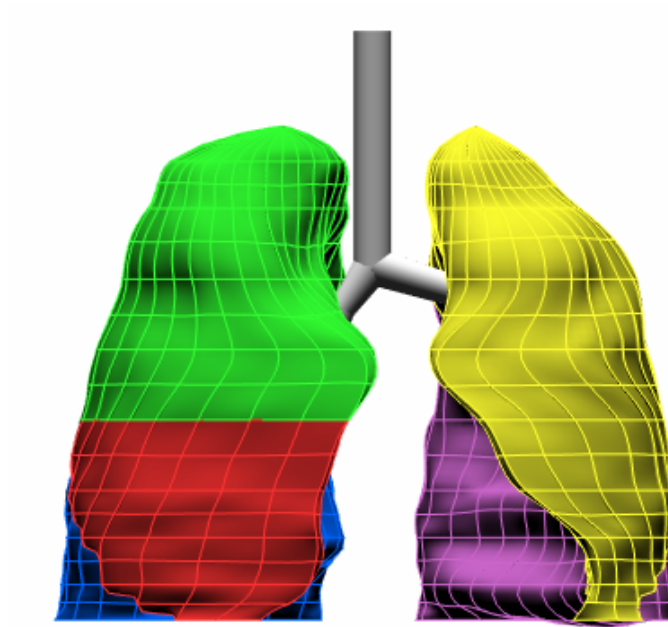
(a) Front view
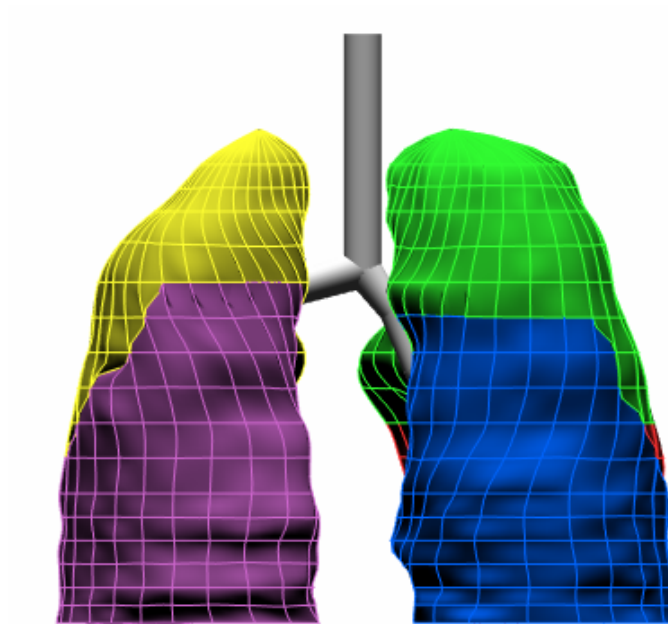
(b) Back view

Figure 2.10: *Host mesh surface and central airways for conducting airway tree generation. (a) Viewed from the front, (b) viewed from the back. Central airways = grey, RUL = green, RML = red, RLL = blue, LUL = yellow, LLL = purple.*
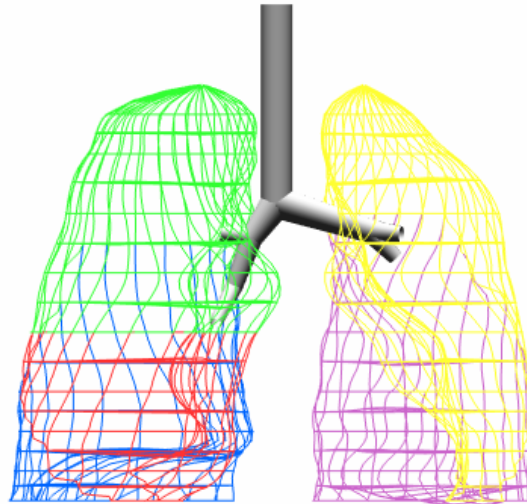
Figure 2.11: *Central airways and host mesh elements for conducting airway tree generation. Central airways = grey, RUL = green, RML = red, RLL = blue, LUL = yellow, LLL = purple.*

2.3.3   Adaptations for three dimensions

The two-dimensional bifurcation algorithm begins with the generation of a large number of random points in the host space. For three-dimensional tree generation, a fine uniform (in x space) grid of points was placed inside the three-dimensional host spaces: a uniform grid was computationally less expensive than generating random points. The irregular shape of the host spaces means that meshes generated using the uniform grid will be 'grown' in response to host geometry rather than according to a defined distribution of the 'random' points. Wang et al. (1992) have stated that the two-dimensional bifurcation algorithm would be equivalent to an area-halving algorithm if the points were numerous and evenly spaced, therefore it is expected that for a fine uniform grid in the host volumes, a three-dimensional bifurcation algorithm should approach a volume-halving algorithm. This assumption is verified in Section 2.4.

   An obvious difference between a two-dimensional and a three-dimensional bifurcation algorithm is that whereas plane branching uses a line to divide the collection of points, volume branching will require a plane. In the two-dimensional

algorithm, using the line from the starting point through the centre of mass to split the points is an obvious choice. For consistency between the three-dimensional and two-dimensional algorithms, the splitting plane in the three-dimensional algorithm should include the line from the starting point through the centre of mass. Definition of a splitting plane requires definition of a second vector: the vectors defined by the parent branch and the line from start point through the centre of mass were chosen to define the splitting plane. This is consistent with the approach used by Kitaoka et al. (1999) in the diameter-flow algorithm.

The two-dimensional algorithm aims to supply each random point in the host space with a terminal branch, hence termination of an airway path occurs when a subcollection of random points contains only one point. In contrast, it is not appropriate to have a terminal branch supplying each uniform grid point in the three-dimensional host volumes, as the terminal airways are not strictly uniformly distributed nor are they as numerous as the number of grid points. The number of grid points could be made equal to the number of 'expected' terminal branches, however this would 1) constrain the terminal branches to have uniformly distributed end points, and 2) constrain the number of generated terminal branches. Hence it is more appropriate to have a far larger number of grid points than terminal branches. This also allows the terminal branches to supply regions with different shapes - where the respiratory unit would be sited.

Terminal branches arise in the three-dimensional model when their length is less than a defined limit, or the subcollection of points the branch supplies is less than a defined number. The limit on the number of points in a subcollection ensures that a space exists at the end of each terminal branch for an acinus of a realistic size. The limit on the number of grid points in a supplied set is calculated using the host volume (3034 ml) and the range of expected terminal branches (26,000 to 32,000) from Haefeli-Bleuer & Weibel (1988). Dividing the total host volume (less 150 ml to account for the volume of the conducting airways) by the mid-range value (29,000) for the number of terminal branches gives a mean respiratory unit volume of 99.45 mm^3. The grid number limit is then the number of grid points that would fit inside this volume, and this number is dependent on the spacing of the grid points. The method used to calculate the grid point number limit provides a sensible estimate of the number of

points for any grid spacing.

Branch length decreases with order in the conducting airway tree. The three-dimensional generation algorithm imposes a limit on the length such that generated branches with a length less than or equal to the length limit are considered to be terminal bronchioles. Since the terminal bronchiole is of the order of 1.0-1.5 mm (Haefeli-Bleuer & Weibel 1988, Weibel 1963), a limit of 1.2 mm was imposed to allow some variation in the terminal bronchiole length. That is, some terminal bronchioles will be longer than the length limit as they will have arisen from the limit on the number of points in a subcollection, and some terminal bronchioles may be far shorter than the length limit. The validity of choosing this length limit is tested in Section 2.4 by generating trees using different values for the length limit.

When a terminal branch arises in the generated conducting airway tree, the grid points assigned to that branch constitute a space that cannot be filled by neighbouring branches. If the terminal branch is of a relatively low generation, then the unfilled volume in the host mesh may be far larger than the size of a single acinus. To enable neighbouring branches to partially fill the space below a terminal branch, the closest branch to the terminal branch is found, and the grid points are reassigned to it. That is, the grid points are placed in the set of points towards which the closest branch generates. A limit is set on the highest generation for which point reassignment occurs (generation 10), and the maximum distance between the terminal branch from which the reassigned points come from and the branch to which they are assigned to (20 mm).

Because of the irregular shape of the host volumes, the centre of mass of a subcollection of grid points could be positioned such that the resulting branch has a large branching angle between itself and its parent branch. In reality, the angle of branching is usually below 60° (Scadding & Cumming 1981b, Thurlbeck & Horsfield 1980, Phalen et al. 1978). Therefore a branch angle limit of 60° is included in the model generation. When a new branch has a branching angle larger than the limit, its angle is reduced to be equal to the angle limit. The branch is altered such that it still lies in the plane defined by its parent branch vector and the line from the end of the parent branch through the centre of mass. The validity of the branch angle limit is investigated in Section 2.4.

As each branch is produced, a check is performed to ensure that the end of the new

(a)   (b)   (c)   (d)
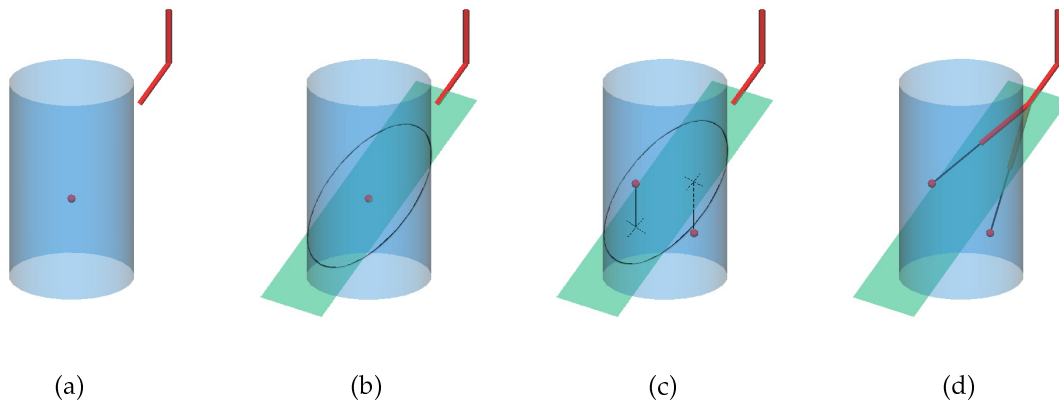
Figure 2.12: *Generation of a three-dimensional tree in a cylinder, using the adapted bifurcating distributive method. (a) Calculation of the centre of mass; (b) Division of uniform points by a splitting plane. The intersection of the plane with the cylinder walls is shown in black; (c) Calculation of centre of mass of subcollections. Black lines are drawn vertically from the centres of mass to the splitting plane; (d) Construction of new branches.*

branch lies inside the host volume. This is done by checking that the end of the new branch lies close enough to one of the grid points to qualify as being inside the host. If the end of the branch is outside of the host volume, then the branch length is reduced until the end is within the host. If this makes the branch shorter than the length limit, then the branch becomes a terminal airway.

2.3.4   The three-dimensional host-filling algorithm

After filling the host volume with a fine uniform grid of points, the algorithm used for generating a volume-filling tree is as follows (illustrated in a simple cylinder in Figure 2.12):

1. The centre of mass of the points contained by a single host lobe is found by averaging the individual coordinate positions (see Figure 2.12(a));

2. The vector in the direction of the corresponding lobar bronchus and the coordinates of the centre of mass are used to define a splitting plane. The splitting plane is extended to the host boundaries, and points on either side of the plane are assigned into two subcollections of points (see Figure 2.12(b));

3. The centre of mass of each subcollection of points is calculated (see Figure 2.12(c));

4. An imaginary line is constructed from the end of the lobar bronchus to each centre of mass (see Figure 2.12(d));

5. For each subcollection of points a branch is generated from the end of the lobar bronchus, lying on the imaginary line, and extending a defined fractional distance (the 'branching fraction') towards the centre of mass (see Figure 2.12(d));

6. The angle between the projection of the parent branch and the new generated branch is calculated. This is the 'branch angle'. If the branch angle is greater than an angle limit then the angle is set equal to the limit, such that the resulting branch continues to lie in the plane of its parent branch and the imaginary dividing line;

7. The length of the branch is calculated. If the length is less than or equal to a length limit, then the branch is a terminal airway;

8. The position of the branch end is checked to make sure it is inside the host space. If the branch end is outside the host space, then its length is reduced until the end point lies within the host;

9. The number of grid points in the subcollection is compared with the point number limit. If the number of points is smaller than the limit, then the branch is a terminal airway;

10. When all branching is completed for a single generation, grid points from terminal branches (up to a generation limit) are reassigned to the closest neighbouring branches;

11. The process continues until all pathways are terminated by a terminal airway.

2.3.5 Diameter of airways

Diameters can be assigned to the branches in the asymmetric conducting airway model (ACA) on the basis of generation, order, the relationship between branch length and diameter, or based on a more complex relationship.

Branches in a given generation may belong to a range of orders, so that their lengths, structure, and distance from the respiratory airways may vary considerably. This means that it would be inappropriate to assign branches in the same generation with the same mean diameter; it would be more appropriate to assign diameters on the basis of order.

Using the average ratio of branch length to diameter observed by Weibel (1963) and Phalen et al. (1978) to calculate the branch diameters would ensure that branch length and diameter were proportional. However, this would mean that a daughter branch that is longer than its parent branch would also have a larger diameter. Investigation of experimental data has shown that small diameters do not imply small lengths, and vice versa (Krause, Bandt, Schulz & Sculz 1995), so constraining the length and diameter to have a defined ratio may not be appropriate.

Kitaoka et al. (1999) defined a relationship between the parent and daughter diameters such that $d_0{}^n = d_1{}^n + d_2{}^n$ where d_0 was the parent diameter, and d_1 and d_2 were the daughter diameters. However, Krause et al. (1995) concluded that n was not a reliable parameter to describe the geometrical structure of the lung. This was based on the observation that n was strongly affected by random perturbations, such as small rounding errors in segment measurements.

Based on the above considerations, the method used for assigning diameters to the ACA model branches is iterative:

1. A pair of random diameters are generated for a daughter set of branches based on the mean value for their Horsfield order from Scadding & Cumming (1981*b*);

2. the daughter diameters are checked to ensure that they are not larger than the parent diameter, and if they are then they are regenerated;

2.3.6   Computational mesh

The ACA model is generated as a finite element mesh. Each branch is initially a single finite element, and each branch junction a node (Zienkiewicz & Taylor 1994).

As the ACA model is generated, the new branches are added as elements to the computational mesh. This is done by recording the element that they are attached to

(their parent), their generation number, and their spatial position. The node number at the start and end of each new element is also recorded. A connectivity matrix is calculated to record all of the elements that a branch is attached to, and in which element direction this attachment lies. This includes the parent and daughter branches. The connectivity matrix is then used to calculate the Horsfield and Strahler orders for the entire tree from the terminal generations up.

Once the Horsfield orders have been calculated, the diameters are assigned. For each branch the diameter, length, generation, and Horsfield and Strahler orders are recorded in a property matrix.

2.4 Results from the conducting airway model

2.4.1 Parameter estimation

The variable length limit, maximum angle limit, and branching fraction affect the branch angles, numbers of branches in each order, and the average generation for the terminal branches in the generated trees. The effects of these parameters were investigated by generating trees into the right middle lobe (the lobe with smallest volume) while aiming for 1) a mean terminal generation close to 15; 2) generation of around 3,000 terminal branches; and 3) maintaining an average branch angle close to the theoretical 'ideal' of 37°28′ (Horsfield & Cumming 1967).

The first condition was based on the observation of Phalen et al. (1978) that the mean terminal generation in the right middle lobe was 15.

The second condition was based on the estimation of the number of terminal branches in the human lungs by Haefeli-Bleuer & Weibel (1988), of 26,000-32,000. The middle of this range is 29,000 acini. Multiplying this value by the percentage volume of the right middle lobe (10.35%) suggests approximately 3,000 acini.

The third condition was used in the absence of detailed information about conducting airway branch angles.

Table 2.3, Table 2.5, and Table 2.4 summarise the trees generated using different values for the length limit, maximum angle limit, and branching fraction, respectively.

2.4.1.1 Sensitivity to transitional bronchiole length limit

The transitional bronchiole is of the order of 1.0-1.5 mm (Haefeli-Bleuer & Weibel 1988, Weibel 1963), therefore a length limit of 1.2 mm was adopted for the conducting airway model generation. The sensitivity of model parameters to the length limit were investigated over the range from 1.0 to 1.4 mm.

The number of terminal branches, mean terminal generation, and mean branch angle are listed in Table 2.3 for the range of tested length limits. Increasing the length limit generally increased the number of terminal branches, increased the mean terminal generation, and increased the mean branch angle. For length limits greater than 1.2 mm the mean branch angle departed from the 'ideal' branch angle. The mean terminal generation and number of terminal branches were not very sensitive to the length limit. To maintain a number of terminal branches greater than 3,000, the length limit must be 1.2 mm or longer. The effect of the transitional bronchiole length limit on the number of terminal branches, mean terminal branch generation, and mean angle indicates that a length limit of 1.2 mm is an appropriate value.

length limit (mm)	#TB	TBgen	mean angle (°)
1.00	2,968	15.86	37.08
1.10	2,991	15.99	37.45
1.15	2,992	16.06	37.54
1.18	2,992	16.08	37.61
1.20	3,022	16.15	37.79
1.22	3,035	16.19	38.02
1.25	3,018	16.19	38.16
1.30	3,065	16.39	38.78
1.40	3,118	15.69	39.61

Table 2.3: *Effect of changing the length limit on generation into the right middle lobe. Angle limit = 60°, branching fraction = 0.4. #TB: number of terminal branches, TBgen: mean terminal branch generation.*

2.4.1.2 Sensitivity to branching fraction

The branching fraction is the proportion of the line from the end of the previous branch to the centre of mass, that forms a new branch in the conducting airway mesh. Sensitivity of the resulting number of terminal branches, mean terminal branch generation, and mean branch angle, were investigated for branching fractions ranging

from 0.30 to 0.50. The results are listed in Table 2.4.

Decreasing the branching fraction generally increased the number of terminal branches and the average terminal generation, and decreased the average branch angle. With a branching fraction of 0.4 the average branch angle was close to the theoretical ideal angle of $37°28'$ (Horsfield & Cumming 1967), the number of terminal branches was in the target range, and the average terminal generation was close to 16. A branching fraction of 0.4 was therefore adopted for all further tree generation.

Fraction	#TB	TBgen	mean angle (^{o})
0.30	3,102	16.58	29.55
0.35	3,104	16.49	34.47
0.37	3,074	16.27	36.17
0.39	2,987	16.11	37.24
0.40	3,022	16.15	37.79
0.41	2,974	16.05	38.41
0.43	2,964	16.01	39.76
0.45	2,984	15.98	44.22
0.50	2,943	15.87	44.22

Table 2.4: *Effect of changing the branching fraction on generation into the right middle lobe. Length limit = 1.2 mm, maximum branch angle = 60°. #TB: number of terminal branches, TBgen: mean terminal branch generation, mean angle: mean branch angle for the generated branches.*

2.4.1.3 Sensitivity to branch angle limit

A limit was imposed on the maximum size of the branching angle between a parent and daughter branch, to prevent unrealistically large branch angles. Sensitivity of the number of terminal branches, mean terminal branch generation, and mean branch angle were investigated over a branch angle range from 30° to 180°.

In Table 2.5 it can be seen that the parameter most affected by the maximum branch angle limit was the mean branch angle. The mean terminal generation and the number of terminal branches did not display consistent trends with, or significant sensitivity to, the branch angle limit. The mean branch angle increased with increasing branch angle limit, with the most change seen for smaller branch angle limits. The mean branch angle was closest to the 'ideal' angle for a limit of 60°, therefore this angle limit was adopted for subsequent tree generation.

angle limit (°)	#TB	TBgen	mean angle (°)
30.0	2,997	16.43	26.80
40.0	3,007	16.14	31.98
50.0	2,976	16.01	35.22
60.0	3,022	16.15	37.79
70.0	2,983	16.11	39.63
80.0	2,977	16.10	40.60
90.0	2,963	16.05	41.22
180.0	2,964	16.07	42.97

Table 2.5: *Effect of changing the maximum angle limit on generation into the right middle lobe. Length limit = 1.2 mm, branching fraction = 0.4. #TB: number of terminal branches, TBgen: mean terminal branch generation.*

2.4.1.4   Sensitivity to grid point number limit

The sensitivity of the generated tree to the calculation of the minimum number of grid points in a subset was investigated. Table 2.6 shows the effect on the generated tree of changing the grid point limit. The mean branch angle and mean terminal generation were not sensitive to changes in the grid point limit. The number of terminal branches was sensitive to this parameter. However, using the method described in Section 2.3 to generate the tree (0.0% change in GPL) produced a total number of terminal branches close to the target value. The method described in Section 2.3 was therefore used for all further conducting airway model generation.

% variation in GPL	#TB	TBgen	mean angle (°)
-22.2	3,526	16.45	37.70
-11.1	3,217	16.26	37.79
-4.44	3,084	16.18	37.81
0.0	3,022	16.15	37.79
4.44	2,939	16.10	37.82
11.1	2,810	16.03	37.91
22.2	2,617	15.94	38.36

Table 2.6: *Effect of changing the grid point limit (GPL) on generation into the right middle lobe. Length limit = 1.2 mm, angle limit = 60°, branching fraction = 0.4. #TB: number of terminal branches, TBgen: mean terminal branch generation, mean angle: mean branch angle for the generated branches.*

2.4.2 Full conducting airway model

A tree was generated in each of the five host volumes using a length limit of 1.2 mm, angle limit of 60°, and a branching fraction of 0.4. The five trees were then combined to produce a full conducting airway model. Generation of the model is illustrated in Figure 2.13, and the full model is shown in Figure 2.14. Generation of the full conducting airway model took approximately one hour of computing time on a Silicon Graphics Origin 2000 computer using a single processor (250 MHz).

Table 2.7 shows the average number of generations from the trachea to the transitional bronchioles for the generated model and comparison studies. Weibel (1963) estimated an average of 16 generations from the trachea to the terminal bronchiole whereas Horsfield & Cumming (1968) estimated an average of 14.6 generations from the trachea to the lobular branches. Assuming that there are two or three further generations with symmetric branching, this gives an average of 16.6-17.6 generations to the terminal bronchioles. Phalen et al. (1978) gave the average number of generations from the trachea to the terminal branches for each lobe. Kitaoka et al. (1999) gave an average for their whole model of 17.6. The average values from the generated ACA model are around 16, which is similar to the comparison studies, except for the right lower lobe which has an average of 17.42 generations. This is higher than the Weibel (1963) study, but closer to the Horsfield & Cumming (1968) and Phalen et al. (1978) studies. It must also be noted that the definition of a terminal bronchiole as used by Weibel (1963) and Phalen et al. (1978) is slightly different to the transitional bronchiole defined by Haefeli-Bleuer & Weibel (1988) that is used in the ACA model as the terminal generation.

Lobe	Weibel	Horsfield	Phalen	Generated
RUL	16	17.6	15	16.37
RML	16	17.6	15	16.15
RLL	16	17.6	17	17.42
LUL	16	17.6	15	16.34
LLL	16	17.6	16	16.16

Table 2.7: *Mean number of generations from the trachea to the terminal bronchioles for each of the five lobes from Weibel (1963), Horsfield & Cumming (1968), Phalen et al. (1978), and the generated model.*

(a) Central airways   (b) to Generation 4   (c) to Generation 5

(d) to Generation 7   (e) to Generation 9   (f) to Generation 11

(g) to Generation 14   (h) to Generation 18   (i) to Generation 27
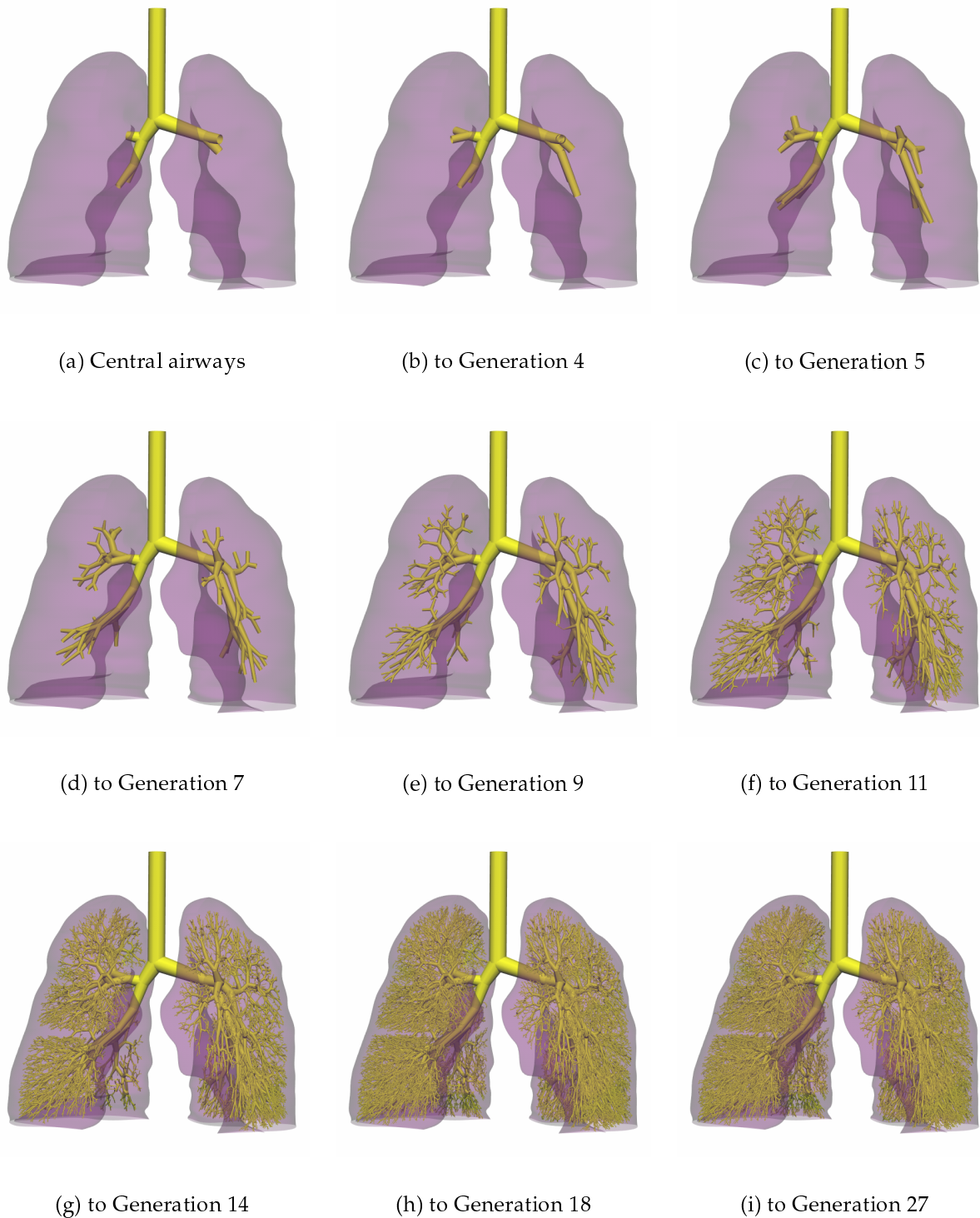
Figure 2.13: *The conducting airway model, by generation. (a) Pre-defined central airways and host boundary, (b) first generated branches from the right upper, left upper, and left lower bronchi, (c) branches to generation 5 (second generation from the right upper, left upper, and left lower bronchi, and first from the right middle and right lower bronchi), (d) to generation 7, (e) to generation 9, (f) to generation 11, (g) to generation 14, (h) to generation 18, (i) all conducting branches (to generation 27).*
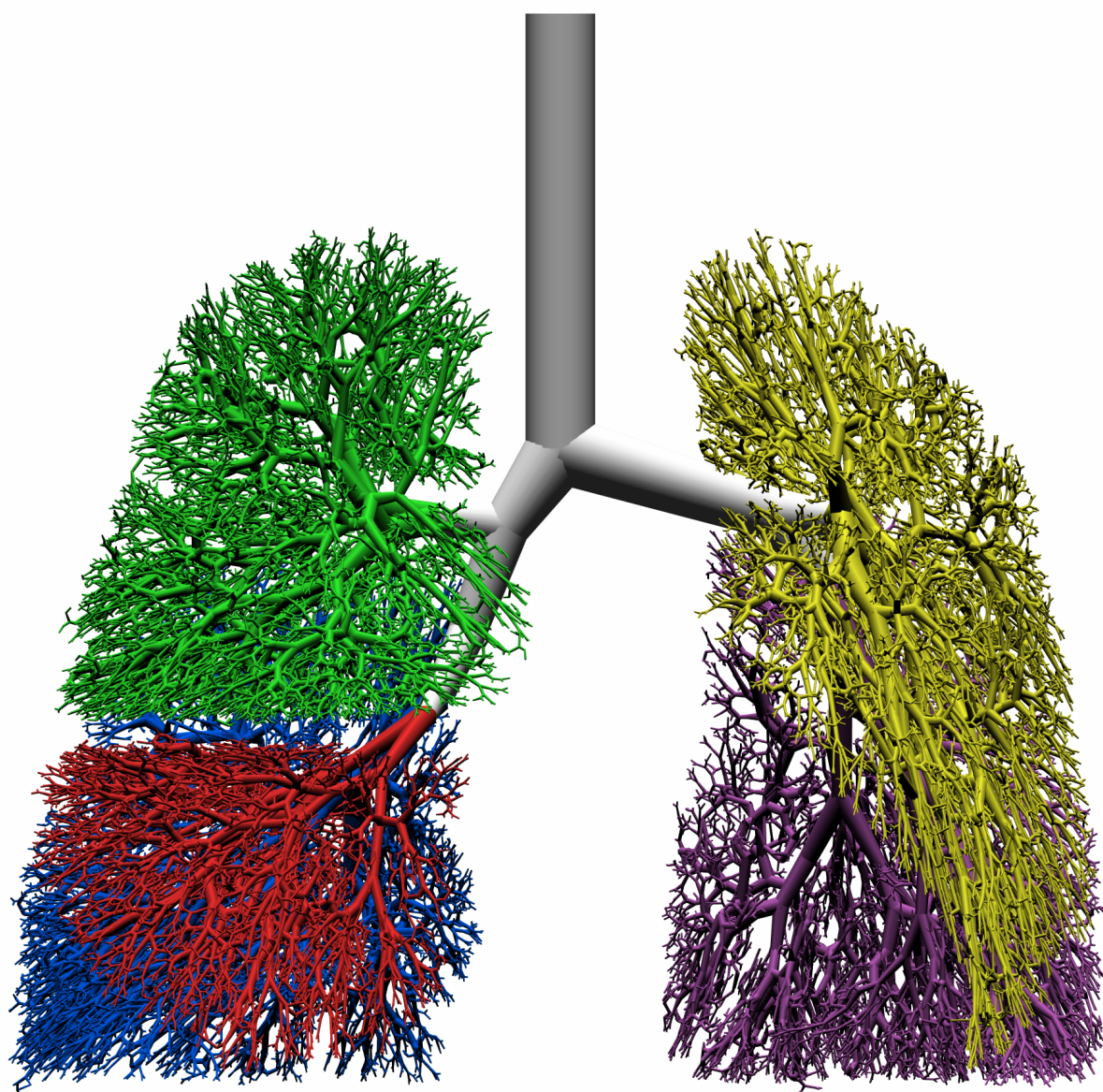
Figure 2.14: *Generated asymmetric conducting airway model, viewed from the front. Green = RUL, red = RML, blue = RLL, yellow = LUL, purple = LLL.*

The shortest path length from the carina (the first division of the trachea) to a lobular branch measured by Horsfield & Cumming (1968) was 75 mm, and the longest was 215 mm. The shortest path from the carina to the end of the terminal bronchiole in the generated model was 102 mm and the longest 239 mm. The path lengths are therefore slightly longer in the generated model, which is partly accounted for by the extra few generations from the lobular branch to the transitional bronchiole in the generated tree. The range of bifurcations to reach a terminal branch in the ACA model is 10 to 26, compared with 8 to 25 from Horsfield & Cumming (1968), 11 to 28 in the delta model, and 8 to 32 in the diameter-flow model.

The number of terminal bronchioles in the generated model is 29,445. Weibel (1963) estimated 65,536 terminal bronchioles, whereas Horsfield & Cumming (1968) estimated 27,992. The more recent study of the respiratory airways by Haefeli-Bleuer & Weibel (1988) estimated the number of terminal bronchioles to be in the range of 26,000 to 32,000. The generated model therefore lies in the middle of this range.

For the Horsfield delta model, a fixed delta of 3 was prescribed for the airways from the lobar bronchi to order 7 (assuming that the terminal bronchioles are order 1). The Horsfield orders and delta values were calculated for the ACA model. Figure 2.15(a) shows the number of branches in a Horsfield order (N_w) divided by the number of branches in the previous order (N_{w-1}) for the generated orders (not for the orders where the numbers of branches were pre-defined). For the delta model this is usually 1.38. For the ACA model, the curve varies around 1.38 in orders 6 to 20. For orders 1 to 5, the branching pattern becomes more symmetric, and this is reflected in the rise of N_w/N_{w-1} for both models. As can be seen in Figure 2.15(b), the mean delta value from the ACA model is similar to that of the Horsfield delta model.

Figure 2.15(c) plots log(number of branches) against Horsfield order for the generated and delta models. The curves are similar for the two models, as are the slopes. The slope of the plot of log(number of branches) against order is the 'branching ratio', R_b. For the generated model R_b is 1.387, compared with 1.38 for the delta model.

The length ratio (R_l) and the diameter ratio (R_d) are calculated from the slopes of log(length) against order and log(diameter) against order, respectively. R_l and R_d were calculated for the generated model from the curves in Figure 2.15(d) and Figure 2.15(e). Their values are 1.114 for R_l and 1.109 for R_d. The branching, length, and diameter
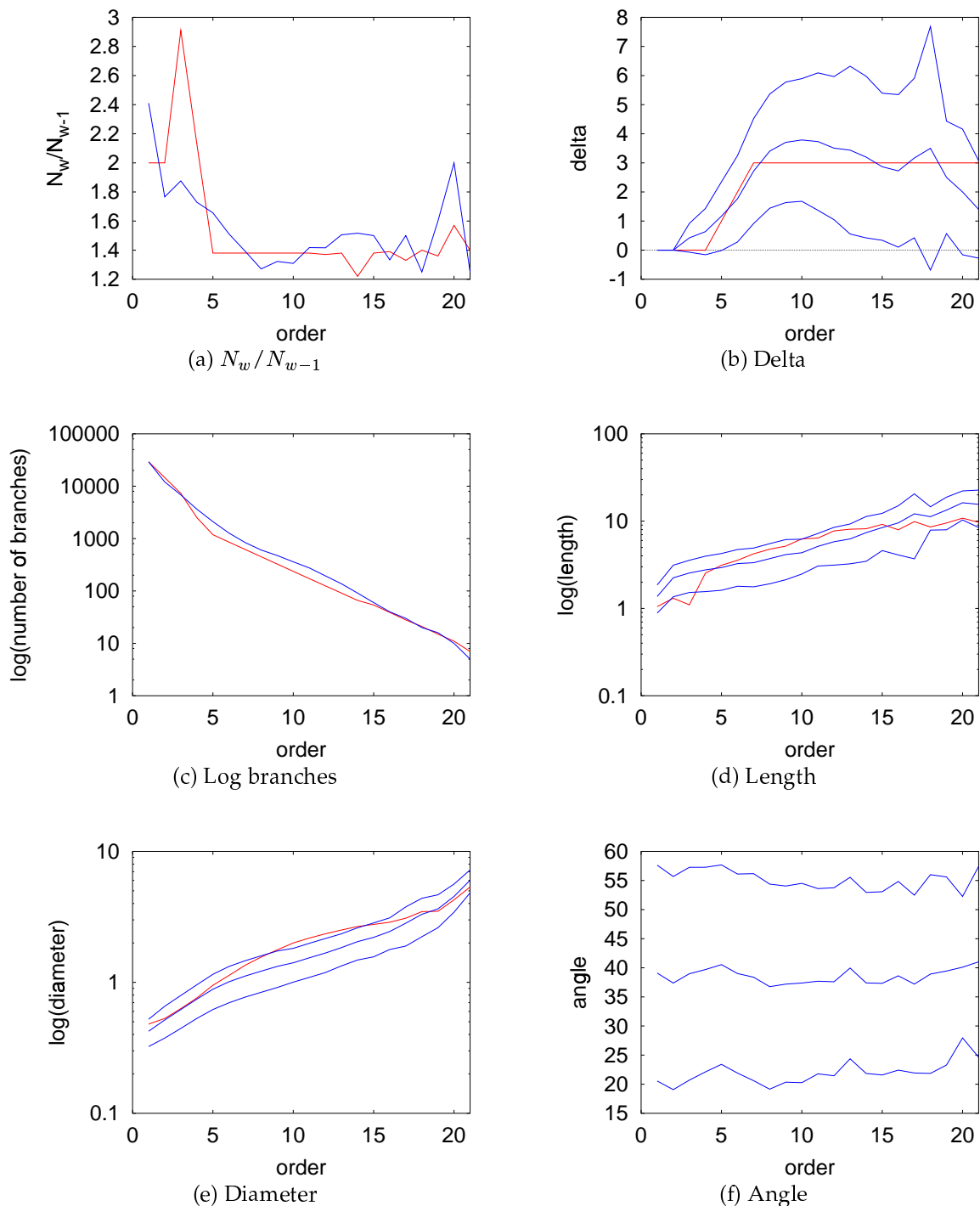
Figure 2.15: *Statistics from the generated ACA model (blue) compared with the Horsfield Delta model, and data from Horsfield and Cumming 1968 (red). (a) Number of branches in an order divided by the number of branches in the next lowest order, compared with Delta model; (b) Mean ± SD for difference in order of daughter branches, compared with Delta model; (c) Log of the number of branches in a Horsfield order against order, compared with Delta model; (d) Log of mean branch length (± SD) against Horsfield order, compared with Horsfield and Cumming 1968; (e) Log of mean branch diameter (± SD) against Horsfield order, compared with Horsfield and Cumming 1968; (f) Mean ± SD for branch angle against order.*

ratios can also be calculated using Strahler ordering. Table 2.8 compares branching, length, and diameter ratios calculated from Strahler ordering in the generated model, from Horsfield, Relea & Cumming (1976), and from Phalen et al. (1978).

Ratio	Horsfield	Phalen	Generated
R_b	2.805	2.508	2.358
R_d	1.427	1.351	1.323
R_l	1.402	1.333	1.344

Table 2.8: *Branching ratios calculated using Strahler ordering from Horsfield et al. (1976), Phalen et al. (1978), and the generated asymmetric conducting airway model.*

The branching angles in the generated model are plotted in Figure 2.15(f). The mean angle is fairly constant around 37° for orders 1 to 22, comprising the sublobar bronchi and bronchioles. Branch angles have been observed to increase towards the periphery of the lung (Horsfield & Cumming 1968, Phalen et al. 1978), but the angles from the generated model do not display this trend. The possibility that varying the branching fraction from the lowest to highest generations could affect the distribution of branch angles was tested in the right middle lobe. That is, the minimum (for lowest order) and maximum (for highest order) branching fractions were specified, and the branching fraction used for a particular branch was a linear interpolation between the maximum and minimum values, based on the new branch generation. Using this approach did not cause significant or consistent changes in the branch angles.

Table 2.9 compares the proportion of terminal branches in each lobe for the generated model with the lobar volumes given by Horsfield & Cumming (1968) for the delta model and for the lung.

Lobe	Horsfield	Delta	Host	Generated
R U L	21	19	23.1	22.8
R M L	9	10	10.4	10.2
R L L	25	26	22.5	22.5
L U L	20	19	23.3	23.7
L L L	25	26	20.8	20.8

Table 2.9: *Percentage volumes of lobes from Horsfield & Cumming (1968), the delta model, the host mesh, and the branches in the generated model.*

The mean ratio of daughter diameter to parent diameter in the ACA model was 0.763, with 0.62% of the diameter ratios greater than one. The mean ratio of daughter length to parent length was 0.893, with 11.9% of the length ratios greater than one. The mean ratio of smallest to largest daughter diameter was 0.814, and the mean ratio of shortest to longest daughter branch length was 0.649. The ratios were evaluated for branches with parent diameters greater than 0.8 mm. This restricts the calculation to bifurcations where less than 10% of the intact branches were observed to be terminal, so avoiding bias that might be introduced by having excluded the most asymmetrical bifurcations in the experimental study (Phillips & Kaye 1997).

The volume of the generated ACA model (the anatomical dead space) from the top of the trachea to the end of the transitional bronchioles is 103.47 ml.

The assumption that the bifurcating-distributive algorithm in three dimensions approximates a volume-splitting algorithm was verified by checking the numbers of grid points in the subspaces at each space division. This check confirmed that the number of points (and therefore the approximate volume) were usually close to evenly divided between the subspaces. Less even divisions arose close to the concave host boundaries, or for subspaces with points reassigned from another subspace.

2.5 Discussion

The purpose of this chapter was to develop an algorithm capable of generating a lung-like tree in a three-dimensional host volume, such that the resulting model tree compares well with morphometric data. The generated tree requires structural characteristics similar to those of the real conducting airways, so that it can be reliably used as a computational mesh for simulating problems such as transport phenomena.

The host space into which the generated model was produced is an anatomically realistic description of the lung surfaces, taken from MRI data and anatomical slices. The resulting model is space-filling into this host, in contrast to the symmetric model of Weibel and the Horsfield delta model which do not specify spatial positioning of branches. The diameter-flow model of Kitaoka et al. (1999) is also space-filling, but it was first generated into an idealised geometry. When Kitaoka et al. (1999) used more

accurate descriptions of host geometry, the number of terminating branches increased because they projected outside the host space. This indicates that the generation algorithm will be more reliable than the diameter-flow algorithm for generating conducting airway models in even more irregularly shaped cavities.

The generation algorithm produces a strictly bifurcating tree; that is, there are no divisions into three or more branches. Trifurcations have been observed in the lung, but on close inspection have usually been found to be two bifurcations connected by a very short branch (Weibel 1963, Horsfield & Cumming 1968, Haefeli-Bleuer & Weibel 1988). The generation algorithm is therefore capable of producing apparent trichotomy, consistent with this observation, when one of the daughter branches is very short (but not shorter than the length limit). Functionally, two bifurcations joined by a short branch behave similarly to a trichotomy.

The parameters used for final model generation (length limit, angle limit, and branching fraction) were chosen based on physiological considerations, and their effect on the resulting tree. A length limit of 1.2 mm was used based on anatomical data: the scaled first respiratory bronchiole length from Haefeli-Bleuer & Weibel (1988) is 1.27 ±0.281 mm, and the transitional bronchiole is assumed to be slightly longer than this. Haefeli-Bleuer & Weibel (1988) defined the acinus as comprising only alveolated branches, hence only the portion of the transitional bronchiole that was alveolated was included in the analysis. Because of this, Haefeli-Bleuer & Weibel (1988) did not present mean lengths for the transitional bronchioles.

By setting the length limit in the generated model to be 1.2 mm, some of the terminal branches will have lengths less than 1.2 mm when they terminate based on the length limit (a generated branch with a length less than or equal to the length limit becomes a terminal branch), and some will be longer because they terminate based on the number of points towards which they branch. The mean transitional bronchiole length in the ACA model is 1.37 ±0.88 mm. The mean is therefore higher than the length limit which indicates that either: 1) more branches terminated because of the number of subtended points than because of their length, or 2) that those branches terminating because of the number of subtended points had long lengths relative to the length limit, and hence had a large influence on the mean. Although the mean transitional bronchiole length is larger than that measured by Haefeli-Bleuer & Weibel (1988) for the first respiratory

bronchiole, it is within one standard deviation of the experimental mean.

The branching fraction of 0.40 was chosen based on its effect on the generation of a tree into the right middle lobe. Increasing the branching fraction generally decreased the number of terminal branches, decreased the average terminal generation, and increased the average branching angle for the entire tree. The reverse trends were observed for decreasing the branching fraction. A value of 0.40 was chosen because it produced an average terminal generation close to 16 (Raabe et al. 1976) and an average branch angle close to the theoretical ideal.

An angle limit of 60° was adopted for model generation. The branching angle limit was based on the observation that the branching angle is usually below this value (Scadding & Cumming 1981*b*, Thurlbeck & Horsfield 1980). Support for including a branching angle limit comes from the observation that acini situated near the hilum of the lung are not supplied directly by branches from the bronchi. They are instead supplied by airway paths consisting of multiple branches angling back through 180° or more to reach them (Horsfield & Cumming 1968). This suggests that airway branching is limited to a range of angles.

Branch angles have been observed, on average, to increase towards the periphery of the lung (Horsfield & Cumming 1968, Phalen et al. 1978). In contrast, the generated model shows fairly constant means and standard deviations for branch angle, and a steadily decreasing minimum angle with order. Although the branching angles in the generated model do not increase towards the periphery, their mean value is close to the theoretical 'ideal' value proposed by Horsfield & Cumming (1967) of $37^o28'$, and the range of angles increases with decreasing order. The branching angles affect flow distribution and resistances. Having angles very different from measured values would induce unrealistic flow distributions when flow was driven by the solution of coupled mechanics and flow equations. Although the generated ACA model does not have increasing branch angle with decreasing order, the mean angle for each generation is close to a theoretical 'ideal' that has been hypothesised to minimise resistance to flow. The minimum angle in the ACA model decreases slightly with order, but the maximum angle is constant at the angle limit. Given that the mean is fairly constant, this indicates that the number of branch angles that are larger than the model mean increases with decreasing order. The branch angle characteristics of the

generated ACA model are therefore similar to the experimental characteristics.

The generation algorithm produces conducting airway branches that are more 'oriented' than in reality. Comparison of Figure 2.13 with Figure 2.7 shows the difference in orientation of the peripheral branches between the model and reality. Introducing a degree of randomness in the algorithm for the more peripheral branches could improve the model's appearance. This could also increase the branching angles for the distal generations.

The fine grid of uniform points in the host volume are split by the plane that contains the parent branch and the centre of mass (the 'splitting plane'). The plane is therefore not constrained to a set angle as in the diameter-flow algorithm, where the splitting plane is generally at 90° to the branching plane of the parent branch. The branching planes in the generated ACA model have an average angle between them of 90.1^o with a standard deviation of 39.0^o. In reality, successive bifurcations often lie in planes at right angles to each other (Horsfield et al. 1976). This arrangement reduces unequal distribution of flow that can be caused by having successive bifurcations arising in the same plane (Snyder, Dantzker & Jaeger 1981).

The volume proportions of the right upper, right middle, and left upper lobes for the host lung are higher than for the lung studied by Horsfield & Cumming (1968). The proportions for the lower lobes are lower, in particular for the left lower lobe. However, the number of terminal branches generated in each lobe is in proportion to the percentage volume of lung. In the absence of evidence suggesting that different lobes have different densities of terminal branches, the approximately equal density of terminal branches generated in the ACA model seems appropriate.

The number of branches in an order, branch length, and branch diameter are generally logarithmic functions of order. From calculations based on minimum flow resistance and minimum entropy production the relationship between R_b, R_d, and R_l has been shown to approximate $R_b^{\frac{1}{3}} = R_d = R_l$ (Horsfield et al. 1976). Values for R_b, R_d, and R_l have been calculated for the generated ACA model using both Horsfield ordering and Strahler ordering. The Horsfield R_b from the ACA and delta models are very close in value, but the Strahler R_b from the ACA model is slightly smaller than values calculated from morphometric studies. The Strahler R_b for the delta model is for branches down to a diameter of 0.7 mm; for branches with smaller

diameter R_b is 2.320 (Scadding & Cumming 1981*b*) therefore R_b from the ACA model (which is for all of the conducting airway branches, regardless of diameter) lies between these measured values. Both the Horsfield and Strahler ratios for branch numbers, length, and diameter in the ACA model exhibit the cube-root relationship. In contrast, the diameter-flow algorithm of Kitaoka et al. (1999) produced a tree with higher asymmetry than the human lungs. Constraining the diameter-flow algorithm to produce a more symmetric tree resulted in more branches terminating because they projected outside the host boundary.

The average terminal generation in the delta model is 17.6, which is an overestimate according to Phalen et al. (1978). This is the same average value obtained using the diameter-flow algorithm. The generated ACA model has average terminal generations within the range observed by the comparison studies of Weibel (1963), Phalen et al. (1978), and Horsfield & Cumming (1968), and a range of bifurcations to the terminal branches similar to Horsfield & Cumming (1968) and the delta model. This is important from a functional point of view, as the number of bifurcations down an airway path has a significant influence on the distribution and behaviour of gas flow.

The delta model prescribes a fixed difference between daughter branch orders from the lobar bronchi down to Horsfield order 6. In contrast, the mean delta values in the ACA model varied between 4 and 2 between the lobar bronchi and order 6 branches. For lower orders, delta decreases rapidly in both models, reflecting more symmetric branching. This is consistent with observation (Horsfield & Cumming 1968).

Although the generation algorithm is used to 'grow' a model into a defined volume, it does not attempt to mimic the actual growth process of a lung; the algorithm is only concerned with simulating a representative adult conducting airway tree. Real 'growth' would require extension of the algorithm to include a deforming host geometry and a more complex set of rules to govern branch splitting.

Krause et al. (1995) defined the 'contraction ratio' as the ratio of daughter to parent branch (either for diameter or length). They calculated the mean contraction ratios as 0.76 ±0.15 (diameter) and 0.94 ±1.37 (length) for the human data from Raabe et al. (1976). 90.6% of diameter contractions were less than 1.0, compared with 71.9% for length contractions. This suggested that diameters decreased more uniformly than lengths. The diameter contraction ratio for the ACA model is slightly larger than the

value calculated from experiment, and the length contraction ratio is smaller than the experimental value. However, the differences between the modelled and experimental values are small, particularly for the diameter ratio. This indicates that, on average, the branch diameters and lengths in the ACA model decrease in a similar fashion to the measured experimental lungs.

The average ratio of smaller to larger daughter branch diameter is 0.814 in the ACA model, compared with 0.86 experimentally (Weibel 1963, Phalen et al. 1978). The average ratios of smallest to largest daughter branch length are also close: 0.649 for the ACA model, and 0.62 experimentally (Phalen et al. 1978).

The ACA model volume of 103.47 ml is smaller than the Weibel volume of 145.1 ml for the conducting airways from the trachea to the terminal bronchioles (generations 1-16), but is very close to the delta model volume of 103.79 ml.

2.5.1 Conclusions

Weibel's symmetric model (Weibel 1963) and Horsfield's delta model (Horsfield et al. 1971) have proved very useful for specific lung function studies, but Weibel's model is limited to cases where asymmetry is not important, and both models are only useful when the spatial distribution of airway paths can be neglected. To thoroughly investigate gas mixing, aerosol deposition, airway mechanics, and water and heat transfers, a more complete model of the conducting airways is required. The diameter-flow algorithm presented by Kitaoka et al. (1999) produces a three-dimensional airway model but the algorithm is relatively complicated, it does not produce a sufficiently realistic airway tree, and it is very sensitive to changes in the assumed host geometry and fundamental model parameters.

The generation algorithm described in this chapter produces a conducting airway model with branching characteristics close to those measured experimentally. The model has branching, length, and diameter ratios consistent with morphometric studies, and the average terminal generation lies within the observed range. The branch angles are consistently close to the ideal angle of 37°28′ proposed by Horsfield & Cumming (1967). The mean branching plane angle is very close to 90°, a value that theoretically minimises flow resistance, and that has frequently been observed

experimentally. The average decrease of length and diameter with distance down the airway tree is consistent with experiment.

The three-dimensional algorithm described in this chapter provides an effective method for generating conducting airway models specific to a given host geometry. This will be useful for 'normal' lungs, but may be of particular use for lungs with different host shapes. It will also be of interest to generate conducting airway models for animals other than humans. The ability to generate realistic animal models will test the adequacy of the algorithm.

Chapter 3

Gas mixing in the respiratory airways

3.1 Introduction

Under normal breathing conditions, the human lungs do not mix inspired and residual gases with perfect efficiency. This 'mixing efficiency' decreases when the lungs are diseased or function is impaired. The inefficiency of the lungs has been investigated over the past 50 years using a variety of mathematical models. These models have proved useful as they have been able to suggest mechanisms contributing to incomplete mixing, without the need for making measurements in the fine airways. The currently held theory is that incomplete mixing is due to inhomogeneous distribution of inspired gas, because of distributed ventilation (non-uniform expansion of the airways) or because of interaction between diffusion and convection at branch points.

The most recent mathematical models of gas mixing in the lungs (Verbanck & Paiva 1990, Scherer et al. 1996, Cruz et al. 1997) have attempted to explain the evolution of a sloping alveolar plateau in phase III of the multiple-breath washout curve (see Section 3.2.4). These three models have focused on different properties to explain incomplete gas mixing. None of the three models can reproduce experimental results entirely satisfactorily.

To date gas mixing models have not incorporated detailed conducting airway asymmetry, although asymmetry in the respiratory airways has been shown to be

important in simulating gas mixing (Paiva & Engel 1984). An asymmetric model of the conducting airways was developed in Chapter 2 as a finite element mesh, where each conducting airway was a single element. If this approach was used to model the combined conducting and respiratory airway system, the resulting model would be too large for currently available computing resources. A new respiratory airway model is required, such that it incorporates the important characteristics of the pulmonary acinus while maintaining a small model 'size'.

This chapter details the development of a general lumped parameter model of a pulmonary acinus. The lumped parameter model is in the form of a regression equation that is used to predict the concentration at the end of expiration at the end of each transitional bronchiole in a conducting airway model. The lumped parameter model is calibrated using gas mixing results from a multi-branching respiratory airway model.

The multi-branching respiratory airway model is based on the anatomical study by Haefeli-Bleuer & Weibel (1988). Each airway in a single respiratory acinus is modelled as a single finite element, and the elements are coupled to form a computational mesh. Gas transport equations (see Section 3.3.1) are solved in the computational mesh using a range of gas pairs, ventilation rates, and model sizes. Information describing the inspiratory characteristics of the breaths are then used to derive the regression equation that forms the basis of the lumped parameter model.

The multi-branching respiratory model is also used to investigate the effect of respiratory airway asymmetry on evolution of the sloping alveolar plateau in phase III of the washout curve.

In the following chapter (Chapter 4) the lumped parameter acinus is coupled with the conducting airway model described in Chapter 2, and the full model is then used to simulate gas mixing.

3.2 Background

3.2.1 Morphology of the respiratory airways

The transitional bronchiole, as defined by Haefeli-Bleuer & Weibel (1988), defines the boundary between the conducting and respiratory zones in the lung. A single transitional bronchiole and all of the respiratory bronchioles, alveolar ducts, alveoli and alveolar sacs distal to it comprises a basic unit of gas-exchange called a pulmonary acinus. There are an estimated 26,000-32,000 acini in the human lungs (Haefeli-Bleuer & Weibel 1988). The acinus is the largest lung unit in which all airways participate, to some degree, in O_2/CO_2 gas exchange.

The structure of the acinus is highly asymmetric, in both branch dimensions and branching pattern. The acini arise at a range of distances down the conducting airway tree, and take the shape of the space created by surrounding structures. Weibel (1963) observed strict dichotomy of branching in the airway tree. In contrast, Hansen & Ampaya (1975) observed trichotomy and occasionally higher order divisions. Haefeli-Bleuer & Weibel (1988) observed apparent trichotomy which they explained as two bifurcations joined by a very short branch. The existence or not of higher order divisions is a matter of definition on the part of the researcher: in a functional sense a trichotomy will perform in the same way as two bifurcations joined by a very short branch.
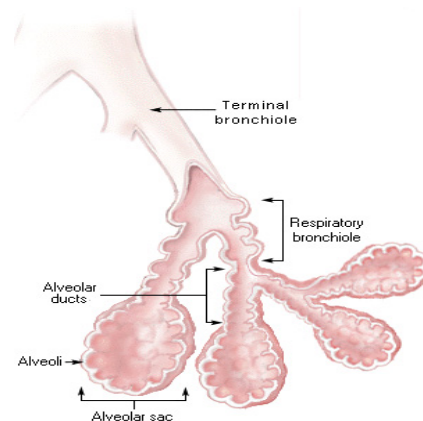
Figure 3.1: *The different types of airways in the pulmonary acinus. Image courtesy of gsm.com (http://www.gsm.com) (c)1993-2000 Gold Standard Multimedia Inc. and its licensors.*

The structural support for the respiratory airways comes from the connective tissue framework of the lung. In addition, the walls of the respiratory bronchioles and alveolar ducts contain a small amount of smooth muscle. Figure 3.1 shows the different airways in the acinus.

The transitional bronchiole is the last branch down an airway path to have a distinctly conductive component. That is, the initial portion of the transitional

bronchiole is not alveolated, whereas the last portion is (Haefeli-Bleuer & Weibel 1988). Distal to the transitional bronchiole are typically three generations of respiratory bronchioles whose walls contain a few alveoli and/or alveolar sacs. Respiratory bronchioles are mainly conductive, but a small amount of gas exchange can take place due to the presence of the few alveoli and alveolar sacs.

Alveolar ducts arise from the last generation of respiratory bronchioles. The ducts are air-spaces rather than branches: their 'walls' are defined as the mesh of entrances to other airways. The network of orifices comprising the alveolar duct boundary can be likened to a roll of chicken wire, where the large holes are the entrances to alveolar ducts, sacs, and alveoli.

Figure 3.2 illustrates the cellular structure of the alveoli. The principal cell type in the alveoli is the Type I cell (broad pavement) which comprises about 95% of the alveolar epithelial surface area. The Type II cells (corner cells) are more active than the Type I cells: they manufacture the phospholipid mixture that forms part of the alveolar surfactant.
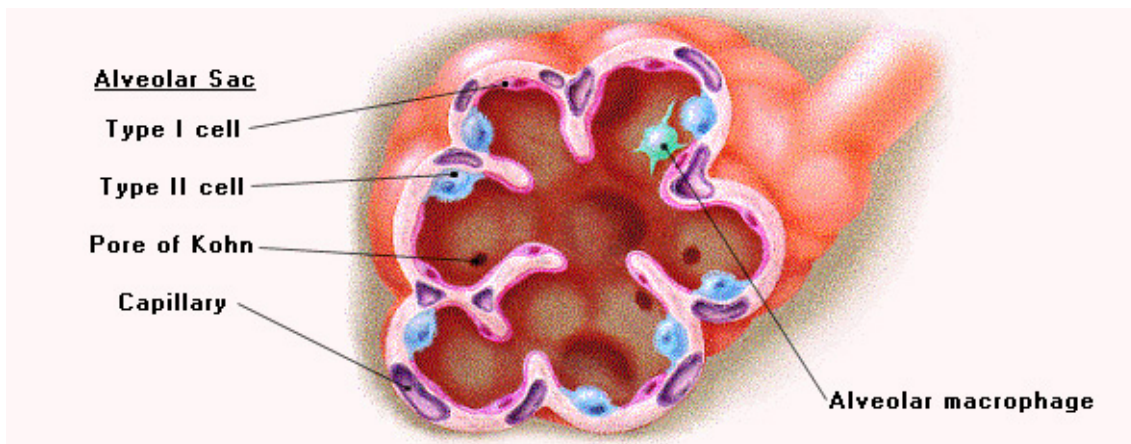
Figure 3.2: *The structure of a single alveolar sac, showing: Type I cell (broad pavement), Type II cell (corner cell), pores of Kohn, capillary wall of alveolus. Image courtesy of gsm.com (http://www.gsm.com) (c)1993-2000 Gold Standard Multimedia Inc. and its licensors.*

Alveolar sacs are air-spaces with alveoli as their only outlets; the alveoli are the site of gas exchange with the bloodstream. An alveolus is a cup-like terminal airspace of about $\frac{1}{4}$ mm in diameter. There are an estimated 300 million alveoli in the adult human lungs (Weibel 1984). The alveolar walls consist of a capillary membrane with air on

one side and blood from the pulmonary circulation on the other. The partial pressure gradient across the membrane is the driving force for gas exchange between alveolar gas and the blood in the pulmonary circulation.

Surface tension arises at any interface between gas and liquid. The alveoli are therefore subjected to large amounts of surface tension which endangers their stability. To counteract surface tension, the capillary network in the alveolar walls is interlaced with a network of fibres. In addition, the surfactant that lines the alveolar walls has a very low surface tension due to the presence of a phospholipid coat. The surface tension of the surfactant varies with surface area expansion and contraction, contributing to the dynamic mechanical behaviour of the lungs (Weibel 1984).

Alveolar pores of Kohn are openings between adjacent alveoli that are normally covered by surfactant. Pores of Kohn increase in number and size with age and certain diseases, but are absent in newborns. They provide an avenue for limited gas transfer between alveoli.

3.2.2 Experimental study of the respiratory airways

Haefeli-Bleuer & Weibel (1988) made a detailed study of the respiratory airways in the human lungs from silicone-rubber casts.

Silicone-rubber casts of two right upper lobes were made from isolated formaldehyde-fixed lungs from two different cadavers. Samples of acini were dissected from the conducting airways in each cast. 103 acini were sampled from one cast, and 106 from the other. The acinar volumes were calculated, the acini were ordered by volume, and then they were divided into six groups. One acinus was randomly sampled from each group for further analysis.

Dissection of the acini from the conducting airways required a precise definition of the boundary between the conducting and respiratory airways. One common definition of the acinus is that it is the complex of branches distal to and including the terminal bronchiole, which is the last non-respiratory airway. An equally common definition is that all of the airways in the acinus take part in gas exchange. Noticing the discrepancy between these two definitions, Haefeli-Bleuer and Weibel decided to define the 'transitional bronchiole' as the first bronchiole to have any alveolisation - the

initial part of the transitional bronchiole is often purely conductive. An acinus was then defined as arising from and including the portion of alveolised transitional bronchiole. It was found to be easier to identify transitional bronchioles by this definition than to identify terminal bronchioles as being the last non-alveolated conducting airway. This is because a conducting airway may bifurcate into a respiratory branch and a non-respiratory conducting airway. The daughter conducting airway may give rise to a further few generations of non-respiratory airways before an alveolated airway is reached. Defining the terminal bronchiole in that situation is difficult, but defining the transitional bronchiole is relatively easy.

Because the entire lung was not able to be cast, an accurate prediction of the degree of cast inflation was not possible. However, it was estimated that the airways were inflated to nearly total lung capacity. The volumes of the individual acini from each inflated cast varied from 50 mm^3 to 450 mm^3, with an average of 187 mm^3. That is, the range of sizes covered nearly an order of magnitude.

Dimensions of the inner and outer diameter and segment lengths were measured on the sampled acini. The inner diameter and length were found to decrease with progressive generations, but the outer diameter remained fairly constant. This is due to the observed increase in size and number of alveoli in the acinar periphery. Very little variation was observed in mean dimensions per generation for different acini, with no apparent dependence of segment size on overall acinus size. Most branch paths were found to terminate at the 9th generation with a mean of 9.1 generations and a range over generations 6 to 12. Because the cast was very close to total lung capacity, the branch length and outer diameter were probably close to maximal. However, the inner diameter was not necessarily maximal. In air-filled lungs the inner diameter has been shown to depend strongly on surface tension acting on the free edge of the alveolar septa. This keeps the ducts wider than they appear in fluid-filled lungs. An estimate from comparison with histological preparations puts the true inner duct diameters at 20-30% larger in air-filled lungs in vivo than in the silicone-filled casts. The alveolar 'sleeve' would be expected to be smaller as a consequence.

Haefeli-Bleuer and Weibel assumed a total acinar air volume at total lung capacity of 5-6 litres and a mean acinar volume of 187 mm^3. This gave an estimate of the number of acini of 26,000-32,000.

3.2.3 Transport of gases inside the lungs

Respiration can be divided into three stages: 1) external respiration which involves the delivery of atmospheric O_2 to the alveoli and the excretion of tissue-produced CO_2; 2) intermediate respiration, which is the vascular transport and hemoglobin transport of O_2 and CO_2 between the lung and tissue cells of the body, and; 3) internal respiration which involves the use of O_2 and the production of CO_2 by the tissues.

3.2.3.1 Ventilation and gas transport

A significant part of external respiration in the human lungs is the movement of gases between the mouth and alveolar surfaces, a process called ventilation. Unlike the sino-atrial node of the heart, the respiratory muscles are not inherently rhythmic. Instead, ventilation is controlled by a specialised feedback system to the brain that ensures a nearly constant level of CO_2 in the lungs and blood.

Contraction of the intercostal muscles of the rib cage and the diaphragm causes the ribs to rise and the diaphragm to move downwards. This enlarges the thoracic cavity, thereby lowering the pressure in the alveoli. A pressure gradient is therefore established between the mouth and the alveoli, and air flows into the lungs. For a normal inspiration, a pressure difference of about -3 mmHg is established. During inspiration, potential energy is stored in the lung's elastic fibres as they are stretched. At the end of inspiration, the stored energy is available to passively retract the system to its original length. Therefore, during normal expiration a positive pressure difference of about 3 mmHg is established along the airways.

Advective flow established by the pressure gradient between the mouth and the alveolar surfaces distributes inspired gas through the system of branching conducting airways, with molecular diffusion working in parallel in response to concentration gradients. Division of flow at branch points slows the forward rate of transport by advection, until in the peripheral branches the main method of transport is by molecular diffusion. Molecular diffusion is a major component of transport in the last 5 mm or so of airways, corresponding mainly to the respiratory zone.

A measure of the relative importance of advection and diffusion is the dimensionless Peclet number, $Pe = u\frac{d}{D}$, where u is mean velocity, d is diameter, and

D is a diffusion coefficient. The Reynolds number, $Re = \frac{ud}{\mu/\rho}$, where μ is the dynamic viscosity of the fluid and ρ is the fluid density, generally indicates whether flow is turbulent or laminar. In the conducting airways with a typical flow of $0.5 \text{ L} \cdot \text{s}^{-1}$, Re is about 2,350 and Pe is between about 530 - 3,800 (for diffusion coefficients of 10.5 - 74.3 $\text{mm}^2 \cdot \text{s}^{-1}$). In the transitional bronchiole Re is about 3.5 and Pe is between 0.8 - 5.6. The Re in the trachea suggests that flow in this region could be transitional between turbulent and laminar - it may or may not be turbulent. However, the cartilaginous ridges on the trachea and airway bifurcations induce turbulent flow even when the Re indicates otherwise. In the respiratory region the flow is laminar. The Pe numbers indicate that advective transport is significant in the tracheal region, whereas in the region of the transitional bronchiole molecular diffusion has become far more significant.

3.2.3.2   Lung volumes

The capacities of the lung are usually classified using a set of conventional definitions. The largest volume of air that the lungs can contain - at maximal inspiration - is the total lung capacity (TLC); the smallest volume of air that the lungs contain, after a maximal forced expiration, is the residual volume (RV). The difference between TLC and RV is the vital capacity (VC). VC is the largest volume of air that can be inspired or expired from the lungs. The tidal volume (V_T) is the volume of air moved into or out of the lungs in a breath. The volume of air contained in the lungs at the end of a relaxed tidal exhalation is the functional residual capacity (FRC). The volume that can be inhaled from FRC is the inspiratory capacity (IC).

3.2.3.3   Non-uniform distribution of flow

If the lung expanded uniformly and synchronously all over, then flow down an airway would be proportional to the volume of lung below the branch. However, the distribution of flow to different regions in the lungs has been shown to be uneven (Milic-Emili et al. 1966, Anthonisen et al. 1970), and this has been attributed to the pleural pressure gradient and deformation of the lung by its own weight.

The pleural pressure gradient causes differences in regional compliance by

modifying the distribution of alveolar stresses in a topologically consistent fashion (Milic-Emili et al. 1966). Because the pleural pressure gradient is only present *in vivo*, it would be expected that the vertical gradient of ventilation would not be observed in excised lungs or in lobes that are exposed to a uniform surface pressure. However, studies of isolated lungs and lobes have shown regional non-uniformities in ventilation which are magnified in the presence of a simulated pleural pressure gradient (Warner, Hyatt & Rehder 1988).

Because the total pressure-volume curve of the lungs is sigmoidal, the upper part of the lung may expand to a different degree than the lower part for a given change in transpulmonary pressure. Ventilation would therefore be distributed unequally to upper and lower regions. Non-uniform distribution between lobes could be due to different pressure-volume curves for the lobes as has been demonstrated in the dog lung (Anthonisen et al. 1970), but this does not explain non-uniformities within a lobe.

It has been shown that deformation of the lung by its own weight is non-uniform, and this must cause a non-uniform distribution of regional volumes and ventilation. The particular distribution depends on lobar shape, means of support, and the mechanical properties of the parenchyma (Kallok, Wilson, Rodarte, Lai-Fook, Chevalier & Harris 1979).

Variability of volume changes may increase towards the periphery of the lung (Wilson, Olsen & Rodarte 1987). In normal upright subjects, changes in lung volume during a maximal inspiration are greater in lower than in upper lung regions. The opposite is true when the lung volume is varied from maximal expiratory volume to FRC. In the range of lung volumes between 20% and 100% of VC the proportion of inspired gas delivered to any lung region is constant. Throughout expiration, upper lung regions tend to empty later than lower lung regions and this phenomenon is gravity dependent (Anthonisen et al. 1970).

3.2.4   Gas mixing

The lungs cannot be completely emptied during expiration, so they contain some residual gas after each breath. This residual gas smoothes out and damps down the changes in concentration that would occur if the lungs emptied completely with each

breath. Inspired fresh air entering the lungs becomes humidified and heated to body temperature, then must mix with the residual gas present in the lungs before it can reach the respiratory surfaces and can take part in gas exchange.

Mixing between inspired and resident gases takes place by means of: 1) molecular diffusion; 2) turbulent mixing; 3) convective mixing; and, 4) Taylor diffusion. Most gas mixing takes place in the respiratory airways where advection is small and the main mechanism of transport is molecular diffusion. Turbulent and convective mixing result from turbulence in the large airways where the Reynolds number is sufficiently large, and from disturbances and secondary motions generated at bifurcations. Convective mixing is associated with non-random eddy currents and secondary motions. Taylor diffusion is when axial streaming of one gas into another during laminar flow enhances mixing between them. In addition, Engel, Menkes, Wood, Utz, Joubert & Macklem (1973) have shown that cardiac oscillations can significantly influence the effective diffusion of gases in the upper airways, particularly for low breathing frequencies.

3.2.4.1   Quasi-stationary interface

Because the advective flow of gas quickly slows, at some point - usually in the respiratory bronchioles - the rate of advective flow is balanced by the rate of retrograde diffusion of residual gas molecules. Where the forward rate of advective transport equals the retrograde rate of molecular diffusion, there is a Quasi-Stationary Interface (QSI) of concentration between inspired and residual gas.

A QSI is defined as beginning at the point where the gas concentration first falls from the inspired gas concentration. Mouthward of all QSIs the airways contain only fresh inspired gas. Beyond the QSIs there are concentration gradients along which inspired gas molecules diffuse in a peripheral, and resident gas molecules in a central, direction. Different airway paths develop QSIs at different distances down them.

3.2.4.2   Anatomical dead-space

At the end of inspiration, gas present in the conducting airways cannot take part in gas exchange. This volume of gas is equal to the volume of the conducting airways, and is called the 'anatomical dead-space'. The anatomical dead-space represents the

minimum volume of inspired gas that does not take part in gas exchange.

Gas mixing is not usually complete in the length of a normal breath, so some of the gas that reaches the respiratory airways will be ineffective. Compared to an ideal lung having uniform flow distribution and infinitely rapid diffusion in the peripheral airways, a lung with an ineffective volume has 'mixing inefficiency'. Mixing inefficiency effectively increases the dead space because the fraction of tidal volume available for gas mixing is incompletely mixed with residual gas.

3.2.4.3 Fowler's method for calculating the anatomical dead-space

Fowler (1948) introduced the Single Breath Washin (SBW) test as a means of calculating the volume of the anatomical dead-space.

Consider inspiration of gas A into a lung containing gas B. The fractional concentration of gas A (F_A) and the expired volume are measured continuously during the following expiration. A SBW curve is constructed by plotting F_A against expired volume. Figure 3.3 shows a representative SBW curve.

The SBW curve typically has three phases:

1. Phase I is from the start of expiration and consists entirely of unmixed washin gas (F_A=1). This represents the volume of inspirate that has been transported solely by advection;

2. Phase II begins where the concentration of washin gas first begins to fall from the inspirate concentration, and ends when the gas concentration starts to plateau. Its curve consists of a sigmoid fall in concentration, which can be attributed to the concentration profile developed in the lung during inspiration in response to finite diffusion rates, and the dispersal of arrival times of QSIs at the mouth;

3. Phase III where F_A settles to a concentration 'plateau'. Phase III usually has a small slope.

Fowler's construction has been superimposed on Figure 3.3. Phase III is produced backwards to establish the end of phase II, and a perpendicular is dropped to give equal areas above and below phase II. The expired volume corresponding to this point
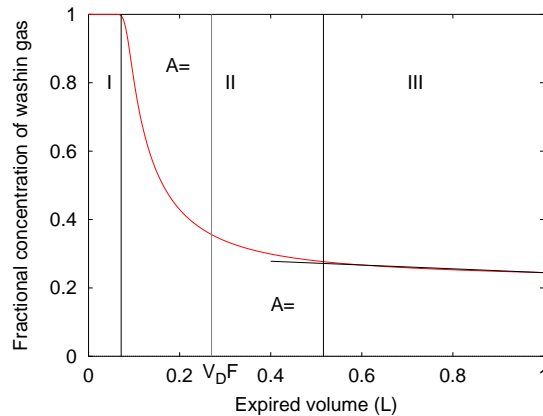
Figure 3.3: *A Single Breath Washin curve, with Fowler's construction superimposed. Phases I, II, and III are shown from left to right. $V_D F$ is positioned such that the areas above and below the curve (A=) are equal.*

is Fowler's estimate of the anatomical dead space, $V_D F$, which is the best estimate of the volume of the conducting airways.

An approximation to $V_D F$ is to find the expired volume at the transition from phase III to phase II, halve the concentration at this expired volume, then find the volume corresponding to the resulting concentration. This method has been shown to result in values of $V_D F$ very close to those obtained using Fowler's method (Crawford, Makowska, Paiva & Engel 1985).

3.2.4.4   Physiologic dead space

Bohr's calculation of dead space ($V_D B$) measures the volume of lung which does not eliminate subject gas. It is therefore called the 'physiologic' dead space because it is a functional measurement rather than an anatomical one, as in the case of $V_D F$. In normal subjects $V_D B$ is close in value to $V_D F$, but for patients with lung disease $V_D B$ may be significantly larger than $V_D F$ because of an impaired match between ventilation and perfusion (West 1979).

Consider inspiring gas A into a lung containing only gas B, and assume that only gas A is present in the dead space at the end of inspiration. Then assume that all of the expired gas B will come from the alveolar region, and none from the dead space. Therefore

$$V_T.F_E = V_{Al}.F_{Al} \tag{3.1}$$

where V_T is the tidal volume, F_E is the mean expired fractional concentration of gas B, V_{Al} is the alveolar tidal volume, and F_{Al} is the fractional concentration of gas B in the alveolar space. The total tidal volume is made up of the dead space volume and the alveolar tidal volume, so

$$V_T.F_E = (V_T - V_D).F_{Al} \tag{3.2}$$

where V_D is a dead space containing only gas A at the end of inspiration. Rearranging Equation (3.2) gives an expression for the Bohr dead space:

$$V_D B = \frac{F_{Al} - F_E}{F_{Al}} V_T \tag{3.3}$$

Experimentally, F_{Al} can be approximated by the end expired gas concentration.

3.2.4.5   Phase III of the washout curve

The slope of phase III in the washout curve has been the subject of much experimental study and investigation with mathematical models. It is thought to reflect mainly ventilation inhomogeneities in the periphery of the lung (Verbanck & Paiva 1990). The mechanisms involved in generating this slope are generally categorised in two groups: 1) Diffusion- and Convection-Dependent Inhomogeneities (DCDI), and; 2) Convection-Dependent Inhomogeneities (CDI).

3.2.4.5.1   *Diffusion- and Convection-Dependent Inhomogeneity*

DCDI is due to interaction of convection and diffusion in the asymmetric lung structure. Consider washin of a gas into two units of equal volume with similar cross-sectional areas, supplied by paths of different volumes. With uniform flow distribution, incoming gas will advect into the units in proportion to their volumes,

but gas diffuses into the units in proportion to their cross-sectional areas and diffusion gradients. Initially the concentration gradients will be the same for each unit, so the amount of gas entering each unit by diffusion will be similar. The unit with the largest path volume will be ventilated by a larger amount of resident gas than the unit supplied by the short path, before washin gas reaches the unit. The average concentration inside the smaller unit will therefore be greater than the larger unit at the end of inspiration. The Phase III slope therefore progressively decreases with each breath of the washin test, and shows a slightly curvilinear shape as a function of cumulative expired volume. DCDI also explains why more diffusive gases produce smaller alveolar slopes than the heavier gases.

3.2.4.5.2   *Convection-Dependent Inhomogeneity*

CDI is determined entirely by lung mechanics. Gravity (interregional mechanism) or uneven parenchymal mechanics (intraregional mechanism) both contribute to CDI.

A vertical gradient of pleural pressure is generated in the presence of gravity. As a consequence, the lungs develop vertical differences in regional pre-expiratory gas concentrations. The concentration of expired gas changes continuously during expiration implying that areas with differing pre-expiratory concentrations may contribute different amounts to the expirate. That is, they empty with variable rates ('sequentially'). Anthonisen et al. (1970) have shown that the lungs empty sequentially throughout the VC, and that this phenomenon is gravity dependent.

Because the concentration of resident gas in airways as small as 3mm in diameter continues to gradually rise during expiration, this implies that significant ventilation heterogeneity can exist within relatively small regions. This may be due to the elastic material properties of the lung causing unequal ventilation and/or flow sequencing among peripheral lung units.

3.2.4.5.3   *Normalised phase III slope*

Crawford et al. (1986) introduced S_n, the slope of the alveolar plateau normalised by the average expired concentration of resident gas, as a means of analysis of Multiple Breath Washin (MBW) curves. Both CDI and DCDI contribute to the increase in S_n over

the initial breaths of a MBW test. Crawford et al. (1986) showed that the contribution of DCDI to increasing S_n becomes fixed after a number of breaths, and further increases in S_n reflect solely the CDI contribution. It was shown that because of the increasing contribution of DCDI to the S_n of the first few breaths of a washout, the difference between the slopes of two inert gases differing in diffusivity should initially increase. After the point where DCDI becomes fixed, the two slopes may be expected to increase in parallel (reflecting CDI). Crawford et al. (1986) also found that short end-inspiratory breath-holds substantially reduced the breath-by-breath increase in S_n for the first five breaths, with the remaining breaths unaffected by breath-holds.

These results suggested that the rise in S_n in the first breaths of a MBW test is mainly due to increasing inhomogeneity of gas concentrations between units that are close enough together such that short breath-holds produce significant equilibration of concentrations. The rise in S_n over the remaining breaths was attributed to concentration differences between units that were too far apart to have their concentration differences reduced by short breath-holds.

3.2.4.6 The ventilatory dead-space and mixing efficiencies

Calculation of the ventilatory dead-space, $V_D V$, is based on comparison of the measured turnovers of lung volume needed to leave a specific residue Z of the residual gas that was initially present in the lungs, with the theoretical amount of turnovers that would be required in perfectly mixing lungs without dead space. From Harris, Buchanan & Whitlock (1987):

$$V_D = V_T - V_L \left(\left(\frac{1}{Z_k} \right)^{1/k} - 1 \right) \tag{3.4}$$

where V_T is the tidal volume, V_L is the pre-inspiratory lung volume, k is the breath number, and Z_k is the fraction of residual gas remaining in the lungs after breath k.

V_D is the estimate of the ventilatory dead-space, $V_D V$, up to and including breath k (Harris et al. 1987). Fuller, Harris & Withy (1990) define it as "that dead space which, in an alveolar uniform lung of the same total volume, would cause it in a given number

of breaths to wash an inert gas, in or out, identically with the lung under examination".

With perfect efficiency, $V_D V$ would be equal to the volume of the conducting airways. Using $V_D F$ as the estimate of the anatomical dead-space, the estimate of inefficiency is therefore the amount by which $V_D V$ exceeds the anatomical dead-space. The difference $V_D V$-$V_D F$ is the effective alveolar dead-space arising from non-uniformity in the real lungs. The Multiple Breath alveolar Mixing Efficiency at the kth breath ($MBME_k$) is therefore given by

$$MBME_k = \frac{V_T - V_D V_k}{V_T - V_D F} \tag{3.5}$$

That is, the mixing inefficiency describes the fraction of inspired gas that reaches the alveolar space but does not take part in gas mixing.

The MBME can be calculated for a single breath, where Z is the fraction of residual gas remaining in the lung at the end of the breath.

The Alveolar Mixing Efficiency (AME) expresses mixing efficiency as the ratio of the volume of residual gas expired in a given breath and the volume that would be expired by the 'ideal' lung under the same conditions.

The AME consistently overestimates the MBME for a single breath by a small amount because AME is calculated from equal turnovers but different clearances, whereas MBME uses equal clearances but different turnovers.

3.2.4.7   Other methods of gas mixing

During breath-holding the magnitude of V_D decreases similarly for gases of different diffusivity (Bartels, Severinghaus, Forster & Briscoe 1954). This has lead to the conclusion that molecular diffusion is not the main contributor to the decrease in V_D.

Bartels et al. (1954) proposed that the churning action of the heart might be the predominant mechanism for reducing V_D with time. This theory is supported by the observations of Engel et al. (1973), who observed a five-fold enhancement in mixing *in vivo* compared with mixing in excised lungs. As the heart beats, it reduces intrathoracic blood volume during systolic ejection, thus contributing to the pressure gradient that drives inspiration. This is referred to as the 'aspirating' action of the heart (Bosman & Lee 1969). The heart also displaces as it pumps blood, which causes displacements and

resulting compression or expansion to different parts of the lung.

Convective mixing occurs as a result of thermodynamic and airway and alveolar geometric factors. Heyder, Blanchard, Feldman & Brain (1988) have demonstrated the influence of airway geometry on convective gas mixing using an aerosol to simulate a non-diffusing gas. They found that the aerosol bolus underwent more axial dispersion the further it penetrated into the lung. The expired bolus was always spread over a volume that was larger than the volume of the inspired bolus.

3.2.5 Past models of gas mixing in the lungs

It is not currently possible to make direct measurements of concentration in the small airways of the human lungs. This inability to perform direct measurements has prompted the development of mathematical models for simulating gas mixing. The increasingly sophisticated models have been used to provide possible explanations for lung gas mixing behaviour and, in particular, to explain the mechanisms that cause the slope of the alveolar plateau in Phase III of the gas washout curve, and to explain the inefficiency of gas mixing (see Section 3.2.4).

The earliest proposed theory to explain the sloping alveolar plateau was that inspired gas did not have time to diffuse completely throughout the lungs during a normal respiratory cycle and that a concentration gradient would therefore persist throughout expiration, resulting in a sloping alveolar plateau. The proposed gradient in gas concentration from the mouth to the alveolar surfaces has come to be called 'stratified inhomogeneity'. However, the first mathematical model of gas mixing in the respiratory region of the lungs (Rauwerda 1946) did not support stratified inhomogeneity as the cause of the slope of the alveolar plateau.

Rauwerda (1946) found that gas mixing was very close to complete over the time of a normal breath in two simple respiratory airway models and therefore no significant concentration gradient persisted. Rauwerda investigated the time for complete gas mixing in the alveolated airways by solving the classical diffusion equation in two models with lumped alveolar and duct volumes: the first model was a circular cylinder, and the second model was a cone truncated by closed spherical surfaces. Both models were rigid structures. The governing equation was solved analytically with only axial

diffusion considered in the cylindrical model and only radial diffusion considered in the conical model.

Later studies of lung morphology (Weibel 1963, Horsfield & Cumming 1968) showed that the geometry employed by Rauwerda to represent the respiratory airways was very different to real lungs. The conical model had end areas close to those published by Weibel (1963), but the cross-sectional areas between the ends were far larger than those subsequently published. Both ends of the models were closed during simulation, hence the terminal bronchioles (at the proximal end of the model) were not able to interact with more proximal conducting airways.

Cumming, Crank, Horsfield & Parker (1966) modelled gas mixing in the distal airways using two rigid truncated cone models: the first model had its small end open and in contact with an infinite reservoir of oxygen and its other end was assumed to be closed; the second model had both ends assumed closed. A planar front separating pure O_2 from air was positioned in the alveolar region, and then the static diffusion equation was solved analytically in the two models. The resulting concentration gradients were found to persist for several seconds, leading to the conclusion that stratified inhomogeneity may contribute to the slope of the alveolar plateau.

Once again, the geometry of the two Cumming models was very different to that eventually published (Weibel 1963, Horsfield & Cumming 1968). In addition, Cumming's model did not take account of alveolar volume, only duct volume.

La Force & Lewis (1970) solved diffusion of O_2 into N_2 using a finite difference method in a symmetric dichotomous branching model with the branch lengths and cross-sectional areas proposed by Weibel (1963), and in a second model that incorporated an additional alveolar cross-sectional area. Both models were rigid. They found no significant concentration gradients persisting after a breath. In fact, they found that the alveolar concentration stratification disappeared in much less than a second. Although the model was claimed to investigate the effects of branching, because it was a symmetric model it was equivalent to later solid-body 'trumpet-shaped' models.

The models of Rauwerda (1946), Cumming et al. (1966) and La Force & Lewis (1970) were all rigid structures (i.e. they did not expand or contract during ventilation), with the boundary conditions 'reflecting' material from the last generation, and they

did not incorporate convective movement of gas. Cumming et al. (1971) attempted to include simultaneous convective flow and longitudinal diffusion in a 'stationary front' model using Weibel's model A to describe the model geometry. They solved the classic static diffusion equation using a modified finite difference method, where they approximated convective flow by shifting the 'stationary' interface by 100 ml after solution of the diffusion equation at each 150 ms time-interval. Finite radial diffusion into the alveoli was included in the solution.

Two sets of boundary conditions were investigated with the model: the first set established an interface between oxygen and nitrogen 500 ml within the model at the beginning of the simulation, followed by 10 s of diffusion; the second boundary condition set the interface 1000 ml within the model and did not include convective flow. For the second set of boundary conditions the model expanded and contracted during simulation.

Although a 1.1% N_2 gradient for the alveolar slope between 750 and 1250 ml expired volume was obtained from the results, the simulations supported the findings of Rauwerda (1946) and La Force & Lewis (1970), namely that diffusion was too rapid for stratification to persist.

Cumming's model was the first to demonstrate the quasi-stationary front between inspired and resident gas. Other convective-diffusive studies have confirmed the stationary interface but have shown almost complete diffusive mixing within the time of a respiratory cycle (Baker et al. 1974, Pack, Hooper, Nixon & Taylor 1977, Paiva 1973, Scherer et al. 1972, Scrimshire, Loughnane & Jones 1978).

Baker et al. (1974) analysed simultaneous convection and longitudinal diffusion using a finite difference solution of the diffusion equation. The model geometry was described by a modified form of Weibel's model A, where the conducting airways were taken to be generations 0 - 17 and the volume of generations 18 - 23 was lumped together in a single well-mixed alveolar compartment. The lung volume was an exponential function of time. From a single breath N_2 washout in this model, Baker et al. (1974) calculated a sloping alveolar plateau of 0.245 vol % $N_2 \cdot L^{-1}$ at 450 ml after 1.7 dead-spaces were expired, which was significantly diminished by 2 s of breath-holding. The anatomic dead space predicted by the model was 70% larger than measured values.

Scherer et al. (1972) and Paiva (1972) independently derived transport equations governing simultaneous flow and longitudinal diffusion where alveoli were considered reservoirs through which no axial diffusion occurs. The transport equations were used in symmetric models based on Weibel's model A. Both of these studies found that concentration stratification existed in the alveolated airways at the end of a normal inspiration, but they did not observe a resulting slope of the alveolar plateau. Paiva therefore concluded that the existence of alveolar stratification is not a sufficient condition for a sloping alveolar plateau since it may be obliterated by diffusional processes occurring during expiration.

Pack et al. (1977) used a model with regular dichotomy and incorporated time-varying flow, model expansion, and gas exchange. They found that when simulating single breath washin tests, a flow-enhanced diffusion coefficient was necessary in their model to obtain any slope in the alveolar plateau. Later studies (Verbanck & Paiva 1990) have shown that it is not necessary to include effective diffusion in gas transport models, so the alveolar slopes resulting from this study do not represent the same mechanisms of generation as in experimental results.

Engel et al. (1979) investigated simultaneous diffusion and convection in a solid model consisting of Weibel's model A for the conducting airways, and a respiratory region based on the study of Hansen & Ampaya (1975). From this study Engel et al. (1979) concluded that Taylor type dispersion (see Section 3.2.4) has a negligible effect on gas mixing. This finding was supported by Chang & Farhi (1973) and Pack et al. (1977), who concluded that Taylor mixing contributes very little to the shape of the concentration profiles down the lung. The model developed by Engel et al. (1979) was unable to even qualitatively predict the different slopes of the alveolar plateaus for gases of different diffusivity.

All of the above models assumed airway symmetry, with most based on Weibel's symmetric model A. The assumption of airway symmetry overestimates the duration of Phase I, since notably shorter path lengths do not exist. Phase II is underestimated because of the lack of 'apparent mixing' caused by a distribution of path lengths. Mon & Ultman (1976) and Paiva & Engel (1979) incorporated asymmetry into their models, and demonstrated that it could have an influence on the slope of the alveolar plateau. Luijendijk, Zwart, de Vries & Salet (1980) and Paiva & Engel (1981) used

geometrically asymmetrical models in an attempt to explain generation of the sloping alveolar plateau by complex interaction between convection and diffusion at intra-acinar branch points subtending units of equal volume.

Luijendijk et al. (1980) represented asymmetry using a model consisting of two acini plus the conducting airways, with respiratory dimensions based on Hansen & Ampaya (1975). Each acinus was axisymmetric, but of different sizes. Comparison of results with a model having acini of the same size showed a marked increase in the alveolar plateau slope due to asymmetry.

Paiva & Engel (1979) and Paiva & Engel (1981) used a similar model to Luijendijk et al. (1980) with two axisymmetric trumpets connected to a bifurcating airway. The relative volumes of the two trumpets and the point in the airways represented by the bifurcation could be varied. The study showed that such a model could produce a sloping alveolar plateau even when the two parts were ventilated synchronously. Although asymmetry was shown to have a significant influence on the alveolar slope, Paiva & Engel (1981) concluded that gas mixing was not very sensitive to the geometry of the last few respiratory generations, based on comparisons of results from a Weibel-based model with a Hansen-based model.

de Vries, Luijendijk & Zwart (1981) performed simulations in expansile lung models that had asymmetries in branching pattern or cross section within the acinus. From single breath washout simulations of He and SF_6, only small differences were found between the results obtained from a lung model with an asymmetric branching pattern using either a local homogeneous or inhomogeneous flow distribution. From these results it was concluded that the branching pattern asymmetry had the most significant influence on generation of the slope of the alveolar plateau, the Phase III contribution of the Bohr dead space, and the end tidal concentration ratio of SF_6 and He observed in single-breath washout experiments.

Davidson & Engel (1982) utilised the acinar model of Parker, Horsfield & Cumming (1971) to simulate gas transport and mixing. The model consisted of five identical subunits, each one with five branch points. The study predicted a distinctly non-homogeneous gas distribution within the model at the end of a 1 L inspiration of O_2 over 1 s, and significant concentration differences between the different transport paths at the end of expiration. The calculated alveolar slope between 750 ml and 1000 ml

expired volume was 3.3%·L^{-1}.

Bowes, Cumming, Horsfield, Loughhead & Preston (1982) considered an arbitrary structure of the acinus with perfect symmetry between the terminal bronchioles and the last respiratory bronchioles and a very asymmetrical pattern of branching distally. The study deliberately used a model with a degree of asymmetry greater than that observed in studies of acinar anatomy, to investigate whether asymmetry of the alveolar ducts could account for incomplete gas mixing. The respiratory bronchioles and proximal conducting airways were assumed to be symmetrical. The conducting airways were assumed rigid, but the respiratory airways were expansile. The calculated alveolar slope for a 1 L inspiration over 2 s, between 750 ml and 1250 ml expired volume was 3.4%·L^{-1}. Bowes et al. (1982) calculated a 97% mixing efficiency, therefore they concluded that although the acinar asymmetry had a significant effect on the slope of the alveolar plateau, it was insufficient to explain the failure of gas mixing, which is closer to 85% (Cumming & Guyatt 1982).

The alveolar slopes from the Bowes and Davidson studies lie in the range measured in normal subjects (Crawford et al. 1986). However, the geometry of the Davidson study was based more on a mathematical concept than on real anatomy, and the Bowes study deliberately chose a degree of asymmetry higher than in the real lung.

Paiva & Engel (1984) simulated gas concentrations in an asymmetrically branching model of the acinus based on the morphometric study of Hansen & Ampaya (1975). The model was radially expansile and used uniform, constant flow. To simplify computation, branch lengths in generations 15 - 18 were assumed to all be 1 mm and in generations 19 - 26 were assumed to be 0.5 mm. This required the cross-sectional areas to be adjusted to maintain measured volumes. The transport equation was only solved down selected pathways.

The Paiva & Engel (1984) study demonstrated substantial inhomogeneity of gas concentration at the end of inspiration of 1 L O_2 into N_2 over 2 s. Gas inhomogeneity persisted even with a 10 s breath-hold. A small alveolar plateau of 0.53% N_2 · L^{-1}, was calculated. Results from the model suggested that while intra-acinar gas inhomogeneity was substantial, it contributed only a small amount to the overall impairment in gas mixing. Diffusive pendelluft was observed to enhance mixing during expiration.

Engel & Paiva (1985) found a very strong dependence of the alveolar slope on tidal volume when flow was kept constant at $0.5 \; \text{L} \cdot \text{s}^{-1}$ in a multi-branching model similar to that presented by Paiva & Engel (1984). Both the strong dependence on tidal volume and the alveolar slope values were different from experimental observations. A 98.7% mixing efficiency was calculated for the multi-branching model. The main difference between simulations in the multi-branching model and experiments was that Phase II for the simulations was far sharper, and the Phase III slopes were much smaller than observed experimentally. The sharp Phase II could be mainly attributed to non-consideration of distribution of transit times from acini with different conducting pathway lengths.

Paiva, Verbanck & van Muylem (1988) compared experimental single breath washin results with results from simulations performed in two multi-branching respiratory airway models with different asymmetries. The first model was the same as Paiva & Engel (1984), and the second model was closer to the respiratory structure of the rat or rabbit. This meant that the second model was more asymmetric than the first in the region where the interface between resident and washin gas usually stands. The alveolar slopes simulated by the second model were always larger than those generated by the first, which lead the researchers to conclude that interdependence of gas transport by convection and diffusion in the periphery of the lung was a major component of the slope of the alveolar plateau.

Verbanck & Paiva (1990) published a full lung model partitioned into an upper and a lower region, each containing two subunits. Each subunit consisted of an asymmetric branching structure based on the morphometric study of Haefeli-Bleuer & Weibel (1988). The model contained equivalent to 27,500 acini. Gas transport in the dead space was assumed purely convective, and diffusive mixing was assumed to occur solely in the acini. Gas concentrations from the subunits were flow-weighted to recombine during expiration. The model was used to investigate the effect of unequal flow distribution to the upper and lower regions, and to the neighbouring acinar models. The resulting plots from the Verbanck & Paiva (1990) model of S_n against breath number for He and SF_6 ran parallel and wider apart than experimental results, giving a larger ΔS_n than measured by Crawford et al. (1985). The shape of the S_n curve for O_2 was found to be qualitatively similar to experiments, but absolute decreases

of S_n with breath-holding were larger in experiments than simulated by the model. The study concluded that the model simulations underestimated the experimental ventilation inhomogeneity. The sloping S_n curve was produced by uneven ventilation of neighbouring acini.

Scherer, Gobran, Aukberg, Baumgardner, Bartkowski & Neufeld (1988) showed that including a source term to allow for the evolution of a gas from the blood into the alveolar gas space could produce a sloping alveolar plateau when using a Weibel-based symmetric model. Scherer et al. (1988) used a single-path trumpet-bell model and included a source term in proportion to the local alveolar blood flow, gas solubility, and gas blood and local air-phase concentration difference. Their geometric model used Weibel's symmetric model A with volume expansion of the alveoli, as described in Scherer et al. (1972). The study was mainly concerned with washout of CO_2, of which a large amount is generated from the blood. Scherer et al. (1996) used the same single-path model with no source term and simulated zero slope for the normalised alveolar plateau over multiple breaths. They showed that inclusion of the source term produced S_n values that increased with each breath. The shape of the simulated S_n curve was different to experiments.

Schwardt, Neufeld, Baumgardner & Scherer (1994), Scherer et al. (1996), and Huang, Yang, Scherer & Neufeld (2000) showed that for the single-path model to simulate normalised slopes more accurately, a scaling factor was required to multiply the cross-sectional area of the respiratory region. The lengths were scaled accordingly to maintain the original volumes for each generation. The scaling factor was different for each gas, and did not produce normalised slopes close to experimental over the whole range of breaths.

Cruz (1991) simulated mixing of Argon and O_2 in a seven region lung model (7RLM). The model incorporated both series and parallel inhomogeneities. Each region in the 7RLM was allocated a different compliance curve based on the results of Milic-Emili et al. (1966). Each region was ventilated with a regional tidal volume that was dependent on the compartment compliance and dead space. Regional dead spaces were allocated "on the basis of increasing path lengths of inspired gas from the apex to the base" (Cruz 1991). Mixing of inspired with resident gas beyond each dead space was assumed to be exponential with respect to expired volume. The seven regions had

identical volumes at TLC.

Cruz et al. (1997) compared simulated O_2/N_2 S_n results from the Scherer et al. (1996) single path model and the 7RLM, both with and without a blood source term as described by Scherer et al. (1996). Cruz et al. (1997) demonstrated that the 7RLM with or without a source term fit the experimental data of Crawford et al. (1985) better than the single path model with a source term. The 7RLM without a source term fit the experimental data well from breath 13 onwards. For breaths 1-12 the S_n curves simulated by the 7RLM with and without a source term were identical and lower than the experimental results. The superiority of the 7RLM over the single path model with source term for the first breaths implied that S_n for the first breaths were mostly due to convective mixing of the seven parallel flows. The Cruz et al. (1997) study showed the increasing contribution of the blood source term to S_n with increasing breath number. Cruz et al. (1997) also showed that the non-uniform distribution of ventilation has a large effect on S_n, particularly over the first portion of the S_n curve.

3.2.5.1 Summary

Mathematical models of gas mixing in the human lungs have evolved from the analytic solution of diffusion in simple rigid structures with arbitrary geometry, to include better descriptions of lung anatomy, expansion and contraction during breathing, and simultaneous convective flow and molecular diffusion. The geometry of these models began with simple cones and cylinders, which became trumpet- or thumbtack-shaped solid models, then coupled trumpet-shaped models of different sizes, and finally multi-branching models that attempt to describe the entire acinar geometry.

Although the models have become more complex and descriptive, they still do not consistently simulate the sloping alveolar plateau, nor do they completely account for the inefficiency of gas mixing seen in experiments. The most geometrically detailed full lung model to date is that of Verbanck & Paiva (1990), yet this includes only eight pulmonary acini, with restrictions on the types of gas transport allowed in the conductive and respiratory regions. The 7RLM of Cruz et al. (1997), incorporating distributed volumes, regional ventilation, and a blood source term, has simulated S_n with close match to experimental results over a portion of the O_2/N_2 curve. The results of Cruz et al. (1997) demonstrated the importance of both non-uniform ventilation and

blood-gas exchange when simulating S_n.

None of the models described in this section have incorporated detailed conducting airway asymmetry, nor have any models combined respiratory airway asymmetry with blood-gas exchange and non-uniform ventilation.

3.3   Modelling gas mixing

3.3.1   Derivation of the gas transport equation

An equation governing transport of binary gas mixtures by convection and diffusion through a system of alveolated airways can be derived by considering conservation of mass of inspired gas in a control volume. i.e a slice across an alveolated airway of a certain thickness. The alveoli are assumed to form a 'sleeve' of uniform thickness along the airway.

Gas can enter or leave the control volume by either advection or diffusion. The governing equation balances the change in concentration of gas inside the control volume with the advective and diffusive contributions to concentration change. That is, the change in concentration of gas in the control volume is equal to the net flux of gas through the control volume surface.

Balancing the change in concentration of inspirate gas over time gives Equation (3.6).

$$\frac{d}{dt} \int_V c \, dV = - \int_S \boldsymbol{q_g} . \boldsymbol{n} \, dS \tag{3.6}$$

where V is a control volume, S is the surface of the control volume, $\boldsymbol{n}$ is the normal to the surface, and $\boldsymbol{q_g}$ is the net flux of inspirate gas ($\boldsymbol{q_g} = \boldsymbol{q_a} + \boldsymbol{q_d}$). $\boldsymbol{q_a}$ is the advective flux, and is given by $\boldsymbol{q_a} = -\boldsymbol{u}c$. Molecular diffusion is governed by Fick's law of diffusion, so the diffusive flux $\boldsymbol{q_d}$ is written $\boldsymbol{q_d} = -D\nabla c$ where D is a diffusion coefficient and c is the concentration of inspirate gas. Substituting these expressions for flux into

Equation (3.6) gives Equation (3.7).

$$\frac{d}{dt} \int_V c \, dV = \int_S (-\boldsymbol{u}c + D\nabla c).\boldsymbol{n} \, dS \tag{3.7}$$

Applying Gauss's theorem to Equation (3.7) gives

$$\frac{d}{dt} \int_V c \, dV = \int_V \nabla \cdot (-\boldsymbol{u}c + D\nabla c) \, dV \tag{3.8}$$

Taking the time derivative inside the integral, and equating the integrands (since the control volume is arbitrary) gives

$$\frac{\partial}{\partial t}(c) = \nabla \cdot (-\boldsymbol{u}c + D\nabla c) \tag{3.9}$$

Rearranging Equation (3.9) gives

$$\frac{\partial c}{\partial t} + \nabla \cdot \boldsymbol{u}c = \nabla \cdot (D\nabla c) \tag{3.10}$$

By neglecting secondary flows (in the r and θ directions) and assuming that there are no radial concentration gradients (instantaneous radial diffusion), a one-dimensional advection-diffusion equation is obtained:

$$\frac{\partial c}{\partial t} + u_x \frac{\partial c}{\partial x} = D \frac{\partial^2 c}{\partial x^2} \tag{3.11}$$

The left-hand-side terms in Equation (3.11) govern advective transport. The right-hand-side term describes axial diffusion in the airways governed by a diffusion coefficient, D.

Integrating Equation (3.11) across the alveolated airway gives:

$$\int\limits_r 2\pi r \frac{\partial c}{\partial t}\,dr + \int\limits_r 2\pi r u_x \frac{\partial c}{\partial x}\,dr = \int\limits_r 2\pi r D \frac{\partial^2 c}{\partial x^2}\,dr \tag{3.12}$$

Assuming that there is no axial diffusion or advection in the alveolar region gives:

$$\int\limits_0^{R_A} 2\pi r \frac{\partial c}{\partial t}\,dr + \int\limits_0^{R_a} 2\pi r u_x \frac{\partial c}{\partial x}\,dr = \int\limits_0^{R_a} 2\pi r D \frac{\partial^2 c}{\partial x^2}\,dr \tag{3.13}$$

where R_A is the radius including the alveolar 'sleeve', and R_a is the radius of the duct. Taking the time and spatial derivatives outside of the integrals gives:

$$\frac{\partial}{\partial t}\int\limits_0^{R_A} 2\pi r c\,dr + u_x \frac{\partial}{\partial x}\int\limits_0^{R_a} 2\pi r c\,dr = D\frac{\partial^2}{\partial x^2}\int\limits_0^{R_a} 2\pi r c\,dr \tag{3.14}$$

$$A\frac{\partial c}{\partial t} + a u_x \frac{\partial c}{\partial x} = aD\frac{\partial^2 c}{\partial x^2} \tag{3.15}$$

where a is the duct cross-sectional area and A is the duct plus alveolar area.

In reality there are secondary flows in the spherical alveoli and the concentration is not radially uniform. However, because the secondary flows in the complex alveolar volumes enhances radial gas mixing, the assumption of instantaneous radial diffusion is acceptable.

3.3.1.1   Generation of washin gas by the blood

Equation (3.15) describes transport of a gas pair with no movement of the subject gas to and from the blood. This is the same type of equation derived by Paiva (1972) and Scherer et al. (1972), and subsequently used widely for gas mixing simulation. As pointed out by Scherer et al. (1996) and Cruz et al. (1997), when the blood and air exchange gases a source term must be added to Equation (3.15). The blood gas

exchange term used in this study has a similar form to that of Scherer et al. (1972) and Cruz et al. (1997), such that the amount of gas exchange is proportional to the concentration of gas in the blood and air, the cardiac output (volume flow-rate of blood), the alveolar volume, and the gas solubility. The blood gas exchange term, Q, is given by

$$Q = \frac{Q_b \, (c_b - c) \, \lambda}{\gamma}.2\pi.R_A \qquad (3.16)$$

where Q_b is the local blood flow per unit tissue volume, c_b is the blood concentration of washin gas, λ is the gas solubility, γ is the surface area of alveoli per unit volume of tissue ($2\pi R_A.\Delta x / \pi R_A{}^2 \Delta x$), and R_A is the outer radius of the alveolated branch.

The local blood flow is equal to the cardiac output (Q_c) multiplied by the ratio of the local surface area of alveoli to the total lung surface area of alveoli.

Scherer et al. (1996) assumed that the cardiac output was constant at 110 cm$^3 \cdot$ s^{-1} over the whole lung. In contrast, Cruz et al. (1997) distributed Q_c according to West (1962) such that Q_c at the apex was 1.67 ml $\cdot$ s^{-1}, and Q_c at the base was 26.7 ml $\cdot$ s^{-1}. This resulted in a total Q_c of 100 cm$^3 \cdot$ s^{-1}.

The final transport equation, incorporating the source term, is:

$$A\frac{\partial c}{\partial t} + a u_x \frac{\partial c}{\partial x} = aD\frac{\partial^2 c}{\partial x^2} + Q \qquad (3.17)$$

3.3.2 Solution of the gas transport equation

3.3.2.1 Solution of advective-dominant transport equations

Using conventional Eulerian methods to solve convection dominated transport problems characteristically introduces oscillations and numerical diffusion in the solution near steep solution gradients. Because traditional mesh-based methods (such as the Finite Difference Method, or Finite Element Method) use a finite grid with a limited spatial resolution, they are unable to adequately represent steep solution gradients. The traditional mesh-based methods can produce accurate results when

diffusion is large, but require excessive mesh refinements or time-step reductions to approach accurate solutions for convection-dominated problems. This makes their use impractical when the mesh is large.

The stability and accuracy of Eulerian schemes is limited to small values of the 'Courant number', Cr, which is defined as

$$Cr = u\frac{\Delta t}{\Delta x} \tag{3.18}$$

where u is the local velocity, Δt is the time-step size, and Δx is the local element size. The Courant number can be thought of as an indicator of the number of elements through which a particle moves in one time step from x^* (start position) to x (final position) under pure convection.

Explicit time-stepping schemes approximate derivatives in the transport equation based on values of the solution at nearby nodes. When the Courant number increases, the 'domain of dependence' (Croucher & O'Sullivan 1998) does not include x^*, and the numerical method cannot mimic movement from x^* to x, causing instability. In contrast, implicit time-stepping schemes use solution values at all grid nodes, c_n, to evaluate the new solution, c_{n+1}. This means that x^* is always within the domain of dependence so stability is assured. Although the domain of dependence is over the whole grid, it is the values at nodes close to x which are primarily used to evaluate the solution. Accuracy therefore decreases when the Courant number increases.

Lagrangian methods improve the solution stability and accuracy by increasing the dependence of the final solution on the solution at x^*. The information flow from x to x^* is simulated more accurately by using the Method of Characteristics to solve the convection equation. These types of methods can be very accurate in idealised infinite flow domains, even in the presence of steep concentration gradients and large Courant numbers, but when irregular boundaries and complex flows are present, the methods do not perform well (Croucher & O'Sullivan 1998).

Combined Eulerian-Lagrangian methods take advantage of the high accuracy of Lagrangian methods, while retaining the simplicity and utility of a fixed Eulerian grid. The Lagrange-Galerkin method (LGM) is a specific Eulerian-Lagrangian method, using a split-operator approach and an implicit time-stepping scheme.

3.3.2.2 The Lagrange-Galerkin method

From the reference frame of a particle being 'tracked' through the flow, the time derivative of c (the 'Lagrangian derivative') is given by

$$\frac{Dc}{Dt} = \frac{\partial c}{\partial t} + \boldsymbol{u} \cdot \nabla c \tag{3.19}$$

Substitution of the Lagrangian derivative into the transport equation gives

$$\frac{Dc}{Dt} = \nabla \cdot (D\nabla c) \tag{3.20}$$

The 'operator splitting' approach solves the equation in two steps: 1) the pure convection equation is solved for an auxiliary unknown, c^*; 2) the pure diffusion equation is solved using c^* as an initial condition.

The LGM discretises the Lagrangian derivative using a Finite Difference approximation, then the Galerkin FEM is applied to the pure diffusion equation. The resulting Lagrange-Galerkin formulation is

$$\int_{\Omega} \varphi_i \frac{c^{n+1} - c^*}{\Delta t} \, d\Omega = \int_{\Omega} \varphi_i \nabla \cdot D\nabla c^{n+1} \, d\Omega \tag{3.21}$$

where φ_i is the finite element basis function associated with node i, and Ω is the flow domain.

The integrals in the equation are evaluated numerically using Gaussian quadrature. The particles are therefore tracked at each quadrature point (x_q) within the element to evaluate $x^*(x_q)$. This gives $c^*(x_q) = c^n(x^*(x_q))$.

Because the integrals are evaluated numerically, the LGM is only conditionally stable. However, using cubic-Hermite basis functions increases the smoothness of $c^*(x)$, resulting in high accuracy in the solution and only very weak instability (Li 1990).

Unlike most conventional numerical methods, LG methods do not automatically guarantee exact mass conservation. This is because of small errors that are introduced by the particle tracking procedure and numerical quadrature. However, the method is very accurate and this implies that the total mass is very nearly conserved.

The LGM has been implemented for solution of the transport equations derived in Section 3.3.1 and Section 5.3.2. The method is particularly appropriate for washin simulations in lung models. The boundary conditions at the model entrance for washin simulation induce steep solution gradients with advective-dominated flows in the upper airways, whereas the respiratory airways have diffusive dominated gas movement.

3.3.3   Modelling gas mixing in the respiratory airways

When asymmetry is introduced into the conducting airway model, either in branch dimension, branching pattern, or distribution of flow, it is no longer possible to model only a single branch from each conducting airway generation. Applying the multi branching approach described in Section 2.3 to the full lung would require attaching around 30,000 multi-branching acinar models to a model of the conducting airways. Because each branch in the system is modelled as at least one element, the amount of computer memory and CPU required to store and run simulations with a model of this size is currently not feasible with available computing power.

An approach to minimise the size of the whole lung model is to use Lumped Parameter Acinar (LPA) models. The LPA model described in this section uses input from inspiration to predict the concentration at the end of the terminal bronchiole during expiration. Predicted expiratory concentrations are applied as boundary conditions at the end of the terminal branches in a model of the conducting airways during expiration.

This section describes development of a LPA model that is calibrated using simulations from a multi-branching acinar model.

3.3.3.1   Generating a multi-branching model of the acinus

An asymmetric multi-branching acinar (MBA) model is generated using data from Haefeli-Bleuer & Weibel (1988) as mean values.

As discussed in Section 3.2.2, the Haefeli-Bleuer-Weibel (HBW) study was performed on casts that were very close to total lung capacity (TLC). The HBW data was therefore first scaled to a 'pre-inspiratory' volume (functional residual capacity -

FRC). The FRC was assumed to be at one half of the TLC (Weibel 1984). The individual branch volumes were assumed to scale in proportion to the total volume reduction - that is, by a half. The branch lengths were scaled as the cube root of volume change (Horsfield et al. 1971, Horsfield 1986), such that their scaled length was the original length multiplied by $0.5^{\frac{1}{3}}$. The outer diameters (including the alveolar area) were then calculated using the scaled volumes and lengths. The ratio of duct to total cross-sectional area (which governs the inner diameter size) was scaled further such that the inner diameters increased by 20% from their scaled size. This was in accordance with the recommendation of Haefeli-Bleuer & Weibel (1988) (see Section 3.2.2). Table 3.1 shows the scaled mean dimensions, and the number of branches in each HBW generation.

The first generation in the MBA model was the first pair of respiratory bronchioles. That is, the MBA model did not include the transitional bronchiole. Haefeli-Bleuer & Weibel (1988) described 11 generations in their average acinus, so for 10 generations in the MBA model, a random number of daughter branches per parent branch in the previous generation was calculated. The mean number of daughters per parent branch for each generation were calculated from the HBW acinus. The standard deviations of the number of daughter branches per parent branch were altered arbitrarily until the resulting number of branches in each generation were the same as, or close to, the numbers of branches in 'acinus 3' from Haefeli-Bleuer & Weibel (1988).

The mean and standard deviation were supplied to a random number generator, which returned a real random number. The real number was rounded to an integer value. When the integer number of daughter branches was equal to one, then the random number generator was used to regenerate a random number of daughter branches, until the number was zero or higher than one.

The generated branches were incorporated into a computational mesh as they were produced. Each branch was stored as a one-dimensional element, and each branch junction or ending was a node. Therefore a tree with N branches produced a mesh with N elements and $N + 1$ nodes.

Dimensions of branches were included in the mesh by generating a random branch length and duct diameter for each element using mean values and standard deviations per generation from the HBW data. If the branch was a terminal branch, then the mean

and standard deviation used were for the terminal sac values.

Random branch angles were also generated. The influence of branch angle was not included in the gas transport model for the respiratory airways, so these random angles were useful only for viewing the resulting model.

The alveolar volume was included in each branch by multiplying the conducting cross-sectional area by the ratio of total (including alveolar) to conducting cross-sectional area calculated from the HBW data.

By varying the random number seed used for generation of the number of branches or for generation of the dimensions, MBA models with different branching patterns or variation in dimensions can be generated. Howatson (1995) showed that differences in gas mixing results from models generated using different random number seeds were not significant. For this reason, only one MBA model was generated in this study to represent an 'average' acinus from the HBW data.

Gen	$\#Branches$	L_{duct}(mm)	L_{sac}(mm)	D_{duct}(mm)	D_{sac}(mm)	a/A_{duct}	a/A_{sac}
0	1	1.270	-	0.395	-	1.000	-
1	2	1.056	-	0.394	-	1.000	-
2	4	0.887	-	0.369	-	1.000	-
3	8	0.738	-	0.315	-	0.531	-
4	16	0.660	-	0.303	-	0.491	-
5	32	0.533	-	0.283	-	0.427	-
6	64	0.549	1.205	0.266	0.199	0.378	0.212
7	126	0.568	1.107	0.247	0.194	0.326	0.200
8	230	0.550	0.926	0.237	0.205	0.301	0.224
9	220	0.532	0.788	0.229	0.199	0.281	0.212
10	78	0.506	0.760	0.215	0.198	0.247	0.210
11	2	0.621	0.618	0.265	0.189	0.376	0.191

Table 3.1: *Numbers of branches and scaled dimensions for HBW data. Dimensions are given for both ducts and sacs. The columns, from left to right, are: Weibel generation, number of branches in the generation, mean duct length (L_{duct}), mean sac length (L_{sac}), mean duct diameter (D_{duct}), mean sac diameter (D_{sac}), mean ratio of duct to total area for alveolar ducts and respiratory bronchioles (a/A_{duct}), and mean ratio of duct to total area for alveolar sacs (a/A_{sac}).*

3.3.3.2   Behaviour of the model during simulation

3.3.3.2.1   Uniform deformation

Although the airways in the lungs do not expand uniformly or linearly, uniform expansion was applied to the MBA model in the absence of a realistic mechanics model. Uniform expansion constrains each branch to change in volume in proportion to the total model change in volume. The individual branch lengths were scaled during model expansion and contraction using the cube-root relationship between volume and length (Horsfield et al. 1971, Horsfield 1986).

Updated branch outer diameters were calculated accordingly from the deformed volumes and lengths. The effect of expansion of the alveolar and duct cross-sections was investigated by calculating the inner diameters using three different methods: 1) assuming that the ratio of total to conducting cross-sectional areas remained constant throughout ventilation (assuming that the alveolar and duct areas expanded at the same rate); 2) only the alveolar area expanded, and; 3) only the duct area expanded. The second method was adopted for further simulations.

3.3.3.2.2   Uniform flow distribution

Uniform model expansion implies that there must be uniform distribution of flow. Uniform flow distribution assumes that flow into a branch is in proportion to the volume of lung which it supplies. At each time interval during simulation, the change in volume of all branches below each branch was calculated. This was then equal to the flow through the branch in the next time-step.

3.3.3.2.3   Sinusoidal pattern of flow

The flow pattern at the mouth has often been assumed to be constant throughout inspiration and expiration (see Section 3.2.5). However, the pattern of flow during normal breathing is more 'saw-toothed'. A better fit to the flow pattern at the mouth is sinusoidal flow (Fuller et al. 1990). Gas mixing simulations presented in this chapter assumed sinusoidally varying flow.

3.3.3.2.4   Symmetric conducting airway model

It was necessary to attach the MBA model to a model of the conducting airways during simulation, to provide a 'delay' between gas entering the model mouth and entering the acinus. If washin tests were simulated directly into the acinus, then excessive amounts of washin gas diffused into the acinus because of the large gradient at the model entrance. The MBA model was attached to a 15 generation symmetric conducting airway (SCA) model based on Weibel's symmetric model A (Weibel 1963). The full-lung model effectively contained 32,768 identical acini. Because the conducting airway model was symmetric, the transport equations were solved down only one representative pathway. The combined MBA and symmetric conducting airway model was denoted 'MBA-SCA'.

3.3.3.2.5   Simulating a washin test

During inspiration a fixed concentration boundary condition was applied at the entrance to the model (the top of the trachea) to simulate inspiration of washin gas of fractional concentration 1. For expiration, a zero diffusive flux boundary condition was applied at the top of the trachea, and the expired concentrations were recorded.

3.3.3.2.6   Standard condition set for washin simulations

The gas pairs used for washin simulations were sulphur hexafluoride (SF_6) and nitrogen (N_2), oxygen (O_2) and N_2, and helium (He) and N_2. The diffusion coefficients assumed for each gas pair were 10.5, 22.5, and 74.3 $mm^2 \cdot s^{-1}$ (Paiva & Engel 1984) for SF_6, O_2/N_2, and He, respectively. The gas solubilities were 0.01, 0.014, and 0.0076 ml.gas(ml.$blood$)$^{-1}$ at atmospheric pressure for SF_6, N_2, and He, respectively (Scherer et al. 1996).

The 'standard' set of conditions was defined as tidal volume (V_T) of 1 L, total breath duration of 4 s (2 s inspiration and 2 s expiration), and a sinusoidal flow pattern. This condition set was used to allow comparison with experimental results from Crawford et al. (1985), and model results from Verbanck, Mangado, Peces-Barba & Paiva (1991), Scherer et al. (1996), and Cruz et al. (1997). Crawford et al. (1985) performed multiple breath washin experiments for N_2/O_2 mixing by having the subject inhale pure O_2

while the expired N_2 was measured. SF_6/N_2 and He/N_2 multiple breath experiments were performed by first equilibrating the subject's blood with the inspired gas mixture. i.e. the subject inspired multiple breaths of a gas mixture containing 5% of the washout gas, until the blood contained an approximately equal concentration. The subject then switched to breathing room air, and the expired SF_6 or He concentrations were recorded.

For the gas mixing simulations presented in this study, N_2 washout refers to mixing of inspired O_2 with resident N_2. The washin plots show expired washin gas concentration (O_2 for the N_2 washout, and air for the SF_6 and He washouts) against expired volume. The normalised alveolar slopes, dead-spaces, and mixing efficiencies are calculated for the washout gases.

3.4 Results from the multi-branching model

3.4.1 The generated MBA model

The volume of the generated MBA model was 82.76 mm^3, which was smaller than the scaled average volume from Haefeli-Bleuer & Weibel (1988) of 93.5 mm^3. This gave a total respiratory volume of 2.71 L in the MBA-SCA model.

The smaller size of the model acinus was because its numbers of branches were based on 'acinus-3' from Haefeli-Bleuer & Weibel (1988), which had an unscaled volume of 161.2 mm^3. The model volume was therefore close to the scaled acinus-3 volume of 80.6 mm^3.

Two further MBA-SCA models with different sizes were generated. The models were constructed using the same average dimensions from Haefeli-Bleuer & Weibel (1988) as the standard MBA model, but the smaller model had 7 generations, and the larger model had 10 generations and was more numerous in its peripheral branches. The volumes of the small and large models were 40.31 mm^3 and 194.00 mm^3, respectively.

Figure 3.4 compares the duct and alveolar cross-sectional areas from the small, standard, and large MBA-SCA models. The lowest coloured line for each corresponding model plots the duct cross-sectional area, and the highest

corresponding line plots the total cross-sectional area.

The duct cross-sectional areas for the three models were identical to generation 23: for further generations the smallest model had smaller duct cross-sectional areas than the other two models because of fewer branches in these generations. The total cross-sectional area for the three models was identical to generation 24, and had the same values as the total cross-sectional areas from Haefeli-Bleuer & Weibel (1988).
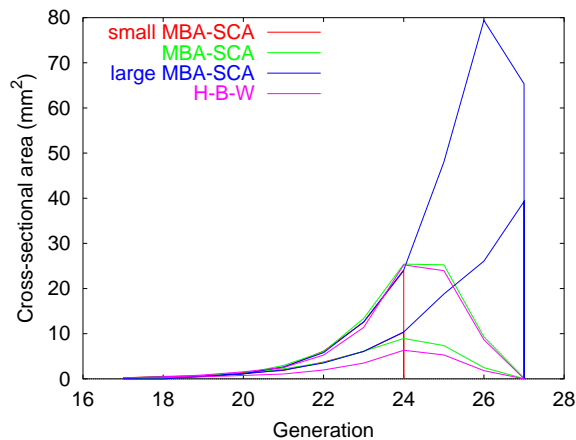
Figure 3.4: *Cross-sectional areas for MBA-SCA models of three different sizes: 40.31* mm^3*, 82.76* mm^3*, and 194.00* mm^3*. Comparison with experimental data from Haefeli-Bleuer & Weibel (1988) 'acinus-3', scaled to FRC at half the original volume.*

Most of the volume of the largest model came from the last few generations, where the alveolar volume was large. Unlike the experimental data or the middle-sized model, the smallest and largest models did not have a gradual decrease in cross-sectional area.

The generated multi-branching model is shown in Figure 3.5, at 0.5 s intervals throughout a 2 s inspiration and 2 s expiration of O_2 ($V_T = 1$ L). The figure illustrates the changes in branch radii and lengths throughout the breath. Concentrations in the model are shown as coloured fields: red corresponds to 100% O_2, and dark blue to 100% N_2. Washin gas at high concentration penetrated no further than the first few generations in the MBA model. The deepest level of penetration of the washin gas front was at mid-inspiration. The concentration front was quickly swept out of the respiratory airways in the early part of expiration, after which there were only small, but significant, differences in concentration in the MBA model.

(a) 0.5 s

(b) 1.0 s, mid inspiration

(c) 1.5 s

(d) 2.0 s, end inspiration

(e) 2.5 s

(f) 3.0 s, mid expiration

(g) 3.5 s

(h) 4.0 s, end expiration
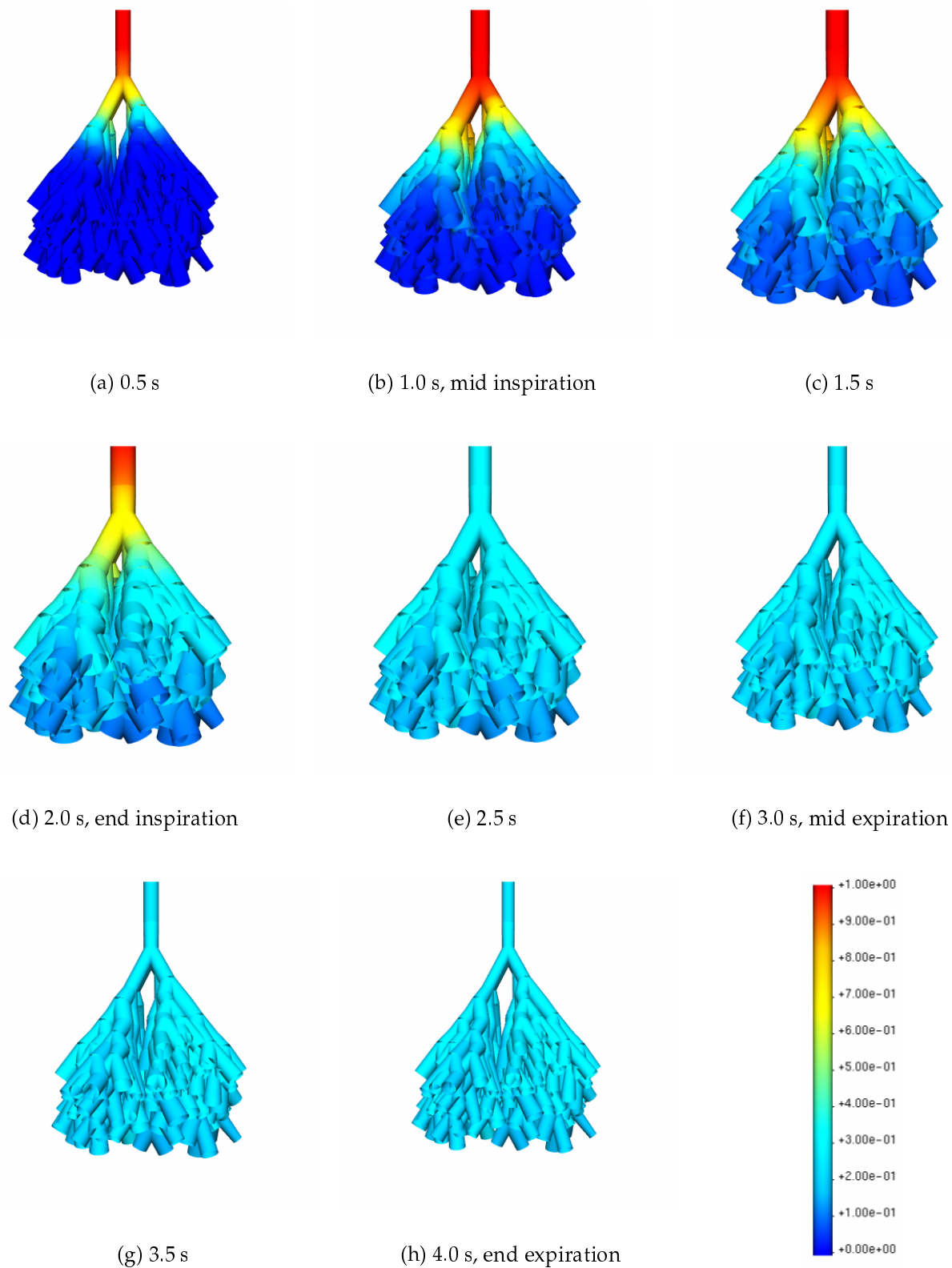
Figure 3.5: *The generated multi-branching acinar model shown at 0.5 s intervals during a 4 s breath of* O_2/N_2, *with tidal volume 1L.*

3.4.2   Convergence tests for the MBA-SCA model

Simulations were run in the MBA-SCA model using SF_6/N_2 under the standard condition set, with varying time-step size. Table 3.2 shows the percentage difference in results for the reducing time-steps. SF_6 was used as the 'test' gas because it has a low diffusivity, therefore errors in the results would be larger for this gas than for the more diffusible gases.

Δt (s)	$c_{ee}\%$	$c_{tb}\%$
0.05 - 0.02	0.7670	0.2324
0.02 - 0.01	-1.0204	-1.0211
0.01 - 0.005	0.2689	0.2877
0.005 - 0.002	0.2154	0.1967

Table 3.2: *Percentage difference in results for decreasing time-step sizes. The Δt column shows the time-step change, c_{ee} is the percentage difference in concentration at the mouth at the end of expiration, and c_{tb} is the percentage difference in concentration at the end of the transitional bronchiole at the end of expiration.*

The change in results from Δt=0.01 s to Δt=0.005 s were very small (less than 0.3%). Δt=0.01 s was therefore used as the time-step size for the MBA-SCA simulations.

If, for example, an explicit time-stepping scheme had been used instead of the LGM, a much smaller time-step would have been necessary. Solutions of the transport equation using explicit time-stepping schemes become unstable when the Courant number exceeds some fixed limit - usually 1 (Croucher & O'Sullivan 1998). If the trachea were assumed to be discretised to sections of 1 mm length, with a diameter of 16 mm and mean flow of $0.5 \, L \cdot s^{-1}$, then to maintain a Courant number of 1 or less, the time-step size would have to be 0.0004 s or less. The time-step of 0.01 s necessary for gas mixing in the MBA-SCA model was therefore 25 times larger than would have been required for an explicit time-stepping scheme.

3.4.3   Effect of relative duct to alveolar expansion

The transport equation derived in Section 3.3.1 effectively delays axial diffusion by the a/A term. If a/A changes during ventilation, then so will the effective delay. Assumptions about the relative expansion of the duct and alveolar areas could
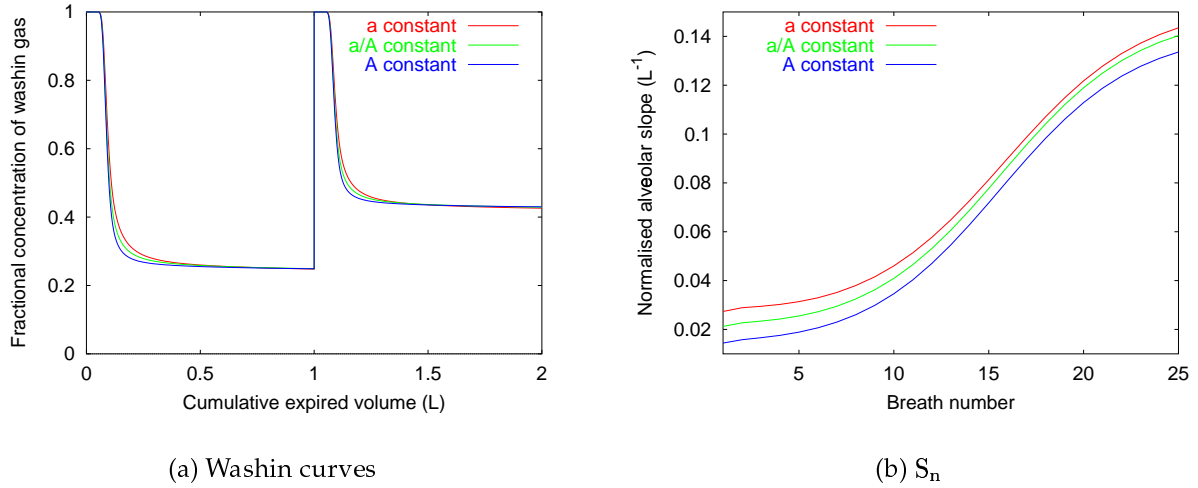
(a) Washin curves   (b) S_n

Figure 3.6: *(a) Washin curves and (b) normalised alveolar slopes, for different ratios of duct to alveolar cross-sectional expansion. 25 breaths of* N_2 *under standard conditions.*

therefore affect the behaviour of the model. To investigate the effect of relative area expansion, simulations were run in the MBA-SCA model with 1) expansion of the duct and alveolar areas at the same rate; 2) expansion of the alveolar area only (duct area constant); and, 3) expansion of the duct area only (alveolar area constant).

Figure 3.6(a) shows fractional concentration against expired volume for the standard conditions for N_2 under the three conditions of expansion over two breaths. S_n against breath number is plotted in Figure 3.6(b) for the N_2 washout simulation under different expansion rules over 25 breaths. The different expansion methods had little effect on the end expired washin gas concentration or on the duration of phase I. However, the slope of phase II was the least steep when expansion was in the alveolar cross-section only, and steepest when only the duct cross-section expanded. Expanding the alveolar cross-section while maintaining a constant duct cross-section also maximised the normalised alveolar slope, shown in Figure 3.6(b). The alveolar mixing efficiencies (AME) for the first breath were 97.02%, 96.42%, and 97.93% for conditions 1), 2), and 3), respectively. Therefore alveolar expansion also had the effect of minimising the AME. For further simulations, expansion in the alveolar area only was used. This is discussed further in Section 4.3.

3.4.4 Asymmetry of the acinar model, and blood gas exchange

Gas mixing was simulated in a symmetric model, with and without a blood gas exchange term to account for generation of washout gas from the blood (see Equation (3.16) in Section 3.3.1.1). Results from these simulations were compared with results from the MBA-SCA model, with and without a blood gas exchange term. Figure 3.7(a) shows washin plots for the four models, and Figure 3.7(b) shows normalised alveolar slopes. The standard condition set was used.

(a) Washin curves

(b) S_n
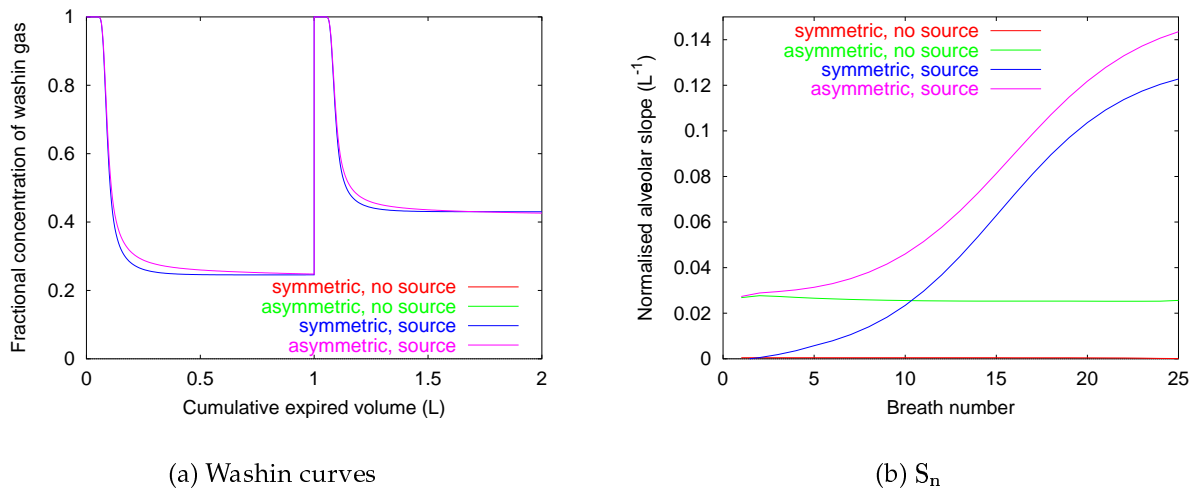
Figure 3.7: *Results from using symmetric and asymmetric respiratory airway models, with and without blood gas exchange terms. (a) Washin curves, and (b) normalised alveolar slopes. 25 breaths of N_2 under standard conditions.*

The washin curves for the symmetric model with and without a blood gas exchange term were so similar that they are indistinguishable in Figure 3.7(a). This was also the case for the asymmetric model with and without a blood gas exchange term. However, the washin curves for the symmetric and asymmetric models were clearly different from each other: the symmetric model produced washin curves with flatter plateaus than the asymmetric model. Although the plateau concentrations from the models for the first two breaths were very similar whether a blood gas exchange term was included or not, the normalised alveolar slopes were very different over multiple breaths. S_n for the models without a blood gas exchange term stayed close to the first

breath value, whereas inclusion of a blood gas exchange term resulted in increasing S_n values for each breath.

Figure 3.8 shows the concentration profiles in the MBA-SCA model and the symmetric model during a single breath of O_2/N_2 under standard conditions. Concentration profiles are compared for simulations with and without a blood gas exchange term.

At mid-way through inspiration (Figure 3.8(a), 1.0 s) the concentration profiles for all four models were quite similar. By the end of inspiration (Figure 3.8(b), 2.0 s) the concentrations from generation 15 to the terminal airways had developed small differences for the MBA-SCA and symmetric models. At that stage the presence of the blood gas exchange term had had no effect: the concentration profiles with or without the blood gas exchange term were identical for each different type of geometric model. The concentration in the terminal generation of the symmetric model (Weibel generation 25) was higher than that in the terminal generation of the MBA-SCA model (Weibel generation 27) at the end of inspiration.

By mid-way through expiration (Figure 3.8(c), 3.0 s) the symmetric model had developed very different concentration profiles to the MBA-SCA model. The concentration throughout the symmetric model was essentially constant for the blood gas exchange and no blood gas exchange simulations, with the model including the blood gas exchange term having developed a higher steady-state concentration. In contrast, the MBA-SCA model still exhibited significant differences in concentration from the trachea to the terminal airways, with a sharp decrease in concentration in the last few generations of the respiratory airways. The concentrations for the MBA-SCA model without a blood gas exchange term were slightly higher than when a blood gas exchange term was included.

At the end of expiration (Figure 3.8(d), 4.0 s) the concentration throughout the symmetric model was constant for both types of simulation, whereas concentration differences still persisted in the MBA-SCA model. There were only small differences in the concentrations for the MBA-SCA model with and without the blood gas exchange term.

Further simulations use the asymmetric model with a blood gas exchange term included in the transport equation. This is discussed in more detail in Section 4.3.
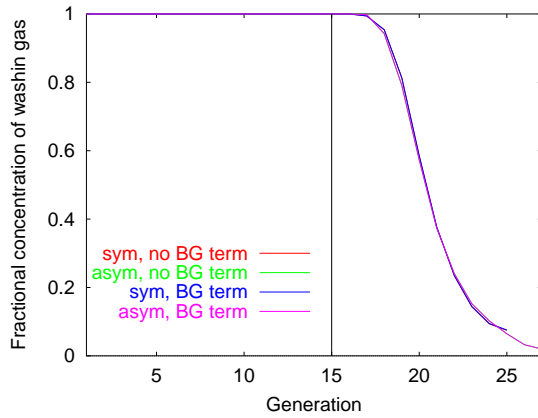
(a) 1.0 s, mid-inspiration
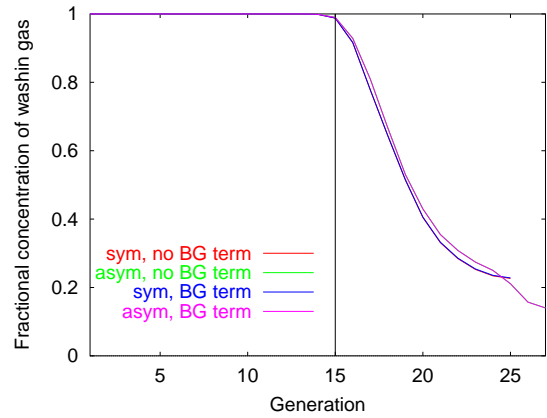
(b) 2.0 s, end-inspiration
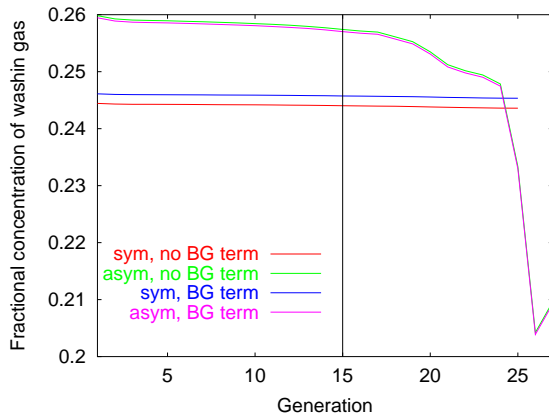
(c) 3.0 s, mid-expiration
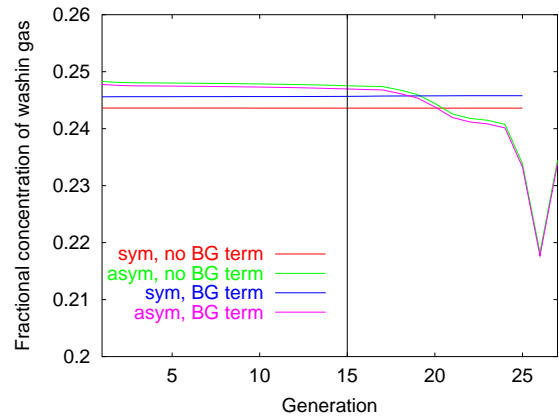
(d) 4.0 s, end-expiration

Figure 3.8: *Mean concentrations in the MBA-SCA model and a symmetric model, with and without a blood gas exchange term, for one breath of O_2/N_2 under standard conditions. Generation 1 is the trachea. The vertical black line divides the conducting and respiratory portions of the model. (a) mid-inspiration, (b) end-inspiration, (c) mid-expiration, (d) end-expiration.*

3.4.5 Simulations using gases with different diffusivities

Multiple-breath simulations were performed in the MBA-SCA model using the three different gas pairs. Figure 3.9(a) plots concentration against cumulative expired volume for the three subject gas pairs under standard conditions over two breaths in the MBA-SCA model. S_n and ΔS_n (the difference between S_n for SF_6 and He) are plotted in Figure 3.9(b) and Figure 3.9(c), respectively, for multiple breaths.

The characteristic three phases can be seen in Figure 3.9(a) for each simulated gas pair, with phase I longest for SF_6, phase II steepest for He and phase III flattest for SF_6. The end expiratory concentration was least for He and highest for SF_6. The difference between the end expiratory concentrations for He and SF_6 increased in the second breath.

S_n was highest for SF_6 over all of the breaths in Figure 3.9(b), which is consistent with theory. The first-breath S_n for SF_6 was close to the experimental first-breath mean for N_2. The S_n curves for N_2 and He had closer values than the SF_6 and N_2 curves, although the diffusion coefficients are closest for N_2 and SF_6.

ΔS_n from the MBA-SCA model is compared with experimental ΔS_n from Crawford et al. (1985) in Figure 3.9(c).
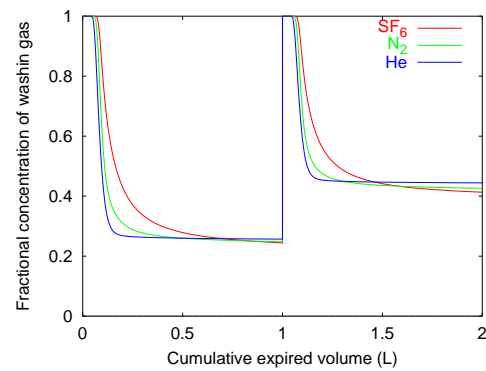
(a) Washin curves

(b) S_n
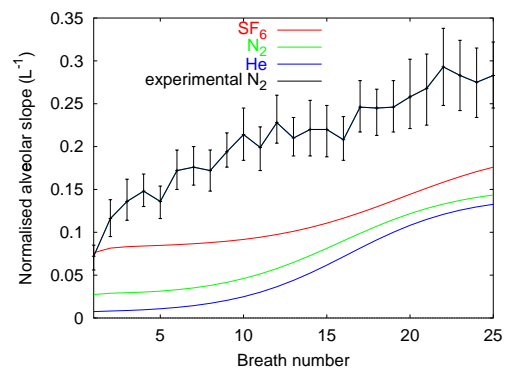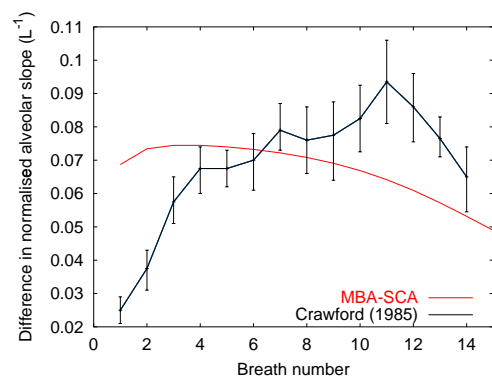
(c) ΔS_n

Figure 3.9: *MBA-SCA results for 15 breaths of* SF_6, N_2, *and* He *under standard conditions.*

Although the range of values for the simulated ΔS_n were generally within $\pm$ one SD of the experimental values, the shape of the numerical ΔS_n curve over fifteen breaths was very different to the experimental curve: the experimental curve showed a definite increase in value from breaths 1 to 11, followed by a decrease to breath 14; the simulated curve increased only to breath 2, then gradually decreased to breath 15.

The AME for the first breath was 92.88%, 96.46%, and 97.90% for SF_6, N_2 and He, respectively. This is consistent with the theory that heavier gases do not mix as fully as light gases, and therefore have lower mixing efficiencies.

Figure 3.10 compares the concentration profiles for the three gas pairs at 1, 2, 3, and 4 s in the MBA-SCA model. The concentration profiles are shown from generation 1 to the last respiratory generation.

By mid-inspiration (Figure 3.10(a), 1.0 s) a small amount of washin gas had reached generation 27 in the MBA model for the N_2 and He simulations. In contrast, no washin gas had reached generation 27 for the SF_6 simulation. The concentration front for He was sited higher up the SCA model (closer to the trachea) than for the other two gases. The concentration front for SF_6 was the least 'smeared' by diffusion, and was sited within the respiratory airways.

At the end of inspiration (Figure 3.10(b), 2.0 s) the respiratory airways contained a more even distribution of washin gas for the He simulation than for the other two gases. The concentration front was still within the respiratory airways for the SF_6 simulation, and the concentration of washin gas in generation 27 was still quite low. There was a 'cross-over' in concentration at generation 23-24 for the three concentration curves.

The concentration of washin gas in generation 27 at mid-way through expiration for the SF_6 simulation remained far smaller than for the two more diffusive gases (Figure 3.10(c), 3.0 s). The concentration of washin gas in the conducting airways was also higher for SF_6 in this simulation than for the other two gases.

By the end of expiration (Figure 3.10(d), 4.0 s) the concentration of washin gas in the conducting airways had settled to an approximately constant value for all three gases. In the respiratory airways, the He simulation showed only a small decrease in washin gas concentration, whereas the SF_6 simulation still had a large decrease in the last four generations. That is, the degree of stratification present at the end of expiration increased with decreasing gas diffusivity.
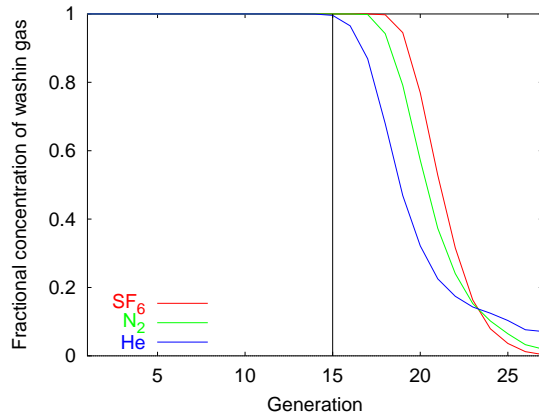
(a) 1.0 s, mid-inspiration
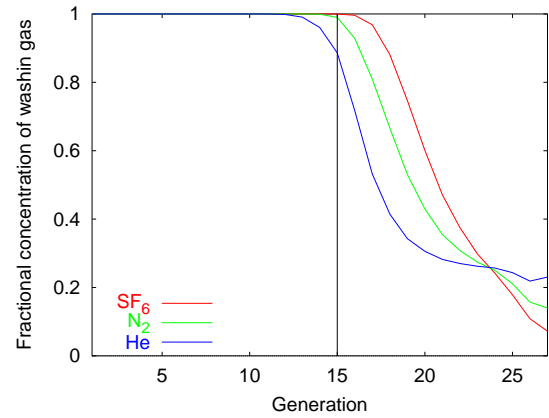
(b) 2.0 s, end-inspiration
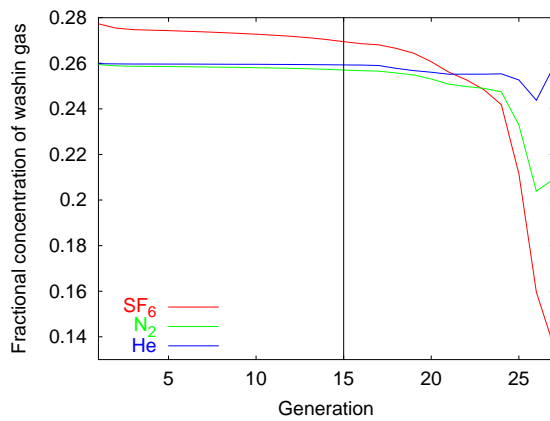
(c) 3.0 s, mid-expiration
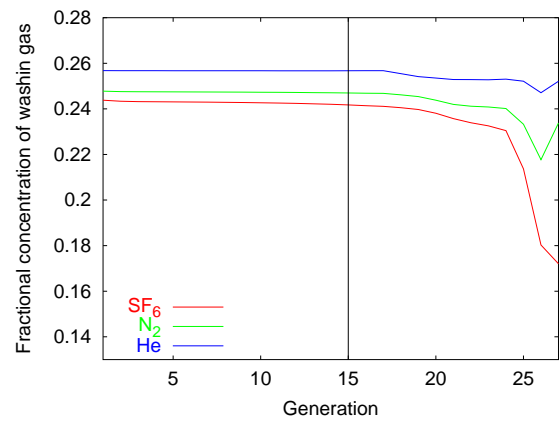
(d) 4.0 s, end-expiration

Figure 3.10: *Concentration profiles in the MBA-SCA model against generation for* SF_6, N_2, *and* He *under standard conditions.* *(a) Mid-inspiration, (b) end-inspiration, (c) mid-expiration, (d) end-expiration. The vertical black line divides the conducting and respiratory portions of the model.*

3.4.6   Concentration at the end of the transitional bronchiole

Figure 3.11 shows a plot of concentration at the end of the transitional bronchiole (generation 15 in the SCA model) against time in the MBA-SCA model. The plot shows two breaths under the standard conditions.

This plot illustrates the penetration of the respiratory airways, from generation 16, by the concentration front for SF_6 and N_2, but not for He: the concentration front for He was situated closer to the mouth, and washin gas at 100% of inspiration concentration did not reach the transitional bronchiole for the ventilation rate described by the standard conditions.

By the end of inspiration (2.0 s) the fractional concentration of washin gas at the end of the transitional bronchiole was close to 100% for SF_6, but was far lower for He. The concentration quickly settled to a plateau for He, settled more slowly for N_2, and settled slowest for SF_6 with the lowest end value. The shape of the concentration curves for the second breath were very similar to those for the first breath. The difference in end-expiratory concentration between He and SF_6 increased for the second breath.
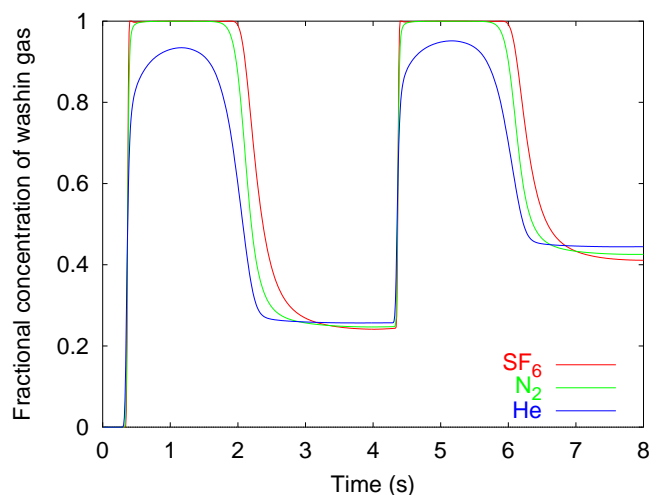
Figure 3.11: *Fractional concentration of washin gas at the end of the transitional bronchiole against time for* SF_6, N_2, *and* He *in the MBA-SCA model under standard conditions.*

3.5 Lumped parameter model of acinar gas mixing

The lumped parameter acinar (LPA) model takes information that describes the simulated inspiration, and uses this to predict the concentration at the end of the transitional bronchiole at the end of expiration (c_{EE}). The LPA model was calibrated using results from the MBA-SCA model. Simulations of multiple-breath washin tests were run in MBA-SCA models of three sizes, using gases of different diffusivities, and varying the breath durations and tidal volumes. The cross-sectional expansion was assumed to occur in the alveolar area only.

Each simulation had a set of parameters that characterised it. These were the pre-inspiratory volume of the MBA, the tidal volume delivered to the MBA, the breath duration, the gas diffusivity, and the amount of washin gas resident in the MBA model at the start and end of inspiration. The concentration at the end of the transitional bronchiole at the end of expiration was also recorded for each simulation.

3.5.1 Regression model for end-expiratory concentration

The predicted end-expired concentration (c_{EE}), the concentration at the end of the transitional bronchiole at the end of inspiration (c_{INSP}), and an estimate of the slope at the end of expiration (s_{EE}) were used to construct a hyperbolic curve of concentration against expired acinar volume. This curve then provided an estimate of the concentration at the end of the terminal bronchiole throughout expiration. The estimated concentration can be used as a boundary condition at the end of the terminal branches in conducting airway models.

Regression analysis was used to investigate the influence of the parameters on the end-expiratory concentration. The regression equation was derived using the regression analysis package in Microsoft Excel. A good fit to the data was found using a very simple relationship - namely, that the end-expiratory concentration was proportional to the steady-state concentration of the acinus plus a constant:

$$c_{EE} = 0.99775 * c_{SS} + 0.00163 \tag{3.22}$$

The steady-state concentration (c_{SS}) is the amount of washin gas contained by

the acinus at the end of inspiration, divided by its end-inspiratory volume. This relationship gave an R^2 value of 0.9997 and SE of 0.0055. Multiple-linear regression using the entire input parameter set and combinations and transformations of the parameters forced the R^2 value to be only slightly closer to 1.0.

Regression analysis was also used to derive two predictive equations for the slope at the end of expiration. The best fit to the MBA-SCA results was obtained using one regression equation for c_{SS} less than 0.975 (Equation (3.23)), and another for c_{SS} greater than or equal to 0.975 (Equation (3.24)).

$$
\begin{aligned}
s_{EE} = & - 5.76189 \times 10^{-4} - 1.04194 \times 10^{-3} * (1 - c_{SS}) \\
& - 1.28785 \times 10^{-3} * S - 3.83714 \times 10^{-8} * D \\
& + 5.70797 \times 10^{-4} * c_{SS} + 7.06053 \times 10^{-2} * (1 - c_{SS}) * S \\
& + 1.11318 \times 10^{-5} * D * (1 - c_{SS})
\end{aligned}
\tag{3.23}
$$

$$
\begin{aligned}
s_{EE} = & - 4.11438 \times 10^{-6} - 1.53560 \times 10^{-3} * (1 - c_{SS}) \\
& - 8.49893 \times 10^{-4} * S - 1.10238 \times 10^{-8} * D \\
& + 4.53066 \times 10^{-2} * (1 - c_{SS}) * S \\
& + 8.79236 \times 10^{-6} * D * (1 - c_{SS})
\end{aligned}
\tag{3.24}
$$

where S is the solubility in blood and D is the diffusion coefficient. The R^2 values were 0.9999 (SE 4.09×10^{-7}) and 0.9897 (SE 4.18×10^{-7}) for Equation (3.23) and Equation (3.24), respectively.

3.5.2 Boundary conditions for the LPA model

The boundary conditions at the entrance to the model (top of trachea) were the same as for the MBA-SCA model (see Section 3.3.3).

During inspiration, a flux boundary condition was specified at the end of the transitional bronchiole. This facilitated diffusion into and out of the LPA model. The boundary condition relied on an estimate of the gradient of concentration at the end of the transitional bronchiole. The gradient was estimated by assuming that

the concentration profile inside the LPA during inspiration could be described by a cubic Hermite function. Examination of Figure 3.8 and Figure 3.10 shows that this is a reasonable approximation: the concentration profile throughout inspiration was s-shaped.

3.5.3   Transfer of gas between the blood and alveoli

Transfer of gas between the alveolar gases and the blood was incorporated into the LPA model. The source term described in Section 3.3.1 for the alveolated airways was applied to the LPA model as a 'lumped' source term to account for gas transfer in all of the alveolated airways.

The initial LPA alveolar volume was assumed to be 73% of the total LPA volume. This proportion was the same as that for the MBA model described in Section 3.3.3. The alveolar volume was assumed to increase with LPA volume increase, and the duct volume was assumed to be constant. The volume increases were assumed to increase the length according to the cube-root relationship (Horsfield et al. 1971, Horsfield 1986). The alveolar surface area was then calculated at each time-step. Equation (3.12) for the alveolated airways then became Equation (3.25)

$$Q_b = \frac{Q_b \left(c_b - c_{SS}(t) \right) \lambda}{\gamma} \tag{3.25}$$

where $c_{SS}(t)$ is the mean gas concentration in the LPA model at the current time-step.

The lumped source term was used to estimate blood-gas transfer for the LPA model over each time-step.

3.5.4   Results from the lumped parameter model

A simple whole lung model consists of a SCA model with a single LPA model attached to the terminal branch. Results from simulations in the LPA-SCA model should mimic results from the MBA-SCA model.

Table 3.3 lists the error in area under the washin curves for simulations of O_2/N_2

under standard conditions over five breaths. That is, the error in the amount of expired washin gas predicted by the LPA-SCA model, as compared to the MBA-SCA model.

Breath	SF$_6$	O$_2$	He
1	-0.6789	0.1648	-0.0368
2	-0.0409	0.4052	0.9814
3	0.0079	0.3510	0.4601
4	-0.1637	0.1845	0.8740
5	-0.4436	-0.0449	0.2557

Table 3.3: *Percentage error in expired washin gas predicted by the LPA-SCA model over 5 breaths.*

The errors in expired washin gas were small (less than 1%), and did not increase with subsequent breaths.

The range of conditions over which the MBA-SCA model was tested were: breath durations from 1 - 4 s, tidal volumes from 200 - 1500 ml, and initial volumes from 40.31 to 194.00 mm^3. The range of conditions over which the LPA model is valid was tested by calculating the error in expired washin gas for simulations under extreme conditions. The error in expired washin gas between the MBA-SCA and the LPA-SCA model results are listed in Table 3.4.

Tidal volume (ml)	Total breath duration (s)	% error
500	4.0	0.99
1000	2.0	6.42
1000	4.0	0.16
1000	8.0	-2.39
1500	4.0	0.23

Table 3.4: *Error in expired washin gas predicted by the LPA-SCA model under extreme simulation conditions.*

The errors became large (greater than 1 %) when the total breath duration departed significantly from 4.0 s. Errors were small for the range of tidal volumes with total breath duration of 4.0 s.

The increase in error when breath length had an extreme value suggests that the LPA will produce results with more error as these breath lengths are approached. For the standard condition set (V_T = 1000 ml, breath length = 4 s) the error in expired washin gas was small (0.16 %).

3.6 Discussion

In this chapter a multi-branching model of a single pulmonary acinus (MBA model) was coupled to a symmetric conducting airway (SCA) model and used to simulate gas mixing. The MBA model was asymmetric with its numbers of branches and branch dimensions based on the experimental study of Haefeli-Bleuer & Weibel (1988). The MBA model incorporated airway asymmetry, evolution of gas from the blood, and expansion of the alveolar areas with constant duct cross-sectional areas. The SCA model was based on the symmetric model described by Weibel (1963) down to generation 15, and had a fixed geometry during simulations. A 'standard condition set' was defined to match the conditions set experimentally by Crawford et al. (1985) and in the models developed by Verbanck et al. (1991), Scherer et al. (1996), and Cruz et al. (1997). The standard conditions were a 2 s inspiration with a 1 L tidal volume, followed by a 2 s expiration. The flow was sinusoidal. Simulations were run in the MBA-SCA model over a wide range of conditions (SF_6, N_2, and He, breath durations from 1 - 4 s, tidal volumes from 200 - 1500 ml, initial volumes from 40.31 - 194.00 mm^3) and the results used to calibrate a lumped parameter acinar (LPA) model. The LPA model was in the form of a regression equation that was used to predict the concentration at the end of the transitional bronchiole during expiration.

The length and diameter of airways in the lungs change during ventilation. Model branch lengths changed as the cube root of volume change (Horsfield et al. 1971, Horsfield 1986), and the updated outer airway diameter was calculated accordingly. Paiva & Engel (1984) and Verbanck & Paiva (1990) maintained a constant ratio of duct to total cross-sectional area. That is, both duct and alveoli expanded uniformly in the radial direction. In contrast, Scherer et al. (1972) kept the duct area constant and expanded only the alveolar area. The ratio of duct to total cross-sectional area ($\frac{a}{A}$) in the conventional gas transport equation (see Section 3.3.1) effectively delays axial diffusion and therefore influences the simulated gas mixing. In Figure 3.6(b) S_n is plotted against breath number for 25 breaths for different relative radial expansions of the alveolar and duct areas. S_n was highest over the entire range of breaths for expansion of the alveolar region only, and lowest for expansion of the duct region only. The first-breath AME for alveolar expansion only was lower than the other two methods; the AME for duct only

expansion was the highest.

The S_n values resulting from assuming only radial alveolar expansion were lower than experimental values, and the AME was higher than experimental values. However, the results were closer to experiment than those obtained when using the other two assumptions. It therefore appears that it is most appropriate to assume that the duct does not expand radially, and that $\frac{a}{A}$ changes with volume. In support of this, Mercer, Laco & Crapo (1987) observed isotropic expansion of ducts and alveoli in rats at high lung volume, but observed progressive non-isotropy as lung volume decreased. At lower lung volumes the alveoli changed dimension at a faster rate.

The effect of respiratory airway asymmetry is shown in Figure 3.7(a) and (b). Incorporating asymmetry caused only small changes in the washin curves for the first two breaths in an O_2/N_2 simulation under standard conditions, but had a more significant effect on S_n. S_n was close to zero for the symmetric model (with no blood gas exchange) over 25 breaths, whereas incorporating asymmetry produced approximately constant S_n with values around $0.026 \cdot L^{-1}$ over the 25 breaths. The S_n values for the MBA-SCA model (without blood gas exchange) were caused by stratification that persisted through to the end of expiration: in Figure 3.8(d) the concentrations in the respiratory airways were lower than those in the conducting airways at the end of expiration. In contrast, the symmetric model quickly developed uniform concentrations throughout, and therefore did not produce a sloping alveolar plateau.

The effect of including evolution of gas from the blood was investigated in a symmetric model and in the MBA-SCA model. Results from these simulations are shown in Figure 3.7(a) and (b). Inclusion of the blood gas exchange term had virtually no effect on the washin curves over the first two breaths, and subsequently the S_n values for the first two breaths were very close to the models with no blood gas exchange term. For further breaths the S_n curves departed from those for the no-blood gas exchange simulations, with increasing values of S_n for both geometric models. The shape of the S_n curves were similar to those obtained by Scherer et al. (1996) and Cruz et al. (1997) for symmetric models with blood gas exchange terms.

Scherer et al. (1996) considered that airway asymmetry was not necessary to model a sloping alveolar plateau. Their results and the symmetric model (with blood gas

exchange) curve in Figure 3.7(b) show that sloping alveolar plateaus with values increasing with breath number can be produced by inclusion of a blood gas exchange term. However, the shape of the S_n curve is significantly different to the shape of the experimental curve (Crawford et al. 1985), and has far lower values than experimental. Scherer et al. (1996) and Huang et al. (2000) attempted to produce results closer to experimental by including an arbitrary parameter, β, in their models. β was used to reduce the model cross-sectional areas. The model lengths were increased to maintain the respiratory airway volumes described by Haefeli-Bleuer & Weibel (1988). Different values for β were required for modelling different gases. This approach produced S_n curves closer to experimental curves, but still with very different shapes: multiplication by β maintained the original curve shape, but increased all of the S_n values. It was shown in Section 3.4.3 that assumptions concerning the relative expansion of the alveoli and duct areas affected the S_n curves. Using the β multiplier to arbitrarily change the geometry of the symmetric model affects the model performance in a similar way: selecting the 'correct' value for β forces the symmetric model to develop a level of stratification that produces S_n values closer to experimental ones.

Cruz et al. (1997) compared results from a symmetric model and a seven-region model with mechanical variation among regions (7RLM) with and without a blood gas exchange term. They showed that although blood gas exchange was important, it was not necessary to include it to produce sloping alveolar plateaus. The results in Figure 3.7(b) also show the importance of blood gas exchange and respiratory airway asymmetry: the blood gas exchange term increased S_n for each breath, and the asymmetry 'shifted' the curve upwards relative to the symmetric model curve. The effect of the respiratory airway asymmetry was therefore similar to the effect of multiplying the symmetric respiratory airways by β (Scherer et al. 1996).

Further simulations were run in the MBA-SCA model under standard conditions with expansion of the alveoli only, and inclusion of a blood gas exchange term. The washin plots in Figure 3.9(a) show the characteristic three phases for each gas pair. Phase I was longest for SF_6 and shortest for He, phase II was steepest for He, and the end-expiratory concentration was lowest for SF_6 and highest for He. The difference in end-expiratory concentration for SF_6 and He increased for the second breath.

Longer phase I is characteristic of heavier gases: the diffusion front does not become

as 'smeared' for a heavy gas as it does for a light gas, so expired concentrations are close to the inspired concentration for a larger proportion of the expirate. The faster diffusion rate of the lightest gas (He) facilitated more complete mixing with resident gas, so the phase III slope was flatter than for the two heavier gases, and the end expiratory concentration was higher. These results are therefore consistent with theory.

One proposed explanation for the shape and duration of phase II is because of different transit times for the diffusion fronts that develop down different airway paths. In the MBA-SCA model, the airway paths to the transitional bronchioles are identical. The diffusion front develops outside of, or close to, the entrance to the acinus. Therefore phase II for the MBA-SCA model cannot be because of a dispersal of transit times. Phase II for the MBA-SCA model represents stratification: concentration differences are present at the end of inspiration.

The difference in phase III slope between the three gas pairs is apparent on the washin plots. The S_n are plotted over 25 breaths in Figure 3.9(b). The results qualitatively followed the experimental trend, such that S_n was highest for SF_6 and lowest for He over the entire 25 breaths. However, the values for S_n were far lower than experimental values (Crawford et al. 1985). This result was consistent with similar multi-branching models of the acinus (Paiva & Engel 1984, Engel & Paiva 1985). Engel & Paiva (1985) produced small S_n values using a multi-branching model, similar to the results obtained using the MBA-SCA model with no blood gas exchange term (Figure 3.7(b)).

The AME of the first breath for O_2/N_2 was 96.46%, compared with 98.7% for the multi-branching model of Engel & Paiva (1985). Both values were higher than experimental values, which are close to 90% for the first breath (Harris et al. 1987). The MBA-SCA model produced a smaller AME than the Engel & Paiva (1985) model because of 1) different geometries, 2) different assumptions about the relative alveolar and duct expansions, and 3) inclusion of a blood gas exchange term in the MBA-SCA model. Engel & Paiva (1985) based the geometry of their model on Hansen & Ampaya (1975) whereas the MBA-SCA model used the geometry of Haefeli-Bleuer & Weibel (1988). Engel & Paiva (1985) assumed that the ratio of duct to total cross-section was constant during branch expansion, whereas the MBA-SCA model expanded in the alveoli only, and Engel & Paiva (1985) did not consider gas exchange.

The LPA model was a regression equation that was derived using results from the MBA-SCA model. Under standard conditions over five breaths, the error in the sum of expired washin gas (from the MBA to the LPA model) was less than 1% for three different gas pairs (see Table 3.3 in Section 3.5). When the breath duration was halved the error increased to 6.42% for a single breath, and when the breath duration was doubled the error was -2.39% (see Table 3.4 in Section 3.5). The LPA model is therefore accurate for conditions close to standard, but is less reliable when the breath duration departs significantly from 4 s (2 s inspiration and 2 s expiration).

Because of the pleural pressure gradient and the weight of the lungs, the acinar tidal volumes are not necessarily identical for acini in different regions. Although the error in expired washin gas increased when the tidal volume was halved or doubled, the errors remained below 1%. The LPA model is therefore more accurate when tidal volume changes than when breath duration changes.

For all gas mixing simulations presented in this study the flow was assumed to be fit to half-sinusoids. Constant flow could be used, but this would require a seperate lumped parameter model. Although experimental results are often quoted as being obtained using constant flow (Crawford et al. 1985), in practise it is difficult to constrain constant flow during inspiration. The assumption of constant flow in the MBA-SCA model increases S_n by only a small amount.

3.6.1 Conclusions

The main results from the simulations in this chapter are: respiratory airway asymmetry has been shown to increase the normalised slope parameter S_n when compared with symmetric respiratory models under equivalent simulation conditions; evolution of gas from the blood increased S_n over multiple breaths; and, the assumption of constant duct area with expanding alveoli was shown to maximise S_n and minimise AME when compared with other relative expansion regimes. The LPA model is accurate at mimicking the behaviour of the MBA model when simulation conditions are close to the standard set; for changes in tidal volume the LPA model is still reasonably accurate, but the model is unreliable for large changes in breath duration (from 4 s).

Chapter 4

Gas mixing in a full lung model

4.1 Introduction

The inability of past lung models to satisfactorily simulate experimental gas mixing results indicates that one or more important effects are missing from the models. Respiratory airway asymmetry, uneven flow distribution, and blood-gas exchange have each been shown to affect the generation of a sloping alveolar plateau in multiple-breath washout curves (Paiva & Engel 1984, Cruz et al. 1997, Scherer et al. 1996). These three effects have not previously been combined in a single model to investigate their cumulative effect. In addition, the effect of the asymmetry of the conducting airways on alveolar slope generation has not previously been investigated in detail.

In Chapter 2 an asymmetric model of the conducting airways was developed that can be used as a computational mesh. In Chapter 3 a simplified model of the respiratory airways was developed for coupling with a conducting airway model, such that gas mixing can feasibly be simulated in the entire lung. In this chapter, a full lung model combining conducting airway asymmetry, representative respiratory airway asymmetry (in the form of a lumped parameter model), blood-gas exchange, and idealised pleural pressure effects is used to simulate gas mixing. The effect of each of these model characteristics on alveolar slope generation is isolated and examined.

A full lung model is constructed by coupling a lumped parameter acinar (LPA) model (described in Chapter 3) to each transitional bronchiole in the asymmetric

113

conducting airway (ACA) model (described in Chapter 2). Gas mixing is then simulated in the LPA-ACA model by setting appropriate boundary and initial conditions. A term is included in the LPA models to account for exchange of gas between the blood and air in the respiratory airways.

The effect of the pleural pressure gradient is investigated by applying idealised gradients of pre-inspiratory acinar volume, and by specifying idealised distributions of tidal volume allocation. The initial acinar volumes are distributed such that the largest acini are at the apex, and the smallest acini at the base; the smallest tidal volumes are supplied to acini at the apex and the largest to acini at the base.

Results from the LPA-ACA model are compared with experimental results from Crawford et al. (1985) and with results from other mathematical models (Verbanck & Paiva 1990, Scherer et al. 1996, Cruz et al. 1997). The gas mixing simulated by the LPA-ACA model shows a better fit to the experimental data than the other lung models. Most importantly, the results show that the asymmetry of the conducting airways is a major contributor to gas inhomogeneity and hence evolution of the sloping alveolar plateau.

4.2 Results from gas mixing in the LPA-ACA model

A LPA model was coupled to each terminal branch (29,445) in the ACA model. The respiratory airway volume was approximately 3.6 L, and the conducting airway volume was 103 ml. In the following sections, gas mixing is simulated in the coupled LPA-ACA model under a wide range of conditions.

4.2.1 Convergence tests for the LPA-ACA model

Table 4.1 lists the percentage errors resulting from decreasing time-step sizes in an LPA-ACA simulation of N_2 washout under standard conditions.

Based on the small errors resulting from decreasing the time-step size from 0.005 s to 0.002 s, a time-step size of 0.005 s was adopted for the LPA-ACA model simulations under standard conditions.

Simulating a single breath with a 2.0 s inspiration and 2.0 s expiration, with a time-step of 0.005 s, took approximately 30 minutes of computing time on a Silicon Graphics Origin 2000 computer, using four 250 MHz processors.

Δt (s)	$c_{ee}\%$	$washin\%$
0.02 - 0.01	-0.4293	-1.2132
0.01 - 0.05	-0.5615	-0.7409
0.005 - 0.002	-0.0789	-0.3176

Table 4.1: *Percentage difference in results for decreasing time-step sizes. The Δt column shows the time-step change, c_{ee} is the percentage difference in concentration at the mouth at the end of expiration, and washin is the percentage difference in the amount of expired washin gas.*

4.2.2   Uniform flow distribution in identical acini

The first simulations run in the model used acini with identical initial volume of 123.40 mm³, giving a total lung model volume of 3.7 L. Ventilation was distributed uniformly throughout the model. This meant that each acinar model expanded by an identical volume during inspiration. Results from simulations under the standard condition set for each of the three gas pairs are presented.

Figure 4.1 shows the concentration fields in the conducting airways of the LPA-ACA model at different times throughout the first breath for He washin simulation. The model had an initial fractional concentration of He of 1 (zero washin gas concentration at 0.0 s) in every branch. The inspired gas (with fractional concentration of 1) moved down the conducting airway tree towards the respiratory airways, from 0.1 s to 0.5 s. By 0.5 s only small regions of the conducting airways did not contain the washin gas at 100% concentration. By 2.0 s (end of inspiration) the concentration of washin gas in the peripheral airways was slightly less than 100% because of mixing with resident gas. During expiration (2.0 to 4.0 s) the unmixed washin gas was quickly eliminated from the model: by 2.4 s there were only small concentration differences throughout the conducting airway system.

(a) 0.0 s   (b) 0.1 s   (c) 0.2 s

(d) 0.3 s   (e) 0.4 s   (f) 0.5 s

(h) 2.0 s, end-insp   (i) 2.1 s   (j) 2.2 s

(k) 2.3 s   (l) 2.4 s   (m) 4.0 s, end-expn
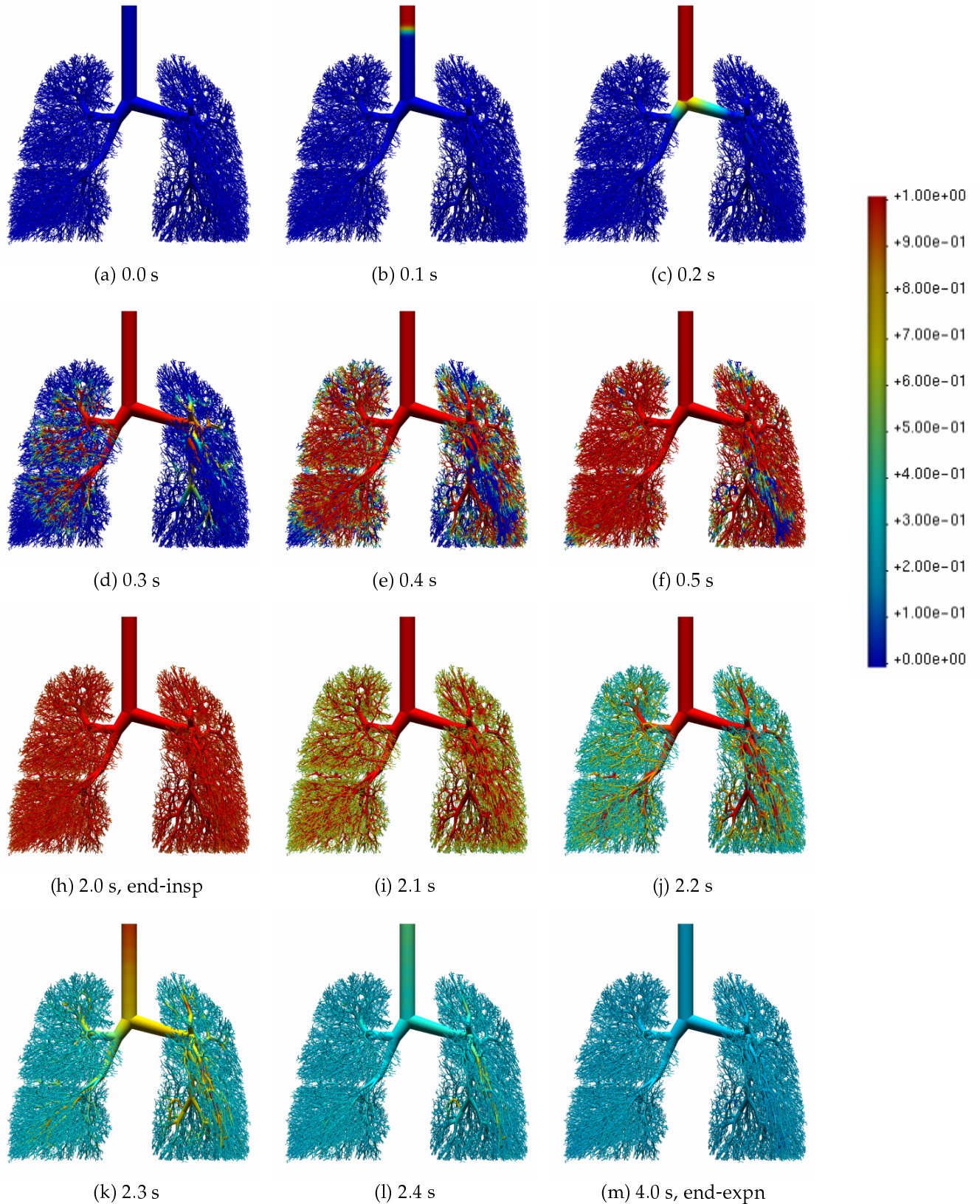
Figure 4.1: *Concentration fields for washin and resident gas in the conducting airways of the LPA-ACA model during a single breath of* He. *Red = 100% air, dark blue = 100%* He.

The washin curves in Figure 4.2(a) show the characteristic three phases for each gas pair. Phase I was longest, phase II was least steep, and phase III was steepest for SF_6 than for the other gases. The magnitude was similar from breath to breath for each individual gas. The end-expiratory concentration for the first breath was very similar for the three gas pairs. For the second breath the end-expiratory concentration was highest for He and lowest for SF_6, which was consistent with greater mixing for the more diffusive gas.
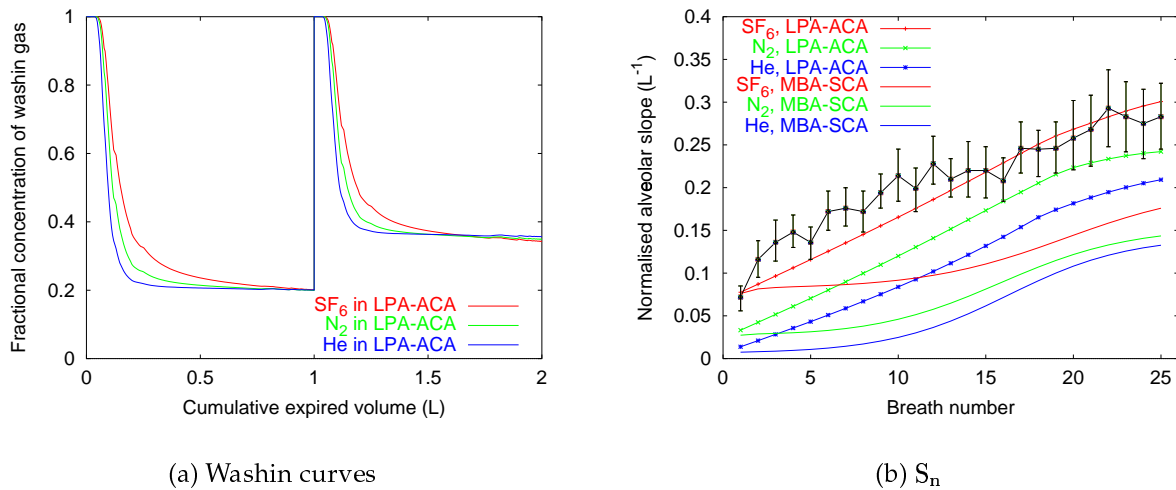
(a) Washin curves   (b) S_n

Figure 4.2: *Results from SF_6/N_2, O_2/N_2, and He/N_2 simulations under standard conditions in the LPA-ACA model. (a) Washin curves for the three gas pairs, over two breaths. (b) Comparison of S_n from the LPA-ACA model and the MBA-SCA model for the three gas pairs over 25 breaths, with experimental results $\pm SD$ from Crawford et al. (1985).*

Figure 4.2(b) plots S_n (the slope of the alveolar plateau in phase III divided by the mean expired concentration) against breath number for 25 breaths in the LPA-ACA model and the MBA-SCA model for the three gas pairs. Experimental mean values $\pm$ one SD are shown for N_2 mixing from Crawford et al. (1985).

S_n for the first breath was close for the MBA-SCA and LPA-ACA simulations for each gas. For the second and subsequent breaths S_n from the LPA-ACA simulations were higher than from the MBA-SCA model. The shape of the LPA-ACA curves were closer to the shape of the experimental curve than those from the MBA-SCA model: the LPA-ACA curves steadily increased in value over breaths 1 - 19, followed by a

slower rate of increase. This was similar to the experimental results for breaths 5 - 25, but the experimental results showed a faster increase in S_n for the initial breaths than produced by the LPA-ACA simulations. By breath 25, the S_n values for each gas pair in the MBA-SCA model were lower than S_n from He in the LPA-ACA model.

The first-breath S_n for SF_6 mixing from both the MBA-SCA and the LPA-ACA models was very close to the experimental first breath S_n for N_2.

(a) 1.0 and 2.0 s   (b) 3.0 and 4.0 s
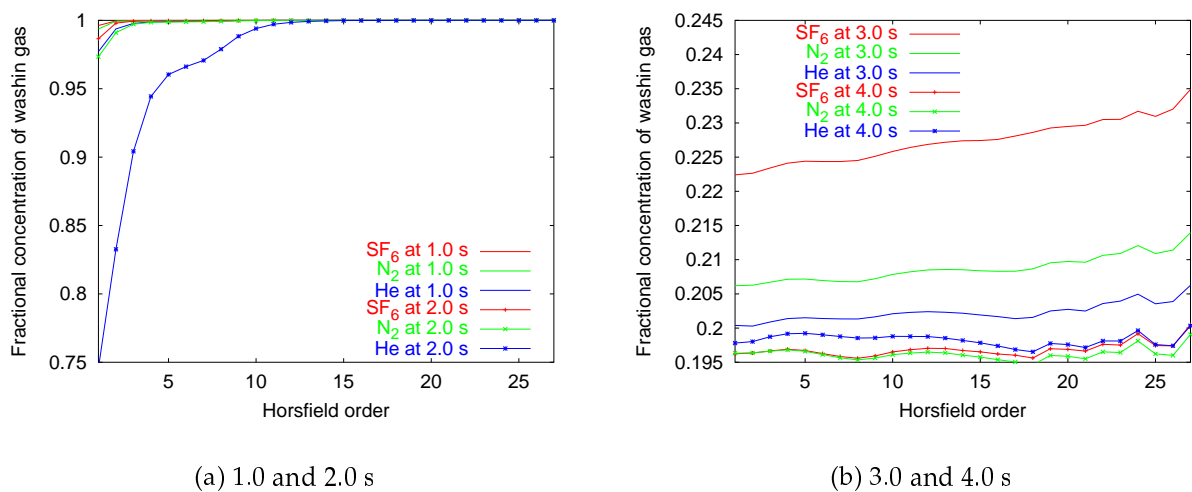
Figure 4.3: *Mean concentration in Horsfield orders 1-27 (conducting airways) in the LPA-ACA model under standard conditions. (a) Concentration against order at mid-way (1.0 s) and end of (2.0 s) inspiration. (b) Concentration against order at mid-way (3.0 s) and end of (4.0 s) expiration.*

In Figure 4.3(a) and (b) the concentration profiles down the conducting airways of the LPA-ACA model are plotted against Horsfield order: because the transitional bronchioles arise in a range of generations, plotting concentration against order rather than generation allows the transitional bronchiole concentrations to be viewed independently. Concentrations at mid-way through and at the end of inspiration are shown in Figure 4.3(a), and concentrations at mid-way through and at the end of expiration are shown in Figure 4.3(b).

By mid-way through inspiration (1.0 s) the mean transitional bronchiole concentration was close to 100% of the washin gas concentration for each gas pair. By the end of inspiration (2.0 s) the mean transitional bronchiole concentration for He had fallen to 75% of the washin gas concentration, compared with very little drop in

the mean transitional bronchiole concentration for SF_6. At the end of inspiration, the mean concentrations were at 100% of washin gas concentration down to order 13 for He, order 9 for N_2, and order 3 for SF_6.

By mid-way through expiration (3.0 s) the concentration of washin gas throughout the conducting airways of the LPA-ACA model had dropped significantly for each gas, with the largest drop for the He simulation. The concentrations fell further still to the end of expiration (4.0 s). Therefore, stratification was not obvious in the conducting airways of this model at the end of expiration for a single breath.

Figure 4.4 shows concentration results for N_2 mixing from the same simulation, but this time plotted against generation instead of order. Grouping the branches by generation places the LPA models at a range of generations down the tree, instead of grouped together in order 1 as was the case when plotting against Horsfield order. Washin gas concentration profiles are plotted at each 0.2 s interval throughout the breath.

During the first half of inspiration, shown in Figure 4.4(a), the concentration front (the interface between 100 % washin gas and mixed washin and resident gas) moved towards the peripheral conducting airways, but by mid-inspiration (1.0 s) the concentration front had not reached the most peripheral LPA models. That is, the LPA models coupled to transitional bronchioles down to generation 22 were being ventilated by washin gas at 100% of the inspiratory concentration by mid-inspiration. The concentration front only entered the LPA models attached to generations 23 to 27 at 1.2 s (Figure 4.4(b)). By the end of inspiration (2.0 s) the concentrations from generation 13 to 27 were lower than the inspired washin gas concentration.

Concentration fell quickly during expiration, with a steady-state reached by mid-expiration (3.0 s, Figure 4.4(c)). For the remainder of expiration the steady-state persisted, with concentrations in generations 1 to 17 at very similar values. Generations 25 to 27 had lower washin gas concentrations than the other generations throughout expiration. This reflected the smaller quantity of washin gas delivered to the LPA models attached to transitional bronchioles in these generations, because of their longer airway paths, on average, than acini in lower generations.
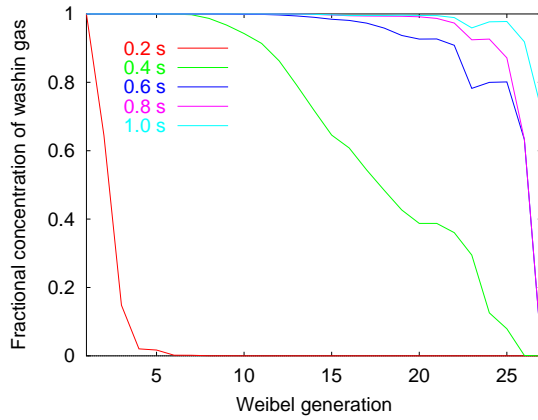
(a) First half of inspiration
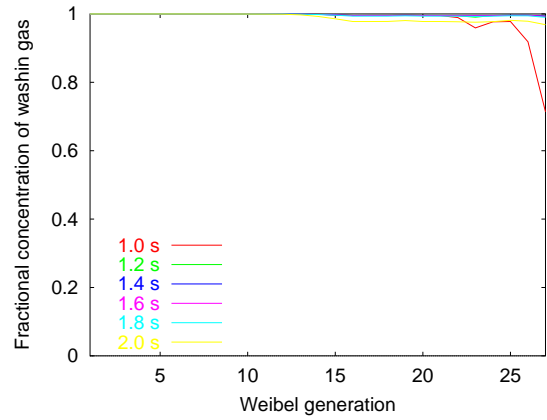
(b) Second half of inspiration
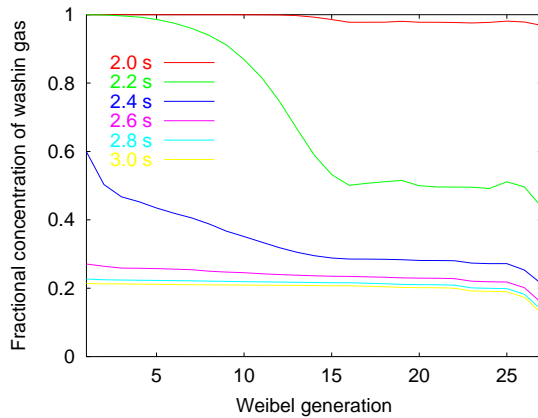
(c) First half of expiration
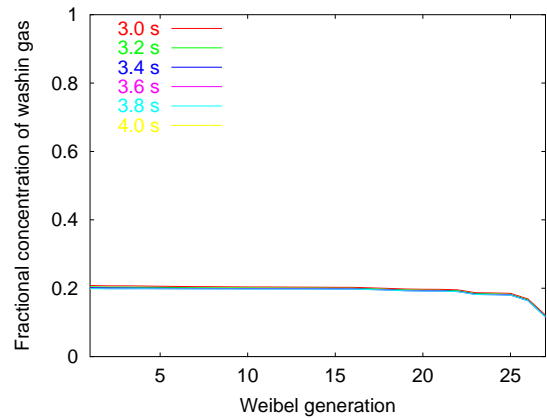
(d) Second half of expiration

Figure 4.4: *Mean concentration in Weibel generations 1-27 (conducting airways) in the LPA-ACA model under standard conditions for* N_2 *simulation. (a) Concentration against generation for the first half of inspiration, (b) concentration against generation for the second half of inspiration, (c) concentration against generation for the first half of expiration, (d) concentration against generation for the second half of expiration.*

Figure 4.5 shows S_n curves for O_2/N_2 mixing simulation in the LPA-ACA model under standard conditions, with and without a blood gas exchange term included.

For the MBA-SCA model results in Section 3.3.3, gas exchange was shown to significantly increase S_n over multiple breaths. For the LPA-ACA model, S_n increased regardless of the inclusion of the blood gas exchange term, but the rate of increase of S_n with breath number was not as fast when gas exchange was not included.

Figure 4.5: *Comparison of S_n curves from O_2/N_2 simulation in the LPA-ACA model under standard conditions, with and without a blood gas exchange term.*

Including the blood gas exchange term also caused the S_n curve to plateau, whereas the S_n curve continued to increase in value at an approximately constant rate when gas exchange was not included in the respiratory model.

Verbanck, Schuermans, van Muylem, Paiva, Noppen & Vincken (1997) used S_{acin} and S_{cond} to represent the contributions of the conductive airways and acinar airways, respectively, to the ventilation inhomogeneity reflected in the alveolar slopes of the N_2 MBW. S_{cond} was the normalised slope difference per unit of lung turnover (TO) in the part of the N_2 MBW where only conductive airways were assumed to contribute to the rate of rise of S_n. i.e. between TO = 1.5 and TO = 6.0. S_{acin} was determined by subtracting S_{cond} multiplied by the TO value of the first breath from the S_n value for the first breath. S_{cond} was calculated for the LPA-ACA model using S_n values between TO = 1.5 and TO = 5.0. This range was used because for higher TO the S_n curves generally began to approach a plateau.

S_{cond} for the LPA-ACA model without gas exchange was $0.0324 \cdot L^{-1}$, giving an S_{acin} of $0.0240 \cdot L^{-1}$. Applying the same analysis to the LPA-ACA model with gas exchange gave $S_{cond} = 0.0389 \cdot L^{-1}$ and $S_{acin} = 0.0228 \cdot L^{-1}$. Inclusion of the blood gas exchange term therefore produced a 5.0% decrease in S_{acin} and a 20.1% increase in S_{cond}.

Figure 4.6(a) compares washin curves for N_2 simulation from the LPA-ACA model using the regression equation predictions, and from perfect mixing assumed in the acini (ACA-perfect). Gas exchange was included for each model. The two models

produced similar phase I, but phase II for the ACA-perfect model was steeper than for the LPA-ACA model. The steep phase II indicates that there was less variation in acinar concentration during expiration from the ACA-perfect model. Phase III for the ACA-perfect model was distinctly linear, and much flatter than that produced by the LPA-ACA model. The end expiratory concentrations were close for each model over this first single breath.
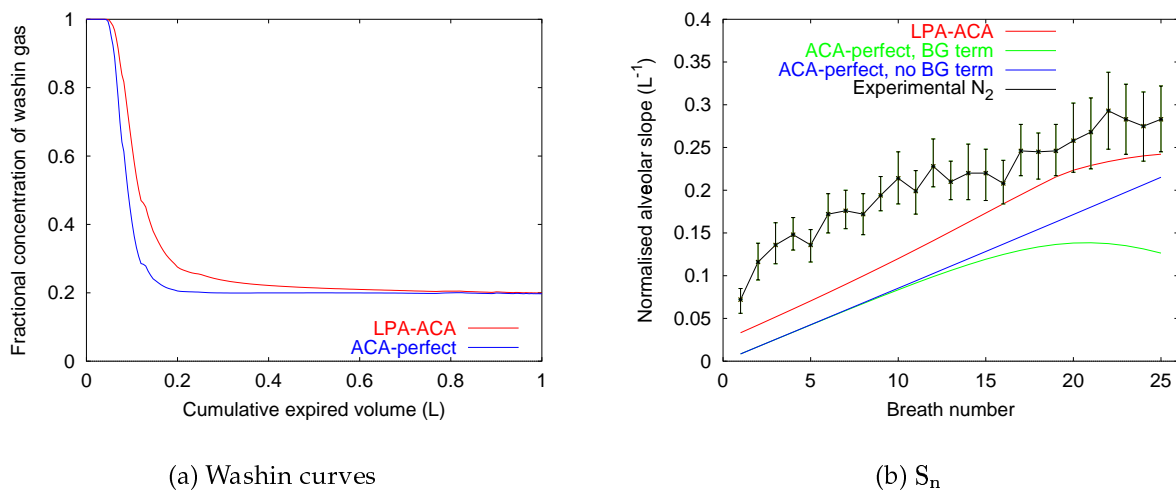
(a) Washin curves   (b) S_n

Figure 4.6: *Results from the LPA-ACA model under standard conditions assuming perfect mixing in the acini. (a) Comparison of N_2 washin curve with LPA-ACA model, (b) S_n curves from models assuming perfect mixing or using a regression equation, compared with experimental results from Crawford et al. (1985).*

Figure 4.6(b) compares O_2/N_2 S_n curves from the ACA-perfect model with and without gas exchange, with the LPA-ACA model using the regression equation predictions, and with results from Crawford et al. (1985) for N_2 over 25 breaths.

The ACA-perfect model S_n curve values were lower than the LPA-ACA model curve over the entire 25 breaths. The rate of increase of the LPA-ACA model curve decreased from breath 20, whereas the ACA-perfect curve with gas exchange peaked at breath 20 and then decreased for breaths 21 to 25. The difference between the LPA-ACA and ACA-perfect (with gas exchange) curves therefore increased with breath number. The ACA-perfect (without gas exchange) S_n curve was linear over the 25 breaths. For the first 10 breaths the gas exchange and non-gas exchange ACA-perfect curves had

identical values. From breaths 11 to 25 the gas exchange curve had lower values than the non-gas exchange curve.

S_{cond} and S_{acin} for the ACA-perfect model with gas exchange were 0.0261 and 0.0014 $\cdot L^{-1}$, respectively. For the ACA-perfect model without gas exchange S_{cond} was 0.0318 $\cdot L^{-1}$ and S_{acin} was -0.0001 $\cdot L^{-1}$.

Concentration against Horsfield order is compared in Figure 4.7 for O_2/N_2 mixing in the LPA-ACA model and in the ACA-perfect model for a single (first) breath. Figure 4.7(a) shows that the concentration profiles in the conducting airways for the two types of acinar model were the same throughout inspiration. During expiration (Figure 4.7(b)) both models displayed decreasing concentrations towards 'steady-state' values. At mid-way through expiration (3.0 s) the mean concentrations throughout the LPA-ACA model were significantly higher than those in the ACA-perfect, at every order. By the end of expiration (4.0 s) the concentration curves were closer in value for the two models, but the LPA-ACA curve values were still slightly higher than the ACA-perfect curve values.

(a) 1.0 and 2.0 s

(b) 3.0 and 4.0 s
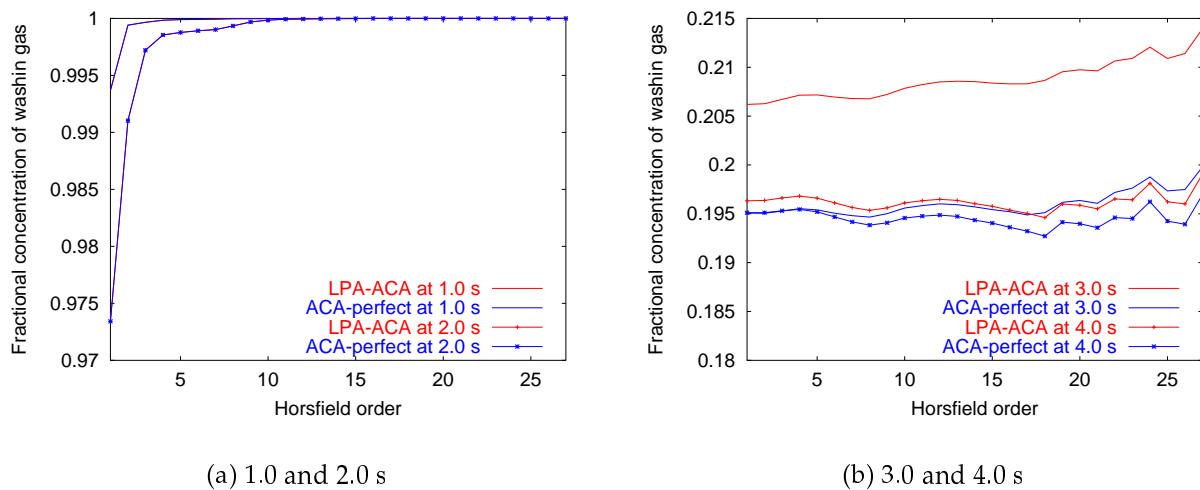
Figure 4.7: *Mean concentration in Horsfield orders 1-27 (conducting airways) in the ACA model under standard conditions, assuming perfect mixing in the acini. (a) Concentration against order at mid-way (1.0 s) and end of (2.0 s) inspiration. (b) Concentration against order at mid-way (3.0 s) and end of (4.0 s) expiration.*

In Figure 4.8(a) the S_n curve from the LPA-ACA model for N_2 over 25 breaths is compared with experimental results from Crawford et al. (1985) and model results from Verbanck & Paiva (1990), Scherer et al. (1996) and Cruz et al. (1997). The S_n values from the LPA-ACA model for the first two breaths were very close to the values from Verbanck & Paiva (1990). The LPA-ACA results were closer to the experimental first breath range than values from Scherer et al. (1996) and Cruz et al. (1997). The S_n values from the 7RLM were higher than those from the LPA-ACA model for breaths 4-25. The 7RLM results were within $\pm$ one SD of the experimental means from breath 13-25, whereas the LPA-ACA model results were within this range from breath 16-25. The SRLM (Scherer et al. 1996) and the Verbanck & Paiva (1990) model did not produce S_n values within $\pm$ one SD of the mean experimental values for any portion of the curves.

Figure 4.8(b) shows the difference in S_n values for SF_6 and He (ΔS_n) for the LPA-ACA model with uniform sizes and acinar V_T (V_{Ta}), compared with experimental results (Crawford et al. 1985). The LPA-ACA results were within $\pm$ one SD of experimental for breath 4 - 12. The LPA-ACA results did not have a sharp increase in ΔS_n over the first three breaths as was seen in the experimental results. For breaths 12 - 14, ΔS_n decreased experimentally, whereas the LPA-ACA curve increased slightly.

(a) S_n (b) ΔS_n
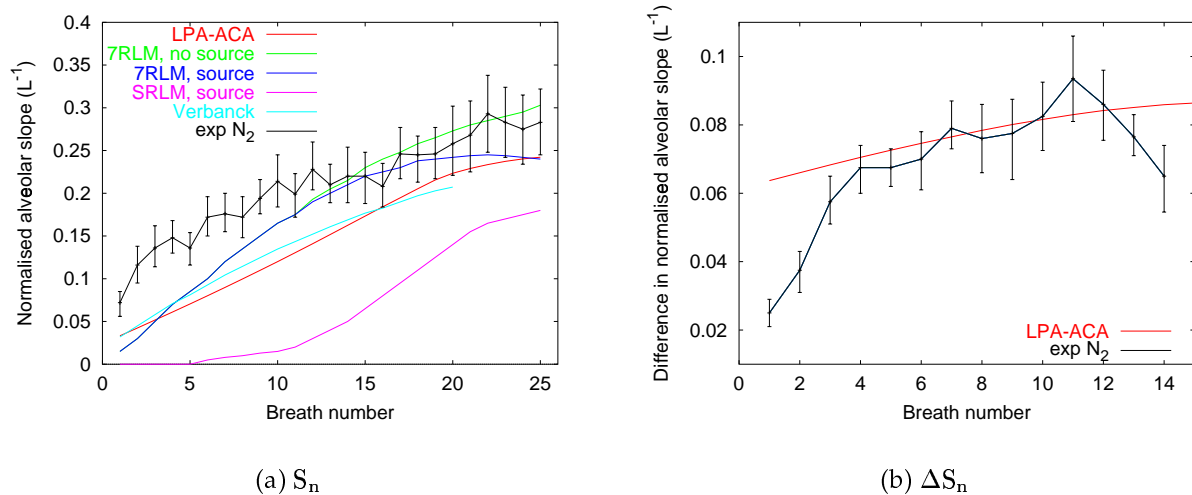
Figure 4.8: *(a) Comparison of S_n from O_2/N_2 mixing in the LPA-ACA model with results from Verbanck and Paiva (1990), Cruz (1997), Scherer et al. (1996), and experimental results (Crawford et al. 1985), (b) comparison of ΔS_n from the LPA-ACA model under standard conditions with experimental results (Crawford et al. 1985).*

4.2.3 Uniform flow distribution in acini with distributed volumes

To investigate the effect of gravity-induced acinar size on evolution of the sloping alveolar plateau, simulations were run using uniform flow distribution in a model with linearly distributed acinar volumes. The minimum, maximum, and mean volume of the LPA models were specified. The volumes were distributed with distance from the base. The maximum and minimum values were adjusted to ensure that the average size of an acinus in the model was the same as that initially specified. The base had the smallest acinar volumes, and the apex the largest. This distribution idealised the gravity-induced distribution that would be present in an upright subject, but it also allowed the effect of volume distributions to be investigated without the influence of non-uniformly distributed flow. Because flow was distributed uniformly, the LPA models changed size in proportion to their volume: the largest acini received the most tidal volume, and the smallest the least. Three size distributions were used for simulation: 111 - 140, 93 - 164, and 62 - 206 mm^3. The mean LPA volume in all cases was 123.40 mm^3, giving a total model volume of 3.7 L.

S_n curves from the three size distributions are compared with results from the LPA-ACA model with identical acini and uniform flow distribution, and experimental results from Crawford et al. (1985) in Figure 4.9(a). Introducing a small size distribution (111 - 140 mm^3) increased S_n by a small amount over the range of simulated breaths. Increasing the size range to 93 - 164 mm^3 increased the S_n values again by a small amount. The S_n curves for the first two size distributions were very close in value to the results for identical LPA sizes for breaths 1 - 5. The difference in S_n values from the identical LPA size curve increased for subsequent breaths. The S_n curves from these two size distributions had shapes similar to the identical LPA size curve, with increasing S_n values for breaths 1 - 19, followed by a slower increase in S_n as a plateau was approached. For the third size distribution (62 - 206 mm^3) S_n for the first breath was larger than for the other distributions. The increase in S_n from breath 1 - 20 was faster than for the other size distributions, and the curve plateaued at a higher value. The simulated S_n curve was within $\pm$ one SD of the experimental mean values for breaths 11 - 25, compared with breaths 16 - 25 for the other three cases.

Figure 4.9(b) compares ΔS_n from the three size distributions with the uniform size

(a) S_n (b) ΔS_n
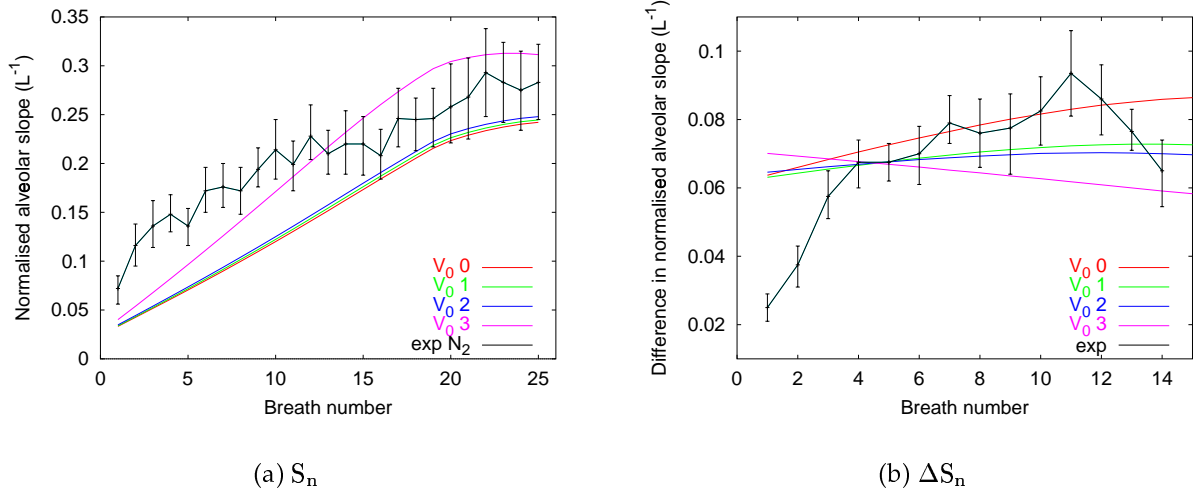
Figure 4.9: *(a) Comparison of S_n from O_2/N_2 mixing in the LPA-ACA model using distributed acinar sizes, with experimental results (Crawford et al. 1985). (b) Difference between S_n for SF_6 and He for distributed acinar volumes, compared with experimental results (Crawford et al. 1985).*

model and Crawford et al. (1985) results. The effect of the first two size distributions on S_n was small, but their effect on ΔS_n was more significant: introducing a small size distribution decreased ΔS_n from the uniform model values. The uniform size model had increasing ΔS_n with breath number, but the first two size distributions quickly reached a plateau followed by a very small decrease in value for breaths 13 - 15. The ΔS_n results for the largest size distribution were different to the other distribution results: instead of increasing ΔS_n values, this distribution showed decreasing ΔS_n with breath number. ΔS_n for the first breath was larger than for the other cases.

S_{cond} and S_{acin} values for the three distributions are listed in Table 4.2, with values from the LPA-ACA model with identical initial LPA volumes for comparison.

Distribution	$S_{cond}(\cdot L^{-1})$	$S_{acin}(\cdot L^{-1})$
Identical	0.0389	0.0228
111 - 140 mm^3	0.0393	0.0231
93 - 164 mm^3	0.0399	0.0240
62 - 206 mm^3	0.0547	0.0254

Table 4.2: *S_{cond} and S_{acin} calculated for the LPA-ACA model with identical initial LPA volumes, and linear initial volume distributions.*

4.2.4   Distributed acinar tidal volumes in identical acini

To investigate the effect of gravity induced flow distribution, simulations were performed in the LPA-ACA model with acini of identical initial size, but with acinar V_T (V_{Ta}) distributed linearly from the apex to the base. That is, acini near the apex received the smallest V_{Ta} and acini near the base received the largest V_{Ta}. The distribution of V_{Ta} was calculated by first defining a minimum and maximum local V_T. The minimum and maximum values were adjusted to ensure that the correct total volume change was achieved. Three V_{Ta} ranges were used : 30.88 - 37.74, 25.73 - 44.60, and 17.16 - 54.90 mm^3. This can be compared with the mean V_{Ta} (for V_T = 1 L) of 34.31 mm^3.

The S_n curves resulting from the V_{Ta} distributions are compared with the LPA-ACA model with uniform flow and experimental results from Crawford et al. (1985) in Figure 4.10(a). Introducing a small V_{Ta} distribution (30.88 - 37.74 mm^3) increased S_n slightly over the range of breaths. The second V_{Ta} distribution (25.73 to 44.60 mm^3) caused the S_n values to increase significantly over the entire 25 breaths, relative to the first distribution curve. The values for the first 12 breaths were closer to the experimental values than for the first distribution, and for breaths 13 - 25 the S_n results were within one SD of the experimental mean values.

(a) S_n (b) ΔS_n
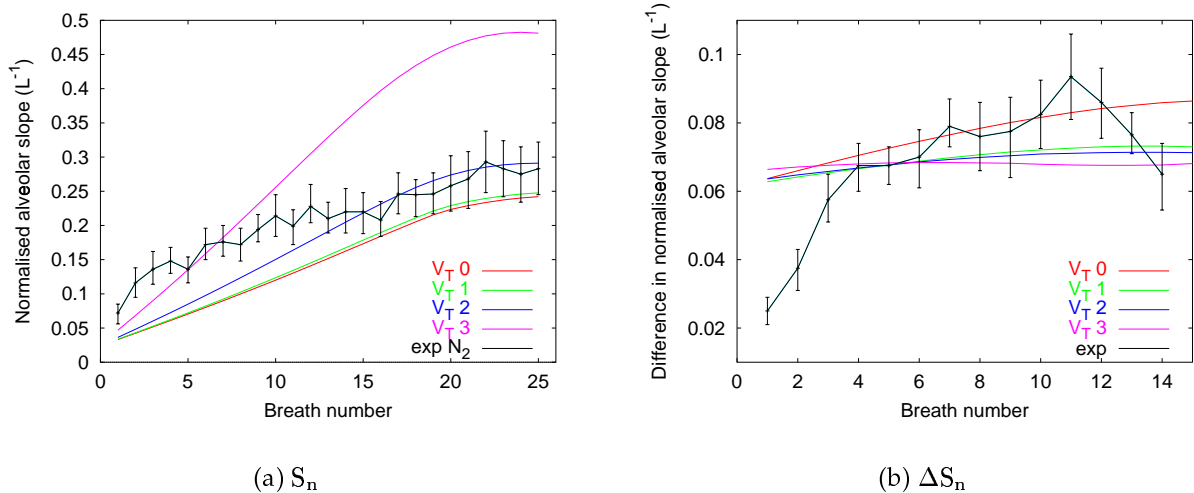
Figure 4.10: *(a) Comparison of S_n from O_2/N_2 mixing in the LPA-ACA model using distributed acinar tidal volumes with experimental results (Crawford et al. 1985). (b) Difference between S_n for SF_6 and He for distributed acinar tidal volumes, compared with experimental results (Crawford et al. 1985).*

The third V_{Ta} distribution (17.16 to 54.90 mm^3) caused large increases in S_n over the entire 25 breaths. The values from breath 8 were larger than the experimental values.

ΔS_n for the V_{Ta} distributions are compared with uniform tidal volumes and experimental results (Crawford et al. 1985) in Figure 4.10(b). All three distributions caused ΔS_n to decrease, except for the first two breaths with the widest distribution: these values were higher than for uniform flow.

S_{cond} and S_{acin} for the three V_{Ta} distributions are listed in Table 4.3. For V_{Ta} = 17.16 to 54.90 mm^3, S_{cond} increased by 122.88% and S_{acin} increased by 3.51%, relative to the identical V_{Ta} results.

Range (mm^3)	$S_{cond}(\cdot L^{-1})$	$S_{acin}(\cdot L^{-1})$
34.31	0.0389	0.0228
30.88 to 37.74	0.0401	0.0228
25.73 to 44.60	0.0494	0.0230
17.16 to 54.90	0.0867	0.0236

Table 4.3: S_{cond} *and* S_{acin} *calculated for the LPA-ACA model with identical LPA tidal volumes, and linear LPA tidal volume distributions.*

4.2.5   Distributed tidal volumes and initial volumes

The effect of combined distributions of initial acinar volumes and V_{Ta} was investigated by simulating combinations of linear distributions. Nine combined distributions were used: the first set used distributed V_{Ta} of 30.88 - 37.74 mm^3 for three initial volume distributions (111 - 140, 93 - 164, and 62 - 206 mm^3); the second set applied a V_{Ta} range of 25.73 - 44.60 mm^3 to the three volume distributions, and; the final set applied a V_{Ta} range of 17.16 to 54.90 mm^3. The mean LPA volume was 123.40 mm^3, giving a total volume of 3.7 L.

Figure 4.11 compares results from gas mixing under standard conditions for the first three combined distributions with experimental results from Crawford et al. (1985) for N_2 mixing, the results from the LPA-ACA model with uniform flow and identical initial LPA models, and the results from the LPA-ACA model with identical initial LPA models and V_{Ta} range 30.88 to 37.74 mm^3. S_n curves are shown in Figure 4.11(a) and ΔS_n curves in Figure 4.11(b).
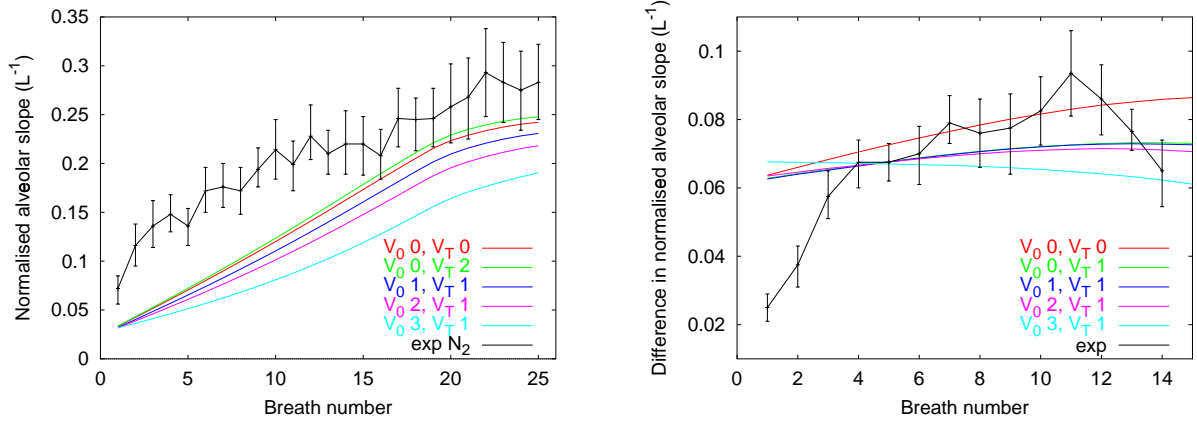
(a) S_n for acinar V_T range 30.88 to 37.74 mm^3

(b) ΔS_n for acinar V_T range 30.88 to 37.74 mm^3

Figure 4.11: *Comparison of S_n and ΔS_n from O_2/N_2 mixing in the LPA-ACA model using distributed acinar tidal volumes and acinar sizes with experimental results (Crawford et al. 1985). Acinar V_T range 30.88 to 37.74 mm^3, with initial volume ranges 111 - 140 mm^3, 93 - 164 mm^3, and 62 - 206 mm^3. (a) S_n for acinar V_T range 30.88 to 37.74 mm^3, (b) ΔS_n for acinar V_T range 30.88 to 37.74 mm^3.*

Applying increasing ranges of LPA volumes decreased S_n over the 25 breaths shown in Figure 4.11(a). None of the distributions produced S_n curves within $\pm$ one SD of the experimental means. All curves began to plateau around breath 20.

ΔS_n increased for the first breath for the widest V_{Ta} distribution. The ΔS_n values for this simulation were smaller than for the uniform flow-uniform initial volume simulation for breaths 3 to 25, and the curve had a negative slope. The ΔS_n curves for the other two combined distributions were very close to the curve for identical initial volumes with V_{Ta} range 30.88 to 37.74 mm^3.

The next set of distributions used a V_{Ta} range of 25.73 to 44.60 mm^3 over the range of initial LPA volumes. In Figure 4.12(a) increasing the initial volume range increased S_n over the 25 breaths for the initial acinar volume range of 111 to 140 mm^3 and acinar V_T range 25.73 to 44.60 mm^3, relative to the S_n curve for uniform initial volumes and uniform flow. The S_n curve for this simulation lay between the curves for uniform flow and initial volumes, and V_{Ta} 25.73 to 44.60 mm^3 with uniform initial volumes. That is, applying the V_{Ta} distribution caused the S_n values to increase, but when combined with the initial volume distribution the S_n values decreased. S_n for breaths 14 to 25 for

initial volume range 111 to 140 mm^3 were within $\pm$ one SD of the experimental mean values, with breaths 16 to 25 very close to the experimental means. The ΔS_n curves for the initial volume distributions were close in value to the curve for identical initial volumes and distributed V_{Ta}. For the widest initial volume range, the first breath value was larger than for the other simulations, and the curve had a negative slope. This was the opposite trend to the experimental data.
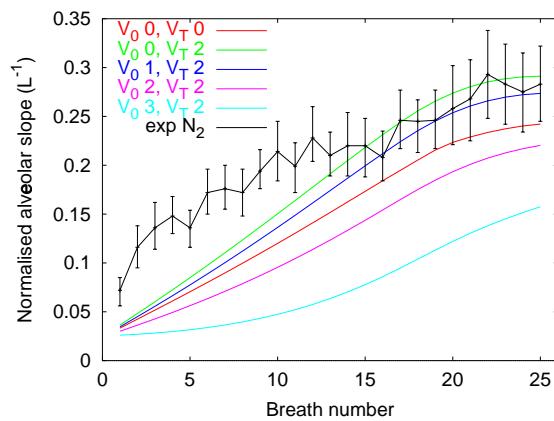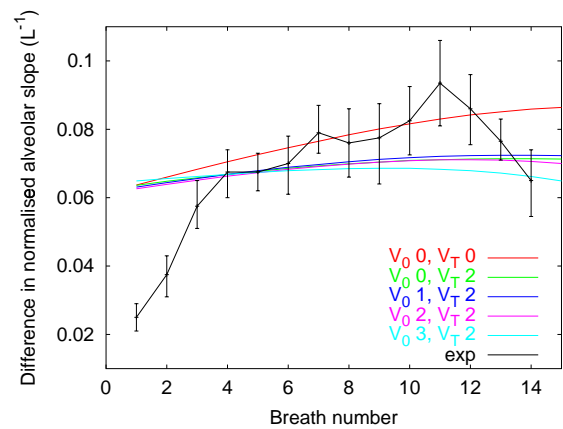
(a) S_n for acinar V_T range 25.73 to 44.60 mm^3 (b) ΔS_n for acinar V_T range 25.73 to 44.60 mm^3

Figure 4.12: *Comparison of S_n and ΔS_n from O_2/N_2 mixing in the LPA-ACA model using distributed acinar tidal volumes and acinar sizes with experimental results (Crawford et al. 1985). (a) S_n for acinar V_T range 25.73 to 44.60 mm^3, (b) ΔS_n for acinar V_T range 25.73 to 44.60 mm^3.*

Results from the final set of combined distributions are shown in Figure 4.13(a) for S_n, and Figure 4.13(b) for ΔS_n. As occurred for the other two flow multiplier ranges, as the volume distribution increased the S_n values decreased. For the most extreme volume distribution the S_n curve had values lower than the curve for uniform flow with identical initial volumes. Results for ΔS_n were also similar to the previous two flow multiplier ranges, such that the curves from the first two volume distributions were close to the model having identical initial volumes, and the widest volume distribution had a negative slope.

Table 4.4 lists S_{cond} and S_{acin} for the LPA-ACA model with combined distributions. S_{cond} decreased for each increase in initial volume range. S_{acin} increased with initial

volume range for V_{Ta} range 30.88 to 37.74 mm^3. S_{acin} decreased for the other two tidal volume ranges with increasing initial volume range.
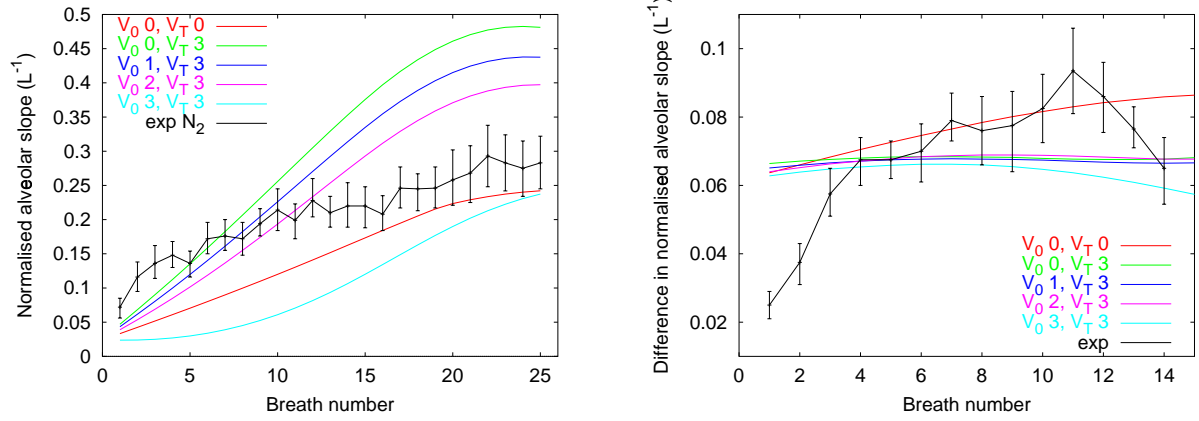
(a) S_n for acinar V_T range 17.16 to 54.90 mm^3

(b) ΔS_n for acinar V_T range 17.16 to 54.90 mm^3

Figure 4.13: *Comparison of S_n and ΔS_n from O_2/N_2 mixing in the LPA-ACA model using distributed acinar tidal volumes and acinar sizes with experimental results (Crawford et al. 1985). (a) S_n for acinar V_T range 17.16 to 54.90 mm^3, (b) ΔS_n for acinar V_T range 17.16 to 54.90 mm^3.*

V_0 range (mm^3)	V_T range (mm^3)	$S_{cond}(\cdot L^{-1})$	$S_{acin}(\cdot L^{-1})$
123.40	30.88 - 37.74	0.0401	0.0228
111 - 140	30.88 - 37.74	0.0365	0.0223
93 - 164	30.88 - 37.74	0.0338	0.0226
62 - 206	30.88 - 37.74	0.0276	0.0242
123.40	25.73 - 44.60	0.0494	0.0230
111 - 140	25.73 - 44.60	0.0458	0.0222
93 - 164	25.73 - 44.60	0.0347	0.0207
62 - 206	25.73 - 44.60	0.0215	0.0203
123.40	17.16 - 54.90	0.0867	0.0236
111 - 140	17.16 - 54.90	0.0784	0.0222
93 - 164	17.16 - 54.90	0.0713	0.0196
62 - 206	17.16 - 54.90	0.0406	0.0127

Table 4.4: *S_{cond} and S_{acin} calculated for the LPA-ACA model for combined distributed initial LPA volumes, and distributed acinar tidal volumes.*

4.2.6 Bohr dead space and alveolar mixing efficiency

The Bohr dead space ($V_D B$) is an estimate of the volume of lung which does not eliminate subject gas (see Section 3.2.4). Figure 4.14 plots $V_D B$ against breath number for a subset of the LPA-ACA simulations presented in the previous sections. The resulting $V_D B$ curves are compared with experimental results from Crawford et al. (1985).

Figure 4.14: *Bohr dead space for* N_2 *mixing in the LPA-ACA model compared with Crawford et al. (1985).*

The mean volume of the upper airways - including the mouth down to the carina - has been estimated to be about 80 ml (Horsfield & Cumming 1968). Subtracting the volume of the trachea in the LPA-ACA model gives close to 60 ml as an estimate of the upper airways proximal to the trachea. This volume was subtracted from the experimental $V_D B$ curve to enable comparison with the simulated results, where the extra-thoracic airways were not included.

The $V_D B$ curves for the simulated results had similar shapes to the S_n curves seen previously. The experimental results had a 41.83% increase in $V_D B$ from the first to the 25th breath, whereas the LPA-ACA model with uniform flow distribution and identical initial acinar volumes had a 72.96% increase in $V_D B$ over the same range.

Figure 4.15 plots the alveolar mixing efficiencies calculated for the LPA-ACA model with identical initial LPA volumes and uniform flow, the small distribution of initial volumes (111 - 140 mm^3), the small distribution of V_{Ta} (30.88 to 37.74 mm^3), the combination of the small initial volume

Figure 4.15: *Alveolar mixing efficiency for* N_2 *mixing in the LPA-ACA model compared with Crawford et al. (1989).*

and V_{Ta} distributions, and experimental results from Crawford, Cotton, Paiva & Engel (1989).

The simulated AME curves all had values higher than the experimental values. The simulated curves followed the trend of the experimental curve, in that AME decreased with decreasing fraction of N_2 remaining in the lungs.

4.2.7   Distributing the pulmonary circulation

Gas transfer between the alveolar gas and the blood is partly determined by the ventilation-perfusion ratio. Studies have shown that the blood flow to the upper parts of the erect lung is less than to the basal regions (West 1962). Cruz et al. (1997) used distributed perfusion in their seven region lung model, such that the regions near the base of the model were perfused with a larger volume of blood than those near the apex. To investigate the effect of distributing the pulmonary circulation, a linear distribution of blood flow was applied to the LPA-ACA model.

Figure 4.16 shows S_n results from the LPA-ACA model with identical initial LPA volumes and V_{Ta} range 17.16 to 54.90 mm^3, and initial LPA volume distribution 111 to 140 mm^3 with V_{Ta} range 17.16 to 54.90 mm^3.

The total pulmonary circulation for all simulations was assumed to be 100 cm$^3 \cdot$ s^{-1}. For the first simulations with even distribution of blood to the alveoli, the circulation within a single LPA model was proportional to the ratio of LPA alveolar surface area to total model alveolar surface area. For linearly distributed circulation, the acini near the top of the model received the least blood (10% of the mean circulation) and those near the bottom received the most (170% of the mean circulation).

Distributing the pulmonary circulation had little effect on S_n. Distributing the circulation in the uniform initial volume model caused S_n to be slightly smaller from breath 16 onwards than when the circulation was uniform. A similar result was seen for the distributed initial volume model. Therefore, S_n does not appear to be sensitive to the distribution of the pulmonary circulation for these gases with very small solubilities. For gases with higher solubility in blood (such as O_2) the distribution of the pulmonary circulation could have a larger effect on S_n.
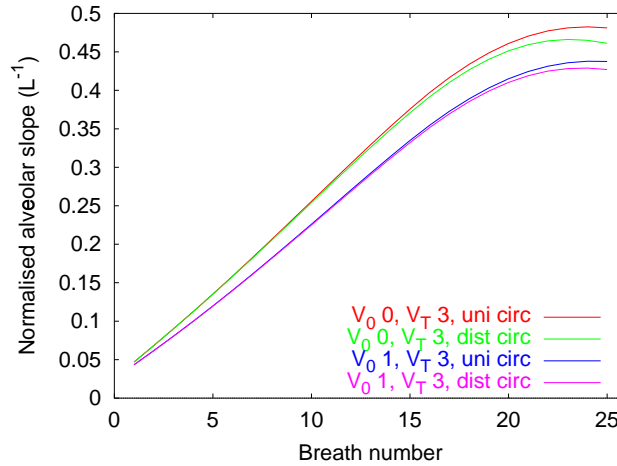
Figure 4.16: *Comparison of S_n from N_2 mixing in the LPA-ACA model with 1) identical initial LPA volumes and tidal volume range 17.16 to 54.90 mm^3, and 2) initial LPA volume distribution 111 to 140 mm^3 with tidal volume range 17.16 to 54.90 mm^3, both with a uniform and a distributed pulmonary circulation.*

4.3 Discussion

The simulations presented in this chapter were run in a full lung model comprising an asymmetric conducting airway system and lumped parameter acini. The lumped parameter acinar (LPA) models were based on a respiratory airway model with airway asymmetry. The influence of conducting and respiratory airway asymmetry, blood-gas exchange, and the pleural pressure gradient were investigated. A 'standard' condition set of V_T 1 L and total breath duration 4 s was used to maintain consistency with experimental results (Crawford et al. 1985) and comparison models (Verbanck & Paiva 1990, Scherer et al. 1996, Cruz et al. 1997)

Calibration of mathematical models of gas mixing has traditionally been against experimentally obtained washin/washout curves and calculated normalised alveolar slopes (S_n), alveolar mixing efficiencies (AME), and various dead spaces. The earlier models focused on qualitatively reproducing washin/washout curves with their characteristic three phases, whereas later models used analysis of model-based S_n values to hypothesise on the basis of the sloping alveolar plateau in phase III. On the basis of these analyses, the sloping alveolar plateau and gas mixing inefficiencies have generally been explained by Convection-Dependent Inhomogeneities (CDI) and

Diffusion- and Convection-Dependent Inhomogeneities (DCDI). These mechanisms are described in full in Section 3.2.4. Analysis of results from the LPA-ACA model under different ventilation strategies confirms the effect of CDI and DCDI on the magnitude of S_n. The results also confirm the importance of incorporating asymmetry in models of the conducting airways, and the necessity of including evolution of resident gas from the blood. The results indicate that an accurate description of the mechanics of the lungs during breathing will be essential to accurately simulate S_n, dead space, and mixing efficiencies over multiple breath washouts.

Crawford et al. (1985) observed an increase in ΔS_n for SF_6 and He over only the first five breaths in multiple breath washout experiments. ΔS_n was approximately constant for subsequent breaths. S_n and $V_D B$ increased progressively in multiple breaths, with the increase in S_n the most significant. They concluded that the increase in S_n after the fifth breath during a multiple breath N_2 washout was diffusion independent and may constitute a sensitive index of CDI. This conclusion was based on comparison of the experimental results with results from analysis by Paiva, van Muylem & Engel (1982). Paiva et al. (1982) found that beyond the third simulated breath in a two-trumpet model, the concentration difference for SF_6 and He (normalised by the difference between inspired and resident gas concentrations) remained constant. This result was explained on the basis of development of a steady-state representing a balance between convection, diffusion, and progressive dilution of N_2 in each trumpet. Results from simulations in the multi-branching acinar model of Paiva & Engel (1984) predicted that S_n reached greater than 95% of its asymptotic value within the first four breaths. Verbanck & Paiva (1990) also showed this result for gas mixing simulation in a model consisting of eight coupled multi-branching acini. From these results Verbanck & Paiva (1990) concluded that the DCDI contribution to S_n could be considered breath independent after breath 5. The results from the MBA-SCA model with gas exchange, and the LPA-ACA model with uniform flow and identical initial LPA volumes show that S_n increases over more than the first four breaths when 'classical' CDI is not prescribed.

Paiva et al. (1982), Paiva & Engel (1984), and Verbanck & Paiva (1990) did not include a source term to account for gas transfer between alveolar gas and the blood. For certain experimental conditions neglecting gas transfer would be appropriate -

such as for the single breath SF_6 and He breaths measured by Lauzon, Prisk, Elliott, Verbanck, Paiva & West (1997).

For the Lauzon et al. (1997) experiments the subject inhaled single breaths of the washin gas, and expired concentration was then measured during expiration. Multiple pre-conditioning breaths were not used to equilibrate the subject gas in the alveolar gas and blood. In contrast, Crawford et al. (1985) required the subjects to breath multiple breaths of the subject gas mixture before switching to breathing room air (in the case of SF_6 and He) or pure oxygen (in the case of N_2). For the single breath experiments, there would be no evolution of washin gas from the blood hence neglecting the gas exchange source term would be appropriate. However, for the Crawford et al. (1985) experiments the evolution of subject gas from the blood has been shown to be significant.

Scherer et al. (1996) was the first to show the importance of including gas exchange when simulating S_n. Cruz et al. (1997) compared S_n curves from including and neglecting gas exchange in a seven-region lung model (7RLM) with volume changes described by a third order polynomial. They also reproduced the results of Scherer et al. (1996) by simulating gas mixing using a single region of their 7RLM. Cruz et al. (1997) showed that gas exchange had essentially no effect on the S_n curve for the first 12 breaths in their model, but had a large effect on subsequent breaths: their simulations showed decreasing S_n values from breath 23 onwards, which was different to the experimental results of Crawford et al. (1985). In contrast, results from the MBA-SCA and LPA-ACA model did not have decreasing S_n values when gas exchange was included. Given that the simulated S_n from including gas exchange in a model with a symmetric respiratory airway structure produced larger S_n values than results from an asymmetric model without gas exchange (see Section 3.3.3), the effect of gas exchange cannot be neglected for simulating multiple breath washins under the experimental conditions used by Crawford et al. (1985).

The effect of gas exchange on S_n was isolated by simulating mixing in a symmetric model. The model was similar to the symmetric model used by Scherer et al. (1996) and the single region model used by Cruz et al. (1997). Results for these simulations can be seen in Figure 3.7, where inclusion of gas exchange had essentially no effect on the first breath S_n, but increased S_n significantly over the next 24 breaths. These simulations showed that including gas exchange caused the S_n curve to approach a plateau around

breath 20, which was similar to the results from Scherer et al. (1996) and Cruz et al. (1997).

The effect of the acinar asymmetry on the S_n curve was to 'shift' the curve up by $0.027 \cdot L^{-1}$. This effect was seen, in Figure 3.7, whether gas exchange was included or not. The 'shift' in the S_n curve induced by the asymmetry of the model suggests that S_n of the first breath was due predominantly to DCDI in the asymmetric respiratory airway model structure. That is, the conducting airway asymmetry, gas exchange, and non-uniform ventilation had little effect on the first breath value.

The first set of simulations run in the LPA-ACA model set the LPA volumes to be identical at the end of each terminal branch, and ventilated the acini uniformly. That is, each LPA increased in volume by an identical amount. Because uniform ventilation was used, the effect of classical CDI was eliminated from these simulations. The generated S_n values over 25 breaths for the three gas pairs were larger than for the MBA-SCA model, but generally lower than the experimental results (see Figure 4.2). The larger values of S_n relative to the MBA-SCA results were due to increased concentration inhomogeneity because of the asymmetry of the ACA model: that is, the ACA model introduced large amounts of CDI. The inhomogeneity has been classified as CDI because it causes non-uniform concentrations by a diffusion-independent method.

The effect of the conducting airway asymmetry was that acini at the end of long and short paths received different amounts of washin gas during inspiration, even though they were ventilated with an identical volume of gas. The acini at the end of long airway paths were ventilated with a larger amount of gas that was resident in the conducting airways at the start of inspiration. This resulted in the acini at the end of the long paths having lower mean concentrations at the end of inspiration, and those down short airway paths having higher concentrations. The LPA models therefore predicted a range of end-expiratory concentrations that generally increased for subsequent breaths. The results show that large values of S_n can develop in the absence of classical CDI, without the acini having different initial volumes. The difference in S_n for the first breath for the LPA-ACA and MBA-SCA models was very small: the initial concentration of resident gas was assumed to be at fractional concentration 1 for both models, so the first breath for the LPA-ACA model did not develop large concentration

differences between the LPA models. For subsequent breaths, the concentrations at the start of inspiration became progressively more inhomogeneous, therefore generating larger values for S_n.

The non-uniform distribution of concentrations resulting from the ACA asymmetry is shown in Figure 4.4(a) and (b), where concentration is plotted against generation for mixing of O_2/N_2 in the LPA-ACA model under standard conditions. Terminal branches arise in generations 11 to 27. By 0.8 s the terminal branches in generations 11-20 were being ventilated by close to 100% washin gas. At 0.8 s the mean concentration in generation 27 was close to zero, indicating that up to this time at least, the acini arising from generation 27 had been ventilated almost entirely by resident gas. In Figure 4.4(c) the concentrations in generations 15-27 decreased rapidly during expiration, and the concentrations in generations 1-14 decreased at a slower rate as unmixed gas from the anatomical dead space was expired. The mean concentrations in the last two generations remained lower than for the earlier generations. This reflects the lower end-expiratory concentrations predicted by the LPA models attached to these last two generations.

The effect of gas exchange on results from the LPA-ACA model is shown in Figure 4.5 for S_n. Not including the gas exchange source term had essentially no effect on S_n for the first 3 breaths, but for breaths 4 to 24 the S_n values were lower than when gas exchange was included. Including gas exchange caused larger S_n values from breaths 4 to 24, and caused the curve to begin to plateau from around breath 20. The two curves intersected at breath 25. So, unlike the MBA-SCA model, the S_n curve for the LPA-ACA model without gas exchange increased significantly over the 25 breaths. This result indicates that the asymmetry of the conducting airway model induced a large part of the S_n increase, by distributing resident gas unevenly to the LPA models.

Using model analyses, Verbanck & Paiva (1990) had concluded that the asymmetric respiratory airway structure contributed to the evolution of S_n. Because the conducting airway structure of their model did not have the degree of asymmetry of the LPA-ACA model, they were unable to observe the influence of conducting airway asymmetry on the evolution of S_n. In contrast, the results from gas mixing simulations under conditions of uniform flow and identical initial acinar volumes in the LPA-ACA model

show that the asymmetry of the conducting airways has a large effect on S_n.

The effect of the asymmetric conducting airway structure is to cause uneven ventilation of the acini with resident gas, although the acini are expanded by an identical volume. The more symmetric the conducting airway model, the less uneven this resident gas distribution would be. This effect is therefore significant CDI in the conducting airway structure - making a large contribution to the evolution of S_n, even with uniform ventilation.

S_{cond} and S_{acin} for the LPA-ACA N_2 simulation using uniform initial volumes and uniform flow were $0.0389 \cdot L^{-1}$ and $0.0228 \cdot L^{-1}$ for S_{cond} and S_{acin}, respectively. S_{cond} is said to represent the contribution of the conducting airways to S_n, and S_{acin} is supposed to represent the contribution of the acinar airways. Therefore, although classical CDI was not explicitly included in the simulation, S_{cond} still had a large value. This supports the hypothesis that CDI was induced by the conducting airway structure. Although S_{cond} is assumed to represent the inhomogeneity caused by the conducting airway structure, it also includes the effect of gas exchange: S_{cond} was 20.1% smaller when gas exchange was not included in the LPA-ACA model.

The S_n curve comparisons in Figure 4.6(b) for perfect acinar mixing (ACA-perfect) and the LPA-ACA model illustrates the effect of both conducting airway asymmetry and blood-gas exchange. When respiratory airway mixing was assumed to be perfect and evolution of gas from the blood was neglected, the plot of S_n against breath number over 25 breaths was linear. However, the increase in S_n over 25 breaths (0.2068) was similar to the experimental increase over the same range (0.2110) and to the increase from the LPA-ACA model with gas exchange (0.2089). The distribution of inspired gas by the conducting airway asymmetry therefore has a major effect on the evolution of S_n. Blood-gas exchange caused the rate of increase of S_n to slow down after breath 19. When respiratory mixing was assumed to be perfect, gas exchange caused S_n to decrease from breath 20. This result is similar to the results from Cruz et al. (1997) for a seven-region lung model with gas exchange: S_n decreased beyond breath 23 when they included gas exchange in their model. Cruz et al. (1997) assumed perfect respiratory mixing for all of their models.

When respiratory mixing was perfect and there was no gas exchange, S_{cond} for the ACA model was $0.0318 \cdot L^{-1}$ and S_{acin} was $-0.0001 \cdot L^{-1}$. The small negative value for

S_{acin} confirms that the respiratory airways did not contribute to S_n evolution for this model. When gas exchange was included, S_{cond} decreased to $0.0261 \cdot L^{-1}$ and S_{acin} increased to $0.0014 \cdot L^{-1}$. That is, even though mixing was assumed to be perfect in the respiratory airways, they still contributed a small amount to S_n evolution because the alveoli in the respiratory airways were the site of blood-gas exchange.

Linear acinar volume distributions were applied to investigate the possible effect on generation of S_n by acinar deformation in the presence of a pleural pressure gradient. The pleural pressure gradient acting on an upright lung causes the acini at the apex to be larger than those at the base (Milic-Emili et al. 1966). Glazier, Highes, Maloney & West (1967) observed that in the upright lung at FRC, the alveoli near the lung apex were about four times larger by volume than those near the base. Most of the observed change in volume was over the top 10 cm of the lung. A linear gradient of acinar volumes does not therefore mimic the effect of the pleural pressure gradient in the erect lung. However, in the absence of an accurate description of the distributed sizes, a linear gradient will provide an indication of the effect of non-uniform sizes that is more realistic than application of uniform volumes. LPA volumes were distributed such that the smallest acini were at the base of the lungs, and the largest were at the apex. Three ranges of volumes were used : 111 - 140, 93 - 164, and 62 - 206 mm^3. The mean LPA volume in all cases was 123.40 mm^3.

Figure 4.9(a) and (b) show S_n and ΔS_n, respectively, for the linearly distributed acinar volumes. The results show that distributing the acinar volumes increased the generated S_n values, with the largest effect for the widest distribution of initial volumes. The ΔS_n curves were close in value for the first two size distributions, with lower values than for the identical initial volumes. For the most extreme volume range (62 to 206 mm^3) the ΔS_n curve sloped in the opposite direction to the experimental curve.

The more linear ΔS_n curves and lower first breath S_n from the model than from experiment indicates that incomplete mixing in the acini is not modelled adequately by the MBA or LPA models. The respiratory airways are the major site of gas mixing in the lungs, and inhomogeneity of gas concentrations in the respiratory airways are the main contributor to first breath S_n. The low first breath S_n produced by the model shows that the MBA and LPA models do not include all of the factors necessary to

accurately simulate respiratory airway mixing inefficiencies. This is supported by the high values for ΔS_n for breaths 1 to 3: gases with very different diffusivities maintain similar differences in inhomogeneity throughout the simulations.

Because ventilation was prescribed to be uniform for these simulations, classical CDI did not contribute to the increase in S_n relative to the identical initial volume simulation. Instead, CDI from the asymmetric conducting airways and a small increase in DCDI in the respiratory airways caused the increases in the S_n values. In this set of simulations, the smallest acini were near the base of the lungs and therefore tended to have longer path-lengths on average. The largest acini were near the apex of the lungs and had shorter average path-lengths. This meant that the smallest acini were ventilated with the most resident gas, and the largest acini with the least. The result was that the model developed a larger range of mean acinar concentrations at the end of expiration when the initial acinar volumes were distributed linearly.

S_{cond} and S_{acin} increased by 40.62% and 11.40%, respectively, from identical initial volumes to a volume distribution of 62 to 206 mm^3. This confirms that distributing the initial volumes had the most effect on conducting airway induced CDI. The small effect of volume distribution on S_{acin} also confirms that the LPA model is not unrealistically sensitive to changes in initial volume.

Wilson et al. (1987) and Rodarte, Chaniotakis & Wilson (1989) suggested that in dog lungs the experimentally observed inhomogeneity of volume expansions could account for a substantial part of the N_2 phase III slope. The acini in the basal region have been observed to inflate faster than those at the apex (Milic-Emili et al. 1966). To investigate the effect of inhomogeneous volume expansions on the evolution of S_n, acinar tidal volumes were distributed linearly in the LPA-ACA model with identical initial volumes. The distributions were applied such that LPA models near the apex had the smallest local tidal volumes, and those near the base had the largest.

Distributing the acinar tidal volumes linearly to acinar models of identical size in the LPA-ACA model increased S_n, as illustrated in Figure 4.10(a), with the largest effect for the widest distribution. The effect of the distributed tidal volumes was to increase the mean acinar concentrations in the basal acini and decrease those in the apical acini, relative to the uniform flow distribution. Therefore a range of mean concentrations at the end of inspiration were developed, causing increased S_n.

S_{cond} and S_{acin} increased by 122.88% and 3.51%, respectively, from uniform flow to the widest tidal volume distribution (17.16 to 54.90 mm^3). Therefore there was little change in acinar model contribution to S_n, but a large change in the contribution of the conducting airways. The small value for S_{acin} confirms that the LPA model was not sensitive to tidal volume changes, and hence did not introduce significant errors into the results.

Under normal conditions, the pleural pressure gradient causes a distribution of alveolar sizes from top to bottom while at the same time causing flow to be distributed non-uniformly. This combined effect was investigated in the LPA-ACA model by simulating O_2/N_2 gas mixing under standard conditions for combinations of distributed initial acinar volumes and distributed acinar tidal volumes.

For the small tidal volume range (30.88 to 37.74 mm^3) applying initial volume distributions caused the S_n curve to decrease in value relative to the uniform initial volume model with either uniform flow or the small tidal volume range (Figure 4.11(a)). For the other combined distribution simulation sets (Figure 4.12(a) and Figure 4.13(a)) the S_n curves decreased with increasing initial volume distribution relative to the curve for uniform initial volume model with distributed tidal volumes. As the acinar tidal volume range widened, the number of S_n curves with values larger than those for the uniform flow-uniform initial volume model increased. i.e. combined distributions of initial acinar volume and tidal volume can either increase or decrease S_n depending on their relative proportions.

The S_n curve will decrease when the distribution of washin gas is effectively made more uniform by the combined distribution. That is, the small acini at the end of long paths are ventilated with slightly more washin gas, and the large ones at the end of short paths with slightly less, such that the range of mean acinar concentrations at the end of inspiration is less. S_n increases when the end-inspiratory mean acinar concentration range increases.

Cruz (1991) and Cruz et al. (1997) used a seven-region lung model (7RLM) with volume changes described by a third order polynomial. Each region was a symmetric structure based on Weibel (1963). The volume changes were based on the work of Milic-Emili et al. (1966) and Anthonisen et al. (1970). The regions assigned the initial volume of the apex region to be largest and the basal region to be smallest, then the

regions converged to the same size as the inspired volume increased. That is, the basal regions received more flow than the apical regions. This is similar to the LPA-ACA simulations where both flow and acinar size were distributed. The 7RLM produced a good match to the experimental data of Crawford et al. (1985) over breaths 13 to 25, but had smaller values for S_n than experimental for breaths 1 to 12. The first breath S_n from the 7RLM had a smaller value than from the LPA-ACA model with identical initial LPA volumes and uniform flow. This difference in the results from the two models supports the premise that first breath S_n is largely due to asymmetry in the respiratory airways: the 7RLM had symmetric respiratory airways.

The LPA-ACA model results show that S_n is generated by the combined effect of asymmetry in both the respiratory and conducting airways, transfer of gas from the blood, the effect of the pleural pressure gradient, and deformation of the alveoli during ventilation. Given the significant effect that each of these factors has on S_n, it would not be appropriate to leave any of them out when simulating gas mixing.

The LPA-ACA model does not match experimental results perfectly, under any conditions of acinar size or flow distribution. However, distributing the initial acinar sizes and tidal volumes both have a significant effect on S_n. The inability of the LPA-ACA model to match the experimental data perfectly is likely to be due to a combination of factors: 1) assumption of uniform flow and deformation in the acini, 2) underestimation of respiratory airway asymmetry, 3) neglecting cardiogenic mixing, and 4) lack of an accurate description of pleural pressure and its effects.

In support of the first factor, Elad, Shochat & Shiner (1998) found that asymmetry in the compliance of the peripheral airways and lung parenchyma greatly increases the degree of asynchronous ventilation in the lungs. In addition, volume expansions have been found to be more inhomogeneous in the more peripheral lung units (Wilson et al. 1987, Rodarte et al. 1989).

A recent study by Dutrieue, Vanholsbeeck, Verbanck & Paiva (2000) concluded that branching asymmetry was underestimated in the first few generations of the Haefeli-Bleuer & Weibel (1988) study. Dutrieue et al. (2000) used multi-branching models with varying degrees of asymmetry to demonstrate that S_{acin} could be modelled more accurately when the asymmetry was increased. The MBA and LPA models are based on the original Haefeli-Bleuer & Weibel (1988) data, and therefore are probably too

symmetric.

Cardiogenic mixing may contribute to increased non-uniformity of ventilation, and therefore development of a wider range of end-inspiratory mean acinar concentrations.

The effect of the pleural pressure gradient has been investigated using idealised distributions in the LPA-ACA model. Results have shown that the S_n curve is affected by these distributions, and consequently the real pleural pressure gradient may have a more complex effect on generation of S_n than modelled here.

The current model only considers the transfer of relatively insoluble gases between the air and blood. That is, oxygen and carbon dioxide exchange is not modelled. O_2/CO_2 exchange is a more complex process than can be modelled using the simple source terms presented in Equation (3.16) and Equation (3.25). Modelling washout of these more soluble gases will require development of a more detailed exchange model than is presented in the current study.

4.3.1 Conclusions

Past gas mixing models have usually approached the problem of reproducing experimental S_n curves with emphasis on only one contributing factor: for example, non-uniform ventilation (Verbanck & Paiva 1990, Cruz 1991), respiratory airway asymmetry (Paiva & Engel 1984), or gas exchange (Scherer et al. 1996). Results from the LPA-ACA model have shown that S_n is significantly affected by all of the factors considered individually by other researchers, and none of these factors should be neglected.

Verbanck & Paiva (1990) attempted to simulate the results of Crawford et al. (1985) without including gas exchange in their model. They attempted to reproduce the experimental results by ventilating non-uniformly between upper and lower regions, and between adjacent multi-branching acini. However, even with very non-uniform flow distributions, their S_n curves had values below experimental.

Scherer et al. (1996) included gas exchange, but used a uniformly ventilated symmetric model. They attempted to reproduce the Crawford et al. (1985) results by altering the cross-sectional areas and lengths in the respiratory portion of their model. This resulted in the S_n curves being 'shifted' up the y-axis on the S_n against breath

number plot, but the shape of the curves was still unrealistic. Their S_n curves had very little increase in S_n over breaths 1 to 8, i.e. very different to the experimental results, where the first few breaths showed the biggest increase in S_n.

Cruz et al. (1997) acknowledged the effect of gas exchange, but felt that the most important factor contributing to evolution of S_n was regionally-based non-uniform distribution of flow. Including gas exchange in their model caused an unrealistic decrease in S_n beyond breath 23 - the current study has shown that this resulted from assuming simplistic respiratory gas mixing. When gas exchange was not included, the Cruz et al. (1997) model fit the experimental results well from breath 13 onwards.

Results from the LPA-ACA model also suggest that non-uniform ventilation is an important factor in generating S_n, but the asymmetry of the conducting airways produced steep S_n curves even with uniform ventilation, therefore conducting airway asymmetry cannot be neglected if a lung model is to have an anatomical rather than a semi-empirical basis.

Results from gas mixing simulations in the LPA-ACA model have shown that S_n can be induced by 1) asymmetry of the acinar airways, 2) asymmetry of the conducting airways, 3) evolution of resident gas from the blood, and 4) the pleural pressure gradient causing uneven flow distribution.

The acinar asymmetry has been shown to be the factor affecting S_n generation the most in the first breath of a washout simulation: results from the MBA-SCA and LPA-ACA models for the first breath were close in value, demonstrating that the conducting airway asymmetry and gas exchange did not make a large contribution to first breath S_n.

The conducting airway asymmetry has been shown to generate a large component of S_n, even when identical acini are uniformly inflated and gas exchange is neglected. Conducting airway asymmetry causes large increases in S_n over the entire range of a 25 breath washout, due to large degrees of asymmetry-induced CDI.

Gas exchange has a small effect on the first breaths, but is the main contributor to S_n curve 'plateau' observed from around breath 15 experimentally. It is essential to include gas exchange when simulating the experimental results of Crawford et al. (1985).

The pleural pressure gradient, idealised as linear distributions of initial acinar

volume and acinar tidal volume, has a small effect on S_{acin}. It modifies the S_n curve such that values can either increase or decrease relative to uniform ventilation simulations, depending on the range of distributions used for the simulation. The results have therefore shown that an accurate description of the pleural pressure gradient and coupling of parenchymal deformation to flow in the airways will be essential to model S_n evolution more accurately.

Chapter 5

Water vapour and heat transport

5.1 Introduction

When a patient is attached to an artificial ventilator via an endotracheal tube, the air delivered to the patient must be preconditioned to avoid damage to the airways and subsequent development of pulmonary infection. Fisher & Paykel Healthcare are a New Zealand company specialising in the manufacture of respiratory humidifiers. These humidifiers actively heat and moisten air that passes from the ventilator to an intubated patient. Fisher & Paykel Healthcare require a mathematical model of respiratory heat and water exchange in an intubated lung, such that the model can be used to investigate penetration of unconditioned air and airway drying for a range of ventilation conditions.

This chapter describes simulation of water vapour and heat transfer in fluid-lined conducting airway models. Simulations are performed in a symmetric geometric model, and in the asymmetric conducting airway model described in Chapter 2. Unlike the majority of previous respiratory heat and mass transfer models, this model does not use experimentally-derived heat and mass transfer coefficients; instead, radial heat and water vapour transfer are solved iteratively with axial transport, assuming that the velocity, temperature, and concentration can be described radially by a power law. Experimentally derived calculations for heat and mass transfer coefficients have been used in past models, but this approach is not appropriate for a model with an

endotracheal tube or for extreme inspiratory conditions.

Validation of the water and heat transfer model is first performed by comparing numerical results from the model without an endotracheal tube with experimental results from McFadden et al. (1985). The experimental results were measured over a wider range of ventilation rates and inspiratory temperatures than the model would generally be subjected to during its use by Fisher & Paykel Healthcare. Further validation of the model is performed by comparing numerical results from the model with experimental results for inclusion of an endotracheal tube (Ryan et al. 2000).

The symmetric model is shown to be sufficient, and computationally inexpensive, under limited inspiratory conditions. As the unconditioned air penetrates further into the model, it becomes necessary to use the asymmetric model to produce results close to those found experimentally.

5.2   Background

5.2.1   Airway surface liquid and latent heat

The airways in the mammalian respiratory tract are lined with a layer of mucus. The mucus layer rests above a layer of watery serous fluid. The surface liquid covers a single layer of epithelial cells which in turn rest on a basement membrane. Below the basement membrane, a capillary layer is embedded in a layer of connective tissue. The lining epithelium is thickest in the upper airways where it is underlain by a thick submucosa (Sleigh, Blake & Liron 1988).

The epithelium of the trachea and bronchi is composed of about 5 ciliated cells for each goblet (secretory) cell. There are approximately 200 cilia on each ciliated cell, from 5 - 7 μm in length (Kilburn 1968). The airways are ciliated down to the non-alveolar walls of the respiratory bronchioles (Sleigh et al. 1988).

The mucus layer is propelled by the beating action of the cilia. The cilia beat in the watery layer to sweep mucus towards the mouth, where it is expectorated or swallowed. The surface liquid is secreted by serous cells. Its depth is carefully regulated by microtubules on the ciliated epithelial cell surfaces (Evrensel, Khan, Elli & Krumpe 1993), to maintain optimal thickness of the surface fluid in which the cilia

are bathed (periciliary fluid). When the surface liquid layer is depleted, the back-sweep of the cilia cannot clear the mucus, and the mucus is swept back and forth with no net movement towards the mouth. Conversely, if the surface liquid layer becomes too deep then the cilia can be decoupled from the mucus. Proper mucus transport is therefore very sensitive to the depth of the surface liquid layer. The cilia and their beating action is illustrated in Figure 5.1.
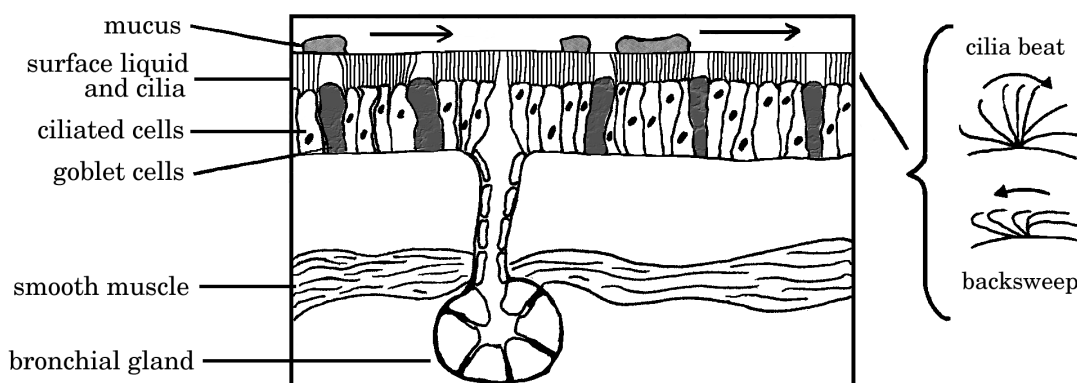
Figure 5.1: *Radial layers in the trachea and bronchi, showing the forward sweep of the cilia and their backsweep clear of the mucus.*

The total energy content of air is made up of sensible heat and latent heat. The temperature of the air reflects its sensible heat content, while water mass reflects its latent heat content. Thus, humid air has more energy to give up than dry air. Sensible heat energy exchanged between inspired gas and the airway surface liquid directly alters the temperature of each, whereas evaporation involves a water and latent heat loss from the surface liquid only, thereby cooling the surface liquid and only affecting the gas temperature indirectly. During condensation, the surface liquid gains water and latent heat, thereby heating only the surface liquid. The end-expiratory temperature and water content of the airway surface liquid are dynamic, being intermediate between plasma, at core temperature, and the temperature and water content of the inspired air.

5.2.2 Temperature and humidity of inspired gas

Under normal conditions the mammalian upper respiratory system - the nose, the pharynx, and the trachea - conditions inspired air to bring it close to body temperature, and to saturate it with water vapour. During expiration, some of this heat is recovered by the surfaces of the upper respiratory airways, but the rest is lost to the environment. The nose recovers around 30% of heat and water from expired air during normal breathing in temperate conditions (Cole 1993).

The nasal turbinate structures (well-perfused 'fin-like' protrusions from the walls of the nasal cavity) are the major site of air conditioning in the mammalian respiratory system, although the upper airways are a secondary site of humidification and heating. The temperature of the turbinate mucosal surface has been shown to increase from close to expired air temperature at the nasal end, to close to body temperature at the posterior end (Schroter & Watkins 1989). Thermoregulation of expired air passing through this region is controlled by the blood temperature and blood flow rate in the nasal turbinate structure.

The Isothermal Saturation Boundary (ISB) is the level in the airways beyond which air temperature and humidity do not fluctuate. For normal breathing the ISB is at around the second or third bronchial generation (Hanna & Scherer 1986c). When ventilation frequency increases, or very cold and dry air is inspired, the ISB shifts further down the airway tree. Under these more extreme conditions the nose and mouth are unable to fully heat and moisten the air as it passes through. Instead, the airways in the lungs perform the final conditioning to body temperature and saturation, and consequently the position within the airways at which full conditioning is attained is more distal from the mouth than under normal breathing conditions.

The rate of conditioning by the airways depends on blood flow rates and temperatures, cell metabolic rates, gas velocity, thermal properties of air and lung tissue, latent heat of evaporation, the rate of surface liquid replenishment, and heat generation by blood perfusion. The wall and airstream temperatures in the central airways have been shown to be slightly below body core temperature for restful room breathing (Hanna & Scherer 1986c).

When an artificial airway such as an endotracheal tube is placed in the upper

airway, the nose and mouth are bypassed. Adequate pre-conditioning of air supplied to the artificially ventilated patient becomes critical: inadequate humidification has been shown to cause thickened secretions, small airway blockage, atelectasis, and impaired gas exchange. When heat and humidity drop below core body temperature and saturation a series of events take place: 1) the mucus (usually 95 % water) thickens as its water content evaporates, 2) the cilia find it more difficult to move mucus so the pulmonary system becomes less able to fend off infections, 3) the mucus becomes thick and inelastic, the cilia are immobilised, and mucociliary clearance stops completely, 4) the lack of moisture causes cilia to break off from cells in the airway, causing damage to the mucosal lining, and 5) atelectasis occurs - mucus blocks some of the airways causing the alveoli distal to the blocked airway to collapse. This leads to a decrease in FRC, decreased pulmonary compliance, and increased shunting (that is, blood entering the arterial system without going through ventilated areas of lung) (West 1979).

With an endotracheal tube in place, the patient is not able to clear particles or mucus from the lungs by sneezing or coughing, and the nose is not available to filter inspired particles. The correct function of the mucociliary escalator therefore becomes critical for the health of the patient.

5.2.2.1 Artificial ventilation and air conditioning

Artificial ventilation is employed when the body is unable to ventilate itself. Ventilator support is required for a wide range of respiratory disorders, which generally fall into three main categories:

1. The body's ventilatory system lacks muscle drive due to muscle weakness or paralysis, or damage to the thoracic wall structure;

2. abnormalities in lung resistance - due to tumour growth, muscle constriction of the airways, inflammation and swelling of airway linings, or excessive mucosal secretion into the airways (often caused by allergic bronchial asthma), or;

3. abnormalities in the compliance of the lungs - when the chest wall is restricted by diseases leading to skeletal deformations, or from traumatic damage.

When the nose and mouth are bypassed, as is the case with patients receiving artificial ventilation via an endotracheal tube, it becomes necessary to warm and moisten air before it is delivered to the patient.

The lung functions that are sensitive to inspired humidity are: gas conditioning, heat and moisture recovery, defence, and airway mechanics (Williams, Seakins, Rankin, Smith & Galler 1996). Table 5.1 from Williams, Seakins, Rankin, Smith & Galler (1996) shows the rate at which airway damage occurs when the inspired air is not adequately conditioned.

AH below 44 mg.L^{-1}	Time to MD (hrs)	Time to CD (hrs)
0	≥ 24	≥ 24
10	≥ 24	≥ 24
20	0.5	18
30	≤ 0.1	4
40	≤ 0.1	1
44	≤ 0.1	0.5

Table 5.1: *Time for damage to occur to the airways under inadequate humidification (from Williams et al. (1996)). The first column lists the absolute humidity (AH) of the inspired gas below 44 mg.L^{-1} (saturation at 37°C), the second column lists the time to mucociliary damage (MD), and the third column lists the time to cell damage (CD).*

For patients ventilated with air with a water content of less than 14 mg.L^{-1}, the time to cell damage is short, and the time to mucociliary dysfunction is a matter of minutes.

5.2.3 Humidification of inspired air

Three main methods of humidification are currently available:

1. Nebulizers. These produce a fine aerosol of water droplets which evaporate on introduction to the inspiratory gas stream;

2. Heat and moisture exchangers (HME). These devices are placed between the patient and tubing circuit. During exhalation, gases at body temperature pass through the device, heating a hygroscopic filter medium in the HME and

condensing water in it. During the next inhalation, the inspired gas is warmed and humidified as it passes through the heat and moisture exchanger;

3. Heated water humidifiers. These consist of a heated water bath over which the inspiratory gas stream is passed.

Of these methods the first is no longer in common use due to inadequate performance. Heated humidifiers and HMEs are commonly used to condition air supplied to artificially ventilated patients.

5.2.4 Active humidification

The heated water humidifiers manufactured by Fisher & Paykel Healthcare condition inspired air by passing the air through a conditioning chamber before it reaches the patient. There is a water bath in the chamber that supplies heat and water vapour to air passing through. The chamber can be set to a selected temperature. Ideally the chamber would condition air to the chamber set temperature and 100% relative humidity, but in reality full conditioning is difficult to achieve.

The active humidification process encounters both a transport and a generation problem. The transport problem involves movement of conditioned air from the chamber to the patient without the air losing heat to the environment, and the generation problem arises when the chamber cannot fully condition all of the air that passes through it.

If conditioned air sits in the supply tube for too long, it loses heat to the environment. As the air loses heat, water vapour condenses on the walls of the tubing. To combat this problem a coiled heating wire is inserted in the tube, and this is used to heat the tube gas above the humidifier setting by approximately $3°C$, to ensure that condensation does not occur. The heated air is then cooled by approximately $3°C$ as it passes through the Y-tube to the mouth. This is the transport problem: moving air from the chamber to the patient without loss of heat or moisture.

For fast inspirations or high flow rates, air is not in contact with the water bath in the humidifier long enough to be conditioned to the chamber setting. This is the generation problem.

Although the chamber is set to a constant temperature, the temperature and humidity of the air supplied to the patient is not constant. The first air inspired by the patient is air that was sitting in the tubing between the Y-tube junction and the mouth; this is the last air that was expired by the patient, and therefore is warm and moist. The next air that is inhaled has been sitting in the supply tube during the previous expiration. This air will have lost heat to the environment during the expiration, and will have been heated by the heating coil, but this may have resulted in patches of gas at higher and lower temperatures than supplied by the chamber. The next volume of gas was sitting in the chamber during the previous expiration, so it is at approximately the chamber set temperature and humidity. Further inspired gas is at lower temperatures and humidities, depending upon the amount of time spent in the chamber.

There is currently debate as to what level of temperature and humidity the air supplied to artificially ventilated patients should be conditioned. Some groups advocate conditioning to body temperature and saturation (Williams, Rankin, Smith, Galler & Seakins 1996, Ryan et al. 2000), while others consider that lower temperatures and absolute humidities would be more appropriate (Irlbeck 1998, Miyao, Hirokawa, Miyasaka & Kawazoe 1992).

Experimental studies have shown that when the airway is exposed to inspired gas at body temperature and saturated with water vapour, the physical properties of the airway mucus are optimised (Richards & Marriott 1974), the cilial beat frequency is maximised (Horstmann, Iravani, Norris-Melville & Richter 1977), and the mucus transport velocity is maximal (King, Tomkiewicz, Boyd, Shao & Ghahary 1995). However, Irlbeck (1998) suggested that delivery of gas at body temperature and saturation would result in particulate water being introduced into the airway via significant condensation onto the ET tube.

5.2.5 Experimental respiratory temperatures and blood flow

Very few studies have been undertaken to measure human respiratory temperatures under increasing thermal loads. The experimental studies used for comparison with numerical results in this chapter are those of McFadden et al. (1985) and Ryan et al. (2000). The first study had subjects breathe through the mouth at different rates of

ventilation, with no endotracheal tube, and the second study had the subjects breathe while artificially ventilated and intubated with an endotracheal tube.

5.2.5.1 Measurements of airway temperatures, no endotracheal tube

McFadden et al. (1985) recorded temperatures down a single path of the airway tree using a flexible 30.2 cm probe that had six thermistors spaced at 4.3 cm intervals and arranged in a spiral pattern. The outer diameter of the probe was 1.4 mm, and the diameter of the thermistors was 250 μm. The 63% response time of the thermistors was 0.250 s in stirred water.

The first set of conditions used room air that was bubbled through a humidifier (26.7 $\pm 0.5^o$C, 8.8 ± 0.3mg $\cdot$ L^{-1}). The second set of conditions used dry compressed air that was cooled to subfreezing temperatures (-18.6 $\pm 1.2^o$C, < 0.05mg $\cdot$ L^{-1}). The ventilation rates chosen for the study were 15, 30, 60, and 100 L $\cdot$ min^{-1}. Each level of ventilation was maintained for 2 minutes. Although the ventilation rates were presented for this study, the tidal volumes and breath durations were not mentioned.

This study demonstrated that the colder the inspired gas or the greater the ventilation rate, the more deeper regions were recruited into the conditioning process.

5.2.5.2 Measurements of airway temperatures, with endotracheal tube

Ryan et al. (2000) recorded temperatures at multiple positions down (and just beyond) the endotracheal tube in intubated, artificially ventilated patients. Their aim was to determine inspiratory conditions that were thermodynamically neutral to the intubated airways, and to investigate the effect of the ET tube on water and heat balance.

The subjects were receiving positive pressure ventilation, and the air was conditioned by a heated pass-over humidifier. The humidifier settings used for the experiments were 30, 34, 37, and 40°C. The ventilator delivered 400 ml of air at a constant flow rate for 2.2 s, followed by a constant flow expiration for 3.6 s.

A miniature thermocouple, built into a suction catheter, was used to record the temperatures at multiple points down the ET tube. Humidity was measured by a hygrometer that was positioned between the supply tube and the patient's mouth.

5.2.5.3   Airway blood flow

The regulation of airway blood flow has been thoroughly investigated in animals, but not in humans. This has been largely due to the invasiveness of the experimental techniques employed to measure blood flow (Le Merre, Kim, Chediak & Wanner 1996).

Using a soluble inert gas uptake technique to measure airway mucosal blood flow in the conducting airways of humans, Breitenbucher, Chediak & Wanner (1994) concluded that mucosal blood flow is inversely related to intrathoracic pressure. Results from Le Merre et al. (1996) showed that during quiet breathing, cold dry air decreased the mucosal blood flow and warm humid air had no effect. From these results, the authors concluded that there is vasoconstriction in the central airways during cold dry air breathing.

In contrast, hyperventilation with a corresponding decrease in both the temperature and humidity of inspired air reaching the lower airways has been reported to lead to an increase in tracheobronchial blood flow in dogs (Baile, Dahlby, Wiggs, Parsons & Pare 1987). In addition, tracheal and bronchial blood flow have been reported to increase with ventilation rate during eucapnic (high partial pressure of CO_2 in blood) dry air hyperventilation in sheep (Parsons, Pare, White & Baile 1989). Eucapnic hyperventilation with frigid air has also been found to increase mucosal blood flow in humans (Kim, LeMerre, Chediak & Wanner 1996).

Based on these conflicting experimental findings, Le Merre et al. (1996) suggested that there could be a biphasic response to increased thermal stress, with vasoconstriction followed by vasodilation. They also suggested that the level of ventilation, independent of the temperature, could increase blood flow, counteracting the effect of cold dry air. An alternative theory is that there may be interspecies differences that are dependent upon anatomical features and physiological needs specific to the experimental animal.

To date there has been no conclusive explanation of the behaviour of airway blood flow in humans in response to thermal challenge.

5.2.6   Literature review

Models of water and heat transport in the airways can be differentiated by their treatment of radial geometry, their approach to transfer of water and heat from the mucus to the gas in the lumen, and their treatment of time-dependence.

Hanna & Scherer (1982) developed a one-dimensional, quasi-steady model of heat and water transfer using conservation of mass and energy balance in a 'slice' through an idealised airway. The model was divided radially into a lumen and a lumped body layer that included the airway surface liquid and surrounding tissue. Blood temperature was assumed to be constant, and at a distance Δy from the air-mucus interface. Transport of water vapour from the mucus into the lumen was governed by mass transfer coefficients. The concentration of water vapour at the air-mucus interface was assumed to be saturated at the air-mucus interface temperature.

The model solved for average concentration and temperature in the lumen, and the temperature and concentration at the air-mucus interface as functions of distance from the tip of the nose, but not of time. The assumption that the system was quasi-steady was justified on the basis of comparing the time to reach steady-state conditions (10^{-3}s) with the time of a normal breath.

Hanna & Scherer (1986a) measured mass transfer coefficients using a naphthalene sublimation technique in an acrylic cast of the human upper respiratory airways (beginning with the nose). The mass transfer coefficients were presented in terms of Sherwood numbers for different regions. Hanna & Scherer (1986b) and Hanna & Scherer (1986c) utilised these mass transfer coefficients to apply the model of Hanna & Scherer (1982) to a Weibel structure.

Simulated results from the models were generally in agreement with experimental data for the upper airways and trachea, but results were too low below the carina. Hanna & Scherer (1986c) found that varying the transfer coefficients had very little effect on the simulated expiratory temperatures, but had a significant effect on the inspiratory temperature profile: increasing the coefficients increased the inspiratory temperature profile by about 10%, and decreasing the transfer coefficients reduced the temperature profile by about 25%. The modelled wall blood temperature was the parameter found to have the most effect on net water flux.

Ingenito et al. (1986) used control volume analysis to derive essentially the same model as Hanna & Scherer (1986b) and Hanna & Scherer (1986c) but with the capillary bed modelled as an infinite thermal reservoir at a distance Δy from the mucosal surface. The capillary bed temperature was estimated by the equation $T_{cap}(x) = 27 + 0.3x$ (^oC) where x is cm from the airway opening. Their results were generally consistent with those of Hanna & Scherer (1986b) and Hanna & Scherer (1986c) for similar simulation conditions.

The models of Hanna & Scherer (1986b), Hanna & Scherer (1986c), and Ingenito et al. (1986) were limited to heat and water exchange with the mucosal surface. Events occurring in the airway mucosa were not considered. Because the surface liquid layer was 'lumped' with the surrounding tissue layer, these models cannot be used to investigate airway drying.

Tsu et al. (1988) developed a model to investigate the exchange of heat, water, and a soluble gas between respired air and the airway surface liquid. This was a one-dimensional model incorporating a mucus layer with changing depth, and secretion of fluid from the tissue to the mucus. Tsu et al. (1988) used a control volume approach to derive their governing equations for heat and water vapour transport in a symmetric Weibel structure. The model was divided radially into three regions: the lumen, a thin mucus layer, and a non-perfused tissue layer. Simulated values of temperature and concentration were averaged values for each region. Heat and mass transfer coefficients from Ingenito (1984) were used to estimate the exchange rates of heat and mass between the air-mucus interface and gas in the lumen. The thickness of the mucus layer in the trachea was initially 10 μm, and for subsequent generations the mucus thickness was set such that the ratio of mucus thickness to compartment diameter was the same as for the trachea. Reduction of the thin mucus layer below 10 μm triggered secretion of liquid from the non-perfused tissue.

Parameters were varied in the Tsu et al. (1988) model to investigate their effect on the results, and to determine the parameters that gave the best fit to experimental data. Varying the tissue layer thickness and capillary blood temperature profiles were chosen to characterise airway perfusion indirectly.

Comparison between measured and predicted end-inspiratory and end-expiratory temperature was poor for all simulations and the set of parameters giving the best

fit for the inspiratory data gave the worst fit for the expiratory data, and vice versa. The choice of the heat transfer coefficient was found to have the biggest effect on the fit of the simulated results to experimental data. It was found better to use Ingenito's coefficients for oral breathing simulations and Hanna's coefficients for nasal breathing simulations. The next most significant parameter was the non-perfused tissue thickness. That is, the effective 'buffer' between the surface liquid and heat supplied by the blood.

Tsai, Saidel, McFadden & Fouke (1990) developed a model of radial water and heat transfer in the trachea during breath-holding. The trachea was idealised as circular with four regions: lumen, airway surface liquid, mucosa-submucosa, and surrounding tissue. The mucosa-submucosa layer was assumed to be the main source of continuously supplied water because of its high density of gland ducts and capilliaries. The model had two heat sources: 1) blood flow in the mucosa-submucosa layer; and, 2) blood flow in the surrounding tissue. Because the airway surface liquid and mucosa-submucosa layers are very thin and have much larger thermal conductivities than air, the simulated temperature drop across them was very small.

Tsai et al. (1990) found that during the first part of warming, the air temperature rises fast until it approaches the wall temperature, then the air temperature and wall temperature are very close and have similar warming rates. The simulated profiles of concentration in the lumen were very similar to those for temperature. The effect of varying the blood flow rate or changing the thickness of the mucosa-submucosa on the airway temperature was small individually, but had a more significant effect when combined.

Daviskas et al. (1990) modelled heat and water transport in a Weibel structure using a time-dependent model based on a single differential equation with an analytical solution. Only radial transport was considered in a single region (the lumen), so an analytical solution to the governing equation was obtainable using Bessel functions. The temperature at the wall was modelled using an iterative process to fit an empirical equation to experimental results. The empirical equation was both time and position dependent. This approach avoided coupling the heat and water vapour equations, but it restricted predictions from the model to the range of the experimental data. That is, the model was restricted to inspiratory conditions close to $8.8 \ \mathrm{mg} \cdot \mathrm{L}^{-1}$ and

26 - 35°C. 99.5% saturation was initially assumed at the air-mucus interface. Good fit to the experimental data of McFadden et al. (1985) were achieved by iteratively fitting wall temperature. However, the simulated expired concentrations at the mouth were significantly higher than the experimental data: most of the experimental concentrations were close to 90% saturation. Daviskas, Gonda & Anderson (1991) adapted the model to incorporate different degrees of saturation at different levels down the airway tree. Saturation at the wall of the mouth was 91%, pharynx 93%, larynx 96%, and the rest of the airways were at 99.5%.

Bui et al. (1998) presented a model describing the simultaneous exchange of heat, water, and an inert gas in a layered model with bronchial circulation. The dimensions of the upper airway were taken from Hanna (1983), and the more distal airway structure was an eighteen generation Weibel symmetric model, with the respiratory bronchioles and alveoli lumped together. Radially, the model was divided into seven layers: 1) lumen, 2) mucus layer, 3) epithelium, 4) connective tissue, 5) bronchial smooth muscle, 6) body-tissue, and 7) core-body layer. Transport between the mucus layer and gas in the lumen was described with heat and mass transfer coefficients. The heat transfer coefficient was taken from an empirical correlation (Ingenito 1984) and the corresponding mass transfer coefficient was calculated from the Chilton-Colburn analogy.

The lumenal surface of the airway wall contains lumenal folds. Bui et al. (1998) used a scaling factor (S) to account for enhanced surface area when mucosal folds are present. The value of S was found to be 2.5 in the small airways and 1.1 in the trachea. S was scaled linearly from the trachea to the 12th generation. Incorporating S improved the model's ability to simulate a Phase III slope, but the end expiratory temperature was insensitive to S. Increasing S enhanced the model's ability to recover heat and water.

Because mucus is 95% water, the physical properties of the mucus layer in the Bui et al. (1998) model (density, specific heat, and thermal conductivity) were assumed to be the same as water. The mucus layer had a minimum thickness of 10 μm in the trachea, and was scaled in subsequent generations such that the volume of mucus in the lower generations was the same as in the trachea. The mucus layer changed thickness with evaporation and condensation.

The physical properties of the epithelium, connective tissue, and smooth muscle were assumed to be equal to water, with the exception of solubility and diffusivity of the inert gas. Fluid was secreted from the non-perfused tissue layer to the epithelium and replaced by filtration from the bronchial circulation within the connective tissue layer. No fluid was secreted from the smooth muscle layer because of its anatomical distance from the mucus layer relative to the perfused connective tissue. The blood flow to the connective tissue and smooth muscle layers was modelled as an evenly dispersed network of capillaries that supplied blood at the condition of the body and exited at a new condition, which was determined by the dynamics of heat and mass transfer.

Simulated results were found to be sensitive to the thickness of the effective buffer between the smooth muscle and the core body. The exhaled temperature was sensitive to the local heat transfer coefficient between the mucus layer and air. The results were not very sensitive to the parameters associated with the bronchial circulation. The thickness of the mucus and epithelial layers did not affect the results significantly, however, the results were extremely sensitive to the thickness of the body-tissue layer. Bui et al. (1998) concluded that it might be more appropriate to vary the body layer thickness axially.

In contrast to the above models which all used transfer coefficients to estimate the amount of heat and mass transfer, Saidel et al. (1983) described the radial velocity profile in a cylindrical model trachea using a parabolic equation. The water vapour concentration at the airway wall was assumed to be in equilibrium with liquid water at wall temperature. The wall temperature was assumed to be body temperature. An alternating-direction algorithm was used to solve axially and radially for temperature and water vapour concentration. The results were then used to calculate local rates of water vapour and heat transfer.

5.2.6.1 Summary

All of the described models have used a symmetric structure (based on Weibel (1963)) for the conducting airways. For simulating nasal or oral breathing without extreme inspiratory conditions, a symmetric model would be adequate because the ISB would not penetrate far beyond the carina, and the symmetric model would also be

computationally inexpensive. However, when more extreme conditions are simulated or when an endotracheal tube has been inserted, the ISB can penetrate far down the airway tree. The symmetric model effectively averages out concentrations over a given generation, whereas concentrations in a given generation of an asymmetric tree could exist over a wide range under the right set of conditions. Over time, the effect of these variations in concentration would be simulated better by an asymmetric model than a symmetric one.

The above models have differed in the number of layers that they have considered necessary. Hanna & Scherer (1982), Hanna & Scherer (1986b), Hanna & Scherer (1986c), Ingenito et al. (1986), Daviskas et al. (1990), and Daviskas et al. (1991) solved for temperature and concentration only in the lumen and at the air-mucus interface. None of these models considered the airway surface liquid or tissue layers separately.

Tsu et al. (1988) incorporated a mucus layer and a non-perfused tissue layer. Tsai et al. (1990) incorporated airway surface liquid, mucosa-submucosa, and surrounding tissue. They observed that the temperature drop across the airway surface liquid and mucosa-submucosa was very small because of the much larger thermal conductivities in the layers than that of air. Bui et al. (1998) presented the most layers, comprising airway surface liquid, epithelium, connective tissue, bronchial smooth muscle, body-tissue, and a core-body layer. They found that the thickness of the mucus and epithelial layers did not have a significant effect on the results, but the results were very sensitive to the thickness of the body-tissue layer.

Based on the findings of Bui et al. (1998) and Tsai et al. (1990), it does not seem to be necessary to model as many layers as Bui et al. (1998), however, results have been shown to be sensitive to the distance of the core-body from the lumenal surface. The number of layers used by Bui et al. (1998) were necessary for modelling inert gas transfer, where transfer properties differed between the layers. For water and heat transfer, the properties of the layers are assumed to be the same as water, therefore the number of layers in the Bui et al. (1998) model could be reduced if inert gas transfer was not included.

A mucus layer of variable thickness was included in the models of Tsu et al. (1988) and Bui et al. (1998). Tsu et al. (1988) triggered secretion of liquid from the non-perfused tissue layer when the surface liquid depth dropped below 10 μm, such that

the minimum depth was always maintained.

The capillary bed temperature profile, gas phase transfer coefficients, and non-perfused tissue thickness have been identified as the parameters having the largest effect on model results (Tsu et al. 1988, Bui et al. 1998). With the exception of Daviskas et al. (1990) and Daviskas et al. (1991), all of the models have relied on heat and mass transfer coefficients derived from experimental data over a limited range of the respiratory airways. The heat and mass transfer coefficients have been taken from Hanna & Scherer (1986*a*) or Ingenito (1984).

The mass transfer coefficients derived by Hanna & Scherer (1986*a*) were from a cast of the upper airways, and their use in lower airways may not be appropriate. Evidence for this is that Hanna & Scherer (1986*c*) found that simulated values below the carina were lower than experimental values. The Hanna mass transfer coefficients approach zero as velocity decreases, so their use would not be appropriate for simulating extreme conditions where air at low temperature and humidity penetrates far down the airway tree to regions of low velocity.

Ingenito (1984) measured intra-thoracic airway temperatures and then used a model of the airways to determine an average heat transfer coefficient for the entire airway tree from the trachea to the bronchioles (the model extrapolates values for generations 7-18). The corresponding mass transfer coefficient is then calculated from the Chilton-Colburn analogy. As velocity decreases, the Ingenito transfer coefficients reach an asymptote. In generations 7-18, where the transfer coefficients were extrapolated and velocities are smaller, it is likely that, as for the Hanna coefficients, the prediction of mass transfer is too low (Bui et al. 1998).

In contrast to the other studies, Daviskas et al. (1991) did not use heat and mass transfer coefficients. Instead they attempted to fit wall temperatures in their model to experimental data. Daviskas et al. (1991) regarded their model as a 'semi-empirical construct' which would be good only over a limited range of simulation conditions. This is because the model relies on fitting the wall temperature behaviour to experimental data that has been measured at relatively few positions down the airways over a narrow range of inspiratory conditions.

In summary, the models described here have not focused specifically on depletion of airway surface liquid, so have usually not incorporated this as a separate layer. Their

geometry has been based on a Weibel symmetric model, which may not be valid for more extreme simulation conditions. The use of transfer coefficients that have been measured in the upper or central airways, and then extrapolated for the rest of the conducting airways may cause underestimation of the mass and heat transfer in the more distal airways under extreme conditions. The derived heat transfer coefficients are not appropriate for estimating heat transfer across an endotracheal tube. Only two studies have compared simulated temperatures with experimental results: Ingenito et al. (1986) and Daviskas et al. (1990) produced simulated temperatures close to the experimental data of McFadden et al. (1985), but both of these models are limited to small ranges of inspiratory conditions.

5.3   Modelling water and heat transfer

5.3.1   Radial structure of the lung model

The conducting airway model described in Chapter 2 describes the conducting airways by their length, inner diameter, and spatial positions of their end-points. To model the radial transfer of water vapour and heat, the layers surrounding the airways must be considered.

Bui et al. (1998) modelled seven radial layers: 1) lumen, 2) mucus layer, 3) epithelium 4) connective tissue 5) bronchial smooth muscle, 6) body-tissue and 7) core-body layer. Although Bui et al. (1998) included water vapour and heat transfer in their model, they were primarily concerned with the transfer of inert gases across the bronchial walls. The physical properties of the epithelium, connective tissue, and smooth muscle were assumed to be equal to water, with the exception of solubility and diffusivity of the inert gas being modelled. Therefore, for water and heat transfer some of the layers were effectively lumped into a single layer. The number of layers used by Bui et al. (1998) are therefore not necessary for modelling water vapour and heat transfer, without additional inert gas transfer.

The airways in the water and heat transfer model presented in this chapter generally have four radial layers: 1) lumen, 2) airway surface liquid (serous liquid and mucus), 3) sub-mucosal layer, and 4) surrounding bronchial circulation. The layers in

this model were therefore the same as used by Tsai et al. (1990) to study radial heat and water transfer in the trachea during breath-holding, but with the only source of heat being from the body-core layer at distance Δy (plus surface liquid depth) from the air-mucus interface. The surface liquid layer was assumed to have a changeable depth, in response to evaporation or condensation. Two additional optional layers can be included from the mouth to a specified depth, to model a PVC endotracheal tube and condensation on the tube. The four basic layers are identified in Figure 5.2.
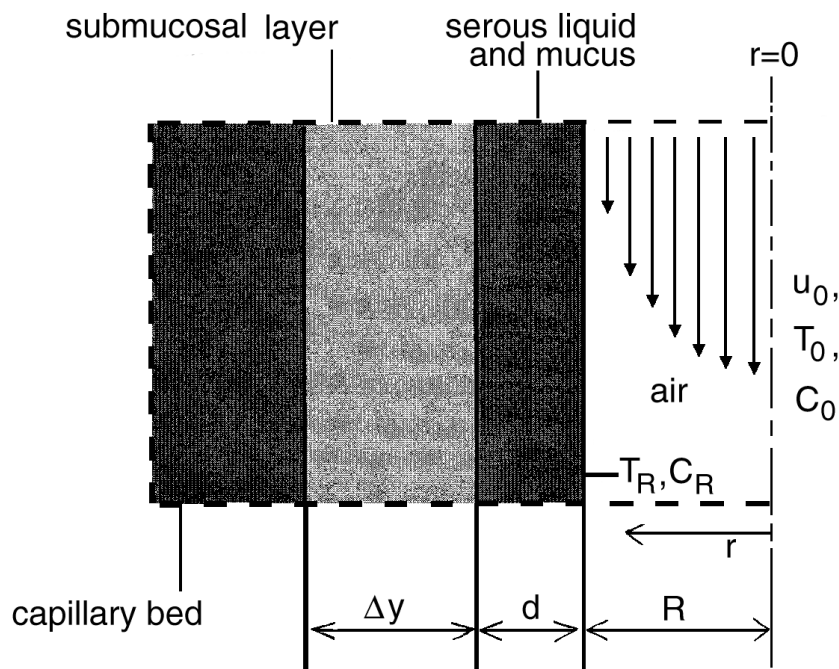
Figure 5.2: *Radial layers in the water and heat transfer model: air in lumen, mucus and surface liquid, submucosal layer ('tissue' layer), and the surrounding capillary bed at fixed temperature.*

5.3.1.1 Power laws for velocity, temperature, and concentration

Because it was not possible to use transfer coefficients from Hanna & Scherer (1986a) or Ingenito (1984), an alternative approach was used where the velocity, temperature, and concentration profiles across the airways were described by power law equations.

For laminar flow, the velocity profile can be described by a parabolic equation (power law with exponent eqaul to 2), with velocity at the walls equal to zero (a

'no-slip' boundary condition). Tsai et al. (1990) found that the temperature and concentration profiles within the lumen were parabolic in nature for breath-holding simulations. However, as the velocity of air increases, the airflow becomes turbulent: flow in the central airways is turbulent under normal breathing conditions. Therefore the parabolic profile that described velocity as a function of radius for laminar flow would not be appropriate for turbulent flow.

As an approximation, the α parameter that describes the shape of the velocity profile (see Equation (5.9)) can be increased to give a profile with a flatter centre and steeper sides. The velocity profile would therefore approach the mean velocity for a more turbulent flow. As turbulence increases, the mixing of heat and water vapour increases in the lumen. It is therefore plausible that the temperature and concentration profiles would follow the same trend as the velocity profile: that is, they would have increased values of β and γ (see Equations (5.3) and (5.4)). The effect of increasing β and γ is to increase the gradient in temperature and concentration at the airway wall. Because transfer of water vapour and heat from the radial layers is dependent on gradients at the wall, larger values of β and γ would cause increased movement of water vapour and heat. This is the same effect that is observed when gas velocity increases.

The water and heat transfer model is ultimately intended to simulate air conditioning in an artificially ventilated patient. Artificially ventilated adults are generally ventilated at a low rate, with an approximately constant flow. The model therefore assumes constant inspiratory and expiratory flow, and hence the Reynolds number (Re) is constant for a given airway throughout the inspiratory or expiratory manouvere. Re is therefore calculated for each branch at the start of inspiration and expiration, and the corresponding α, β, and γ values are calculated. When the Re indicates that the flow is laminar, α, β, and γ are set equal to 2. For larger Re, α, β, and γ are equal to the Re multiplied by a specified constant. The sensitivity of the numerical results to this constant is investigated in Section 5.4.

5.3.1.2   Equations describing radial heat transport

A water and heat transport model has been developed which assumes each airway to be comprised of a lumen, airway wall (including air surface liquid and mucus) and an

outer capillary network. The blood in the capillary layer provides heat to the system. Radial heat transport through the layers is described by:

$$c_p \rho \frac{\partial T}{\partial t} = K \left(\frac{1}{r} \frac{\partial}{\partial r} \left(r \frac{\partial T}{\partial r} \right) \right) \tag{5.1}$$

where c_p is the specific heat of the material in the layer, ρ is the material density, T is temperature, K is the thermal conductivity of the tissue, and r is the radial coordinate.

If the temperature and water vapour concentration profiles in the lumen are described by power law curves, then the transfer of heat from the surface liquid into the lumen can be described by considering energy balance at the air-mucus interface. Heat is provided by the capillary layer at a finite rate, which is dependent on a thermal conductance, the distance between the interface and the capillary layer, and the temperature gradient across the layers. Change in temperature of the gas in the lumen will be due to heat movement across the mucus-air interface in response to a gradient of temperature, and latent heat from evaporation of, or condensation onto, the surface liquid. Then:

$$K_{mucus} \left. \frac{\partial T}{\partial r} \right|_{R_+} = K_{air} \left. \frac{\partial T}{\partial r} \right|_{R_-} + D \Delta H \left. \frac{\partial C}{\partial r} \right|_{R_-} \tag{5.2}$$

where K_{mucus} is the thermal conductivity for the mucus layer, R is the radial position of the air-mucus interface, K_{air} is the thermal conductivity for the air and water vapour mixture, D is a diffusion coefficient for water vapour, C is water vapour concentration, and ΔH is the heat of evaporation. Equation (5.2) balances the rate of heat moving through the mucus to the air-mucus interface with the rate of heat moving into the lumen via conduction and via latent heat.

By assuming that the temperature and water vapour concentration profiles are described by power laws across the airway (with r), then T and C can be replaced by:

$$T(r) = T_R + (T_0 - T_R) \left(1 - \left(\frac{r}{R} \right)^{\beta} \right) ; \beta \geq 2 \qquad (5.3)$$

$$C(r) = C_R + (C_0 - C_R) \left(1 - \left(\frac{r}{R} \right)^{\gamma} \right) ; \gamma \geq 2 \qquad (5.4)$$

where T_0 and C_0 are temperature and water vapour concentration in the centre of the airway (peak values), and T_R and C_R are temperature and water vapour concentration at the air-mucus interface. Note that T_0, C_0, T_R, and C_R are all time-dependent. β and γ are coefficients which describe the shape of the profiles. Substituting these descriptions into Equation (5.2) gives an expression for the temperature gradient at the air-mucus interface, as it is approached from the tissue side:

$$\left. \frac{\partial T}{\partial r} \right|_{R_+} = \frac{1}{K_{mucus}} \left(\frac{K_{air} (T_R - T_0) \beta}{R} + \frac{D \Delta H (C_R - C_0) \beta}{R} \right) \qquad (5.5)$$

The maximum amount of water vapour that a volume can hold for a given temperature and pressure is described by the Clausius-Clapeyron equation (Ragone 1995). An approximation to the Clausius-Clapeyron equation over a 15^oC range near body temperature is (Hanna & Scherer 1986c):

$$C = 0.4035584 e^{-4970/T} \qquad (5.6)$$

where T is in units of K, and C is in units of $g \cdot \text{mm}^{-3}$.

The immediate source of water vapour at the air-mucus interface is from the mucus layer. The water is in a liquid state until enough energy is supplied to enable evaporation. If it is assumed that incremental changes in temperature will be small, then it can be assumed that the concentration of water vapour at the air-mucus interface (C_0) is described by Equation (5.6). That is, there is 100% relative humidity at the air-mucus interface (Saidel et al. 1983).

Equation (5.5) provides a boundary condition at the air-mucus interface, and

Equation (5.1) describes the movement of heat through the radial layers, excluding the lumen. Temperature in the body layer is assumed to be constant at core body temperature, providing a fixed boundary condition at this radial position. Radial heat transfer can therefore be solved for through the layers using a finite element method (Zienkiewicz & Taylor 1994).

5.3.2 Axial equations for water and heat transport in the lumen

Equations describing axial transport of water vapour and heat through the lumen of cylindrical branches in an airway model are derived by considering conservation of mass and energy in a 'slice' through a single non-alveolated airway, using the approach described in Section 3.3.1. This provides equations (5.7) and (5.8) in radial coordinates:

$$c_p\rho\frac{\partial T}{\partial t} + c_p\rho u\frac{\partial T}{\partial x} = K\left(\frac{1}{r}\frac{\partial}{\partial r}\left(r\frac{\partial T}{\partial r}\right) + \frac{\partial^2 T}{\partial x^2}\right) \tag{5.7}$$

$$\frac{\partial C}{\partial t} + u\frac{\partial C}{\partial x} = D\left(\frac{1}{r}\frac{\partial}{\partial r}\left(r\frac{\partial C}{\partial r}\right) + \frac{\partial^2 C}{\partial x^2}\right) \tag{5.8}$$

where $T(x,r,t)$ is temperature, $C(x,r,t)$ is water vapour concentration, c_p is specific heat of air, ρ is the density of air, $u(x,r,t)$ is axial velocity, K is a thermal transfer coefficient, D is a water vapour diffusion coefficient. x and r are the axial and radial coordinates.

By assuming that the time-dependent velocity profile follows a power law across the airway (with r), then u can be replaced by:

$$u(r) = u_0\left(1 - \left(\frac{r}{R}\right)^\alpha\right); \alpha \geq 2 \tag{5.9}$$

where u_o is the velocity in the centre of the airway (peak value), and α is a coefficient that describes the shape of the velocity profile.

Substituting equations (5.3), (5.4), (from Section 5.3.1.2) and (5.9) into equations (5.7)

and (5.8), and integrating each term over the lumenal cross-section A gives:

$$Ac_p\rho\left(\frac{\partial T_0}{\partial t}\left(\frac{\beta}{\beta+2}\right)+\frac{u_0\alpha}{\beta+2}\left(\frac{\partial T_0}{\partial x}\left(\frac{\beta\left(\alpha+\beta+4\right)}{\left(\alpha+2\right)\left(\alpha+\beta+2\right)}\right)+\frac{\partial T_R}{\partial x}\left(\frac{2}{\left(\alpha+\beta+2\right)}\right)\right)\right)$$
$$=AK\left(\frac{2\beta\left(T_R-T_0\right)}{R^2}+\frac{\partial^2 T_0}{\partial x^2}\left(\frac{\beta}{\beta+2}\right)+\frac{\partial^2 T_R}{\partial x^2}\left(\frac{2}{\beta+2}\right)\right) \quad (5.10)$$

$$A\left(\frac{\partial C_0}{\partial t}\left(\frac{\gamma}{\gamma+2}\right)+\frac{u_0\alpha}{\gamma+2}\left(\frac{\partial C_0}{\partial x}\left(\frac{\gamma\left(\alpha+\gamma+4\right)}{\left(\alpha+2\right)\left(\alpha+\gamma+2\right)}\right)+\frac{\partial C_R}{\partial x}\left(\frac{2}{\left(\alpha+\gamma+2\right)}\right)\right)\right)$$
$$=AD\left(\frac{2\gamma\left(C_R-C_0\right)}{R^2}+\frac{\partial^2 C_0}{\partial x^2}\left(\frac{\gamma}{\gamma+2}\right)+\frac{\partial^2 C_R}{\partial x^2}\left(\frac{2}{\gamma+2}\right)\right) \quad (5.11)$$

Integrating (5.9) over the lumen cross-section to calculate the average velocity gives:

$$u_{av}=\frac{1}{A}\int_r 2\pi r.u_0\left(1-\left(\frac{r}{R}\right)^{\alpha}\right)\,dr$$
$$=u_0\left(\frac{\alpha}{\alpha+2}\right) \quad (5.12)$$

Rearranging (5.12) gives

$$u_0=u_{av}\left(\frac{\alpha+2}{\alpha}\right) \quad (5.13)$$

Substituting (5.13) into (5.10) and (5.11), and multiplying (5.10) and (5.11) by $\left(\frac{\beta+2}{\beta}\right)$ and $\left(\frac{\gamma+2}{\gamma}\right)$, respectively, results in:

$$Ac_p\rho\frac{\partial T_0}{\partial t}+Ac_p\rho u_{av}\left(\frac{\partial T_0}{\partial x}\left(\frac{\alpha+\beta+4}{\alpha+\beta+2}\right)+\frac{\partial T_R}{\partial x}\left(\frac{2(\alpha+2)}{\beta(\alpha+\beta+2)}\right)\right)$$
$$=A\frac{2K\left(\beta+2\right)\left(T_R-T_0\right)}{R^2}+AK\left(\frac{\partial^2 T_0}{\partial x^2}+\frac{\partial^2 T_R}{\partial x^2}\left(\frac{2}{\beta}\right)\right) \quad (5.14)$$

$$A\frac{\partial C_0}{\partial t} + Au_{av}\left(\frac{\partial C_0}{\partial x}\left(\frac{\alpha + \gamma + 4}{\alpha + \gamma + 2}\right) + \frac{\partial C_R}{\partial x}\left(\frac{2(\alpha + 2)}{\gamma(\alpha + \gamma + 2)}\right)\right)$$
$$= A\frac{2D\left(\gamma + 2\right)\left(C_R - C_0\right)}{R^2} + AD\left(\frac{\partial^2 C_0}{\partial x^2} + \frac{\partial^2 C_R}{\partial x^2}\left(\frac{2}{\gamma}\right)\right) \quad (5.15)$$

Equation (5.14) and Equation (5.15) describe axial movement of heat and water vapour in the airways of a non-alveolated system (i.e. not the respiratory airways).

5.3.2.1 Condensation and evaporation

The model airway surface liquid is assumed to have a variable depth. In the model, surface liquid evaporates in response to absolute concentration gradients. Although a concentration gradient might be present that drives movement of water vapour from the surface liquid into the lumen, the temperature in the lumen might be such that it cannot contain any more water vapour. i.e. it is at saturation. In this case, the evaporated water is assumed to deposit back onto the surface liquid, with no net transfer of energy. The volume of water evaporating from the surface liquid is estimated by assuming that the gradient in water vapour concentration is constant over a time interval, Δt, and that this gradient directly reflects the amount of water vapour evaporating into the lumen. Equation (5.4) is used to estimate the concentration gradient. Multiplying by the surface area and the diffusion coefficient, and dividing by the density of water (ρ_{water}) gives the volume estimate:

$$V_{evap} = \frac{D\gamma\left(C_R - C_0\right)2\pi L\Delta t}{\rho_{water}} \quad (5.16)$$

where V_{evap} is the volume of water evaporating, D is the diffusion coefficient of water vapour in air, and L is the length of the portion of branch element being considered.

The rate of replenishment of water in the surface liquid layer, or rate of reabsorption by the surrounding layers, is assumed to be constant and 'switched' on by changes in depth of the surface layer. That is, if the depth drops below 10 μm then a water source is switched on, or if the depth becomes deeper than 10 μm the tissue reabsorbs some water. The rates of replenishment and reabsorption are assumed to be equal and opposite, at 2.0 $\mu L \cdot cm^{-2} \cdot min^{-1}$ (Phillips, Wong & Yeates 1998).

5.3.2.2 The endotracheal tube

A layer of liquid can condense onto the endotracheal tube, generally during expiration as warm moist air passes over the cool tube surface. This can also evaporate off as dry gas passes over it in the next inspiration. The amount of evaporation from the tube surface is calculated and the condensate depth updated at each time-step.

5.3.3 Solving the transfer equations

Equation (5.1) describes the radial movement of heat through the tissue layers surrounding the lumen in a model airway. Equation (5.5) provides a gradient boundary condition at the air-mucus interface that depends upon knowledge of the temperatures and concentrations within the lumen. A second boundary condition is provided by the fixed temperature at the body core position.

Equation (5.14) and Equation (5.15) describe axial movement of heat and water vapour, respectively. Their solution depends upon knowledge of the temperature and concentration at the air-mucus interface. These non-linear coupled equations can be solved by assuming that T_R and C_R are constant over a time-step. The Lagrange-Galerkin method is used to solve the coupled system, where the advective components are first solved using the Method of Characteristics, then the diffusive components are solved using the Galerkin Finite Element method (see Section 3.3.2.1). Equation (5.1) can then be solved by assuming that the temperature and concentration in the centre of the airway (T_0 and C_0) are constant over a time-step. This assumption allows estimation of the gradient in temperature at the air-mucus interface over the time-interval, and therefore provides the boundary condition at this position for solution. Solving (5.1) provides temperatures at the air-mucus interface, the surface liquid-tissue interface, and interfaces with the endotracheal tube (if present). The concentration at the air-mucus interface is then calculated using Equation (5.6).

Equation (5.1), Equation (5.14) and Equation (5.15) are coupled by their inter-dependence upon $T_0, C_0, T_R,$ and C_R. The system of three equations is therefore solved iteratively: the axial equations (5.14) and (5.15) are solved first, using values of T_R and C_R from the end of the previous solution, to give values for T_0 and C_0; the radial Equation (5.1) is then applied to the layers outside the lumen and solved using the

updated values for T_0, and C_0, and assuming constant $\left.\dfrac{\partial T}{\partial r}\right|_R$, to give new values for T_R and C_R; the axial and radial solutions are iterated, using updated temperature and concentration values, until there is convergence in the solution.

Convergence is tested by separately summing the errors in solutions at individual node points (for the axial solution), and the errors at individual Gauss points (Zienkiewicz & Taylor 1994) (for the radial solution).

$$Error = \sum_{n=1}^{N} \frac{|X_n(t + \Delta t) - X_n(t)|}{1 + |X_n(t)|} \tag{5.17}$$

where X is either T_0 or C_0 at node n, or T_R at Gauss point n, and N is the number of nodes or Gauss points in the model. When all of the summed errors are below 10^{-5}, then the solution is assumed to have converged.

5.3.3.1 Boundary and simulation conditions

Transfer of water vapour and heat from the airway walls into unconditioned air in the lumen was simulated in a symmetric lung model and in an asymmetric conducting airway (ACA) model, both with radial layers (see Section 5.3). Inspired temperatures and water contents were set to mimic the experimental conditions of McFadden et al. (1985) and Ryan et al. (2000). Flow was constant, and uniformly distributed.

For the numerical simulations without an endotracheal tube, a fixed temperature and humidity were applied at the top of the trachea during inspiration. When an endotracheal tube was placed to 2/3 of the way down the trachea, the inspired temperatures were raw data from a single breath, supplied by Ryan et al. (2000). The raw data are listed in Appendix A. That is, the experimental inspired temperature changed with time, so a time-varying fixed boundary condition was applied at the entrance to the endotracheal tube. The temperatures at 0.2 s intervals were experimentally measured values, and values between these time were calculated by linear interpolation between the measured values.

During expiration the fixed boundary condition was changed to a zero diffusive flux boundary condition. Zero diffusive flux boundary conditions were applied

at the end of the transitional bronchioles in the models during inspiration; fixed concentrations and humidities (at body core conditions) were applied during expiration. The temperature and humidity at the end of the transitional bronchioles was monitored during inspiration to check that it did not drop below core conditions.

A body temperature of 36.5^oC was assumed in the tissue surrounding the model for simulations without an endotracheal tube, unless otherwise specified. For the simulations where an endotracheal tube was included, the body temperature was different for each set of simulation conditions: Ryan et al. (2000) measured the body temperature to be $37.2\pm1.0°C$, but inspection of their results showed convergence towards different expiratory temperatures at the most distally measured point. This suggests that the body temperature may have varied between the different inspired condition set experiments. The body temperatures used in the following simulations were all within one standard deviation of the experimental mean.

In the McFadden et al. (1985) experiments, the subjects breathed either room air or frigid air at a range of ventilation frequencies. The air temperature and humidity were specified for the pre-inspired gas, and the temperatures within the airway tree were recorded by multiple thermistors. For these experiments the subjects inspired through the mouth, therefore the inspired air was partly conditioned before it entered the trachea. The ACA model begins at the trachea, so the inspiratory temperatures used for simulations were those given experimentally for the sub-glottis region. The inspired air was assumed to be nearly saturated at the sub-glottis temperature.

The physical properties assumed in the model are listed in Table 5.2. In addition to these properties, the latent heat of vaporisation was assumed to be 2411 kJ $\cdot$ kg^{-1}, and the water vapour and thermal diffusivities were assumed to be 27.7 mm$^2 \cdot$ s^{-1} and 23.7 mm$^2 \cdot$ s^{-1}, respectively (Saidel et al. 1983).

Material	ρ (g $\cdot$ mm^{-3})	C_p (kJ $\cdot$ g$^{-1} \cdot$ K^{-1})	K (kJ $\cdot$ mm$^{-1} \cdot$ s$^{-1} \cdot$ K^{-1})
Air[1]	0.112 x 10^{-5}	1.0059 x 10^{-3}	0.268 x 10^{-7}
Water (ASL)	0.110 x 10^{-2}	0.4184 x 10^{-2}	0.550 x 10^{-6}
PVCETT[2]	0.1714 x 10^{-2}	0.105 x 10^{-2}	0.920 x 10^{-7}
Tissue[3]	0.161 x 10^{-3}	0.4174 x 10^{-2}	0.110 10^{-6}

Table 5.2: *Material parameters used in the water and heat transfer model. 1. from Naftali et al. 1998, 2. provided by Fisher & Paykel Healthcare, 3. from Schweikert and Keanini 1999.*

5.4 Results

5.4.1 Ensuring convergence of the solution

5.4.1.1 Convergence with time-step size

An appropriate time-step (Δt) size was determined by examining the difference in simulated temperatures as Δt was decreased. Table 5.3 lists the percentage difference in temperatures from one Δt to a smaller size, for temperatures at 43 mm from the top of the trachea, at the end of the tenth inspiration and expiration. Changing Δt from 0.005 s to 0.002 s changed the temperature at the end of inspiration by 0.174%, and the temperature at the end of expiration by 0.201%. Halving Δt again produced very small changes in the end-manouvere temperatures. A Δt of 0.005 s was chosen for solution of the water and heat transfer equations.

Δt (s)	$T_{\mathrm{insp}}\%$	$T_{expn}\%$
0.05 - 0.02	2.76	2.06
0.02 - 0.01	1.28	1.11
0.01 - 0.005	0.297	0.377
0.005 - 0.002	0.174	0.201
0.002 - 0.001	0.130	0.139

Table 5.3: *Percentage difference in temperature from one time-step size to a smaller size, for temperatures at 43 mm from the top of the trachea in the ACA model.* T_{insp} *is the percentage difference in end-inspiratory temperature, and* T_{expn} *is the percentage difference in end-expiratory temperature.*

5.4.1.2 Convergence of the iterated solutions

Convergence in the iterated solution at each time-step was achieved after two solutions of each system of equations. That is, an initial solution of the axial transport equations with fixed interface values, solution of the radial heat equation with fixed centre-lumen values, a further axial solution with updated interface values, and a final radial solution with updated centre-lumen values. Convergence was therefore achieved with the minimum possible number of solutions.

5.4.1.3 Convergence with number of breaths

Convergence in the numerical solutions for end-phase temperatures was achieved by the tenth breath, regardless of the breath characteristics. Figure 5.3(a) and (b) demonstrate convergence over ten breaths for the temperature at the centre of the airway lumen (T_{lumen}) and the temperature at the mucus-air interface (T_{mai}), respectively, for an inspired temperature (T_{insp}) of 32.0°C, and a ventilation rate ($\dot{V}$) of $15 \, L \cdot min^{-1}$ in the ACA model.

(a) T_{lumen} (b) T_{mai}
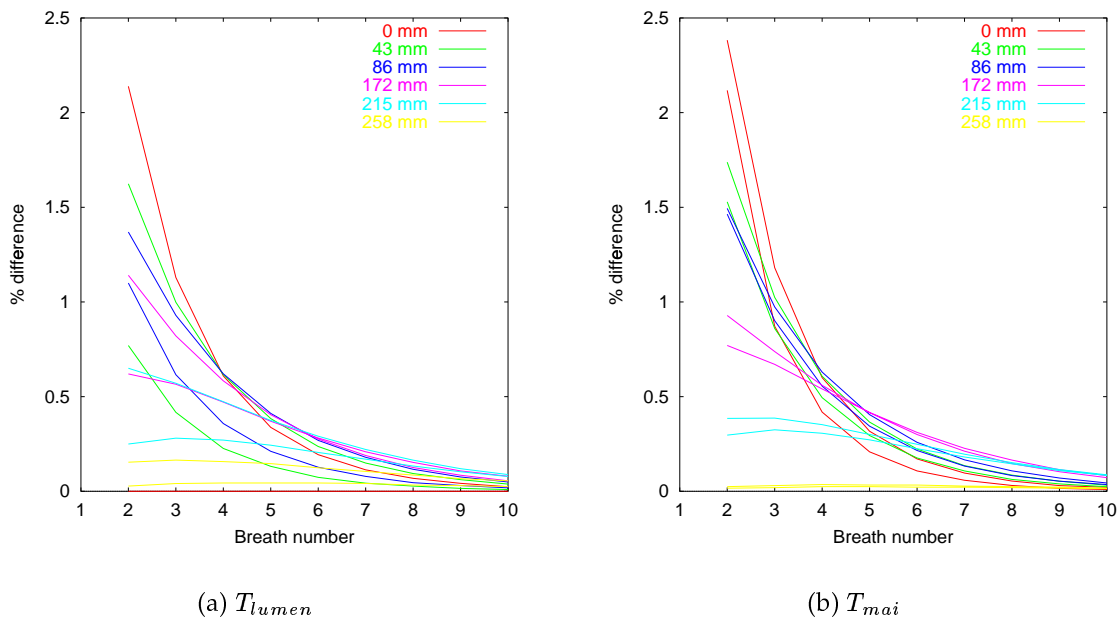
Figure 5.3: *Percentage difference in temperatures from breath to breath, at each data point over ten breaths.* $T_{insp} = 32.0°C$, $\dot{V} = 15 \, L \cdot min^{-1}$. *The end-inspiratory temperatures for a given data point are on the corresponding curve with the lowest values, and the end-expiratory temperatures are on the corresponding curve with the highest values. (a) Temperature in the centre of the airway lumen, (b) temperature at the air-mucus interface.*

By the tenth breath, every point at distances corresponding to the measurement points of McFadden et al. (1985) had less than a 0.1% change in temperature relative to its temperature at the previous breath. Table 5.4 lists the percentage difference in T_{lumen} from the temperature at the previous breath for the second data point (43 mm from the top of the trachea) for the eight different inspiratory condition sets investigated by McFadden et al. (1985). The inspired relative humidity was assumed to be 98% for

each simulation. The end-inspiratory percentage change at the tenth breath was less than 0.1% for all simulations; the end-expiratory percentage change was less than 0.5% for all simulations. All subsequent simulations solved for a minimum of ten breaths.

$T_{mouth}(^\circ\text{C})$	V_{rate} (L $\cdot$ min^{-1})	$T_{insp}\%$	$T_{expn}\%$
32.0	15	0.0092	0.0382
31.3	30	0.0411	0.1595
30.3	60	0.0268	0.1661
29.2	100	0.0238	0.1398
28.1	15	0.0205	0.0619
25.2	30	0.0839	0.3524
23.5	60	0.0041	0.1496
20.5	100	0.0845	0.4625

Table 5.4: *Percentage difference in temperature from previous breath for different inspiratory conditions. 43 mm from the top of the trachea in the ACA model.* T_{insp} *is the percentage difference in end-inspiratory temperature, and* T_{expn} *is the percentage difference in end-expiratory temperature.*

Simulating a single breath with a 0.5 s inspiration and 0.5 s expiration, with a time-step of 0.005 s, took approximately 40 minutes of computing time on a Silicon Graphics Origin 2000 computer, using four 250 MHz processors. Solution of the water and heat transfer system was therefore more than five times slower than solution of the gas mixing system described in Chapter 3.

5.4.2 Comparison of numerical results with experimental data

Water and heat transfer simulations were performed using the experimental conditions of McFadden et al. (1985): the $\dot{V}$ ranged from 15 L $\cdot$ min^{-1} to 100 L $\cdot$ min^{-1}, and the inspired temperatures were those measured in the sub-glottis region. α, β, and γ were equal to the Re divided by 50 for each simulation, and the inspired air was assumed to be at 98%RH. The sensitivity of the results to these assumptions is investigated in Section 5.4.4.

McFadden et al. (1985) recorded temperatures in the lungs down an airway path from the trachea to a subsegmental bronchus of the anterior segment of the right lower lobe. In this section, the temperatures down a corresponding individual path in the ACA model are compared with the experimental results.

5.4.2.1 Ventilation rate 15 $L \cdot min^{-1}$, inspired temperature 32.0°C

Figure 5.4(a) and (b) show model temperatures at the end of inspiration and the end of expiration, respectively. The red line in Figure 5.4(a) plots T_{lumen}; the blue line plots T_{mai}; the black line plots experimental results ($\pm$ one standard error, SE) from McFadden et al. (1985).

At the end of inspiration T_{lumen} was within one SE of the experimental mean values from the top of the trachea to the fourth data point (172 mm from the top of the trachea). T_{mai} was warmer than T_{lumen} at each data point at the end of inspiration, with the difference decreasing moving distally. At the most distal data point, T_{mai} was close to body temperature (36.5°C) but T_{lumen} was closer to 36.0°C. The modelled temperatures in the trachea (0 to 100 mm from the entrance to the model) were very close to the mean experimental values.

(a) End of inspiration   (b) End of expiration

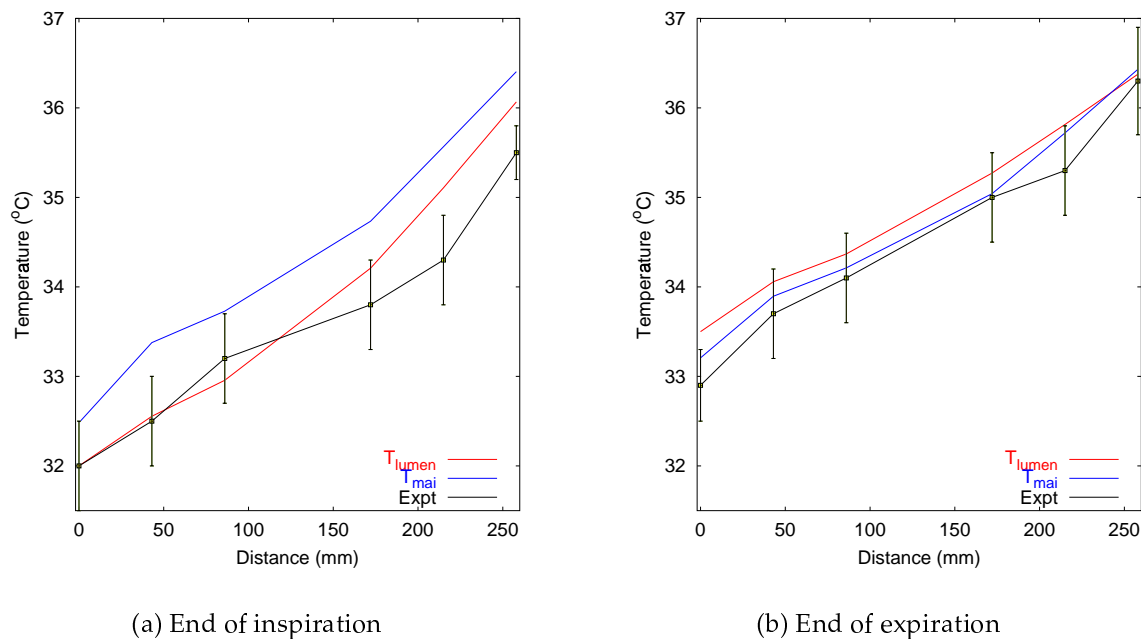**Figure 5.4:** *End-inspiratory and end-expiratory temperatures in the ACA model, with T_{insp}=32.0°C and $\dot{V}$ = 15 $L \cdot min^{-1}$. Red = T_{lumen}, blue = T_{mai}, black = experimental results (McFadden et al. 1985). (a) Temperatures at the end of inspiration, (b) temperatures at the end of expiration. Note the upper boundary of the graphs are higher than body temperature (36.5°C).*

The temperatures at the end of expiration were closer to the experimental values than at the end of inspiration: T_{lumen} and T_{mai} were both within one SE of the mean experimental values for all data points except at the top of the trachea. At this point, T_{mai} was within one SE of the experimental mean, but T_{lumen} was slightly higher. The difference between T_{mai} and T_{lumen} was less at the end of expiration than at the end of inspiration. Whereas at the end of inspiration T_{mai} was warmer than T_{lumen}, at the end of expiration this had reversed, except at the most distal data point.

Because the thermistors used by McFadden et al. (1985) had a relatively slow response time (63% response time of 0.250 s in stirred water), the temperatures they recorded at the end of inspiration and expiration would have actually been temperatures from an earlier portion of the breath. In Figure 5.5, T_{lumen} and T_{mai} are plotted against distance from the top of the trachea for 50%, 75%, and 100% through inspiration and expiration. The difference in temperatures for both T_{lumen} and T_{mai} from 50 to 100% of inspiration were very small, but the difference for expiration was larger: the temperatures were lower at 50% expiration than 100% expiration, particularly in the trachea. The 50% expiratory temperature was within one SE of the experimental mean at the top of the trachea.
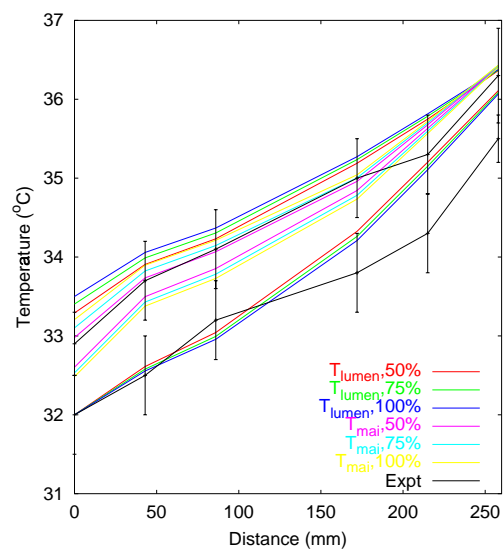
Figure 5.5: T_{insp}=32.0°C, $\dot{V}$ = 15 L · min^{-1}: *temperatures in the centre of the airway lumen at 50%, 75%, and 100% through inspiration and expiration, compared with experimental results (McFadden et al. 1985).*

The mean, maximum, and minimum central lumen temperatures at each data point distance were calculated down the ACA model. That is, the temperatures were calculated using values from every airway in the model that was a distance of 0, 43, 86, 155, 225, or 258 mm from the top of the trachea. Figure 5.6 plots the mean, minimum, and maximum central lumen temperatures for the ACA model against distance from the top of the trachea. The curves are compared with the temperatures in the individual

path used in this study for comparison with experimental results. The experimental results from McFadden et al. (1985) are also shown, ±SE.

The maximum temperature reached body temperature (36.5°C) 225 mm from the top of the trachea, at the end of both inspiration and expiration. The end-inspiratory mean temperatures were higher than one SE from the mean for the last three data points. At both the end of inspiration and expiration, the mean temperature was close to body temperature for the last two data points. This indicates that most of the temperatures at these distances were at, or close to, body temperature, and the lower temperatures in the individual path were not common at this distance. The minimum temperatures were lower than those in the individual path for the last two data points at the end of inspiration, and for every data point distal to the trachea at the end of expiration. In both cases, the minimum temperatures were

Figure 5.6: $T_{insp}=32.0$°C, $\dot{V} = 15$ L $\cdot$ min^{-1}: *mean, minimum, and maximum temperatures down the airways in the ACA model at the end of inspiration and expiration, compared with experimental results (McFadden et al. 1985) ±SE, and temperatures down an individual path.*

closer to the mean experimental values than the selected path.

5.4.2.2 Increasing the rate of ventilation

Figure 5.7 (a) and (b) compare T_{lumen} (red) and T_{mai} (blue) from the ACA model with experimental results from McFadden et al. (1985) (black) for a $\dot{V}$ of 30 L $\cdot$ min^{-1}, and a T_{insp} of 31.3°C. Only mean experimental values are shown, as McFadden et al. (1985) supplied values for the SE for only $\dot{V}$ = 15 and 100 L $\cdot$ min^{-1}.

The simulated temperatures in the airway centre were very close to the mean experimental values for the end of both inspiration and expiration. T_{mai} was also close to the experimental values. As was observed for a ventilation rate of 15 L $\cdot$ min^{-1} with T_{insp} 32.0°C, T_{mai} was higher than T_{lumen} during inspiration and lower during

expiration. The exception to this was for the most distal point during expiration, where T_{mai} was warmer than T_{lumen}.

(a) End of inspiration   (b) End of expiration
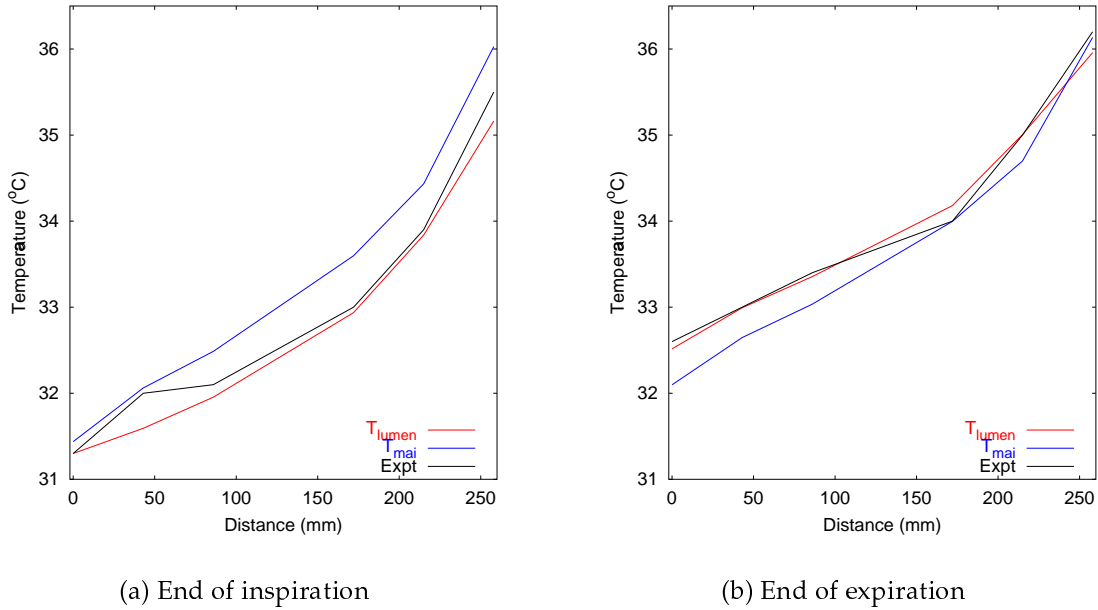
Figure 5.7: *End-inspiratory and end-expiratory temperatures in the ACA model, with T_{insp}=31.3°C and $\dot{V} = 30$ L · min^{-1}. Red = T_{lumen}, blue = T_{mai}, black = experimental results (McFadden et al. 1985). (a) Temperatures at the end of inspiration, (b) temperatures at the end of expiration. Note the upper boundary of the graphs are at body temperature (36.5°C).*

Increasing the $\dot{V}$ to 60 L · min^{-1} with a T_{insp} of 30.3°C, resulted in the end-inspiratory and end-expiratory curves shown in Figure 5.8. The end-inspiratory and end-expiratory values for both T_{lumen} and T_{mai} followed the shapes of the experimental curves, with the simulated curves close in value to the experimental mean curves. However, T_{lumen} was slightly lower than the experimental values for each data point at the end of inspiration.

Figure 5.9 (a) and (b) show end-inspiratory and end-expiratory temperatures for a $\dot{V}$ of 100 L · min^{-1}. The temperatures at the end of inspiration were close to, or within, one SE of the experimental mean values. T_{mai} at the end of expiration was close to the experimental mean values, but T_{lumen} was significantly higher than the experimental values for the first three data points (within the trachea).

(a) End of inspiration   (b) End of expiration
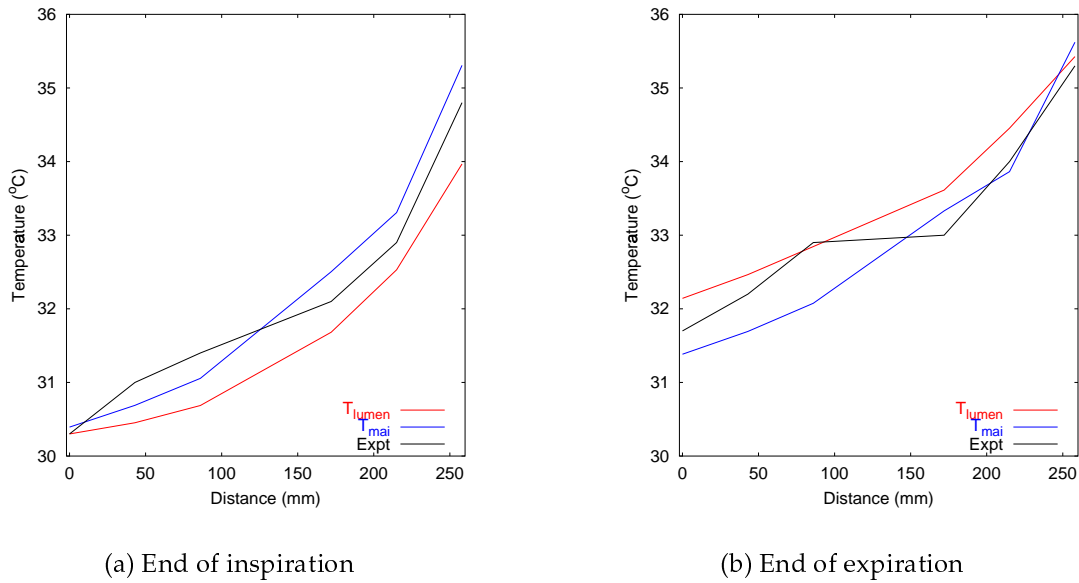
Figure 5.8: *End-inspiratory and end-expiratory temperatures in the ACA model, with* T_{insp}=*30.3°C and* $\dot{V}$ = *60* L · min^{-1}. *Compared with experimental results (McFadden et al. 1985). (a) Temperatures at the end of inspiration, (b) temperatures at the end of expiration. Note the upper boundary of the graphs are lower than body temperature (36.5°C).*

(a) Inspiration   (b) Expiration

Figure 5.9: *End-inspiratory and end-expiratory temperatures in the ACA model, with* T_{insp}=*29.2°C and* $\dot{V}$ = *100* L · min^{-1}. *Compared with experimental results (McFadden et al. 1985). (a) Temperatures at the end of inspiration, (b) temperatures at the end of expiration. Note the upper boundary of the graphs are lower than body temperature (36.5°C).*

Simulated temperatures for each $\dot{V}$ are compared with experimental values in Figure 5.10 (a) and (b) for the end of inspiration and expiration, respectively. The experimental and simulated curves all have lower values for high $\dot{V}$ and low T_{insp}. The simulated curves followed the trend of the experimental curves, such that the temperatures decreased with increasing $\dot{V}$ and decreasing T_{insp}.

(a) End of inspiration   (b) End of expiration
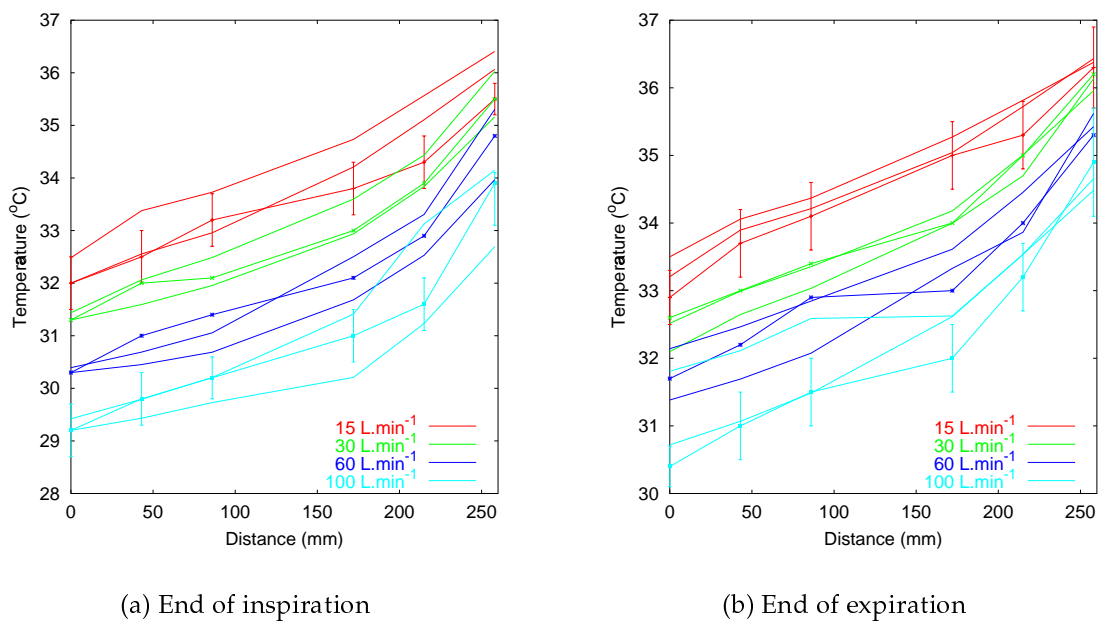
Figure 5.10: *Temperatures at the end of inspiration and end of expiration compared with experimental values (dotted lines, McFadden et al. 1985) for inspiration of room temperature air through the mouth. Experimental mean values $\pm SE$ is shown for $\dot{V}$ of $15\, \mathrm{L} \cdot \mathrm{min}^{-1}$ and $100\, \mathrm{L} \cdot \mathrm{min}^{-1}$. T_{lumen} curves are the lower of the paired lines in (a) and the upper in (b).*

The experimental curves are bracketed by the simulated T_{lumen} and T_{mai} curves for each corresponding simulation, for each $\dot{V}$ at the end of inspiration, and for each $\dot{V}$ at the end of expiration except $\dot{V} = 100\, \mathrm{L} \cdot \mathrm{min}^{-1}$.

Penetration of cool air into the ACA model for the four $\dot{V}$ described in this section is illustrated in the temperature fields (T_{lumen}) shown in Figure 5.11 down to generation 12. Only the first 12 generations are shown so that the penetration of unconditioned air is not obscured by the higher temperatures in the distal airways.

(a) End of inspiration, $\dot{V} = 15 \, \text{L} \cdot \text{min}^{-1}$

(b) End of expiration, $\dot{V} = 15 \, \text{L} \cdot \text{min}^{-1}$

(c) End of inspiration, $\dot{V} = 30 \, \text{L} \cdot \text{min}^{-1}$

(d) End of expiration, $\dot{V} = 30 \, \text{L} \cdot \text{min}^{-1}$

(f) End of inspiration, $\dot{V} = 60 \, \text{L} \cdot \text{min}^{-1}$

(g) End of expiration, $\dot{V} = 60 \, \text{L} \cdot \text{min}^{-1}$

(h) End of inspiration, $\dot{V} = 100 \, \text{L} \cdot \text{min}^{-1}$

(i) End of expiration, $\dot{V} = 100 \, \text{L} \cdot \text{min}^{-1}$
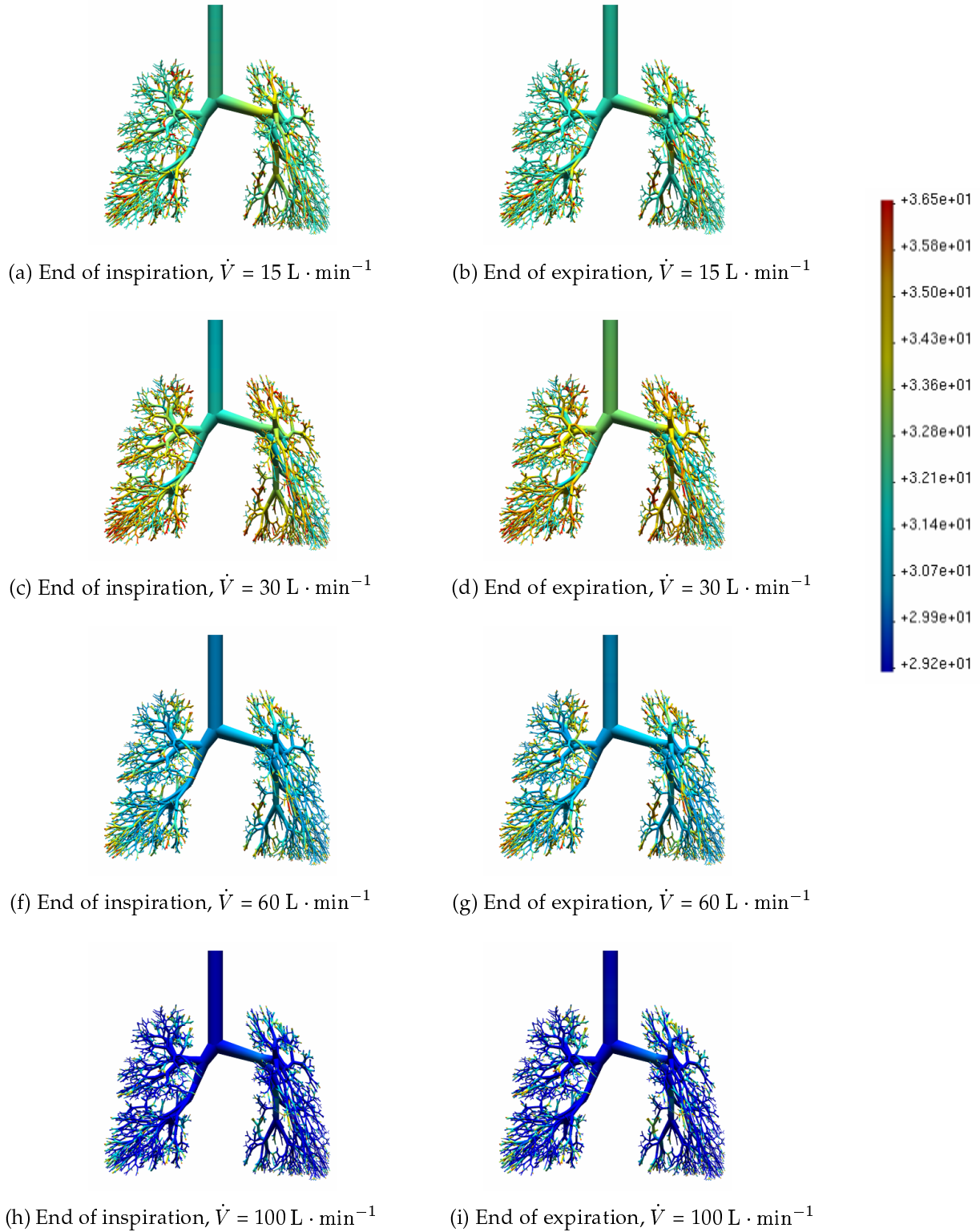
Figure 5.11: *Temperature fields in the first 12 generations of the ACA model at the end of inspiration and the end of expiration, for $\dot{V}$ = 15, 30, 60, and 100 $\text{L} \cdot \text{min}^{-1}$, and mouth inspiration of room temperature air. The temperatures are in degrees C.*

5.4.2.3   Decreasing the inspired temperatures

McFadden et al. (1985) performed a second set of simulations using the same $\dot{V}$ as in the first set, but with inspiration of frigid air (-18.6 $\pm$1.2°C). Figure 5.12, Figure 5.13, and Figure 5.14 compare results from the ACA model with experimental results from McFadden et al. (1985) for inspiration of frigid air with $\dot{V}$ of 15 L $\cdot$ min^{-1}, 30 L $\cdot$ min^{-1}, and 60 L $\cdot$ min^{-1}, respectively.

The simulated end-inspiratory T_{lumen} values were close to the experimental values, particularly in the trachea (0 mm to 100 mm). However, the end-expiratory T_{lumen} and T_{mai} curves were both higher than the experimental values. The air-mucus interface did not cool enough during inspiration to facilitate sufficient cooling of the lumenal gas during expiration. That is, T_{mai} did not reach values as low as the experimental end-expiratory values, therefore it was not possible for the model to cool the expired gas to the end-expiratory experimental temperatures.

(a) End of inspiration
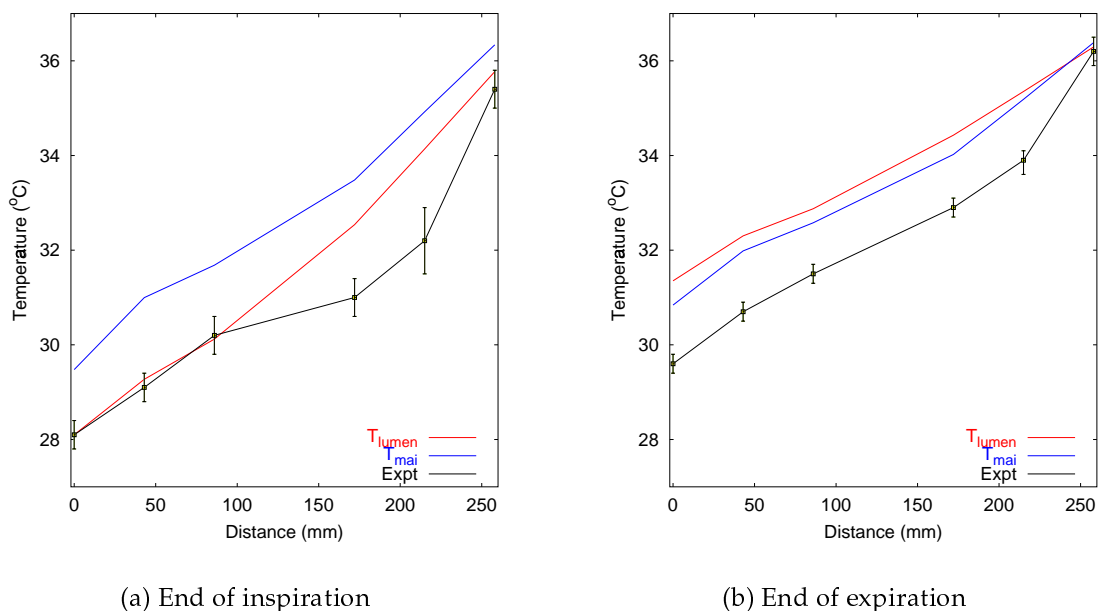
(b) End of expiration

Figure 5.12: *End-inspiratory and end-expiratory temperatures in the ACA model, with T_{insp}=28.1°C and $\dot{V}$ = 15 L $\cdot$ min^{-1}. Red = T_{lumen}, blue = T_{mai}, black = experimental results (McFadden et al. 1985). (a) Temperatures at the end of inspiration, (b) temperatures at the end of expiration. Note the upper boundary of the graphs are at body temperature (36.5°C).*
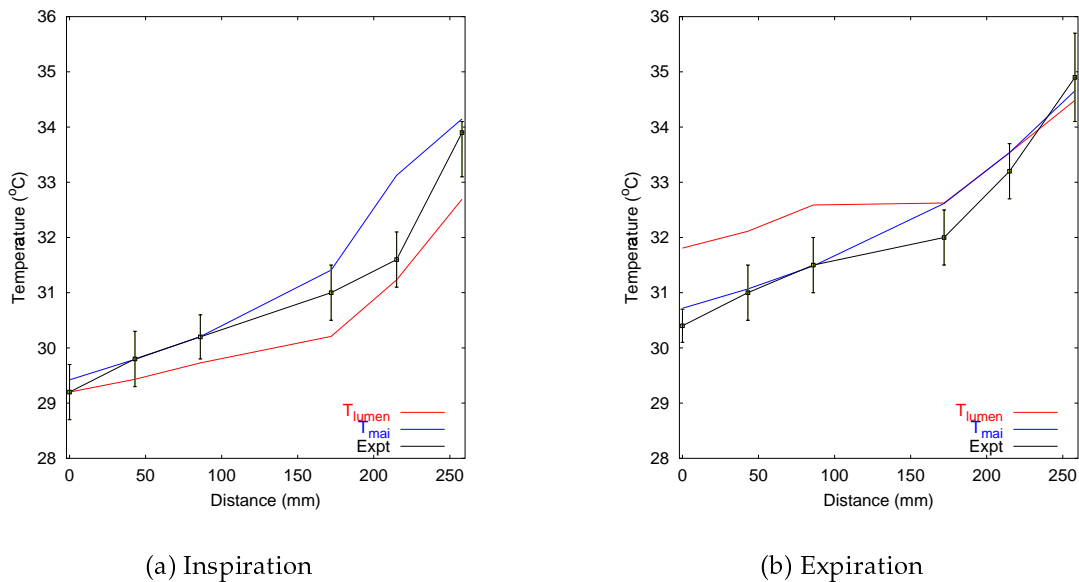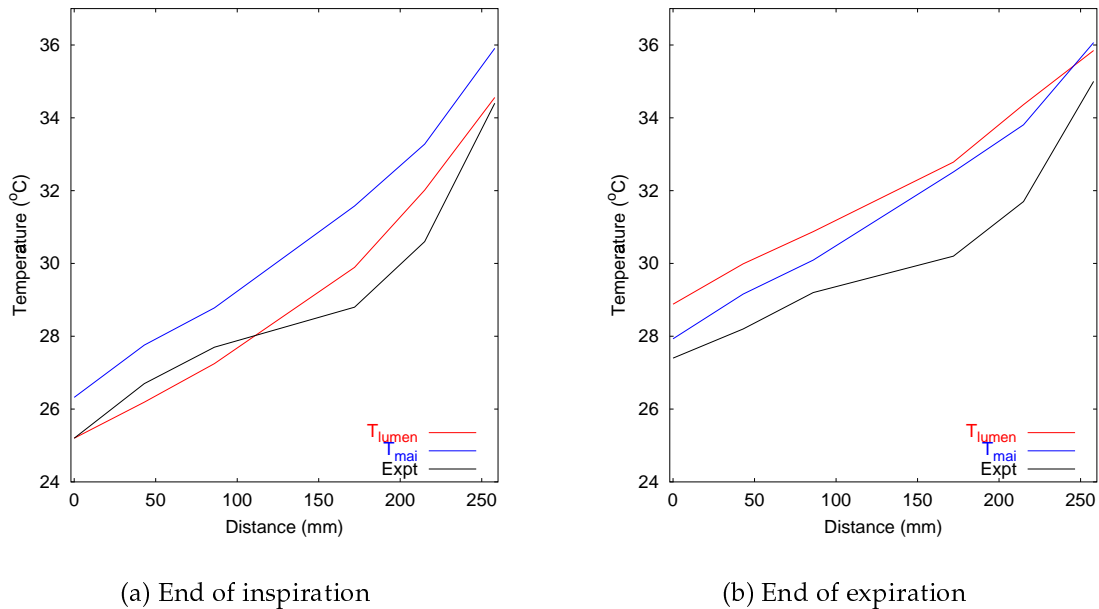
(a) End of inspiration

(b) End of expiration

Figure 5.13: *End-inspiratory and end-expiratory temperatures in the ACA model, with* T_{insp}=25.2°C *and* $\dot{V}$ = 30 L · min^{-1}. *Red* = T_{lumen}, *blue* = T_{mai}, *black* = *experimental results (McFadden et al. 1985). (a) Temperatures at the end of inspiration, (b) temperatures at the end of expiration. Note the upper boundary of the graphs are at body temperature (36.5°C).*

Increasing $\dot{V}$ to 30 L · min^{-1} and reducing the inspired temperature to 25.2°C produced the curves shown in Figure 5.13(a) and (b) for the end of inspiration and the end of expiration, respectively. T_{lumen} at the end of inspiration was very close to the experimental curve over the range of data points. At the end of inspiration T_{mai} was slightly higher than the experimental mean curve at the end of expiration, and therefore T_{lumen} at the end of expiration was also higher than the experimental curve.

Increasing $\dot{V}$ to 60 L · min^{-1}, with T_{insp} 23.5°C produced the end-phase curves in Figure 5.14. Once again, T_{lumen} was very close to the experimental curve at the end of inspiration. However, at the end of expiration T_{lumen} at the top of the trachea (0 mm) was warmer than the experimental mean by more than 2°C. For the lower $\dot{V}$, T_{mai} at the most distal data point (258 mm) was always warmer than the experimental value at this point, but for $\dot{V}$ = 60 L · min^{-1}, T_{mai} at the most distal data point at the end of both inspiration and expiration was cooler than the corresponding experimental value.

(a) End of inspiration (b) End of expiration
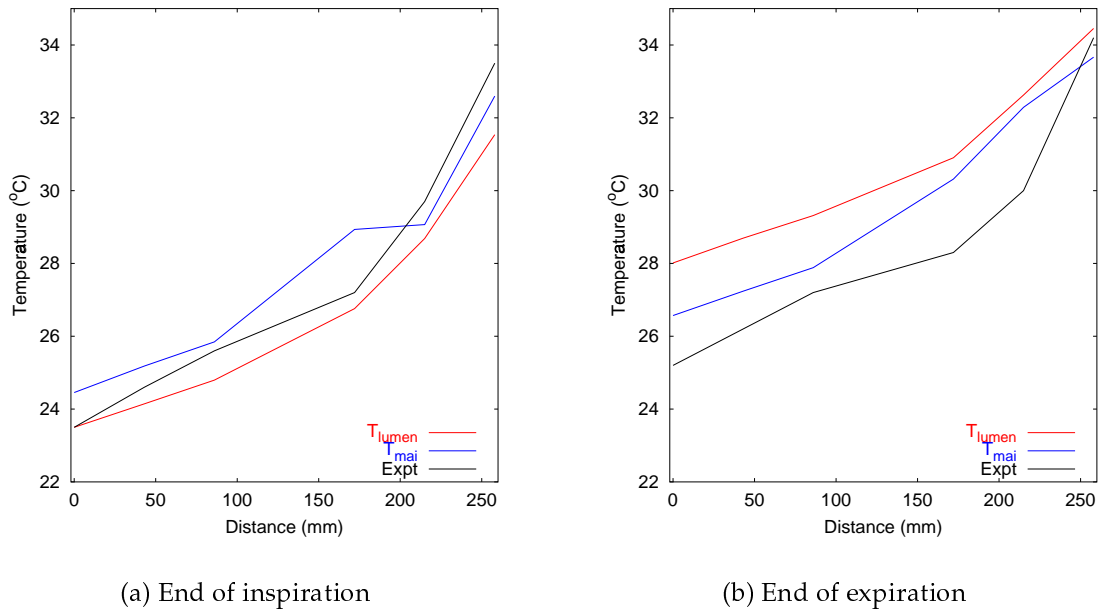
Figure 5.14: *End-inspiratory and end-expiratory temperatures in the ACA model, with T_{insp}=23.5°C and $\dot{V}$ = 60 L · min^{-1}. Red = T_{lumen}, blue = T_{mai}, black = experimental results (McFadden et al. 1985). (a) Temperatures at the end of inspiration, (b) temperatures at the end of expiration. Note the upper boundary of the graphs are lower than body temperature (36.5°C).*

Simulated temperatures for each $\dot{V}$ are compared with experimental values in Figure 5.15 (a) and (b) for the end of inspiration and the end of expiration, respectively. The experimental and simulated curves all have lowest values for high $\dot{V}$ and low T_{insp}.

The simulated curves do not bracket the experimental curves as tightly as in the previous section (with inspiration of room temperature air). For the results at the end of inspiration, the simulated values in the trachea (down to 100 mm) are distinctly related to the corresponding experimental curve, but for the more distal data points there is more of a cross-over between the results. That is, the numerical results for $\dot{V}$ = 30 L · min^{-1} are closest to the experimental results for $\dot{V}$ = 15 L · min^{-1} for the last three data points. At the end of expiration, there was cross-over between the numerical results for $\dot{V}$ = 60 L · min^{-1} and the experimental results for $\dot{V}$ = 30 L · min^{-1}, over the entire range of data points.

(a) End of inspiration
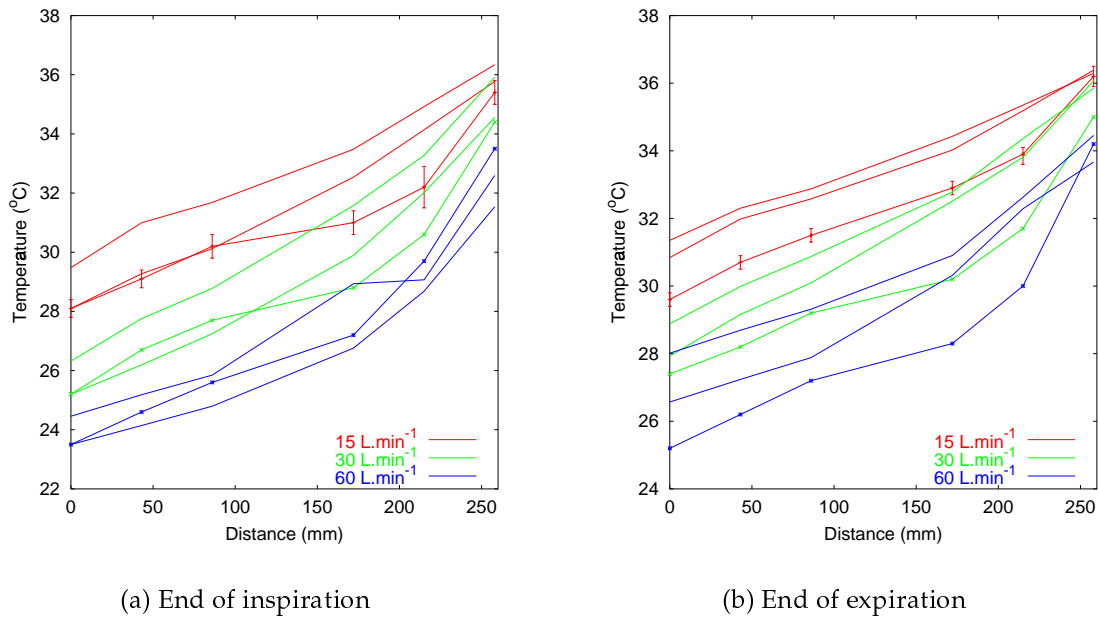
(b) End of expiration

Figure 5.15: *Temperatures at the end of inspiration and end of expiration compared with experimental values (dotted lines, McFadden et al. 1985) for inspiration of frigid air through the mouth. Experimental mean values ±SE are shown for $\dot{V} = 15\,\mathrm{L} \cdot \mathrm{min}^{-1}$. (a) Temperatures at the end of inspiration ($\mathrm{T_{lumen}}$ curves are the lower of the paired lines), (b) temperatures at the end of expiration ($\mathrm{T_{lumen}}$ curves are the upper of the paired lines).*

5.4.3 Comparing models with different levels of complexity

Numerical results from a symmetric model (red and green) and the ACA model (blue and purple) are compared in Figure 5.16 (a) and (b) for $\dot{V} = 15\,\mathrm{L} \cdot \mathrm{min}^{-1}$, $\mathrm{T_{insp}} = 32.0°\mathrm{C}$ and $\dot{V} = 100\,\mathrm{L} \cdot \mathrm{min}^{-1}$, $\mathrm{T_{insp}} = 29.2°\mathrm{C}$, respectively.

Results from the two models for $\dot{V} = 15\,\mathrm{L} \cdot \mathrm{min}^{-1}$ were close for both $\mathrm{T_{lumen}}$ and $\mathrm{T_{mai}}$ within the trachea (0 mm to 100 mm). The difference in results from the two models increased moving distally: the temperatures from the symmetric model approached body temperature at the last two data points, whereas those from the ACA model were closer to the experimental measurements.

For the higher rate of ventilation and lower $\mathrm{T_{insp}}$, $\mathrm{T_{lumen}}$ and $\mathrm{T_{mai}}$ from the two models were close at the first three data points at the end of inspiration. For the more distal data points $\mathrm{T_{lumen}}$ from the ACA model was lower than from the symmetric

model, and T_{mai} was higher at the fourth data point and then lower for the remaining points. T_{mai} at the end of expiration had close values for the two models for the first three data points, but T_{lumen} showed a larger difference in temperatures for the same points. Both T_{mai} and T_{lumen} from the two models showed large differences for the more distal data points at the end of expiration.

(a) T_{insp}=32.0°C, $\dot{V}$ = 15 L · min^{-1} (b) T_{insp}=29.2°C, $\dot{V}$ = 100 L · min^{-1}
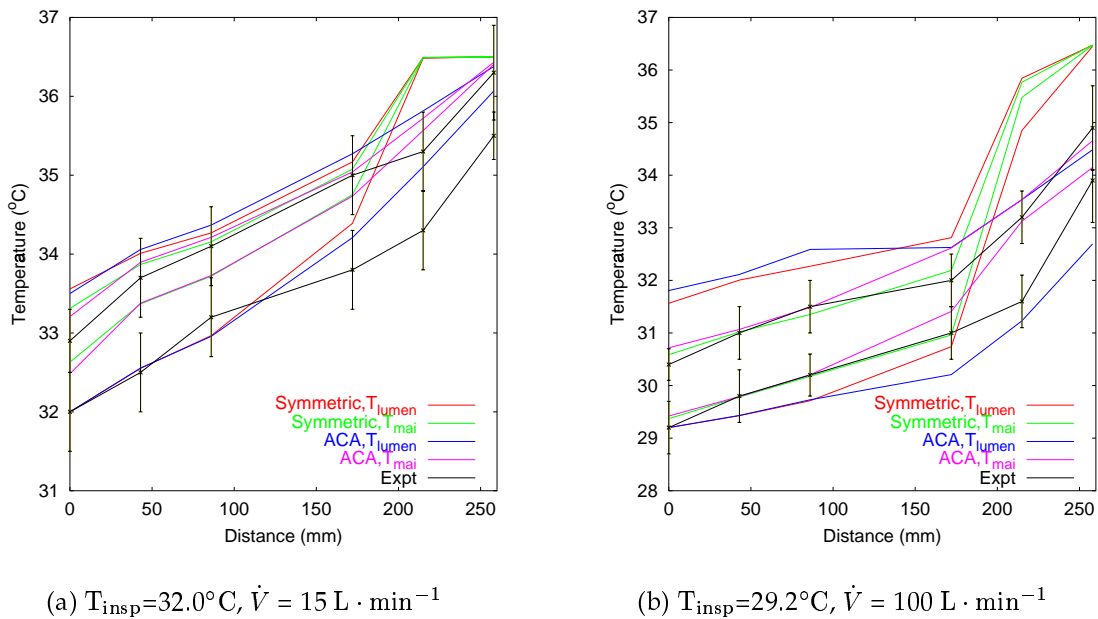
Figure 5.16: *Comparison of numerical results from a symmetric model and the ACA model. Temperatures in the centre of the airway lumen (T_{lumen}) and at the air-mucus interface (T_{mai}) are compared at equidistant points down airway paths in a Weibel (1963) lung model and in a model with a degree of asymmetry that is representative of the human lungs. (a) For inspiration of air at 32.0°C with ventilation at 15 L · min^{-1}, (b) for inspiration of air at 29.2°C with ventilation at 100 L · min^{-1}.*

5.4.4 Sensitivity of the results to model parameters

5.4.4.1 Sensitivity to inspired relative humidity

For the previous simulations, the inspired *RH* was assumed to be 98%. To investigate the sensitivity of the numerical results to this assumption, simulations were run in the symmetric model using T_{insp} = 31.3°C, a $\dot{V}$ of 30 L · min^{-1}, and inspired relative humidity (RH_{insp}) = 80, 90, 92, 94, 96, 98, and 100%.

Figure 5.17(a) plots the temperature at each experimental data point against distance from the top of the trachea, for each simulated RH_{insp}. In Figure 5.17 the difference in temperatures from those produced with $RH_{insp} = 98\%$ is plotted against RH. Increasing the RH from 98 to 100% had little effect on the end-inspiratory and end-expiratory results. Decreasing the inspired RH decreased both the end-inspiratory and end-expiratory temperatures. Although changing the inspired RH changed the simulated temperatures, the changes were small, even for large differences in RH; changing from 98 to 80% RH produced a 1.2°C change in the temperature at the entrance to the model at the end of expiration.

(a) T_{lumen} (b) Temperature differences (°C)
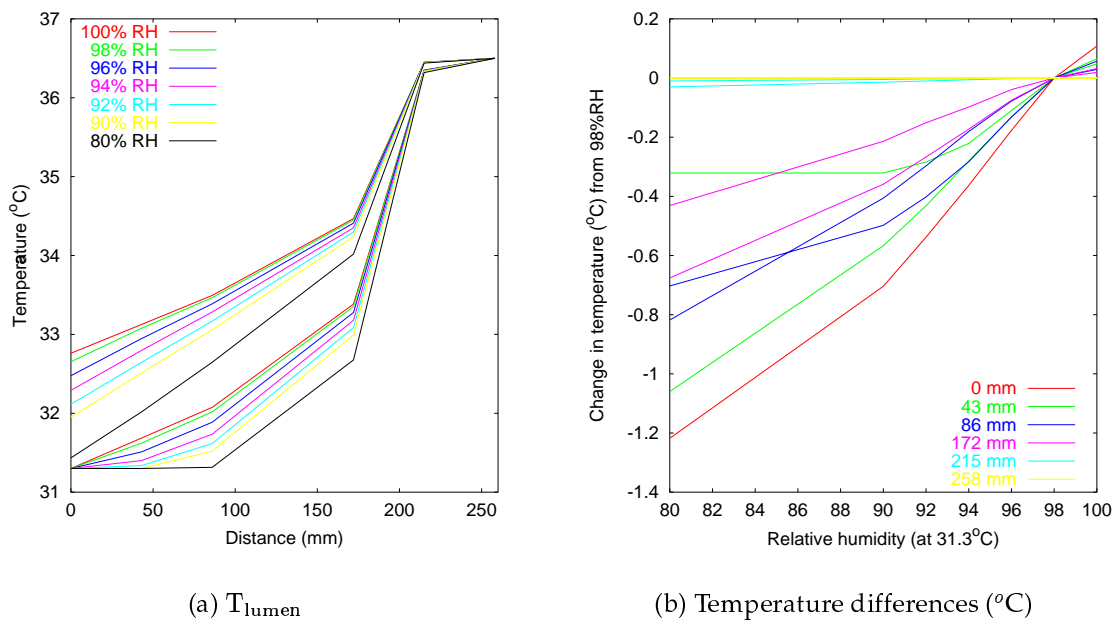
Figure 5.17: *Sensitivity of* T_{lumen} *to inspired humidity. (a)* T_{lumen} *at selected points in a symmetric lung model, for different levels of inspired humidity, (b) difference in* T_{lumen} *at selected points in a symmetric model, from temperatures obtained using an inspired relative humidity of 98%.*

5.4.4.2 Sensitivity to core temperature

The body temperature (T_{core}) was assumed to be at 36.5°C, because the experimental measurements approached this value in the distal branches. Sensitivity of the results to this assumption were tested in the symmetric model using $T_{insp} = 31.3$°C, a $\dot{V}$ of

30 L · min^{-1}, and T$_{core}$ = 38.0, 37.0, 36.5, 36.0, and 35.0°C.

Figure 5.18(a) plots T$_{lumen}$ against distance from the model entrance, at the end of inspiration and expiration, for each body temperature. Figure 5.18(b) plots the difference in T$_{lumen}$ from the temperatures resulting from assuming T_{core} = 36.5°C, against T$_{core}$. The temperature results were sensitive to the assumed body temperature: increasing T_{core} increased both the end-inspiratory and end-expiratory temperatures, but the magnitude of the change at the most distal data point was not carried forward to the mouth. The change in the end-inspiratory temperatures was less than in the end-expiratory temperatures.

(a) T$_{lumen}$

(b) Temperature differences (^{o}C)
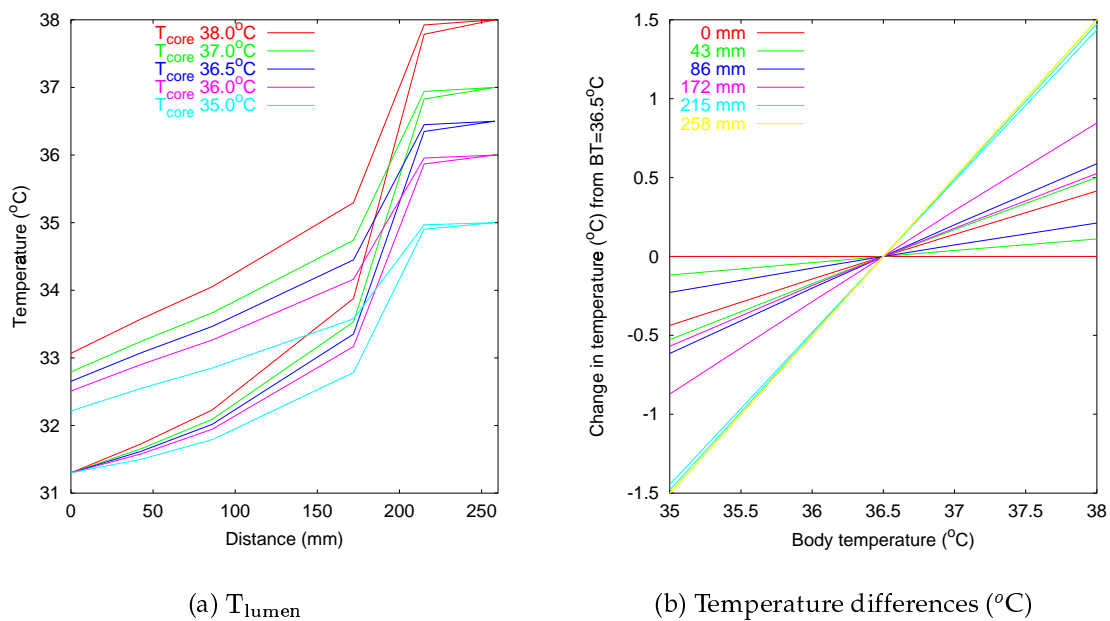
Figure 5.18: *Sensitivity of* T$_{lumen}$ *to core temperature.* (a) T$_{lumen}$ *at selected points in a symmetric lung model, for different body temperatures, (b) difference in* T$_{lumen}$ *at selected points in a symmetric model, from temperatures obtained using a body temperature of 36.5°C.*

5.4.4.3 Sensitivity to entrance wall temperature

In the previous simulations the body temperature was assumed to be constant over the entire model. Tsu et al. (1988) varied the body temperature linearly from a low value at the mouth to core temperature at approximately half-way down the trachea.

This approach was investigated using the symmetric model with $T_{insp} = 31.3°C$, a $\dot{V}$ of $30\ L \cdot min^{-1}$, and temperature at the model entrance $T_{entrance} = 36.5, 36.0, 35.0, 34.0, 33.0, 32.0$, and $31.3°C$. The temperature at the capillary bed was varied linearly from $T_{entrance}$ at the top of the trachea to $36.5°C$ at halfway down the trachea.

Figure 5.19(a) plots T_{lumen} against distance from the top of the trachea for the different entrance temperatures. Figure 5.19(b) plots the difference in T_{lumen} from the results obtained when assuming that $T_{entrance}$ was the same as the core temperature. Reducing $T_{entrance}$ from $36.5°C$ to $35.0°C$ had little effect on the resulting end-inspiratory and end-expiratory temperatures: less than a $0.2°C$ change in T_{lumen} along the airway path. As $T_{entrance}$ decreased, the temperatures at the end of inspiration and expiration decreased. However, decreasing $T_{entrance}$ from $36.5°C$ to $31.3°C$ resulted in maximum temperature differences that were less than $1.2°C$.

(a) T_{lumen} (b) Temperature differences (^{o}C)
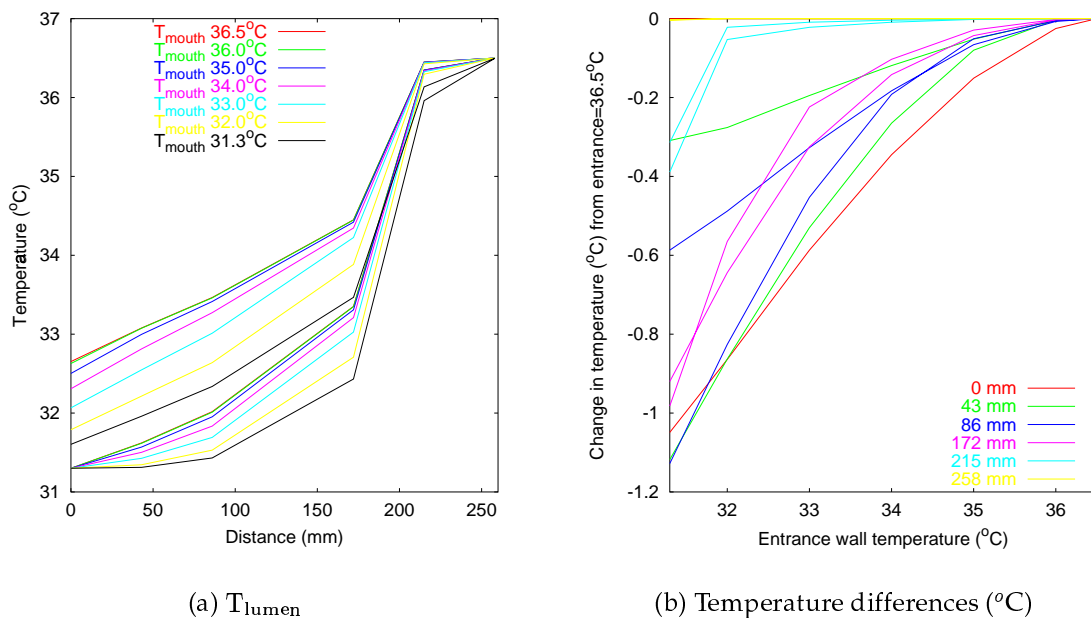
Figure 5.19: *Sensitivity of* T_{lumen} *to model entrance wall temperature. (a)* T_{lumen} *at selected points in a symmetric lung model, for different capillary bed temperatures at the top of the model trachea, (b) difference in* T_{lumen} *at selected points in a symmetric model, from temperatures obtained using a capillary bed temperature of 36.5°C (body temperature) over the entire model.*

5.4.4.4 Sensitivity to tissue depth

In the previous simulations the distance from the air-surface liquid interface to the capillary bed at constant temperature (T_{core}) was assumed to be the changeable depth of the surface liquid plus 1.0 mm (Δy). The sensitivity of the numerical results to the magnitude of Δy was tested using the symmetric model with T_{insp} = 31.3°C, a $\dot{V}$ of 30 L · min^{-1}, and Δy = 2.0, 1.5, 1.0, 0.8, 0.6, 0.4, and 0.2 mm.

(a) T_{lumen} (b) Temperature differences (^{o}C)
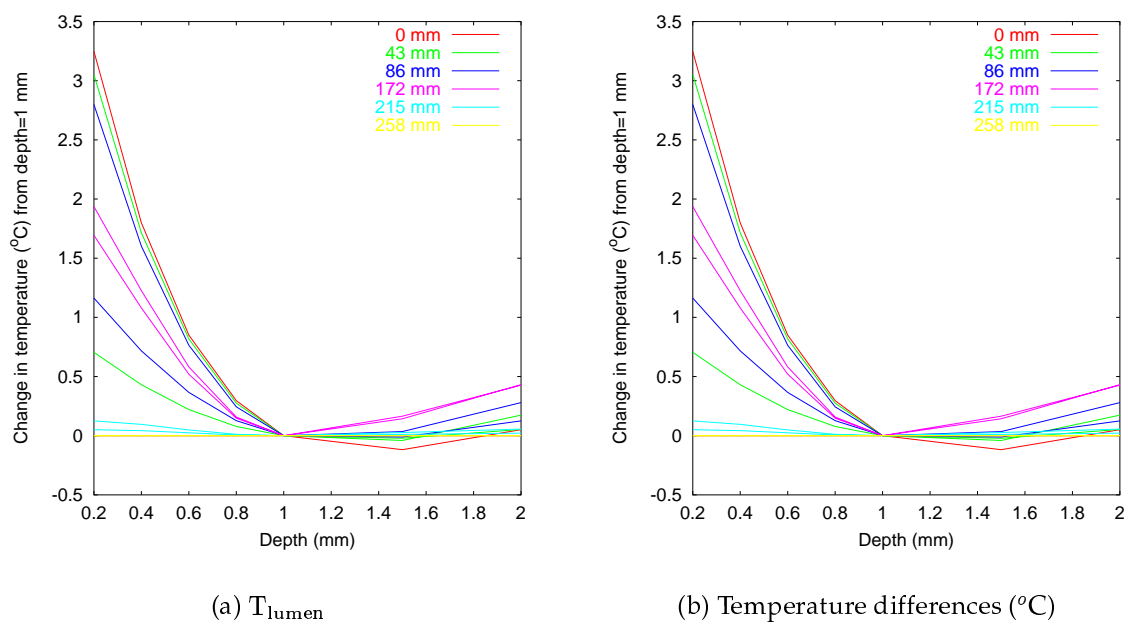
Figure 5.20: *Sensitivity of* T_{lumen} *to tissue depth. (a)* T_{lumen} *at selected points in a symmetric lung model, for different tissue layer depths, (b) difference in* T_{lumen} *at selected points in a symmetric model, from temperatures obtained using a tissue layer depth of 1.0* mm.

Increasing Δy from 1.0 to 2.0 mm caused only small changes in T_{lumen} (less than 0.5°C). Decreasing Δy had more effect on T_{lumen} than increasing Δy, particularly for the temperatures at the end of expiration. Decreasing Δy brought the capillary bed closer to the air-mucus interface, therefore reducing the rewarming time of the liquid surface. Although the effect of reducing Δy was significant, the percent difference in results was far less than the percent reduction in Δy. That is, a 40% reduction in Δy caused a maximum difference from the 1.0 mm results of less than 3% (1°C), and an 80% reduction in Δy caused a maximum difference of 10% (3.2°C).

5.4.4.5   Sensitivity to flow divider

The α, β, and γ parameters define the shape of the velocity, temperature, and water vapour concentration profiles, respectively, across the airways. These parameters are constrained to be equal to the Reynolds number (Re) for each individual airway, divided by a constant. This constant is called the 'flow divider'. For the previous simulations the flow divider has been equal to 50.0 for all three profile parameters, such that the velocity, temperature, and concentration profiles across an airway have the same shape. The magnitude of the profile parameters reflects the level of turbulence in the airway, and hence the magnitude of transfer of heat and water vapour between the surface liquid and the air in the lumen.

(a) $\mathrm{T_{lumen}}$ (b) Temperature differences (^{o}C)
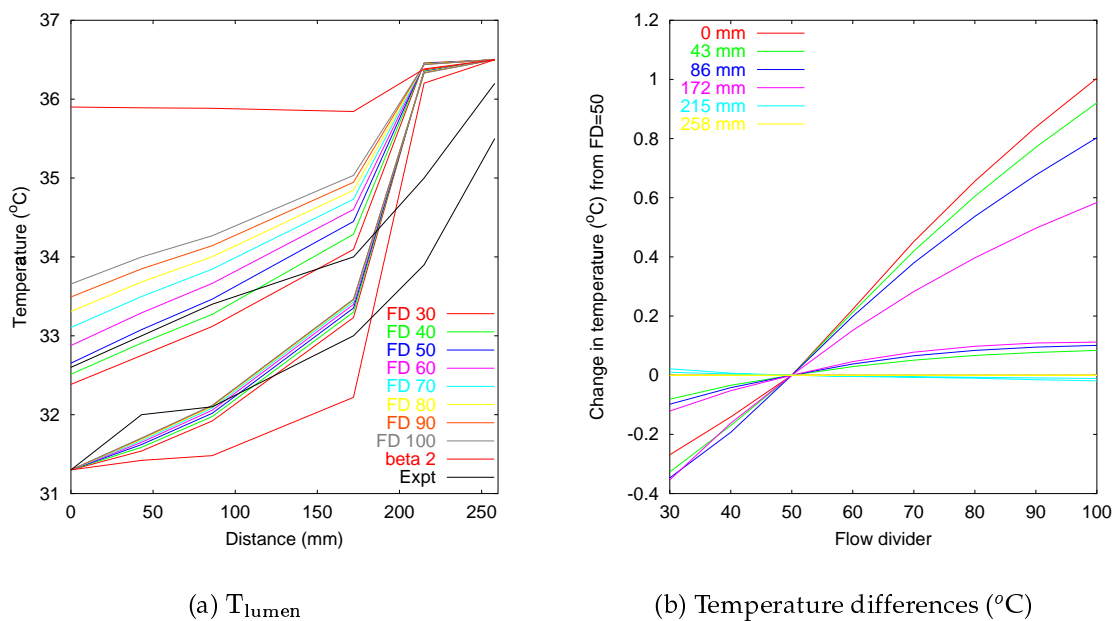
Figure 5.21: *Sensitivity of* $\mathrm{T_{lumen}}$ *to flow divider. (a)* $\mathrm{T_{lumen}}$ *at selected points in a symmetric lung model, for different values of the flow divider, (b) difference in* $\mathrm{T_{lumen}}$ *at selected points in a symmetric model, from temperatures obtained using a flow divider of 50.0.*

The sensitivity of $\mathrm{T_{lumen}}$ to changes in the flow divider (FD) was investigated in the symmetric model with $\mathrm{T_{insp}}$ = 31.3°C, $\dot{V}$ = 30 L · min^{-1}, and FD = 100 to 30, in decrements of 10. A simulation was also run with α, β, and γ all equal to 2.0. This final simulation would be appropriate for laminar flow throughout the entire model.

Figure 5.21(a) and (b) plot T_{lumen} against distance from the top of the trachea, and difference in T_{lumen} from the FD = 50.0 results, respectively.

For α, β, γ = 2.0, there was minimal transfer of heat in the trachea during inspiration: T_{lumen} remained far cooler than for the other FD conditions over most of the data points. However, by the time that the most distal data point was reached, the gas had been heated to body temperature. During expiration there was very little recovery of heat from the lumenal gas for α, β, γ = 2.0.

Varying the magnitude of FD produced only very small changes in T_{lumen} at the end of inspiration. Increasing FD (and thereby decreasing α, β, and γ) increased the end-expiratory temperatures as less heat was able to be recovered during the expiration. The maximum difference in T_{lumen} for increasing FD from 50 to 100 was close to $1.0°C$.

5.4.5 Including an endotracheal tube

Ryan et al. (2000) measured temperatures down the endotracheal tube in intubated subjects, for a range of inspired temperatures. The endotracheal tube was inserted to two-thirds of the way down the trachea, which in the ACA model corresponds to approximately 67 mm in the 100 mm long model trachea.

To simulate the experimental conditions of Ryan et al. (2000), the ACA model was extended to the patient threshold (the lips) by including an internal PVC layer from the threshold to two-thirds of the way down the trachea, and surrounding the PVC layer between the threshold and the trachea with a layer of tissue. The PVC layer was 4 mm thick, the surrounding tissue layer was 1 mm thick, and a 100 μm thick layer of surface liquid sat between the endotracheal tube and the tissue layer.

A FD of 50.0 was used, Δy = 1.0 mm, and the body temperature was assumed to be constant over the entire model at a temperature corresponding to the experimental results. That is, a mean body temperature of 37.2 $\pm 1.0°C$ was measured by Ryan et al. (2000), but the experimental results indicate that higher body temperatures may have been present in the experiments with higher inspired temperatures. The body temperature was therefore set equal to the temperature at the most distal data point (just beyond the tip of the endotracheal tube) at the end of expiration, unless this temperature was higher than one SD from the mean experimental body temperature.

That is, body temperatures of 37.7, 37.8, 38.2, and 38.2°C were used for the 30, 34, 37, and 40°C simulations, respectively. None of the body temperatures were more than one standard deviation from the mean experimental body temperature.

The temperature and pre-mouth absolute humidity were recorded every 0.2 s during the Ryan et al. (2000) experiments. The temperatures that were recorded 10 mm before the threshold were used to specify the temperatures at the model threshold during inspiration. The temperatures from single representative breaths from the Ryan et al. (2000) raw data (provided by the authors) are listed in Appendix A. The experimental inspired humidities were at approximately saturation, therefore the model applied relative humidities of 100% at the threshold. These changing temperatures and humidities were used to define time-varying fixed boundary conditions at the model threshold. The tidal volume was 400 ml, inspired over 2.2 s, and expired over 3.6 s. This $\dot{V}$ was consistent with the experimental results.

Figure 5.22 plots temperature (T_{lumen}) against distance from the threshold for chamber settings of 30, 34, 37, and 40°C. Simulated numerical results are compared with averaged end-phase experimental results from Ryan et al. (2000), ± one SD. For the 30, 34, and 37°C temperature simulations, the lower lines correspond to the end of inspiration and the upper lines correspond to the end of expiration. This is reversed for the 40°C simulation and experimental results.

The temperatures from the ACA model were very close to the experimental values for both the end of inspiration and the end of expiration, for each of the four different condition sets. The model produced results

Figure 5.22: *Comparison of mid-lumen temperatures for the ACA model with an endotracheal tube, with experimental results from Ryan et al. (2000).*

close to experimental not only for inspiratory temperatures below body temperature, but also when the inspired temperatures were warmer than body temperature.

5.4.6 Depletion of the surface liquid layer

The estimated rate of replenishment of the airway surface liquid at normal levels of ventilation is 2.0 $\mu L \cdot cm^{-2} \cdot s^{-1}$ (Phillips et al. 1998). The effect of altering the rate of replenishment on surface liquid depletion was investigated using decreasing replenishment rates.

Figure 5.23 demonstrates drying of the airway surface liquid in the exposed portion of trachea, for T_{insp} 23 °C, RH 30%, inspiration time 2.2 s, expiration time 3.6 s, and V_T = 400 ml. The rate of replenishment of the surface liquid was decreased from the maximum in 10% steps. Figure 5.23 plots the surface liquid depth at a single point in the trachea, 220 mm from the patient threshold (the first point beyond the ET tube).

For replenishment at 100, 90, and 80% of the maximum rate, the surface liquid did not show noticeable changes in depth. For replenishment at 70 to 30% of the maximum rate, the liquid depth decreased during inspiration but recovered fully to its optimal depth during expiration. For replenishment rates at 20, 10, and 0% of the maximum rate, the volume of water supplied to the surface liquid by the surrounding tissue was not enough to recover the depth back to its optimum level.

In Figure 5.24 the surface liquid depth is plotted against time for multiple positions down the exposed portion of trachea in the intubated ACA model. The portions of airway closest to the ET tube lose the most water, which is displayed in Figure 5.24 as greatest decreases in surface liquid depth.

Figure 5.23: *Drying of the airway surface liquid just beyond the end of the endotracheal tube in the ACA model, for different rates of surface liquid replenishment.* T_{insp} *= 23 °C, RH = 30%,* V_T *= 400 ml, inspiration = 2.2 s, and expiration = 3.6 s. Note the decrease in surface liquid depth during each inspiration, and the slower increase in depth during expirations.*

The difference in depth for the multiple points increases for each breath. The change in depth is not linear with distance from the ET tube.

Figure 5.25(a), (b), and (c) plot the loss and gain of water over eight breaths for (1) constant T_{insp} = 23 °C, RH = 30%, (2) chamber setting 30 °C, and (3) chamber setting 34 °C, respectively.   The red lines plot the net loss of water (in mg) from the model.   The green lines plot the amount of water required for to fully condition all of the inspired tidal volume.   The blue line plots the total amount of water supplied or recovered by the model. Surface liquid replenishment was maximal in these simulations. The water vapour supplied to the inspired air was close to the volume needed for total conditioning, for each breath and for all three condition sets. Water recovery during expiration for the cold air was around 20%, and for the warm air was around 29%.
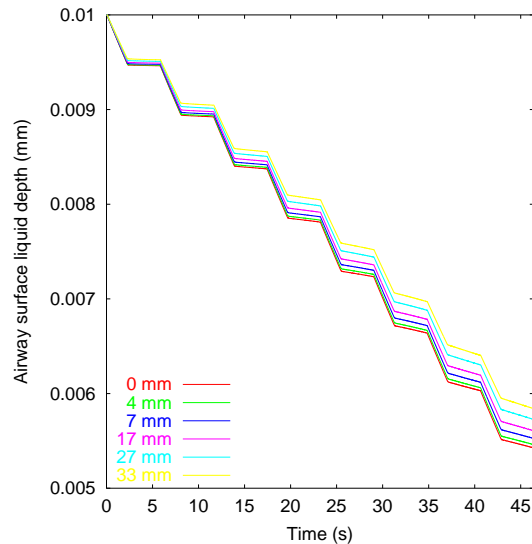
Figure 5.24:   *Drying of the airway surface liquid in the ACA model with no replenishment of the surface liquid.* T_{insp} = 23 °C, RH = 30%, V_T = 400 ml, inspiration = 2.2 s, and expiration = 3.6 s.

(a) 23°C,30%RH (b) 30°C chamber setting   (c) 34°C chamber setting
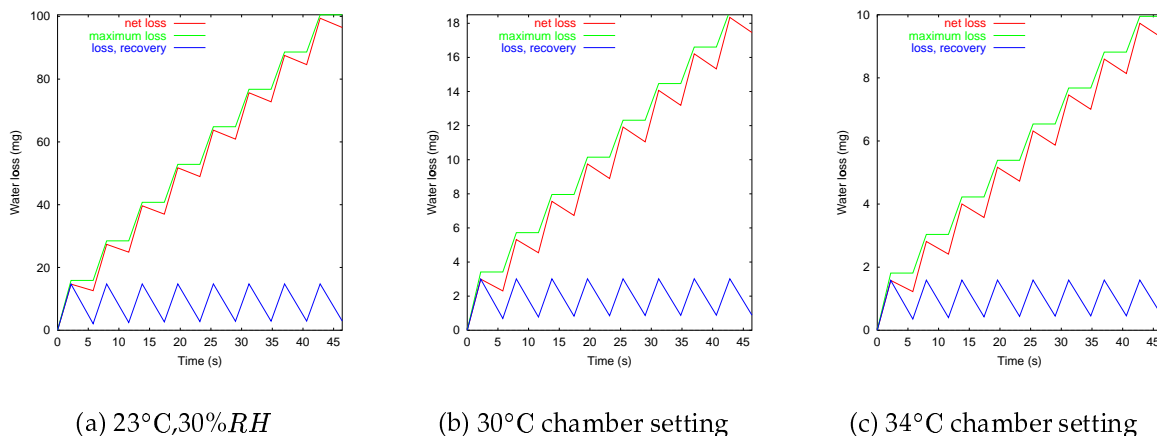
Figure 5.25: *Amount of water lost and recovered by the surface liquid in the ACA model with an ET tube with maximal replenishment of airway surface liquid. (a) constant 23°C at 30%RH, (b) chamber set at 30°C, (c) chamber set at 34°C.*

The much larger water loss for the coldest and driest air is illustrated in Figure 5.26. In this plot it can be seen that both the supply and recovery of water under the cold dry conditions is much larger than for the warmer inspired air. If water had not been recovered during expiration, and conditioning of the inspired air was complete, then the amount of water lost after eight breaths would have been 126.98, 27.34, and 14.50 mg for the 23, 30, and $34°C$ simulations, respectively. The actual amounts of water lost after eight breaths were 96.46, 17.46, and 9.27 mg for the coolest to warmest inspired gases, respectively.
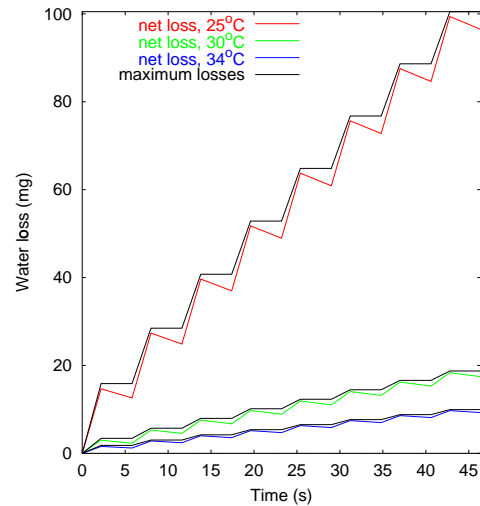
Figure 5.26: *Comparison of the water losses from the surface liquid in the ACA model with an ET tube for different inspired temperatures and humidities.*

5.5 Discussion

Loss of heat and moisture from intubated lungs can lead to drying of the airway walls, damage to the airway cilia, and lead to pulmonary infection and changes in airway mechanics. To prevent airway damage, air supplied to artificially ventilated patients is usually heated and humidified by an external device. Fisher & Paykel Healthcare manufacture respiratory humidifiers for active conditioning of inspired air. Only limited experimental measurements can be taken from intubated patients, so a mathematical model that can simulate transfer of water vapour and heat in intubated lungs could provide information on airway penetration by unconditioned air, and airway drying. The water and heat transfer model presented in this chapter was developed with the aim of being used for investigating unconditioned air penetration and airway drying in intubated lungs.

In this chapter the development of a radially layered conducting airway model was described. The radial layers comprised an outer capillary bed with constant

temperature, a tissue layer with thickness Δy = 1 mm, a surface liquid layer with variable depth, and an optional PVC endotracheal (ET) tube layer and associated condensate layer on the ET tube. The radial layers were applied to the asymmetric conducting airway (ACA) model described in Chapter 2, and to a symmetric model based on Weibel (1963).

The velocity, temperature, and water vapour concentration profiles across each airway were described using power law equations with variable profiles. Using a profile parameter of 2.0 gave a velocity profile appropriate for laminar flow; larger profile parameter values produced 'flatter' profiles with steeper gradients near the air-liquid interface. The profile parameter for a particular airway was proportional to the Reynolds number (Re) for the airway under the current simulation conditions. Profile parameters were used instead of heat and mass transfer coefficients because transfer coefficients were not available for the ET tube, and because the transfer coefficient approach has not been shown to be reliable for simulating heat and water vapour transfer (see Section 5.2.6).

The water and heat transfer model was validated by comparison with experimental results, for lungs with and without an ET tube in place. The first set of experimental results (McFadden et al. 1985) were performed by having subjects breath room air and then frigid air through the mouth at a range of ventilation rates. McFadden et al. (1985) presented their results as plots of mean measured temperature against distance. They also included $\pm$ one standard error (SE) for ventilation rates of 15 $L \cdot min^{-1}$ and 100 $L \cdot min^{-1}$. For the McFadden et al. (1985) experiments, errors may have been introduced into the temperature measurements by the slow thermistor response time, flow disturbance, non-central thermistor positioning, and displacement during high frequency ventilation. The thermistors used by McFadden et al. (1985) had a 63% response time of 0.250 s in stirred water. McFadden et al. (1985) recognised that the relatively slow response time (compared with ventilation times) of the thermistors would have lead to errors in the temperature measurements, but they felt that the measurements "if anything, minimised the actual variations in airstream temperatures".

The presence of the probe in the airway disturbs the normal flow pattern: the probe could contribute to increased turbulence and therefore increased mass and heat

transfers. In the smaller airways, the effect of the probe would be more pronounced: as the ratio of probe diameter to airway diameter increased, the heat and mass transfer would be affected more by changes in pressure and flow distribution.

Because the air flow is fastest in the more proximal airways, their Re is higher and hence values for α, β, and γ are higher than in the more distal airways. This means that the velocity, temperature, and water concentration profiles in the proximal airways are 'flatter' than those in the more distal generations. That is, the temperature or concentration in, for example, the trachea is very close to the central value across most of the lumen; there are very steep gradients in temperature, concentration, and velocity at the airway walls. In the more distal generations the profiles are less flat (approaching laminar flow) and therefore there is more variation in concentration or temperature across the airway. This means that a small displacement of the thermistor from the centre of the airway lumen in this region could introduce errors in the recorded temperature. McFadden et al. (1985) did not specify whether they had used a mechanism to ensure that the thermistors remained central in the airway, and particularly that they did not touch the airway wall. If a thermistor was in contact with the surface liquid then it would record significantly lower temperatures than in the centre of the airway.

During high frequency ventilation the movement of the airways could cause relative displacement of the thermistors: inspiration would cause relative upwards displacement and expiration would cause relative downwards displacement. The thermistors would therefore not be measuring temperature at a single point.

Because of the errors that are almost certainly present in the experimental results presented by McFadden et al. (1985), comparison with numerical results is not expected to produce a close match between the mean experimental values and numerical mid-lumen temperatures for the higher ventilation rates with cooler inspired temperatures.

For the lowest ventilation rate ($15 \, \text{L} \cdot \text{min}^{-1}$) with the warmest inspired air ($32°\text{C}$) there was a close fit between the experimental and numerical results in the trachea at the end of inspiration, but the more distal model data points had values higher than one SE from the experimental means. At the end of expiration the model temperatures were generally within one SE of the experimental means. However, although the end-

expiratory temperatures were within the experimental range, they were all higher than the experimental mean values. These results can be seen in Figure 5.4. In Figure 5.5 the model temperatures at 50%, 75%, and 100% through inspiration and expiration are compared with the experimental temperatures. From 50 to 100% of inspiration there was only a small decrease in the mid-lumen and air-liquid interface temperatures, whereas for 50 to 100% of expiration there was a slightly larger increase in the temperatures. The 50% expiratory temperature at the entrance to the model was within one SE of the experimental mean at this point. Because of the slow thermistor response time, the temperatures anywhere within the 50 to 100% phase range might correspond to the temperatures which were actually measured by the thermistors.

The experimental measurements were made in an airway path from the trachea into a subsegmental bronchus of the right lower lobe. The temperatures selected for comparison with McFadden et al. (1985) are from a similar path through the model. In Figure 5.6 it can be seen that the path has close to minimum values for the end of inspiration, but has more 'mid-range' values for the end of expiration. That is, there are other airway paths that had cooler end-phase temperatures than the selected path at the data point distances. It is therefore possible that selecting a different path in the model for comparison with the experimental results would produce an even closer match. However, it would not be appropriate to just select the path with the 'best fit' for comparison. Instead, it is noted that there is a range of temperatures from the model for the more distal generations. It would also not have been appropriate to compare with distance averaged temperatures over the whole model, because the variation in airway path length causes variations in flow rates and therefore different temperatures at the same distance down long and short airway paths (in terms of distance to the respiratory airways).

The numerical and experimental results were close for increased rates of ventilation (30 and 60 $L \cdot min^{-1}$) for both the end of inspiration and end of expiration. For ventilation at 100 $L \cdot min^{-1}$ with inspired temperature 29.2°C, the temperatures at the end of inspiration were close to the experimental values, but those at the end of expiration were outside the experimental range from the model entrance to beyond the trachea. It is possible that there were more errors in the experimental results for the higher ventilation rates, but there are possibly also more errors in the numerical

results as ventilation increases. This could be because the profile parameters should have had a non-linear variation with Re, or because there should have been cooling of the surrounding bronchial circulation with increased thermal load (Bui et al. 1998, Le Merre et al. 1996).

Decreasing the inspired temperatures for ventilation at 15, 30, and 60 L·min^{-1} produced end-inspiratory temperatures close to the experimental values, but the end-expiratory values were 2 - 3°C higher than the experimental values for most of the measured data points. The warm end-expiratory temperatures were due to insufficient decrease in the air-liquid interface temperatures by the end of inspiration: if the mucus-air interface was not cooler than the experimental end-expiratory temperatures by the end of inspiration, then it was not possible for the end-expiratory mid-lumen temperatures to be as cool as the experimental values. If the blood flow was decreased in response to ventilation of cooler air, then rewarming of the surface liquid would be slower. Because the effect of airway wall cooling is cumulative with each breath, slower surface liquid rewarming would have lead to cooler temperatures at both the airway wall and for the air in the lumen, at both the end of inspiration and expiration.

There are conflicting studies of airway blood flow response to thermal load that indicate either increased or decreased airway blood flow in response to decreasing inspired temperatures or increased ventilation rates. Le Merre et al. (1996) performed experiments in normal human subjects that indicated that quiet breathing of frigid air causes vasoconstriction in the central airways. In contrast, other studies have shown that tracheobronchial blood flow can increase with thermal challenge (Baile et al. 1987, Parsons et al. 1989, Kim et al. 1996). It is therefore not clear how the airway blood flow responds to increased thermal challenge. Because the aim of the water and heat transfer model is to simulate air conditioning under ventilation conditions generally similar to those experienced by intubated patients, the response of the bronchial circulation to cooling of the airway walls can be neglected without significant effect on the results under the important ventilation and temperature condition range.

The simulations for comparison with experiment were performed in the ACA model. The adequacy of a symmetric model for simulating the experiments of McFadden et al. (1985) was tested by comparing results from the ACA model with results from a symmetric model based on Weibel (1963) for ventilation at 15 and

100 L · min^{-1} (see Figure 5.16). At 15 L · min^{-1} the temperatures from the ACA and symmetric model were close in value within the trachea and down to the data point 172 mm from the top of the trachea. For more distal points, the temperature quickly increased to body temperature in the symmetric model, but was closer to the cooler experimental values for the ACA model. For ventilation at 100 L · min^{-1}, the temperatures in the trachea (down to 100 mm) in the two models were close in value, but not as close as for the 15 L · min^{-1} simulations. The difference in results from the two models increased for more distal data points. The appropriateness of the symmetric model for simulating water and heat transfer is therefore limited to less severe ventilation conditions, such that full conditioning can be achieved in the central airways.

A number of assumptions had to be adopted in the model: the relative humidity of the inspired gases was assumed to be 98%, the body temperature was 36.5°C, the capillary bed temperature was assumed to be constant over the entire model, the distance from the surface liquid to the capillary bed was 1.0 mm, and the flow divider used to calculate the profile parameters was set at 50.0. The sensitivity of the results to these assumptions was tested using the symmetric model with inspired temperature 31.3°C and ventilation rate 30 L · min^{-1}.

For the McFadden et al. (1985) experimental results, the humidity of the inspired gas prior to entering the mouth was presented, but the humidities down the airways were not measured. Because the ACA model does not include a nose or mouth, the inspired temperatures used for the simulations were those given for the top of the trachea at the end of inspiration. In the absence of data on the humidity at this point, a relative humidity of 98% was adopted for all simulations. The sensitivity of the results to this assumption were tested using relative humidities ranging from 80 to 100%. Decreasing the inspired relative humidity decreased both the end-inspiratory and end-expiratory temperatures, because the decrease in inspired water vapour caused increased movement of water vapour from the surface liquid into the air in the lumen, with associated cooling of the surface liquid. It is possible that the relative humidity of the inspired gas was at 100%, or it could have been at a lower value. However, it is not likely that the relative humidity was much lower than 98%: the mouth is a relatively efficient conditioner of air. If the relative humidity was at 96%, then the maximum

difference in results from 98% would be less than 1%. The results are therefore not very sensitive over the expected possible range of inspired relative humidities, and the assumption of 98% relative humidity does not influence the results to a significant degree.

The body temperature was assumed to be 36.5°C because this is the value towards which the experimental results appeared to converge at the most peripheral data point. The sensitivity of the numerical results to this assumption was tested over a body temperature range of 35 to 38°C. Increasing the body temperature increased the end-inspired and end-expired temperatures, with the largest changes in temperature at the peripheral symmetric model airways, where the temperatures were always at body temperature. Examining the experimental results shows that the most likely body temperature range was 36 to 37°C. For this range of body temperatures, the maximum difference in results from using a body temperature of 36.5°C was approximately ±1%. Therefore the numerical results are not very sensitive to the body temperature over the expected range.

The body temperature was assumed to be constant over the entire model. That is, the temperature of the capillary bed at every point was assumed to be at body temperature. Tsu et al. (1988) assumed that the temperature of the capillary bed varied from a low temperature at the mouth to body temperature mid-way down the trachea. The effect of this assumption was tested using temperatures at the top of the trachea ranging from 31.3°C (inspired air temperature) to 36.5°C (body temperature). Decreasing the entrance wall temperature decreased the end-phase temperatures, but the results were not very sensitive to the change in entrance wall temperature. Reducing the entrance wall temperature from 36.5 to 35.0°C created maximum differences in the results of approximately 0.5%, and an extreme reduction to 31.3°C caused a maximum difference from the 36.5°C results of 3.5%.

The tissue depth (Δy) was assumed to be 1.0 mm over the entire model. The effect of this assumption was tested over a Δy range of 0.2 to 2.0 mm. Decreasing Δy generally caused the end-phase temperatures to increase. Increasing Δy caused smaller changes in the resulting temperatures than reducing Δy: doubling Δy (to 2.0 mm) caused a maximum change in the results of less than 2%. Increasing or decreasing Δy by 20% (from 1.0 mm) resulted in maximum temperature changes of less than 1%. The

increase in end-phase temperatures with decreasing Δy was because the heat from the fixed temperature capillary bed has less distance to travel, and therefore rewarmed the surface liquid faster than for thicker Δy. Bui et al. (1998) suggested that Δy should vary with airway diameter. This would act as an additional thermal buffer for the respiratory airways: the smaller Δy in the more distal airways would ensure fast heating of cool air that reached the more distal (and therefore smaller) airways.

The final model assumption that could affect the numerical results was the use of profile parameters (α, β, and γ) to describe the shape of power law velocity, temperature, and water vapour concentration profiles across the airways. The profile parameters were assumed to vary with Re, so that higher Re flow would have larger profile parameters, and therefore have flat radial profiles and steep gradients near the air-mucus interface. Low Re flows had profiles approaching that for laminar flow. The constant by which the Re was divided to calculate the profile parameters is the 'flow divider'. The sensitivity of the results to the flow divider was tested over a range of 30 to 100, and also for α,β,γ = 2.0. Varying the flow divider had a very small effect on the end-inspiratory temperatures, but increasing the flow divider noticeably increased the end-expiratory temperatures. That is, increasing the flow divider caused decreasing gradients at the airway wall, which did not have a significant effect on the transfer of heat into the cool lumenal gas, but did reduce the recovery of heat during expiration. Doubling the flow divider (to 100) caused maximum temperature differences of less than 2%, and nearly halving the flow divider (to 30) caused less than 1% differences. For α,β,γ = 2.0, the transfer of heat during inspiration was not enough to increase the mid-lumen temperatures to within the experimental range. During expiration, there was very little recovery of heat. Therefore the numerical results were not particularly sensitive to changes in the flow divider from 50.0.

α ,β, and γ were not varied independently. For a high α value the velocity profile is very flat, except close to the mucus-air interface, which is characteristic of turbulent flow. If the flow is highly turbulent, then the heat and water vapour would be well-mixed across the airway, and hence their profile parameters would also be large. As laminar flow is approached α and β approach 2.0 and γ is assumed to also approach 2.0. The concentration profile for saturated gas could be more complex than a simple power law curve, however, as the relationship between saturation water vapour concentration

and temperature is not linear.

An ET tube was included in the ACA model by adding a PVC layer from the mouth threshold to 67 mm down the model trachea. The ET tube was surrounded by a surface liquid layer and a tissue layer from the top of the trachea to the threshold. Model validation was performed by simulating multiple breaths using the experimental conditions described by Ryan et al. (2000). Two of the experiments had temperatures lower than body temperature, and the last experiment had temperatures higher than body temperature.

The numerical and experimental results (see Figure 5.22) were very close for each set of conditions, for both the end of inspiration and the end of expiration. The ventilation rate for the Ryan et al. (2000) experiments was $4.14 \text{ L} \cdot \text{min}^{-1}$, which was much lower than the ventilation rates in the McFadden et al. (1985) experiments. The model performs reliably for lower ventilation rates, as seen in Figure 5.22.

The replenishment of the airway surface liquid had a maximum rate of $2.0 \ \mu L \cdot \text{cm}^{-2} \cdot \text{s}^{-1}$ (Phillips et al. 1998). The effect of reducing the replenishment rate was investigated in the ACA model with an ET tube, for $V_T = 400$ ml, inspiration = 2.2 s, expiration = 3.6 s, inspired temperature = 25°C, and inspired relative humidity = 30%. The replenishment rate was reduced in 10% steps, and the effect on the surface liquid depletion was investigated. When the rate of replenishment was reduced to 60% of the maximum, recoverable decreases in surface liquid depth were observed. When the rate of replenishment dropped to 20% or lower, the decrease in depth was not recoverable during expiration.

The surface liquid does not have to be entirely evaporated for the function of the cilia to be impaired. In fact, only a small change in depth may be needed for the cilia to be unable to complete their backsweep without contacting the mucus on the periciliary fluid surface. The cilia are also sensitive to the temperature in the airways: their beat frequency decreases with lower temperatures.

The method for replenishing the surface liquid that was adopted in the water and heat transfer model is very simplistic: the response of the surrounding tissue to water loss is actually complex and involves a number of processes. It is not likely that water replenishment or absorption is a constant 'switched on' process as was assumed in the model, but without more detailed experimental information on the effect of the

mechanisms involved, then any alternative approach to replenishment would have to involve numerous assumptions. It is therefore possible that the model underestimates the decrease in surface liquid depth. In future studies the replenishment mechanism could be easily altered in the model to investigate its effect on surface liquid depletion, and to possibly provide a fit to experimental data.

Water loss and recovery were compared for simulations under two of the Ryan et al. (2000) condition sets, and for a constant inspired temperature of 25 °C with 30% RH. The cold and dry air showed more supply of water to the lumenal air, but also showed more recovery of water than for the simulations with warm inspired air. For the cold inspiration the mucus-air interface was cooled to low temperatures, which facilitated the recovery of a larger amount of water during expiration. However, the percentage of water recovered for the cold inspired air was less than the percentage recovered for the warm inspired air.

5.5.1 Conclusions

The radial water and heat transfer model, incorporating power law profile parameters to describe radial velocity, temperature, and water vapour concentration profiles has been validated by comparison with two sets of experimental results. The model has been validated both with and without a PVC ET tube, and has been shown to not be too sensitive to any model parameters.

Using power law profiles to describe velocity, temperature, and water vapour concentration has been shown to be a useful alternative to using empirically derived transfer coefficients to calculate the amount of heat and water vapour transfer.

The water and heat transfer model has been shown to be reliable for ventilation rates lower than $60 \, \text{L} \cdot \text{min}^{-1}$ combined with a top-tracheal temperature of greater than 23.5°C. It is expected that a limited range of lower temperatures could be simulated reliably, as long as the ventilation rate remained low.

It has been shown that an asymmetric model is essential to simulate the experimental results of McFadden et al. (1985). For this experimental study, temperatures were measured in an airway path down to a subsegmental bronchus in the right lower lobe. At this level in the asymmetric conducting airway tree there

can be differences in temperature compared with paths in other regions of the lung. This makes it necessary to use an asymmetric model to reproduce the McFadden et al. (1985) results.

The water and heat transfer model has been shown to be suitable to use for investigating airway penetration by unconditioned air, and airway drying.

Discrepancies between the simulated and experimental results under high rates of ventilation with cool gas can be partly attributed to neglecting the bronchial circulation in the current model. It is also possible that a more detailed description of surface liquid replenishment by the tissue may affect the rate of replenishment and therefore the end-phase temperatures.

Chapter 6

Conclusions

There have been four distinct and important outcomes from this study: (1) an algorithm has been developed for generation of three-dimensional conducting airway models that have characteristics similar to those of the real lungs[1]; (2) a lumped parameter model of a single pulmonary acinus has been developed, based on results from an anatomically based multi-branching model; (3) the coupled conducting airway and lumped parameter model has been used to simulate gas mixing, and has demonstrated the importance of airway asymmetry, mechanics, and blood-gas exchange; and (4) a water and heat transfer model has been developed using the conducting airway model, and results from this model have highlighted the importance of model asymmetry for reproducing experimental results.

A bifurcating distributive algorithm originally developed for generating lung-like trees in two-dimensions (Wang et al. 1992) has been extended for generation of anatomically based models into a three-dimensional space. The 'host' space is defined using MRI data, and the generated model is 'grown' from pre-defined lobar bronchi. One aim of this study was to develop a conducting airway model that could be used as a computational mesh for a wide variety of investigations. It was therefore important that the model had characteristics very close to those of the real lungs. Extensive comparison of the model with experimental data has shown this to be the case.

To enable gas mixing to be investigated using the asymmetric conducting airway

---

[1] A paper detailing the algorithm for conducting airway model generation has been published in the Annals of Biomedical Engineering (Howatson Tawhai, Pullan & Hunter 2000).

model and incorporating respiratory airway asymmetry effects, it was necessary to develop a computationally small model of the respiratory airways: the size and complexity of the conducting airway model necessitated coupling to a small respiratory airway model to make solution of transport equations in the model feasible. This lumped parameter respiratory airway model was calibrated using results from an anatomically based multi-branching model. The lumped parameter model developed in this study uses regression equations to predict concentrations expired from each respiratory unit. The predicted concentrations match those that would be expired by the multi-branching model, over a limited range of simulation conditions.

Coupling each terminal branch in the conducting airway model with a single lumped parameter acinar model allowed detailed investigation of gas mixing in the full lung system. Important outcomes from using the full model to investigate gas mixing were that both conducting and respiratory airway asymmetry, gas exchange, and the pleural pressure gradient were all important contributing factors to generation of a sloping alveolar plateau in phase III of the washout curve.

This study showed that asymmetry in the respiratory airways has the greatest influence on the first breath normalised slope (S_n). The inability of the full lung model to produce first breath S_n with values as high as those measured experimentally indicates that the respiratory airway models developed in this study overestimated the degree of gas mixing in the respiratory region. This is likely to be because asymmetry was underestimated in the first few generations of the experimental data upon which the model was based (Dutrieue et al. 2000).

The conducting airway asymmetry was shown to cause large increases in S_n with increasing breath number. Gas exchange with the pulmonary circulation moderates this increase so that S_n approaches a plateau with increasing breath number. A previously published model with large-scale ventilation inhomogeneity (Cruz et al. 1997) also approached a plateau as the breath number increased, but inclusion of blood gas exchange in the model caused S_n to decrease in the later breaths. This result was also observed for the full lung model in this study, when mixing in the respiratory airways was assumed to be complete by the end of inspiration, and blood gas exchange was included.

The pleural pressure gradient (idealised as vertical gradients of respiratory unit size

and ventilation) had a complex, but significant effect on S_n from the full lung model. This result supports the results of Cruz et al. (1997), who produced increasing S_n curves by introducing experimentally based pre-inspiratory volumes and regional ventilation to a symmetric lung model, with no blood gas exchange and full respiratory mixing. This study therefore highlights the importance of including realistic mechanics when modelling gas mixing.

The water and heat transfer model presented in this study was developed with the aim of being used by Fisher & Paykel Healthcare for investigating airway penetration of unconditioned air, and airway surface liquid drying. The method used to describe transfer of heat and water from the airway walls into the lumenal air differed from previous models in that the velocity, temperature, and water vapour concentration across the airway were described using power law curves. Past models have used empirically derived transfer coefficients to calculate the amount of heat or water transferred, but that approach has not enabled adequate predictions of experimental results. In this study the use of power law curves has been shown to be a useful alternative to the transfer coefficient approach: results from the model developed in this study show a close match to experimental results both with and without an endotracheal tube included in the model. The model has therefore been shown to be adequate for investigating the phenomena of interest to Fisher & Paykel Healthcare.

6.1 Limitations and future extensions to the lung model

Some of the assumptions used in the development of the lung model limit its use to certain ranges of simulation conditions. Improvements to the model could overcome these limitations.

Although the conducting airway model compares very well with experimental data for most measurements, the mean branch angle with order does not increase in a manner observed experimentally. Branch angles have been observed to increase towards the periphery of the lung (with decreasing order), but in the conducting airway model the mean branch angle varies around the ideal angle proposed by Horsfield & Cumming (1968). For the transport simulations performed in this study

there would be no significant effect from changing the branch angles: the transport equations are independent of branch angle. However, if more detailed flow dynamics are incorporated, then the branch angles would become important. A single branching fraction was used to define branching in the algorithm. Varying the branching fraction with generation could impact on the generated branch angles, and this could be investigated in future studies.

The lumped parameter acinar model reproduces results from a multi-branching respiratory airway model, but only over a limited range of conditions. For conditions departing significantly from $V_T = 1$ L, and inspiration and expiration = 2 s, the model is not reliable. A more general model could be developed that allows simulation over a wider range of conditions. The lumped parameter model was also developed using only uniform ventilation. Although transport in the respiratory region is largely by molecular diffusion, the mechanics of the respiratory airways might not be uniform. This could impact on the distribution of gas, and the generation of S_n, as evidenced by the numerical values for first breath S_n that were lower than those measured experimentally. Increased asymmetry should also be considered.

Experimental measurements for airway temperatures under different ventilation conditions are not numerous. The model has been compared with results from the only suitable published experimental study of airway temperatures (McFadden et al. 1985) and has compared well up to ventilation at $60 \text{ L} \cdot \text{min}^{-1}$ with inspired temperature $30.3°\text{C}$. The model has also compared well with results from Ryan et al. (2000) for temperatures measured in intubated patients. However, the model is limited in its ability to simulate cold inspired air at high ventilation rates. This could be because there is no bronchial circulation included in the model. The effect of thermal challenge on the bronchial blood flow is still not clear, but as more experimental studies are published and the details of airway response to cold air are understood, then the relevant additional physical factors should be included in the model. Neglecting the bronchial circulation is not expected to affect the model's ability to simulate conditions close to those experienced by intubated patients.

The water and heat transfer model is able to be used to investigate airway drying, but the mechanism for replenishment of surface liquid is simplistic and will require refinement as more experimental information becomes available. The model currently

supplies a specified percentage of the maximum expected replenishment rate to the surface liquid when any water vapour leaves the liquid for the air. In reality, the mechanisms of transfer of fluid from the tissue to the surface liquid are more complex, and are probably not 'switched on' instantaneously. A more sophisticated approach should eventually be used for determining the amount of water provided by the tissue. This will require development of a more detailed model solely for the water transfer from the tissue to the surface liquid.

The importance of an accurate description of airway mechanics and resulting flow distribution was highlighted by the gas mixing results from incorporating idealised pleural pressure effects. The effect of the pleural pressure gradient was idealised by applying linear vertical gradients of initial respiratory model size, or respiratory model tidal volume. The results in this study have shown that the pleural pressure gradient can have a significant effect on gas mixing results, but a more accurate description of the pleural pressure field, coupled with its effect on airway mechanics and air flow, is necessary.

Coupling of soft tissue mechanics with air flow will provide a more accurate description of the movement of air in the lung branches. Solution of soft tissue mechanics equations, with appropriate constitutive laws describing the behaviour of the lung tissue, will enable a more accurate description of ventilation distribution than the idealised distributions applied in this study. Detailed mechanics solutions will also enable more accurate descriptions of the plueral pressure gradient, and will be a necessary step before coupling with a detailed model of the pulmonary circulation.

Appendices

AppendixA

Raw data from Ryan et al. 2000 for inspired temperatures with humidifier set at 30, 34, 37, and 40°C. Times and temperatures are listed for measurements taken 10 mm outside the mouth.

Time (s)	30°C	34°C	37°C	40°C
0.0	36.440	37.271	37.686	38.271
0.2	36.416	37.246	37.539	38.247
0.4	35.073	36.685	37.539	38.247
0.6	34.512	36.270	37.588	38.418
0.8	34.170	36.050	37.637	38.613
1.0	33.950	35.903	37.661	38.687
1.2	33.755	35.806	37.637	38.809
1.4	33.608	35.757	37.686	38.931
1.6	33.511	35.684	37.832	39.004
1.8	33.389	35.635	37.759	39.053
2.0	33.340	35.586	37.588	39.150
2.2	33.267	35.562	37.979	39.175

Appendix B

CMISS uses .command files to define finite element or boundary element meshes, or collocation grids. The .command files listed below are used to generate lung models, and to solve gas mixing or water and heat transport problems over the finite element lung meshes. The .ip files used in the following .command files can be found at http://www.esc.auckland.ac.nz/Groups/Bioengineering/CMISS/help/examples/9/.

Generating conducting airway models

.command file for right middle lobe generation

```
fem define parameters;r;grow                       # Define the size of the required arrays
fem define coordinates 3,1                          # Define 3-D rectangular cartesian coordinates
fem define region;r;two                             # Define two regions (host and central airways)
fem define base;r;3dlungs_ch                        # Define basis functions: 3-D bi-cubic Hermite
                                                      (in ξ₁ and ξ₃)+ linear Lagrange ( in ξ₂) for host
                                                      mesh, and 1-D linear Lagrange for branches
fem define data;r;rml                               # Define the uniform grid (already generated)
fem define node;r;rml region all                    # Define the nodes for host and central airways
fem define elements;r;rml region all                # Define elements for host and central airways
fem define mesh;r;rml            # Generate the RML mesh: define a stochastic fractal tree, a conducting
                                   airway model as a volume-filling mesh, single lobe model of the right
                                   middle lobe, and default from highest node #s which are read in.  The
                                   region number of the RML is 1, the element number of lobe bronchus
                                   is 676, the element number of the trachea is 668, the region number of
                                   the central airways is 2, the basis function for host lobe is 1, the angle
                                   limit is 60, the length limit is 1.2, the fraction for branching is 0.4,
                                   the spacing limit is 0.5, and the basis function for the airways is 3.
fem define node;w;rml_b region 2                    # Write the generated nodes to file
fem define elements;w;rml_b region 2                # Write the generated elements to file
fem quit
```

Gas mixing

.command file for gas mixing in the MBA-SCA model

```
fem define parameters;r;acinus          # Define the size of the required arrays
fem define coordinates 3,1              # Define 3-D rectangular cartesian coordinates
fem define base;r;acinus                # Define basis functions: 1-D linear Lagrange for branches
fem define mesh;r;MBASCA                # Define a MBA-SCA model: a stochastic fractal tree that is a
                                          full lung model, with a multi-branching acinar mesh based on
                                          Haefeli-Bleuer and Weibel (1988). The conducting portion is 16
                                          'tube' generations using dimensions from Weibel (1963). Random
                                          Number Seed 0 is used for variability in the number of branches,
                                          branch length, and branch diameter. The basis function for the
                                          airways is 1, there is uniform ventilation, and the compliance
                                          relationship is cube-root of volume change.
fem define equation;r;gasmix            # Define solution of gas transport equation: time integration
                                          (Navier-Stokes equations), for lung gas transport. Solution
                                          is by Galerkin finite elements with a Linear analysis, and no
                                          equation coefficients are time-varying. The basis number
                                          is 1, and sparsity structures are used for the solution arrays.
fem define material;r;d225              # Define the gas properties
fem define motion;r;standard            # Define the tidal volume and breath duration
fem define initial;r;gasmix             # Define the initial and boundary conditions
fem define solve;r;MBASCA               # Define the solution method and output
fem solve from 0 to 100                 # Solve the transport equation from 0 to 100 s
fem quit
```

.command file for gas mixing in the LPA-SCA model

```
fem define parameters;r;acinus          # Define the size of the required arrays
fem define coordinates 3,1              # Define 3-D rectangular cartesian coordinates
fem define base;r;acinus                # Define basis functions: 1-D linear Lagrange for branches
fem define mesh;r;LPASCA                # Define a LPA-SCA model (as in previous .command file, but
                                          using BBM for respiratory model)
fem define equation;r;gasmix            # Define solution of gas transport equation
fem define material;r;d225              # Define the gas properties
fem define motion;r;standard            # Define the tidal volume and breath duration
fem define initial;r;acinus             # Define the initial and boundary conditions
fem define solve;r;LPASCA               # Define the solution method and output
fem solve from 0 to 100                 # Solve the transport equation from 0 to 100 s
fem quit
```

.command file for gas mixing in the LPA-ACA model

```
set num_threads 4                      # Set the number of processors for parallel processing
fem define parameters;r;LPAACA                       # Define the size of the required arrays
fem define coordinates 3,1                    # Define 3-D rectangular cartesian coordinates
fem define base;r;3dlungs_ch                                        # Define basis functions
fem define nodes;r;ACA binary                         # Define the nodes for the ACA model
fem define elements;r;ACA binary                   # Define the elements for the ACA model
fem define mesh;r;LPAACA               # Define a LPA-ACA model: a stochastic fractal tree that is a
                                           full lung model. Volume-filling mesh for a full lung model
                                       (5 lobes).The trachea comprises multiple elements (252). The
                                       model consists of lungs only. The respiratory airway model
                                       type is a Black-Box model, which represent acini. The acinar
                                       volume distribution is the same volume throughout the lung
                                           model. The coefficient of variation for diameter is 0.1, the
                                          BBM volume is 123.4013, and the basis function for the
                                          airways is 3. Uniform ventilation is assumed, and the
                                          compliance relationship is cube-root of volume change
fem define equation;r;gasmix                       # Define solution of gas transport equation
fem define material;r;d225                                     # Define the gas properties
fem define motion;r;standard                   # Define the tidal volume and breath duration
fem define initial;r;gasmix                    # Define the initial and boundary conditions
fem define solve;r;LPAACA                         # Define the solution method and output
fem solve from 0 to 100                          # Solve the transport equation from 0 to 100 s
fem quit
```

Water and heat transfer

.command file for water and heat transfer in the ACA model

```
set num_threads 4                      # Set the number of processors for parallel processing
fem define parameters;r;WHT                          # Define the size of the required arrays
fem define coordinates 3,1                    # Define 3-D rectangular cartesian coordinates
fem define base;r;3dlungs_ch                                        # Define basis functions
fem define nodes;r;ACA binary                              # Define nodes for the ACA model
fem define elements;r;ACA binary                        # Define elements for the ACA model
fem define mesh;r;LPAACA                                        # Define a LPA-ACA model
fem define equation;r;WHT             # Define solution of water and heat transport equations
fem define material;r;WHT                        # Define the water vapour and heat properties
fem define motion;r;WHT_15lpm                  # Define the tidal volume and breath duration
fem define initial;r;WHT_15lpm                 # Define the initial and boundary conditions
fem define solve;r;WHT_15lpm                      # Define the solution method and output
fem solve from 0 to 20                           # Solve the transport equations from 0 to 20 s
fem quit
```

.command file for water and heat transfer in the ACA model, with an ET tube

```
set num_threads 4                    # Set the number of processors for parallel processing
fem define parameters;r;WHT                     # Define the size of the required arrays
fem define coordinates 3,1                  # Define 3-D rectangular cartesian coordinates
fem define base;r;3dlungs_ch                            # Define basis functions
fem define nodes;r;ACA binary                     # Define nodes for the ACA model
fem define elements;r;ACA binary               # Define elements for the ACA model
fem define mesh;r;LPAACA_ET                # Define a LPA-ACA model, with an ET tube
fem define equation;r;WHT         # Define solution of water and heat transport equations
fem define material;r;WHT               # Define the water vapour and heat properties
fem define motion;r;WHT_ET               # Define the tidal volume and breath duration
fem define initial;r;30_ryan              # Define the initial and boundary conditions
fem define time;r;30_ryan           # Define the changing boundary temperatures
fem define solve;r;30_ryan                    # Define the solution method and output
fem solve from 0 to 58                   # Solve the transport equations from 0 to 58 s
fem quit
```

Bibliography

Anthonisen, N. R., Robertson, P. C. & Roos, W. R. D. (1970), 'Gravity-dependent sequential emptying of lung regions', *J. Appl. Physiol.* **28**, 589–595.

Baile, E. M., Dahlby, R. W., Wiggs, B. R., Parsons, G. H. & Pare, P. D. (1987), 'Effect of cold and warm dry air hyperventilation on canine airway blood flow', *J. Appl. Physiol.* **62**, 526–532.

Baker, L. G., Ultman, J. S. & Rhoades, R. A. (1974), 'Simultaneous gas flow and diffusion in a symmetric airway system: a mathematical model', *Resp. Physiol.* **21**, 119–138.

Bartels, J., Severinghaus, J. W., Forster, R. E. & Briscoe, W. A. (1954), 'The respiratory dead space measured by single breath analysis of oxygen, carbon dioxide, notrogen, or helium', *J. Cli. Invest.* **33**, 41–48.

Bosman, A. R. & Lee, G. d. J. (1969), 'The effects of cardiac action upon lung gas volume', *Clinical Science* **28**, 311–324.

Bowes, C., Cumming, G., Horsfield, K., Loughhead, J. & Preston, S. (1982), 'Gas mixing in a model of the pulmonary acinus with asymmetrical alveolar ducts', *J. Appl. Physiol.: Respirat. Environ. Exercise Physiol.* **52**(3), 624–633.

Bradley, C. P., Pullan, A. J. & Hunter, P. J. (1997), 'Geometric modelling of the human torso using cubic Hermite elements', *Ann. Biomed. Eng.* **25**, 96–111.

Breitenbucher, A., Chediak, A. D. & Wanner, A. (1994), 'Effect of lung volume and intrathoracic pressure on airway mucosal blood flow in man', *Resp. Physiol.* **10**, 316–321.

Bui, T. D., Dabdub, D. & George, S. C. (1998), 'Modeling bronchial circulation with application to soluble gas exchange: description and sesitivity analysis', *J. Appl. Physiol.* **84**(6), 2070–2088.

Chang, H. K. & Farhi, L. E. (1973), 'On mathematical analysis of gas transport in the lung', *Resp. Physiol.* **18**, 370–385.

Cole, P. (1993), *The respiratory role of the upper airways*, Mosby Year Book, St Louis.

Crawford, A. B. H., Cotton, D. J., Paiva, M. & Engel, L. A. (1989), 'Effect of lung volume on ventilation distribution', *J. Appl. Physiol.* **66**(6), 2502–2510.

Crawford, A. B. H., Makowska, M., Kelly, S. & Engel, L. A. (1986), 'Effect of breath holding on ventilation maldistribution during tidal breathing in normal subjects', *J. Appl. Physiol.* **61**(6), 2108–2115.

Crawford, A. B. H., Makowska, M., Paiva, M. & Engel, L. A. (1985), 'Convection- and diffusion-dependent ventilation maldistribution in normal subjects', *J. Appl. Physiol.* **59**(3), 838–846.

Croucher, A. E. & O'Sullivan, M. J. (1998), 'Numerical methods for contaminant transport in rivers and estuaries', *Computers and Fluids* **27**(8), 861–878.

Cruz, J. C. (1991), 'A combined parallel and series distribution model of inspired inert gases', *Resp. Physiol.* **86**, 1–14.

Cruz, J. C., Jeng, D.-R., Han, D., Wu, G. & Flores, X. F. (1997), 'Ventilation inhomogeneities and mixed venous blood n_2 in multibreath n_2 washout', *Resp. Physiol.* **110**, 47–56.

Cumming, G., Crank, J., Horsfield, K. & Parker, I. (1966), 'Gaseous diffusion in the airways of the human lung', *Resp. Physiol.* **1**, 58–74.

Cumming, G. & Guyatt, A. R. (1982), 'Alveolar gas mixing efficiency in the human lung', *Clinical Science* **62**, 541–547.

Cumming, G., Horsfield, K. & Preston, S. B. (1971), 'Diffusion equilibrium in the lungs examined by nodal analysis', *Respiration Physiology* **12**, 329–245.

Darquenne, C. & Paiva, M. (1994), 'One-dimensional simulation of aerosol transport and deposition in the human lung', *J. Appl. Physiol.* **77**(6), 2889–2898.

Darquenne, C. & Paiva, M. (1996), 'Two- and three-dimensional simulations of aerosol transport and deposition in alveolar zone of human lung', *J. Appl. Physiol.* **80**(4), 1401–1414.

Darquenne, C., Paiva, M., West, J. B. & Prisk, G. K. (1997), 'Effect of microgravity and hypergravity on deposition of 0.5- to 3-um-diameter aerosol in the human lung', *J. Appl. Physiol.* **83**(6), 2029–2036.

Davidson, M. R. & Engel, L. A. (1982), 'Gas transport in an asymmetrical acinus', *Bull. Europ. Physiolpath. Resp.* **18**, 203–214.

Daviskas, E., Gonda, I. & Anderson, S. D. (1990), 'Mathematical modeling of heat and water transport in human respiratory tract', *J. Appl. Physiol.* **69**(1), 363–372.

Daviskas, E., Gonda, I. & Anderson, S. D. (1991), 'Local airway heat and water vapour losses', *Resp. Physiol.* **84**, 115–132.

de Vries, W. R., Luijendijk, S. C. M. & Zwart, A. (1981), 'Helium and sulfur hexaflouride washout in asymmetric lung models', *J. Appl. Physiol.* **51**, 1122–1130.

Dutrieue, B., Vanholsbeeck, F., Verbanck, S. & Paiva, M. (2000), 'A human acinar structure for simulation of realistic alveolar plateau slopes', *J. Appl. Physiol.* **89**, 1859–1867.

Elad, D., Shochat, A. & Shiner, R. J. (1998), 'Computational model of oscillatory airflow in a bronchial bifurcation', *Resp. Physiol.* **112**, 95–111.

Engel, L. A., Menkes, H., Wood, L. D. H., Utz, G., Joubert, J. & Macklem, P. T. (1973), 'Gas mixing during breath holding studied by intrapulmonary gas sampling', *J. Appl. Physiol.* **35**(1), 9–17.

Engel, L. A. & Paiva, M., eds (1985), *Gas mixing and distribution in the lung*, Vol. 25 of *Lung biology in health and disease*, Marcel Dekker, New York, chapter 6, pp. 221–285.

Engel, L. A., Paiva, M., Siegler, D. I. M. & Fukuchi, Y. (1979), 'Dual tracer single breath studies of gas transport in the lung', *Resp. Physiol.* **36**, 103–119.

Evrensel, C. A., Khan, M. R. U., Elli, S. & Krumpe, P. E. (1993), 'Viscous airflow through a rigid tube with a compliant lining: a simple model for the air-mucus interaction in pulmonary airways', *Transactions of the ASME* **115**, 262–269.

Fowler, W. S. (1948), 'Lung function studies II. the respiratory dead space', *Am. J. Physiol.* **154**, 405–416.

Fuller, G. M., Harris, E. A. & Withy, S. J. (1990), 'Gas mixing efficiency in a mathematical model of the lung', *Clin. Phys. Physiol. Meas.* **2**, 149–158.

Gillis, H. L. & Lutchen, K. R. (1999), 'How heterogeneous bronchoconstriction affects ventilation distribution in human lungs: a morphometric model', *Ann. Biomed. Eng.* **27**, 14–22.

Glazier, J. B., Highes, J. M. B., Maloney, J. E. & West, J. B. (1967), 'Vertical gradient of alveolar size in lungs of dogs frozen intact', *J. Appl. Physiol.* **23**(5), 694–705.

Haefeli-Bleuer, B. & Weibel, E. R. (1988), 'Morphometry of the human pulmonary acinus', *Anat. Rec.* **220**, 401–414.

Hanna, L. M. (1983), Modelling of heat and water vapour transport in the human respiratory tract, PhD thesis, University of Pennsylvania, Philadelphia, Pennsylvania.

Hanna, L. M. & Scherer, P. W. (1982), Analysis of respiratory heat and water transport, *in* '35th ACEMB'.

Hanna, L. M. & Scherer, P. W. (1986*a*), 'Measurement of local mass transfer coefficients in a cast model of the human upper respiratory tract', *ASME J. Biomech. Eng.* **108**, 12–18.

Hanna, L. M. & Scherer, P. W. (1986*b*), 'Regional control of local airway heat and water vapour losses', *J. Appl. Physiol.* **61**(2), 624–632.

Hanna, L. M. & Scherer, P. W. (1986*c*), 'A theoretical model of localized heat and water vapor transport in the human respiratory tract', *ASME J. Biomech. Eng.* **108**, 19–27.

Hansen, J. E. & Ampaya, E. P. (1975), 'Human airspace shapes, sizes, areas and volumes', *J. Appl. Physiol.* **38**, 990–995.

Harris, E. A., Buchanan, P. R. & Whitlock, R. M. (1987), 'Human alveolar gas-mixing efficiency for gases of differing diffusivity in health and airflow limitation', *Clinical Science* **73**, 351–359.

Heyder, J., Blanchard, J. D., Feldman, H. A. & Brain, J. D. (1988), 'Convective mixing in human respiratory tract: estimates with aerosol boli', *J. Appl. Physiol.* **64**(3), 1273–1278.

Horsfield, K. (1986), *Handbook of physiology: The respiratory system III*, American Physiological Society, Bethseda, Md., chapter 7.

Horsfield, K. & Cumming, G. (1967), 'Angles of branching and diameters of branches in the human bronchial tree', *Bull. Math. Biophys.* **29**, 245–259.

Horsfield, K. & Cumming, G. (1968), 'Morphology of the bronchial tree in man', *J. Appl. Physiol.* **24**, 373–383.

Horsfield, K., Dart, G., Olsen, D. E., Filley, G. F. & Cumming, G. (1971), 'Models of the human bronchial tree', *J. Appl. Physiol.* **31**, 207–217.

Horsfield, K., Gordon, W. I., Kemp, W. & Phillips, S. (1987), 'Growth of the bronchial tree in man', *Thorax* **42**, 383–388.

Horsfield, K., Relea, F. G. & Cumming, G. (1976), 'Diameter, length and branching ratios in the bronchial tree', *Resp. Physiol.* **26**, 351–356.

Horstmann, G., Iravani, J., Norris-Melville, G. & Richter, H. G. (1977), 'Influence of temperature and decreased water content of inspired air on the ciliated bronchial epithelium: a physiological and elctron microscopical study', *Acta Otolaryngol* **84**, 124–131.

Howatson, M. (1995), An anatomically accurate mathematical model of the human pulmonary acinus, Master's thesis, University of Auckland, Auckland, New Zealand.

Howatson Tawhai, M., Pullan, A. J. & Hunter, P. J. (2000), 'Generation of an anatomically based three-dimensional model of the conducting airways', *Ann. Biomed. Eng.* **28**(7), 793–802.

Huang, J. W., Yang, G. C., Scherer, P. W. & Neufeld, G. R. (2000), 'Airway cross section strongly influences alveolar plateau slope of capnograms for smaller tidal volumes', *Resp. Physiol.* **119**, 51–55.

Hutchins, G. M., Haupt, H. M. & Moore, G. W. (1981), 'A proposed mechanism for the early development of the human tracheobronchial tree', *Anat. Rec.* **201**, 635–640.

Ingenito, E. P. (1984), Respiratory fluid mechanics and heat transfer, Phd, Massachusetts Institute of Technology, Cambridge.

Ingenito, E. P., Solway, J., McFadden, E. R. J., Pichurko, B. M., Cravalho, E. G. & Drazen, J. M. (1986), 'Finite difference analysis of respiratory heat transfer', *J. Appl. Physiol.* **61**(6), 2252–2259.

Irlbeck, D. (1998), 'Normal mechanisms of heat and moisture exchange in the respiratory tract', *Respiratory Care Clinics of North America* **4**(2), 189–198.

Kallok, M. J., Wilson, T. A., Rodarte, J. R., Lai-Fook, S. J., Chevalier, P. A. & Harris, P. D. (1979), 'Distribution of regional volumes and ventilation in excised canine lobes', *J. Appl. Physiol.* **47**(1), 182–191.

Kilburn, K. H. (1968), 'A hyp[othesis for pulmonary clearance and its implications', *Am. Rev. Resp. Dis.* **98**, 449–463.

Kim, H. H., LeMerre, C., Chediak, A. D. & Wanner, A. (1996), 'Effect of hyperventilation on airway mucosal blood flow in normal subjects', *Am. J. Respir. Crit. Care Med.* **154**(5), 1563–1566.

King, M., Tomkiewicz, R. P., Boyd, W. A., Shao, A. & Ghahary, A. (1995), 'Mucociliary clearance and epithelia potential difference in dogs mechanically ventilated with air humidified by heated hot water and heat and mositure exchange devices', *Journal of Aerosol Medicine* **8**(1), 80–84.

Kitaoka, H. & Suki, B. (1997), 'Branching design of the bronchial tree based on a diameter-flow relationship', *J. Appl. Physiol.* **82**(3), 968–976.

Kitaoka, H., Takaki, R. & Suki, B. (1999), 'A three-dimensional model of the human airway tree', *J. Appl. Physiol.* **87**(6), 2207–2217.

Krause, E., Bandt, C., Schulz, A. & Sculz, H. (1995), 'Fractal exponents for the upper airways of mammalian lungs', *The Statistical Software Newsletter* **20**, 583–590.

La Force, R. C. & Lewis, B. M. (1970), 'Diffusional transport in the human lung', *J. Appl. Physiol.* **28**(3), 291–298.

Lauzon, A.-M., Prisk, G. K., Elliott, A. R., Verbanck, S., Paiva, M. & West, J. B. (1997), 'Paradoxical helium and sulfur-hexafluoride single-breath washouts in short-term vs. sustained microgravity', *J. Appl. Physiol.* **82**(3), 859–865.

Le Merre, C., Kim, H. H., Chediak, A. D. & Wanner, A. (1996), 'Airway blood flow responses to temperature and humidity of inhaled air', *Resp. Physiol.* **105**, 235–239.

Li, C. W. (1990), 'Least-squares characteristics and finite elements for advection-dispersion simulation', *International Journal of Numerical Methods in Engineering* **29**, 1343–1358.

Luijendijk, S. C. M., Zwart, A., de Vries, W. R. & Salet, W. M. (1980), 'The sloping alveolar plateau at synchronous ventilation', *Pflugers Arch.* **384**, 267–277.

McFadden, E. R. J., Denison, D. M., Waller, J. F., Assoufi, B., Peacock, A. & Sopwith, T. (1982), 'Direct recordings of the temperatures in the tracheobronchial tree in normal man', *J. Clin. Invest.* **69**, 700–705.

McFadden, E. R. J., Pichurko, B. M., Bowman, H. F., Ingenito, E., Burns, S., Dowling, N. & Solway, J. (1985), 'Thermal mapping of the airways in humans', *J. Appl. Physiol.* **58**(2), 564–570.

Mercer, R. R., Laco, J. M. & Crapo, J. D. (1987), 'Three-dimensional reconstruction of alveoli in the rat lung for pressure-volume relationships', *J. Appl. Physiol.* **62**(4), 1480–1487.

Milic-Emili, J., Henderson, J. A. M., Dolovich, M. B., Trop, D. & Kaneko, K. (1966), 'Regional distribution of inspired gas in the lung', *J. Appl. Physiol.* **21**(3), 749–759.

Miyao, H., Hirokawa, T., Miyasaka, K. & Kawazoe, T. (1992), 'Relative humidity, not absolute humidity, is of great importance when using a humidifier with a heating wire', *Critical Care Medicine* **20**, 674–679.

Mon, E. & Ultman, J. S. (1976), 'Monte carlo simulation of simultaneous gas flow and diffusion in an asymmetric distal pulmonary airway model', *Bull. Math. Biol.* **38**, 161–192.

National Library of Medicine, U. (1996), 'Visual Man Project', CD-ROM.

Nelson, T. R. & Manchester, D. K. (1988), 'Modeling of lung morphogenesis using fractal geometries', *IEEE Transactions on Medical Imaging* **7**(4), 321–327.

Pack, A., Hooper, M. B., Nixon, W. & Taylor, J. C. (1977), 'A computational model of pulmonary gas transport incorporating effective diffusion', *Resp. Physiol.* **29**, 101–124.

Paiva, M. (1972), 'Computation of the boundary conditions for diffusion in the human lung', *Comput. Biomed. Res.* **5**, 585–595.

Paiva, M. (1973), 'Gas transport in the human lung', *J. Appl. Physiol.* **?**(3), 401–410.

Paiva, M. & Engel, L. A. (1979), 'Pulmonary interdependence of gas transport', *J. Appl. Physiol.* **47**, 296–305.

Paiva, M. & Engel, L. A. (1981), 'The anatomical basis for the sloping n2 plateau', *Resp. Physiol.* **44**, 325–337.

Paiva, M. & Engel, L. A. (1984), 'Model analysis of gas distribution within human lung acinus', *J. Appl. Physiol.: Respirat. Environ. Exercise Physiol.* **56**, 418–425.

Paiva, M., van Muylem, A. & Engel, L. A. (1982), 'The slope of phase III in multibreath nitrogen washout and washin', *Bull. Eur. Physiopathol. Respir.* **18**, 273–280.

Paiva, M., Verbanck, S. & van Muylem, A. (1988), 'Diffusion-dependent contribution to the slope of the alveolar plateau', *Resp. Physiol.* **72**, 257–270.

Parent, R. A., ed. (1992), *Treatise on pulmonary toxicology I, Comparative biology of the normal lung*, CRC Press, Boca Raton, chapter 5, pp. 49–61.

Parker, H., Horsfield, K. & Cumming, G. (1971), 'Morphology of distal airways in the human lung', *J. Appl. Physiol.* **31**, 386–391.

Parsons, G. H., Pare, P. D., White, D. A. & Baile, E. M. (1989), 'Airway blood flow response to eucapnic dry air hyperventilation in sheep', *J. Appl. Physiol.* **66**, 1443–1447.

Phalen, R. F., Yeh, H. C., Schum, G. M. & Raabe, O. G. (1978), 'Application of an idealized model to morphometry of the mammalian tracheobronchial tree', *Anat. Rec.* **190**, 167–176.

Phillips, C. G. & Kaye, S. R. (1997), 'On the asymmetry of bifurcations in the bronchial tree', *Resp. Physiol.* **107**, 85–98.

Phillips, J., Wong, L. & Yeates, D. (1998), 'Bidirectional actively coupled water transport across trachea epithelia', *Resp. Crit. Care Med.* **157**(3), A848.

Raabe, O. G., Yeh, H. C., Schum, G. M. & Phalen, R. F. (1976), 'Tracheobronchial geometry - Human, Dog, Rat, Hamster', *Lovelace Foundation for Medical Education and Research* .

Ragone, D. V. (1995), *Thermodynamics of materials*, Vol. II, Wiley, New York.

Rauwerda, P. E. (1946), Unequal ventilation of different parts of the lung and determination of cardiac output, Phd, Groningen State University, Netherlands.

Richards, J. H. & Marriott, C. (1974), 'Effect of relative humidity on the rheological properties of bronchial mucus', *American Review of Respiratory Disease* **109**, 484–486.

Rodarte, J. R., Chaniotakis, M. & Wilson, T. A. (1989), 'Variability of parenchymal expansion measured by computed tomography', *J. Appl. Physiol.* **67**(1), 226–231.

Ryan, S. N., Rankin, N. & Williams, R. (2000), 'Energy balance in the intubated human airway is an indicator of optimal gas conditioning', *submitted to Critical Care Medicine* .

Saidel, G. M., Kruse, K. L. & Primiano, F. P. J. (1983), 'Model simulation of heat and water transport dynamics in an airway', *ASME J. Biomech. Eng.* **105**, 188–193.

Scadding, J. G. & Cumming, G., eds (1981*a*), *Organisation of the tracheobronchial tree*, number 5 *in* 'Scientific foundations of respiratory medicine', William Heinemann, London.

Scadding, J. G. & Cumming, G., eds (1981*b*), *Scientific foundations of respiratory medicine*, William Heinemann, London, chapter 6.

Scherer, P. W., Gobran, S., Aukberg, S. J., Baumgardner, J. E., Bartkowski, R. & Neufeld, G. R. (1988), 'Numerical and experimental study of steady-state co_2 and inert gas washout', *J. Appl. Physiol.* **64**(3), 1022–1029.

Scherer, P. W., Neufeld, J. D., Baumgardner, J. E. & Neufeld, G. R. (1996), 'The importance of a source term in modeling multibreath inert gas washout', *Resp. Physiol.* **103**, 99–103.

Scherer, P. W., Shendalman, L. H. & Green, N. M. (1972), 'Simultaneous diffusion and convection in a single breath lung washout', *Bull. Math. Biophys.* **34**, 393–412.

Schroter, R. C. & Watkins, N. V. (1989), 'Respiratory heat exchange in mammals', *Resp. Physiol.* **78**, 357–368.

Schwardt, J. D., Neufeld, G. R., Baumgardner, J. E. & Scherer, P. W. (1994), 'Noninvasive recovery of acinar anatomic information from co_2 expirograms', *Ann. Biomed. Eng.* **22**, 293–306.

Scrimshire, D. A., Loughnane, R. J. & Jones, T. J. (1978), 'A reappraisal of boundary conditions assumed in pulmonary gas transport models', *Resp. Physiol.* **35**, 317–334.

Sleigh, M. A., Blake, J. R. & Liron, N. (1988), 'The propulsion of mucus by cilia', *Am. Rev. Resp. Dis.* **137**, 726–741.

Snyder, B., Dantzker, D. R. & Jaeger, M. J. (1981), 'Flow partitioning in symmetric cascades of branches', *J. Appl. Physiol.: Respirat. Environ. Exercise Physiol.* **51**(3), 598–606.

Strahler, A. N. (1950), 'Equilibrium theory of erosional slopes approached by frequency distribution analysis', *Am. J. Sci.* **248**, 673–696.

Taulbee, D. B. & Yu, C. P. (1975), 'A theory of aerosol deposition in the human respiratory tract', *J. Appl. Physiol.* **38**(1), 77–85.

Taulbee, D. B., Yu, C. P. & Heyder, J. (1978), 'Aerosol transport in the human lung from analysis of single branches', *J. Appl. Physiol.: Respirat. Environ. Exercise Physiol.* **44**(5), 803–812.

Thurlbeck, A. & Horsfield, K. (1980), 'Branching angles in the bronchial tree related to order of branching', *Resp. Physiol.* **41**, 173–181.

Tsai, C. L., Saidel, G. M., McFadden, E. R. J. & Fouke, J. M. (1990), 'Radial heat and water transport across the airway wall', *J. Appl. Physiol.* **69**(1), 222–231.

Tsu, M. E., Babb, A. L., Ralph, D. D. & Hlastala, M. P. (1988), 'Dynamics of heat, water, and soluble gas exchange in the human airways: 1. a model study', *Ann. Biomed. Eng.* **16**(6), 547–571.

Verbanck, S., Mangado, G., Peces-Barba, G. & Paiva, M. (1991), 'Multiple-breath washout experiments in rat lungs', *J. Appl. Physiol.* **71**(3), 847–854.

Verbanck, S. & Paiva, M. (1990), 'Model simulations of gas mixing and ventilation distribution in the human lung', *J. Appl. Physiol.* **69**(6), 2269–2279.

Verbanck, S., Schuermans, D., van Muylem, A., Melot, C., Noppen, M., Vincken, W. & Paiva, M. (1998), 'Conductive and acinar lung-zone contributions to ventilation inhomogeneity in COPD', *Am. J. Respir. Crit. Care Med.* **157**, 1573–1577.

Verbanck, S., Schuermans, D., van Muylem, A., Paiva, M., Noppen, M. & Vincken, W. (1997), 'Ventilation distribution during histamine provocation', *J. Appl. Physiol.* **83**(6), 1907–1916.

Wang, C. Y., Bassingthwaighte, J. B. & Weissman, L. J. (1992), 'Bifurcating distributive system using Monte Carlo method', *Mathl. Comput. Modelling* **16**(3), 91–98.

Warner, D. O., Hyatt, R. E. & Rehder, K. (1988), 'Inhomogeneity during deflation of excised canine lungs. I. Alveolar pressures.', *J. Appl. Physiol.* **65**(4), 1757–1765.

Weibel, E. R. (1963), *Morphometry of the human lung*, Springer-Verlag, Berlin.

Weibel, E. R. (1984), *The pathway for oxygen: Structure and function in the mammalian respiratory system*, Harvard University Press, Cambridge, Massachusetts, chapter 11.

West, J. B. (1962), 'Regional differences in gas exchange in the lung of erect man', *J. Appl. Physiol.* **17**(6), 893–898.

West, J. B. (1979), *Respiratory physiology - the essentials*, 2nd edn, Williams and Wilkins, Baltimore.

Williams, R., Rankin, N., Smith, T., Galler, D. & Seakins, P. (1996), 'Relationship between the humidity and temperature of inspired gas and the function of the airway mucosa', *Crit. Care Med.* **24**(11), 1920–1929.

Williams, R., Seakins, P., Rankin, N., Smith, T. & Galler, D. (1996), 'A new model of how respired humidity affects airway function', *Proc. of 9th Eur. Cong. on Int. Care Med.* pp. 7–10.

Wilson, T. A., Olsen, L. E. & Rodarte, J. R. (1987), 'Effect of variable parenchynal expansion on gas mixing', *J. Appl. Physiol.* **62**(2), 634–639.

Zienkiewicz, O. C. & Taylor, R. L. (1994), *The Finite Element Method*, fourth edn, McGraw-Hill Book Company Europe, Berkshire.